



January 2023

Neuromodulatory Mechanisms Of Neuropeptides In The Amygdala

Cody Adam Boyle

[How does access to this work benefit you? Let us know!](#)

Follow this and additional works at: <https://commons.und.edu/theses>

Recommended Citation

Boyle, Cody Adam, "Neuromodulatory Mechanisms Of Neuropeptides In The Amygdala" (2023). *Theses and Dissertations*. 5284.

<https://commons.und.edu/theses/5284>

This Dissertation is brought to you for free and open access by the Theses, Dissertations, and Senior Projects at UND Scholarly Commons. It has been accepted for inclusion in Theses and Dissertations by an authorized administrator of UND Scholarly Commons. For more information, please contact und.common@library.und.edu.

NEUROMODULATORY MECHANISMS OF NEUROPEPTIDES IN THE AMYGDALA

by

Cody Adam Boyle

Master of Science, University of North Dakota, 2017
Bachelor of Science, University of North Dakota 2014

A Dissertation

Submitted to the Graduate Faculty

of the

University of North Dakota

In partial fulfillment of the requirements
for the degree of Doctor of Philosophy in Biomedical Sciences

Grand Forks, North Dakota

August

2023

Name: Cody Boyle
Degree: Doctor of Philosophy

This document, submitted in partial fulfillment of the requirements for the degree from the University of North Dakota, has been read by the Faculty Advisory Committee under whom the work has been done and is hereby approved.

DocuSigned by:
Saobo Lei
34403D426773495
Saobo Lei

DocuSigned by:
Thad Rosenberger
C218E05F001482
Thad Rosenberger

DocuSigned by:
Dr. Jonathan Geiger
F65A73E2FAC64E3
Dr. Jonathan Geiger

DocuSigned by:
Dr. James D. Foster
A386FD8E38614E4
Dr. James D. Foster

DocuSigned by:
Peter Meberg
FE5057AF857C460
Peter Meberg

This document is being submitted by the appointed advisory committee as having met all the requirements of the School of Graduate Studies at the University of North Dakota and is hereby approved.

DocuSigned by:
Chris Nelson
2E0A7088C733403

Chris Nelson
Dean of the School of Graduate Studies

6/28/2023

Date

PERMISSION

Title: Neuromodulatory Mechanisms of Neuropeptides in the Amygdala

Department: Biomedical Sciences

Degree: Doctor of Philosophy

In presenting this dissertation in partial fulfillment of the requirements for a graduate degree from the University of North Dakota, I agree that the library of this University shall make it freely available for inspection. I further agree that permission for extensive copying for scholarly purposes may be granted by the professor who supervised my dissertation work, or in her absence, by the Chairperson of the department or the dean of the School of Graduate Studies. It is understood that any copying or publication or other use of this dissertation or part thereof for financial gain shall not be allowed without my written permission. It is also understood that due recognition shall be given to me and to the University of North Dakota in any scholarly use which may be made of any material in my dissertation.

Cody Adam Boyle
August, 2023

TABLE OF CONTENTS

LIST OF TABLES.....	x
LIST OF FIGURES.....	xi
ACKNOWLEDGEMENTS.....	xiii
ABSTRACT.....	xv
PREFACE.....	xvii
CHAPTER	
1. INTRODUCTION TO THE AMYGDALA AND NEUROPEPTIDES.....	1
Study of the Limbic System.....	1
Early Theories of Emotion.....	1
Lesion Studies of the Medial Temporal Lobe and the Amygdala.....	2
Early Structural and Functional Investigations of the Amygdala.....	3
Connectivity and Neuroanatomy of the Rodent Amygdala.....	4
Neuroanatomy of the Rodent Amygdala Nuclei.....	4
Cell Types of the Amygdala.....	5
Connectivity of the Amygdala.....	7
Amygdala and Hippocampal Connections.....	10

	Pathophysiology of the Amygdala	11
	Fear vs. Anxiety	11
	Anxiety and Depression.....	13
	Therapeutic Strategies	16
	Neuropeptides and the Amygdala	19
	Neuropeptides as Neuromodulatory Molecules	20
	Mechanisms of Neuropeptide Release	20
	Neuropeptides as Therapeutics.....	22
	Dissertation Research Objective.....	25
2.	METHODS	26
	Preparation of Amygdala Slices	26
	Electrophysiology.....	27
	Recordings of Resting Membrane Potentials, Action Potentials, Holding Currents, and Current-Voltage Relationships from Amygdala Neurons.....	28
	Recordings of sEPSCs, mEPSCs, and eEPSCs	30
	Stereotaxic Surgery, Microinjection, and Histology	31
	Acoustic Startle and Fear-potentiated Startle Responses	33
	Recordings of Mean Arterial Pressure and Heart Rate.....	34
	Vogel Conflict Test.....	35
	Data Analysis.....	36
	Chemicals.....	37

3.	RESULTS.....	38
	Study 1 - Neuromedin B-mediated Modulation of Central Amygdala Neurons	38
	Introduction	38
	NMB Increases Neuronal Excitability in the CeL.....	39
	NMB-induced Excitation of CeL Neurons Requires the Functions of G Proteins and PLC β	42
	Intracellular Ca ²⁺ Release is Unnecessary, but PKC is Required for NMB-Elicited Excitation of CeL Neurons	43
	NMB Depolarizes CeL Neurons and Increases the Input Resistance and Membrane Time Constants of CeL Neurons	45
	Activation of BB1 Receptors Inhibits an Inwardly Rectifying K ⁺ Channel in CeL Neurons	47
	GIRK Channels are Involved in BB1 Receptor-Mediated Excitation of CeL Neurons.....	50
	G proteins, PLC β and PKC are Required for BB1 Receptor-Mediated Depression of Kir Channels.....	57
	BB1 Receptor-Mediated Excitation of CeL Neurons Promotes Inhibitory Cardiovascular Responses	60
	BB1 Receptor Activation Augments ASR but Attenuates FPS.....	64
	Study 2- Activation of Bombesin-1 Receptors Excites the Principal Neurons in the Basolateral Amygdala by Multiple Signaling and Ionic Mechanisms	70
	Introduction	70
	Activation of BB1 Receptors Excite BLA Principal Neurons.....	71

	BB1 Receptors Stimulate a Cation Current and Inhibit an Inwardly Rectifying K ⁺ Current.....	73
	TRPV1 Channels are Involved in NMB-Mediated Inward Currents	79
	BB1 Receptor-Mediated Excitation of BLA Neurons is Dependent on PLC β and PLC β -Mediated Hydrolysis of PIP ₂ and PI3/4K Signaling	85
	BB1 Receptor Activation Modulates Glutamatergic Transmission in the BLA.....	86
	BB1 Receptor Activation in the BLA Produces Anxiogenic Phenotypes	96
	TRPV1 and GIRK Channels are Involved in BB1 Receptor-Mediated Anxiety-Like Behaviors in the BLA.....	101
	Study 3- Neurokinin-3 Receptor-Mediated Modulation of Basolateral Amygdala Neurons.....	103
	Introduction	103
	Activation of NK3Rs Excites BLA Principal Neurons.....	104
	Stimulation of NK3Rs Activates a Cation Channel and Inhibits an Inwardly Rectifying K ⁺ Channel	106
	TRPC4 and TRPC5 Channels are Involved in NK3R-Elicited Excitation of BLA Principal Neurons.....	114
	NK3R-Mediated Excitation of BLA Neurons is Dependent on PLC β and PLC β -Mediated Hydrolysis of PIP ₂	115
	NK3R-Mediated Excitation of BLA Neurons Augments Cued Startle Responses.....	118
	GIRK Channels and TRPC4/5 Channels are Involved in NK3R-Mediated Enhancement of Startle Responses	121
4.	DISCUSSION.....	127

Study 1 - Neuromedin B-Mediated Modulation of Central Amygdala Neurons	127
Study 2 - Bombesin-1 Receptors Excites Neurons of the Basolateral Amygdala by Multiple Signaling and Ionic Mechanisms	134
Study 3- Neurokinin-3 Receptor-Mediated Modulation of Basolateral Amygdala Neurons.....	142
Limitations and Future Experiments.....	148
Exogenous Application of NPs	148
Lack of Neuronal and Circuit Specificity	148
NP Administration Lacks Temporal Specificity.....	151
LIST OF ABBREVIATIONS	153
LIST OF REAGENTS AND DRUGS	155
COPYRIGHT CLEARANCE	156
REFERENCES.....	157

LIST OF TABLES

Table	Page
1. Cardiovascular parameters	69

LIST OF FIGURES

Figure	Page
1. NMB increases AP firing frequency in CeL neurons.....	41
2. G proteins, PLC β and PKC are required for NMB-mediated potentiation of AP firing frequency.....	46
3. NMB induces membrane depolarization and increases the input resistances and membrane time constants.....	48
4. NMB-mediated inhibition of Kir currents is Ba ²⁺ -sensitive but insensitive to the Kir2 subfamily blocker ML 133	52
5. GIRK channels are involved in NMB-elicited depression of Kir channel currents	55
6. G proteins and PLC β are involved in BB1 receptor-mediated depression of Kir channels	58
7. PKC is involved in NMB-induced depression of Kir channels.	61
8. Schematic diagram showing the cardiovascular recording, ASR and FPS procedures and cannula placement.	65
9. BB1 receptor activation in the CeA reduces cardiovascular output and affects ASR and FPS	67
10. Activation of BB1 receptors excites BLA neurons.....	74
11. NMB-elicited excitation of BLA neurons is mediated by inhibiting a Kir channel and opening a cation channel	77
12. GIRK channels are required for BB1 receptor-elicited inward currents in BLA neurons	80
13. TRPV1 channels are involved in BB1 receptor-induced inward currents in BLA neurons	82
14. BB1 receptor elicited excitation of BLA neurons requires PLC β -mediated intracellular signaling	87

15.	Activation of BB1 receptors enhances spontaneous glutamate release in BLA neurons	91
16.	BB1 receptor-mediated spontaneous glutamate release requires TRPV1 channels in BLA neurons	93
17.	BB1 receptors suppress evoked glutamate release through a presynaptic mechanism	97
18.	Application of NMB into the BLA dose-dependently increase anxiety-like behaviors	100
19.	Activation of NK3Rs excites BLA principal neurons.....	107
20.	Senktide-elicited excitation of BLA neurons is mediated by opening a cation channel and inhibiting a Kir channel.....	110
21.	GIRK channels are required for NK3R-elicited inward currents in BLA neurons	113
22.	TRPC4 and TRPC5 channels are involved in NK3R-induced inward currents in BLA neurons	116
23.	NK3R-elicited excitation of BLA neurons requires PLC β -mediated hydrolysis of PIP ₂	119
24.	Microinjection of senktide into the BLA dose-dependently enhances cued startle responses.....	122
25.	Roles of NK3Rs, GIRK and TRPC4/5 channels in senktide-mediated augmentation of cued startle responses.....	124
26.	The proposed cellular and molecular mechanisms underpinning BB1 receptor-elicited excitation of CeA neurons and decreased FPS and cardiac output.....	128
27.	Working model illustrating the cellular and molecular mechanisms underpinning BB1 receptor-elicited excitation of BLA principal neurons and increased anxiety-like behaviors in the VCT.....	135
28.	Working model illustrating the cellular and molecular mechanisms underpinning NK3R-elicited excitation of BLA principal neurons and augmentation of FPS response.....	144
	Supplementary Figure 1. BB1 receptor-mediated excitation requires release of intracellular Ca ²⁺	102

ACKNOWLEDGEMENTS

I would like to express my appreciation and gratitude to my mentor Dr. Saobo Lei. His commitment to his work and passion for science are qualities that I admire and aspire to model throughout my career. Throughout my time in his lab, his advice, both professionally and personally, has helped me grow as a scientist, person, and parent. Finally, I am thankful for his patience and support, as I have explored various projects throughout my training. Thank you. Dr. Lei.

I want to thank my committee members Drs. Jonathan Geiger, Thad Rosenberger, James Foster, and Peter Meberg. I would also like to thank my former committee member Dr. Walter Kemp. Each of you has been a wonderful resource throughout my training, and has contributed to my professional and personal growth. On countless occasions, each member graciously handled an unannounced office visit to discuss scientific methodologies, career advice, or troubleshoot issues.

Throughout my tenure in graduate school, the faculty, staff, and graduate student body of the Department of Biomedical Science have played a significant role in shaping my academic journey. I would like to thank the principal investigators and members of laboratories of Drs. John Watt, Colin Combs, Catherine Brissette, Holly Brown-Borg, Keith Henry, Archana Dhasarathy, Sergei Nechaev, Alexei Tulin, and Bo Liang. Each of these laboratories has provided some form of assistance through technical support, troubleshooting, or shared equipment and consumables. I would also like to thank

Jennifer Hershey, Michael Ullrich, and Bonnie Kee for their administrative assistance over the last several years. The mentorship and friendship of

Drs. Tim Casselli and Yvonne Tourand means the world to me. I would like to extend my heartfelt gratitude to Bonnie Kee. Her kindness, conversation, support, and assistance on everything from travel to the formatting of this dissertation have always been above and beyond.

I want to thank my family for everything they have done during my time in graduate school. My parents, Tammy, Jason, and Vince have always been the most supporting group. I am grateful for their encouragement in my academic pursuit. My siblings, Drew, Maci, and Misty (and her husband, Jimmy), have enriched my life beyond measure and I am grateful for the memories we have made together over the last five years. My in-laws, Barb, Nancy, and Carly have been incredible support systems during my graduate school tenure. Without their help with projects outside the laboratory, and with my daughter, this degree would have been nearly impossible.

Finally, I want to thank my wife, Emily, and our daughter, Gigi. I would not be the person I am today without them. Emily has sacrificed so much to help me pursue this degree. Her ability to balance so many tasks has allowed me to focus as a scientist. I do not know what I would have done without her. I am sincerely grateful for her encouragement, support, and love as I finish graduate school.

ABSTRACT

The amygdala is a limbic structure critical for emotional processing as well as roles in learning and memory. Disruption of the normal activity of the amygdala has been implicated in several disorders including phobia disorders, anxiety-like disorders, and substance abuse. The function of the amygdala and its role in various disorders is directly related to its underlying cellular activity. The amygdala is both a cortical- and striatal-like structure containing mainly glutamatergic and GABAergic neurons, respectively. This dissertation has three aims related to the neuropeptide modulation of these cell types in the basolateral (BLA) and central amygdala (CeA). The first aim addresses how the neuropeptide, neuromedin B (NMB), alters excitability within the CeA and contributes to cardiac output and fear responses. The second aim addresses how NMB modulates neuronal activity in the BLA and anxiety-like behaviors. Finally, the third aim studies the roles and mechanisms of neurokinin B-mediated modulation of neuronal excitability and fear responses.

For Study 1, bath application of NMB excited CeL neurons *in vitro*. NMB selectively activated bombesin 1 receptors (BB1Rs) increasing action potential firing that was dependent on the activity of PLC and PKC, but excitation was independent of Ca^{2+} flux. NMB enhanced CeL neuronal excitation by inhibiting inwardly rectifying K^+ channels. Direct application of NMB into the CeA reduced mean arterial pressure and heart rate and reduced fear potentiated startle responses.

For Study 2, activation of BB1Rs excited BLA neurons and enhanced glutamatergic transmission. NMB-mediated excitation of BLA neurons was mediated through the activation of non-selective cation channels and depression of inwardly rectifying K⁺ channels. NMB enhanced spontaneous glutamatergic transmission but inhibited evoked glutamate responses through TRPV1 channels. Direct application of NMB into the BLA produced anxiogenic phenotypes in the Vogel Conflict Test.

For Study 3, selective activation of neurokinin 3 receptors (NK3Rs) with senktide or the endogenous ligand neurokinin B enhanced neuronal excitability of BLA neurons. NK3R-elicited excitation of BLA neurons is mediated by the activation of non-selective cation channels and depression of inwardly rectifying K⁺ channels. The NK3R-mediated excitation of BLA neurons required the function of PLC and cleavage of membrane phosphatidylinositol 4,5-bisphosphate. Direct application of senktide into the BLA augmented fear potentiated startle responses. TRPC4/5 and GIRK channels are involved in senktide-induced augmentation of fear potentiated startle responses.

PREFACE

The topic of this dissertation is focused on neuropeptide modulation within the amygdala, an amalgam of nuclei comprised of the basolateral and central amygdala (BLA and CeA, respectively). As a component of the limbic system, the amygdala is critical in the interpretation and processing of sensory stimuli as well as encoding of emotional memory. To improve our understanding of the function of the amygdala and its role in disease, it is important to better understand the neuromodulatory mechanisms that alter amygdala activity.

The principal neurotransmitter of the CeA is γ -aminobutyric acid (GABA), whereas in the BLA the principal neurotransmitter is glutamate. The purpose of this dissertation will be to address some gaps in our knowledge regarding the modulation of GABAergic neurons in the CeA and glutamatergic neurons in the BLA by neuropeptides. A fundamental understanding of the amygdala neuroanatomy, neuronal circuitry, and both physiological and pathophysiological functionality will be needed to provide the reader with the needed background information framing the work presented herein.

For this dissertation, three separate studies were conducted. The first two concern the neuropeptide NMB and NMB-mediated modulation of neuronal activity in the CeA and BLA using *in vitro* and *in vivo* methods. The third study concerns the modulation of BLA principal neurons by the tachykinin neuropeptides. Specifically, examining neurokinin B-mediated modulation of glutamatergic neurons in the BLA using *in vitro* and *in vivo* technique.

CHAPTER 1

INTRODUCTION TO THE AMYGDALA AND NEUROPEPTIDES

Study of the Limbic System

Early Theories of Emotion

Early theorists believed distinct brain regions are involved in the circuitry and behavioral responses underlying emotion. The anatomical basis of emotion was first proposed by Dr. James Papez as a collection of interconnected structures within the mammalian brain [1]. His theory is based on clinical findings that excitatory activity in the cingulate gyrus, hippocampus, and hypothalamus could alter a patient's personality and affective state. Extending the work of Papez, Dr. Paul MacLean defined the 'visceral brain', comprising the hippocampus, thalamus, basal ganglia, cingulate gyrus, and amygdala. Together, their connections to the hypothalamus and the association areas of the temporal lobe were thought to control the expression of emotion [2]. Maclean referred to this circuitry between the visceral brain and hypothalamus as the limbic system [2, 3]. As a corollary to this idea, the visceral brain directs efferent and afferent signals between the hypothalamus to simultaneously generate the physiological actions of emotion, in agreement with the Cannon-Bard Theory of Emotion [4, 5]. Additional studies by Brown and Schäfer , and Klüver and Bucy, who received the most recognition, demonstrates that uni- or bilateral temporal lobe lesions could alter behavior in rhesus monkeys including hypersexuality, inappropriate emotional responses to novel or salient stimuli, and cognitive deficits [6, 7]. Although these brain regions and their associated

functions have been further characterized, these early studies were the first to identify the involvement of the temporal lobe with the affective behavioral response of emotion.

Lesion Studies of the Medial Temporal Lobe and the Amygdala

Therapeutic brain lesions of the medial temporal lobe provide early insights into the behaviors associated with the amygdala. In 1957, patient H.M. underwent bilateral excision of the medial temporal lobe, removing portions of the hippocampus and amygdala. As a result, patient H.M. presented with partial retrograde amnesia and complete anterograde long-term memory deficits. These observations suggest the medial temporal lobe is critical in memory consolidation [8]. Five additional patients underwent bilateral amygdalotomy, without resultant damage to the surrounding cortical and hippocampal tissue [8]. These patients displayed only minor associative and retrograde memory deficits, and their phenotypic psychosis and aggressive paroxysms were largely eliminated [8]. Bilateral lesions of the amygdala are reported to cause associative memory deficits and poor performance in word and visual association tests [9]. Later investigations of more selective amygdalotomy showed that removal diminished aggressive behaviors without the loss of other neurological functions [10]. Mammalian models have also demonstrated similar results as observed in these patients. Rhesus monkeys with selective lesions targeting the amygdala lost the ability to associate shock with predictive cues [11]. Lesions of the amygdala in rodents produced reduced stress responses, motivation, and associative memory deficits [12, 13]. Together, these reports of medial temporal lesions indicate that the amygdala has a role in processing sensory input and responsive behavioral outputs, including aggression, whereas the hippocampus is more intricately involved in memory [7].

Early Structural and Functional Investigations of the Amygdala

The term amygdala is Greek in origin, denoting an almond-shaped collection of gray matter found in the medial temporal lobe below the uncus and adjacent to the hippocampus of the mammalian brain. While the amygdala was first recognized by Dr. Karl Burdach in 1822 [14], an improved characterization of amygdala function has grown over the last 35 years [15]. J. Johnston pioneered the theory of functionally distinct nuclei within the amygdala based on comparative neuroanatomy [16]. He proposed that the amygdala is subdivided into distinct structures based on their phylogenetic relationship to sensory systems; an old division with striate-like neurons associated with the olfactory system (i.e., the central amygdala) and a new division of nuclei with cortical-like neurons (i.e., the basal and lateral amygdala) [16]. Further studies built upon this theory and discovered a complex neuronal network intertwined with the amygdala. In studies of rhesus monkeys, afferent neurons from the orbitofrontal cortex, insular cortex, cingulate, subcallosal gyri and temporal association areas project to amygdala nuclei, which suggests that multisensory information may converge at the amygdala [17]. Indeed, lesions of afferent fibers projecting to the amygdala can alter motivated and affective behaviors as well as produced alterations in autonomic and endocrine function [18]. Further reports in cats and dogs demonstrated that damage to fibers traversing lesions in subcortical brain structures can degenerate downstream efferent neurons in the amygdala. Overall, afferent neurons bring sensory information to the amygdala for emotional processing then these are transmitted to the peripheral nervous system to initiate a behavioral response. Taken together the amygdala is central within this network to transmit sensory information into action, and damage at either point within the pathway can disrupt sensory processing.

The combinatorial use of electrophysiological and neurohistological fiber tracing has further characterized the interconnectivity of the amygdala efferent network [19-21]. Electrical stimulation of the amygdala initiates monosynaptic and polysynaptic efferent projections to sensory association areas in subcortical nuclei, as well as throughout the neocortex [21]. Microelectrode recordings demonstrated that cerebellar [22] and medullary synaptic contacts [23] also converge at the amygdala to relay multisensory information about the proprioceptive and internal physiological state of the animal. Together, these reports indicate that the amygdala is anatomically and functionally positioned to incorporate multisensory information received from cortical and subcortical brain regions. In addition, the efferent fibers responsible for carrying signals from the amygdala to brainstem effector regions can coordinate the behavioral response to sensory information and coordinate behavioral responses via its efferent brainstem connections. Conservation of the amygdala, its distinct nuclei, and their connectivity suggests that findings in one species can inform our understanding of others. Studies of the amygdala in rodent models has enhanced our understanding of anatomical and functional aspects of the amygdala in human brains. The following sections describe how rodent models have provided key insight and knowledge of the amygdala, its connections, and functions.

Connectivity and Neuroanatomy of the Rodent Amygdala

Neuroanatomy of the Rodent Amygdala Nuclei

Anterograde and retrograde tracing techniques have provided a more detailed understanding of the intra- and inter-connectivity of the rodent amygdala. The colloquial almond structure refers to the basal portion of the amygdala, which comprises the lateral, basal, and basomedial nuclei of the amygdala (LA, BA, and BM, respectively; collectively referred to as BLA) [24]. The BLA complex has the most highly agreed upon

interconnectivity between species; however, many subdivisions have been described for each main division (e.g., ventral, dorsal, and lateral portions). Each subdivision is differentiated by its neuronal microarchitectures and peptide-expressing circuits [25]. The central amygdala (CeA) complex is comprised of ~8 structures, but data acquired with the use of Nissl, Golgi, histochemical, and immunohistochemical staining agree on three major divisions; a striatum-like cap that encases the central amygdala proper; a lateral division of the central amygdala (hereafter referred to as CeL); a ventral pallium-like medial nucleus of the CeA (CeM)(Figure 1, a) [26-28]. Collections of intercalated GABAergic neurons encase the BLA, acting as anatomically and functionally distinct units of the amygdala [29]. These studies lay the groundwork for understanding the flow of information into and out of the amygdala nuclei.

Cell Types of the Amygdala

Numerous morphological and functional investigations of the amygdala identified two neuronal populations; Class I projection neurons expressing vesicular glutamate transporter 1 [30] and Class II local inhibitory GABAergic interneurons [31-34]. Golgi stain indicates that the Class I projection neurons represent the major population of neurons in the human, primate, cat and rodent BLA [32, 35, 36] described morphologically as pyramidal or stellate, each with distinct electrophysiological properties [37]. Pyramidal neurons are characterized by spiny apical and basal dendrites with dense collateral arborizations in the vicinity of the parent soma and prominent AP-firing accommodation [24, 37, 38], whereas the stellate cells have smaller dendritic arbors whose axons pass between amygdala nuclei [37, 38]. Intracellular recordings from BLA Class I neurons suggest a heterogeneity of firing patterns that correlate with characteristically high input resistance and variable membrane time constants. For example, BLA projection neurons can fire an initial burst of APs in response to

depolarizing current injection before spike accommodation, fire near the end of the depolarizing step, or display a bursting pattern [38]. These patterns parallel firing patterns observed elsewhere in the neocortex. Regardless of the firing pattern, accommodation of action potential firing is mediated by a prolonged afterhyperpolarization potential (AHP) [38], likely due to differences in the density and distribution of calcium-activated potassium channels [39].

Local interneurons neurons are a minor population representing around 20% of the neurons found within the BLA and are the primary neuronal type of the CeA. These Class II neurons have highly variable electrophysiological and functional properties [34, 40], presenting with or without action potential (AP)-firing accommodation, medium to short duration AHPs, and can be further characterized by their AP firing patterns [33, 41, 42]. Like interneurons in the hippocampus and striatal regions, amygdala GABAergic neurons possess dense dendritic webs to provide both feedforward and feedback inhibition both locally between interneurons and on projection neurons [43-49]. Amygdala interneurons express GAD67/65 [33] and can be further grouped according to their expression of calcium-binding proteins and neuropeptide expression [33, 50]. Specific neuropeptide expressing interneuron circuits include, but are not limited to, parvalbumin (PV+), somatostatin (SOM+), cholecystokinin, calbindin, and calretinin expressing circuits [33]. These interneurons robustly regulate the activity of neuronal activity during synaptic plasticity and fear learning [51, 52] and dysregulation of the excitatory-inhibitory balance in the amygdala is a hallmark of numerous pathologies [53].

Intercalated cells (ITCs) are GABAergic neurons encircling the BLA and CeA that develop from the dorsolateral ganglionic eminence, unlike the GABAergic interneurons of the BLA and CeA arising from the medial ganglionic eminence and ventrolateral ganglionic eminence, respectively [54]. The majority of ITCs are medium spiny neurons although larger ITCs with aspiny dendritic processes have been reported [29]. ITCs have

a large input resistance (520-860 mΩ) and small capacitance (25-70 pF) correlating to their small size, hyperpolarized resting membrane potentials (-76 ~ - 90 mV), and prominent AHPs [55]. These clusters of neurons are theorized to provide feedforward inhibition to normalize amygdala output in response to varying levels of excitatory input, increasing the signal to noise ratio [56]. ITCs possess a slowly de-inactivating K⁺ channel that is inactivated by cell firing but slowly de-inactivates producing after-depolarization in response to excitatory inputs [57]. Thus, these K⁺ channels allow for a self-renewing excitability in the ITCs increasing the feedforward inhibition and narrowing the output from downstream targets. Continued investigations into ITCs are underway to clarify their role in amygdala function and emotional processing.

Connectivity of the Amygdala

Broadly speaking, the generalized view of information transfer through the amygdala is as follows: the LA is the main entry point into the amygdala receiving sensory input, whereas the CeM is the output nucleus of the amygdala that sends projections to behavioral effector regions [58]. The principal neurons in the LA make glutamatergic synapses onto glutamatergic neurons in the BLA and GABAergic neurons in the medial ITCs [59] as well as the CeL. The BLA then sends glutamatergic projections to the CeL, the CeM [60-62] and the ITCs which further innervate CeA neurons [63]. The CeL and CeM also receive GABAergic afferents from other structures [64] and contain local GABAergic interneurons to inhibit each other via axon collaterals [65] and GABAergic projection neurons to relay information out of the amygdala [66, 67]. The CeL projects to the CeM, with no reciprocal projection from the CeM to the CeL [68]. The CeM is the major output nucleus of the amygdala and projects to the structures involved in emotional [68-70] and autonomic control [71-74], although the CeL sends GABAergic projections to behavioral and physiologic effector regions as well [75].

The amygdala is a site of sensory synaptic integration from the thalamic and sensory cortices. Injection of an anterograde tracer (*Phaseolus vulgaris*) into specific regions of the prefrontal cortex (PFC) revealed that deep layer projection neurons topographically innervate the amygdala [76]. Quantitatively, approximately 12% of the prelimbic projection neurons, 21% of the infralimbic neurons, and 10% of the projection neurons from the cingulate cortex send efferent projections to the BLA with increasing density at more distal sites [77, 78], indicating that the sensory cortices send projections about cognitive and polysensory information as well as aspects of reward associations directly to the amygdala. A neuroanatomic comparison of amphibian and mammalian cortico-amygdala interconnectivity supports the phylogenetic conservation of sensory and motor projections, whereas the ontogenetic divergence of the sensory association area in rats may represent mammalian specific circuits, for example suckling behavior and lactation [28]. In support of this developmental evolution of the amygdala, olfactory and gustatory information reaches the amygdala at earlier stages of cortical processing compared to visual, auditory, and somatosensory information which relay first at the level of the thalamus, where modality-specific projections then selectively innervate amygdala nuclei [28, 79, 80]. For example, projects from posterior thalamic nuclei strongly label afferents in the LA and CeL, whereas central medial thalamic projections densely labeled terminals in the BLA and not the CeA [80]. Injection into the medial geniculate nucleus, the principal thalamic relay station of auditory information between the auditory cortex and inferior colliculus, labeled axons that traveled through the thalamic peduncle with terminals found in the BLA and ITCs, with minor localization in the nuclei of CeA [80]. Initial reports of direct projections carrying visual stimuli information to the amygdala were thought to be scarce likely due to the convergence of olfactory and visual tracts [80], whereas other findings indicated visual projections of the posterior allocortex or retinal ganglia indirectly reach the LA or CeA [28, 81]. Subsequent

work employing more sensitive tract tracing dyes suggested that thalamic visual nuclei (i.e. lateral posterior and posterior limitans nuclei) target the anterior LA as well as posterior BLA [82]. The findings that lesions to visual cortex in rats did not eliminate visually conditioned fear expression provide evidence of direct visuo-thalamic projections to the amygdala [82].

Following the convergence and integration of sensory input at the amygdala, the amygdala sends projections to behavioral and physiologic effector regions. Typically, BLA and CeA send projections to different brain regions [83]. The majority of projections to the brainstem nuclei generating behavioral output originate from the CeA, whereas BLA projections typically terminate in the striatum, thalamus, and cerebral cortex [84]. CeA contributes projections involved in autonomic adaptation via projections to the solitary tract nucleus [85] as well as receives information on sympathetic activity and respiratory responses [86]. CeM efferents for somatosensory information (i.e., pain, itch), reward and ingestive behaviors, as well as signals for hypervigilance reach distinct brain regions, including periaqueductal grey, parabrachial nucleus, and substantia nigra [87-91]. Additional amygdala outputs target various hypothalamic nuclei and may regulate the excitability of the entire forebrain through projections to other neuromodulatory cell groups in the forebrain and brainstem (i.e. acetylcholine, noradrenaline, dopamine, and serotonin) [58], though direct projections from the BLA to brainstem nuclei have not yet been fully characterized. It is most likely that sensory information integrated within the BLA projects first to the CeA before reaching brainstem nuclei [92, 93]. However, brainstem monoaminergic afferents from the solitary tract, locus coeruleus, periaqueductal grey area robustly innervate the BLA to modulate its output to the CeA [94-96]. The cortico-amygdala and thalamo-amygdala pathways together with bidirectional synaptic contacts from the brainstem center the amygdala as important

brain structure in processing sensory information to coordinate appropriate responsive behaviors.

Amygdala and Hippocampal Connections

Temporal lobe lesions targeting the amygdala and hippocampus generated deficits in emotional processing and memory, suggesting a functional interaction between the amygdala and hippocampus [6-8]. The hippocampal formation includes the dentate gyrus, areas CA1, CA2, and CA3 (CA4 in humans), and the subiculum as well as the entorhinal and perirhinal cortex in the adjacent parahippocampal area. Together, these areas are responsible for integrating highly processed sensory information from all modalities into complex representations of context (i.e., memory). Information processing within the hippocampus proceeds through a well characterized series of connections known as the tri-synaptic circuit. Briefly, excitatory connections from the entorhinal cortex to the dentate gyrus relay cortical information to the hippocampus. Information is then transmitted via the mossy fibers from the dentate gyrus to CA3. The Schaffer collateral pathway connects CA3 to CA1, which then has projections out of the hippocampus to the septum, hypothalamus and contralateral hippocampus [97]. The structures of this circuit are critical for memory formation and constitute the medial temporal lobe memory system. Together with its interconnectivity between the amygdala, this circuit is important for emotional memory.

The subiculum, entorhinal and perirhinal cortex robustly innervate the amygdala [78]. Subicular projections targeting the BLA form excitatory synapses on pyramidal neurons but may also contact dendritic branches of inhibitory interneurons to provide feedforward inhibitory signaling [98]. These projections directly or indirectly with projections from the prelimbic cortex convey contextual cues mediating fear extinction [99]. Parahippocampal projections targeting the BLA arise mainly from the entorhinal

cortex providing excitatory input onto the spines and dendritic shafts of projection neurons [100], whereas projections originating from the perirhinal cortex differential target populations of BLA interneurons. Efferents of the BLA and CeA reciprocally innervate these hippocampal structures as well as target the temporal regions of CA2 and CA3 [25]. The ventral hippocampal structures receive excitatory contact from all regions of the BLA thought to convey behaviorally relevant information [101, 102]. LA and BLA projections target parahippocampal structures providing excitatory inputs on dendritic spines of principal neurons and their dendritic arbors [67]. The large populations of interconnected neurons between the BLA and hippocampus have synchronized rhythmic firing (i.e., oscillations) that reflect brain states [69]. Disruption of these oscillatory patterns produces behavioral deficits in fear and stress responses and spatial navigation, indicating that these are important for emotional memory [69, 103].

Pathophysiology of the Amygdala

Amygdala dysfunction is implicated in various pathophysiological conditions. The amygdala is implicated in neurodevelopmental disorders, such as Autism Spectrum Disorder [104, 105], and neuropsychiatric disorders, such as anxiety [106, 107], depression [108, 109], and schizophrenia [110, 111]. However, a detailed discussion of all these disorders is beyond the scope of this dissertation. Instead, this section provides a more detailed examination of fear and anxiety-related disorders, with an emphasis on the contributions of the amygdala.

Fear vs. Anxiety

Fear is an emotional response of increased arousal to a specific stimulus and produces internal states of increased vigilance to perceived threats [112]. Fear serves as a protective function to enable an animal to perceive potential threats from their environment and prepare appropriate behavioral responses [113, 114]. This internal

state, or the physiological fear response, leads to abrupt changes in behavior that include active or passive coping strategies used to palliate the physiological fear response. These active coping strategies result in sympathetic activation and a fight-or-flight response, activating the hypothalamic-pituitary axis to release neuroendocrine hormones, resulting in an increase in glucocorticoids and cardiovascular output [115]. Escape is the goal during active coping states, whereas passive coping strategies perceive escape as unlikely. Passive coping strategies are observed in rodent models as immobility or freezing behavior, which acts as measurable endpoints for quantifying the fear response.

Fear conditioning paradigms are effective tools for understanding the neural basis of fear responses. In fear conditioning, a neutral conditioned stimulus (i.e., a light or tone) is paired with an emotionally salient stimulus, (i.e., aversive electric shock) during the conditioning phase to form a learned association of these stimuli. This acquisition of a fear response is then assessed by measuring the conditioned responses, ranging from a startle, or a complete lack of movement, produced by the conditioned stimuli without the unconditioned aversive stimuli. This paradigm models real-life experiences, where threatening stimuli experienced with harm, stress, or pain are learned to prepare the animal for future situations.

Like fear, anxiety is an innate emotional response to threatening stimuli and produces internal states of increased vigilance encompassing physiological, affective and cognitive changes [116], however; unlike fear, anxiety is an internal state in response to non-specific stimuli from the environment. Mild anxiety is believed to increase performance, but chronic or severe levels of anxiety will lead to anxiety-related behaviors and disorders. Behavioral paradigms used to measure anxiety-like behaviors in rodents include, but are not limited to, the elevated plus maze, light-dark box, open-field, and conflict tests. The first three paradigms measure anxiety by quantifying the

amount of time a rodent spends in an 'anxious' or vulnerable location, including the open arms of the plus-shaped maze, center of an open box vs. near the walls, and illuminated vs. dark chambers. The conflict tests differ in that the animal is presented with a choice between a physiological drive (i.e., water, food) and safety. These paradigms do not present a specific threat per se, but rodents must perceive their environment and decide between their innate drive to explore or pursue safety. Optimizing behavioral paradigms for rodent models has advanced our understanding of learning memory, and anxiety. Furthermore, manipulating the neurological pathways involved in fear- and anxiety-driven responses will reveal the components that prevail in fear- and anxiety-like behaviors.

Anxiety and Depression

The neuropsychiatric disorders of anxiety and depression present with a spectrum of symptoms that are characterized by negative emotional states. The primary symptoms and comorbidities of depression include, but are not limited to, social withdrawal, sadness, apathy, problems with memory or attention, and thoughts of suicide [117]. The Diagnostic and Statistical Manual of Mental Disorders, Fifth Edition, Text Revision (DSM-5TR) recognizes several forms of depression with major depressive disorder being the most prevalent affecting an estimated 20% of people during their lifetime [118, 119]. Likewise, symptoms of anxiety and anxiety-related disorders include persistent and excessive worry, irritability, insomnia, weight loss, and difficulty concentrating. The DSM-5TR recognizes several distinct anxiety-related disorders based on symptoms and comorbidities, including post-traumatic stress disorder (PTSD), agoraphobia, and social anxiety disorder. The prevalence of anxiety disorders in the general population varies, but the lifetime prevalence of any anxiety disorder is estimated to be around 15-20%, with higher rates of anxiety among women [120].

Anxiety and depression can arise from the interplay of psychological, genetic, epigenetic, and social factors, with an estimated 50% comorbidity rate of major depressive disorder and some forms of anxiety [121], whereas chronic stress is likely the most important risk factor [108, 122]. Chronic stress can produce structural and functional alterations in brain regions involved in discriminating positively and negatively valenced stimuli [123]. As the involvement of the limbic system in emotion regulation is well established [93, 124], there has been continued interest in the role of the amygdala in anxiety and depression.

The amygdala is an essential brain structure in the circuit of anxiety. Patients with bilateral loss of the amygdala struggle to assess fear in face expression paradigms and have diminished startle responses to threatening simulations [125-127]. Conscious awareness is a significant aspect of fear responses in humans and is related to the level of activation in the PFC, a brain region involved in higher cognitive functions such as attention and the regulation of subcortical systems [128]. As such, higher self-reported anxiety levels in both children and adults are associated with increases in gray matter volume of the amygdala [129, 130]. In patients with PTSD, fMRI-imaging studies have shown exaggerated amygdala activation in response to fearful faces and a simultaneous decrease in PFC activity [131]. However, this exaggerated amygdala activation was not observed in patients with social phobia [132]. As the amygdala regulates multiple components of sensory association [127], the different amygdala activation found in anxious patients may represent failures in amygdala habituation or sensitization to salient stimuli [133]. Collectively, these findings support a role for amygdala activity in depression and anxiety disorders.

Fear conditioning paradigms have revealed specific circuits of the amygdala mediate environmental processing and process the cued associations during fear responses [93, 134]. Exposure to anxiogenic contexts, including open spaces, predatory

odors, or aversive shocks, drives activity-dependent immediate-early gene expression, markers of neuronal activation, in the BLA and CeA [135]. In contrast, disruption of function in the BLA or CeA diminishes fear or anxiety-like behaviors in rats and mice [123, 136]. Single-unit recordings of BLA or CeA neurons demonstrated that single-unit activity of these neurons increases in response to conditioned, both positively and negatively valenced, stimuli and silencing of these neurons during acquisition results in deficits in behavioral output [96, 137, 138]. Indeed, diverse populations of BLA neurons are reciprocally active during exploratory or defensive behaviors such that neurons active in exploration are only active when defensive neurons are inactive [139]. Likewise, improved fluorescent labeling has identified two distinct cell types within the CeL that regulate anxiety---CeL_{ON} neurons which are rapidly activated by the conditioned stimuli and CeL_{OFF} neurons which are inhibited by the conditioned stimuli and express PKC δ [140, 141]. Both CeL_{ON} and CeL_{OFF} neurons send projections to CeM neurons and function through an inhibitory loop within the CeL [140, 141]. These findings indicate that fear- and anxiety-like behaviors occur by activation of CeL_{ON} neurons, and simultaneous downregulation of CeL_{OFF} inhibitory projections to CeM neurons. Additionally, a SOM⁺-expressing subset of GABAergic neurons, largely non-overlapping with PKC δ -expressing CeL_{OFF} neurons, receive excitatory inputs from LA projection neurons, producing experience-dependent alteration in synaptic strength to promote anxiety-like behaviors [142]. Anxiety and depression are associated with widespread changes in the excitability of amygdala neurons and these studies suggest anxiety/depression likely involve distributed and cell-type specific alterations in the excitatory-inhibitory balance within the amygdala as well as interconnected structures [139]. Moreover, an improved understanding in the stress-induced alterations in the neuronal ensembles stemming from the amygdala will highlight how animals cope and subsequently, succumb to anxiety and/or depression.

Specific circuits within the amygdala are believed to regulate anxiety-like behaviors in rodents. Recent advances in tract tracing techniques enable manipulation of specific circuits within the amygdala and identification of synaptic targets during anxiety-related behaviors. Optogenetic activation of glutamatergic neurons in the BLA produces anxiogenic behaviors; however, selective photoactivation of BLA-CeL terminals reduces the behavioral expression of anxiety in mice [143]. BLA neurons labeled with activity-dependent fluorescent tags increased projections to the PFC and hippocampus after fear conditioning [144], suggesting temporal plasticity within these circuits. Whereas PFC-BLA fluorescent intensity increases during specific stimulus extinction, there is a strengthening of synaptic contact between the BLA and ventral hippocampus in context-dependent paradigms and silencing these projections attenuates anxiety-like behavior [102]. These indicate that specific and non-specific negatively valenced stimuli differentially recruit efferent amygdala projections. Similarly, afferent projections to the amygdala may contribute more strongly to phenotypes of one disorder than the other. Projections from the solitary tract and locus coeruleus differentially contribute to positive memory formation in the BLA [96], whereas ventral tegmental projections to the amygdala are required for anxiety-like phenotypes in mice, but not depressive-like phenotypes [145]. These studies highlight the complexity in circuitry and distinct cell types within the amygdala that contribute to anxiety-related disorders and emphasize the shortcomings in current therapeutic options for these disorders.

Therapeutic Strategies

The neurological causes of anxiety and depression are not fully understood. An initial hypothesis proposed these disorders arise from a decreased function of certain monoaminergic neurotransmitters, including norepinephrine (NE), 5-hydroxytryptophan (5-HT or serotonin), and dopamine (DA). This theory was supported by clinical and

animal studies that used reserpine, a drug used to treat hypertension that results in symptoms associated with depression [146]. However, the monoamine hypothesis has some limitations. For example, quantification of NE, 5-HT, or the levels of their metabolites in post-mortem tissue, cerebrospinal fluid, or urine are largely inconsistent [147-149]. Likewise, the activity levels of the rate-limiting enzymes for DA and NE synthesis, as well as the activity of the catabolic enzyme monoamine oxidase, cannot explain changes in DA or NE neurotransmission [148]. Selective depletion of NE or 5-HT does not produce anxiety or depression-like symptoms in healthy controls, but can exacerbates symptoms in patients with major depressive disorder [150]. These observations suggest that these disorders are likely not caused by problems with a single neurotransmitter system, but rather suggest these disorders result from dysfunction of multiple interconnective pathways across different regions of the brain including the cortex, subcortex, and limbic regions, as well as associated neurotransmitter systems [151]. In the context of limbic-cortical system dysfunction, current pharmacological approaches used to treat anxiety and depression aim to bring about adaptive chemical and molecular changes to re-establish a normal mood state [122].

Treatments for anxiety and depression focus on the manipulation of monoamines, specifically 5-HT, DA, NE, and to a lesser extent, GABAergic transmission. Medications, including selective serotonin reuptake inhibitors (SSRIs), selective norepinephrine reuptake inhibitors (SNRIs), and tricyclic antidepressants target transport proteins that regulate the availability of monoamines in the synaptic cleft, reducing the effects of the neurotransmitter at pre- and post-synaptic sites. In contrast, benzodiazepines are positive allosteric modulators of GABAergic transmission [152, 153]. SSRIs and SNRI are potent neuromodulators of amygdala activity. The midbrain raphe nucleus, which is responsible for releasing serotonin into the BLA neurons in response to aversive stimuli

[154], innervates the amygdala [155] and is implicated in anxiety and fear learning [156, 157]. SSRI treatment also modulates neuronal function within the amygdala, depending on the duration of treatment and method of administration in both humans and rodents. In non-depressed patients, acute intravenous citalopram produces a dose-dependent increase in bilateral amygdala activation in response to fearful faces [158], but acute oral administration does not cause amygdala activation in response to a similar facial recognition paradigm [159]. In patients with major depressive disorder, fMRI-imaging revealed significantly higher amygdala activation in response to fearful faces compared to healthy controls, but this difference normalized after 7 days of oral citalopram treatment [160]. The dichotomous relationship between the acute and chronic application of SSRIs in humans has been mirrored by studies conducted in rodents. In rats, acute systemic administration of the SSRI citalopram produces marked increases in 5-HT release in the CeA, which can augment the acquisition of fear memory [161, 162], whereas chronic administration of citalopram induces a reduction in time spent frozen after fear conditioning, indicating an anxiolytic effect [162]. Although a conclusive answer to the delay in SSRI therapeutic action is yet to be determined, SSRI application produces systemic adaptive changes to serotonergic transmission and may also produce alterations in structural rearrangement and synaptic plasticity within the amygdala [163, 164], unfortunately a large number of patients see minimal to no therapeutic benefit from these treatments.

Benzodiazepines are a class of anxiolytic drugs commonly used to treat anxiety. While these drugs can be effective in treating anxiety, benzodiazepines are often used acutely as second-line or adjunct therapy prior to the onset of SSRI/SNRI because of their potential for tolerance and abuse [165]. They function by enhancing fast GABAergic inhibitory signaling within the brain by binding to GABA_A complexes. GABA_A complexes are pentameric chloride channels built from heteropentameric combinations of α -, β -, γ -

δ -, ϵ -, θ -, π -, and ρ -subunits, which contribute to unique electrical and pharmacological properties [166]. The most prevalent form of GABA_A complex within the amygdala is composed of two α -subunits, two β -subunits, and one γ -subunit. The mechanism by which benzodiazepines treat anxiety stems from their interaction with a binding pocket located between the α - and γ -subunits [166]. The γ_2 subunit, which is robustly expressed in the nuclei of the amygdala in humans [167] and rats [168], plays an important role in anxiety and its etiology. A mutant mouse model with a 35% reduction in the γ_2 -subunit displayed increased anxiety-like behaviors in the elevated plus maze and light-dark box, without any changes in the sedative effects of diazepam or ethanol [169]. However, selective ablation of the γ_2 -subunit in SOM-expressing neurons produced a disinhibitory effect, increasing the inhibitory signaling on principal neurons promoting anxiolysis [170]. The α_{1-3} -subunits may also play different roles in the anxiolytic action of benzodiazepines, with the α_2 -subunit suggested to induce anxiolysis, the α_1 -subunit contributing to sedation, and the role of the α_3 -subunits having a controversial role in both phenomena [171]. Functionally, diazepam increases the frequency of IPSC events in the BLA and CeA via GABA_A complexes containing α_1 - and α_2 -subunits [172]. In the CeA, another α -subunit, the α_5 -subunit, is expressed at low levels [168] and selective ablation of α_5 -containing GABA_A complexes in CeL_{OFF} neurons promotes fear generalization and anxiety-like behaviors [173]. Collectively, these studies suggest that a deeper understanding of the specific neural circuits involved is necessary to achieve targeted anxiolytic effects.

Neuropeptides and the Amygdala

Neuropeptides (NPs) are a diverse group of neuromodulators that control a variety of innate behaviors including pain, reward, reproduction, and stress responses [174-176] making neuropeptidergic systems a promising target for the development of effective

therapeutics [175, 177]. This section will provide a basic introduction of the current understanding of neuropeptides as well as discuss the clinical findings of neuropeptide therapy. A specific discussion of the neuropeptides studied in this dissertation are included as an introduction to each study.

Neuropeptides as Neuromodulatory Molecules

NPs share many mechanistic similarities to amino acid neurotransmitters. NPs can exert their direct biological effect on target cells in seconds to minutes or generate prolonged indirect effects via gene regulatory mechanisms on the time scale of hours to days. Like amino acid neurotransmitters, NP release is highly regulated within the presynaptic site, but NPs are also released from non-synaptic sites, for example from preganglionic axons [178], while still targeting postsynaptic neuronal targets. The non-synaptic release of NPs along with their theorized long extracellular half-life may explain reports of *volume transmission* whereby these neuromodulators signal at long distances within the brain [179, 180]. Indeed, the NP synthesizing cell and the cognate receptor are not always anatomically expressed in the same brain region. However, it is likely that most neurons express some NPs in addition to their fast amino acid transmitters and NP release occurs over short distance (e.g., micron) to act at local targets [181]. Furthermore, endogenous peptidases non-selectively break down NPs modifying their bioactive duration and dispersion, depending on the modulators intrinsic chemical composition, supporting the hypothesis that NPs exert local effects [182].

Mechanisms of Neuropeptide Release

Neurotransmitter and NP secretion is regulated by separate organellar vesicles-- clear synaptic vesicles and dense core vesicles (DCVs), respectively. Synaptic vesicles preferentially reside within active zones in association with presynaptic specializations, whereas DCVs localize within release sites more distally from the active zone [181],

likely requiring unique proteins for secretion [183]. It is appreciated that Ca^{2+} is a critical ion in both synaptic vesicle and DCV exocytosis. NP release is positively correlated with action potential spike frequency from axons and dendrites [184, 185], theorized to result from a rise in cytoplasmic Ca^{2+} that increases the probability of DCV release [186]. Furthermore, Ca^{2+} release from intracellular stores mediated by NP receptor activation or pharmacologically can augment DCV release independent of APs [187, 188]. Following release, clear vesicles are rapidly repackaged with amino acid neurotransmitters via transport proteins, whereas DCV refilling is a significantly slower process. DCVs must be resynthesized in the Golgi apparatus of the cell body. Neuropeptides are resynthesized in rough endoplasmic reticulum, and the reloaded DCVs must then be transported to the site of release [189]. There is significant variability in DCV size and likely NP content [189]. For example, estimates of oxytocin and vasopressin in large neurosecretory vesicles at neurohypophyseal boutons may contain between 60,000 and 90,000 molecules of these NPs with peptide content correlating with vesicle size [190]. Upon release, the actions of NP can directly modify neuronal excitability and neurotransmitter release, as well as directly or indirectly effect ion channel activity.

Most NPs generate their physiological effects by interacting with G-protein coupled receptors (GPCRs). Upon binding, GPCRs undergo conformational changes, which initiate intracellular signal cascades. In their resting state, G proteins exist as a heterotrimeric complex of $G\alpha$, $G\beta$, and $G\gamma$ subunits bound to GDP. The exchange of GDP for GTP activates the complex leading the dissociation of the $G\alpha$ subunit from the $G\beta$ and $G\gamma$ subunits. The activated monomeric or dimeric G proteins can interact directly or indirectly with various ion channels, leading to modulations in neuronal activity [191-193]. Moreover, modulation of the neuropeptide signal can occur at the level of the

receptor, as G protein-modulators alter the kinetics of G proteins and their downstream effectors [194]. NP signaling is further amplified via the activation of various intracellular signaling pathways that may include phospholipase C β , adenylyl cyclase, and many other downstream phosphorylated targets. Unlike classic neurotransmitter systems, NPs and their receptor are often discretely expressed. Therefore, the signaling pathways activated by peptidergic systems represent unique therapeutic targets.

Neuropeptides as Therapeutics

The large repository of preclinical data in rodent models had implicated corticotrophin-releasing hormone (CRH in humans, Corticotrophin-releasing Factor, CRF in rodents) as a promising therapeutic target in fear-related and anxiety disorders. CRF is released in response to stress from the parvocellular neurons in the hypothalamus to activate the HPA, and glucocorticoids from the adrenal glands [195]. CRF generates its physiological effect by activating CRF1 and CRF 2 receptors that signal through cAMP-PKA-mediated signaling pathways, though often these receptors generate opposing actions [196, 197]. High expression of CRF is observed in the amygdala and bed nucleus of the stria terminalis (BNST), and CRF is involved in regulating synaptic function [198]. Indeed, CRH is elevated in the cerebrospinal fluid of veterans with PTSD and the levels positively correlate with active psychosis [199, 200]. Unfortunately, no selective CRF1 receptor antagonist has passed the safety and efficacy standards in Phase III clinical trials for anxiety-like psychiatric disorders. The selective CRF-1 antagonist pexacerfont failed to prove more efficacious than the placebo-treated group, with a lower response rate than escitalopram in a cohort of patients with generalized anxiety disorder [201]. Another CRF1 antagonist, verucerfont, has shown limited clinical utility as trials only included female subjects due to a reversible testicular toxicity [202]. In another verucerfont clinical trial interested in anxiety and alcohol use in woman,

verucerfont reduced CRH levels and decreased right amygdala activation in response to fearful faces but did not reduce self-reported alcohol cravings [203]. In addition, a large number of participants in the verucerfont group discontinued the study owing to adverse side effects [203]. Another CRF1 antagonist, GSK561679, augmented the startle response to predictable threats but had no significant responses to unpredictable threats, indicating that GSK561679 increased fear responses while failing to reduce anxiety-like responses [204]. Clinical trials are currently ongoing; however, positive clinical data are still lacking. For a comprehensive review of the potential pitfalls in CRF1 antagonist clinical trials see [205].

Neuropeptide Y (NPY) is known for its role in orexigenic and anxiolytic functions through activation of five NPY receptor subtypes that are expressed throughout the brain with high expression found in the hippocampus, amygdala, and brainstem [206]. The involvement of NPY in the behavioral effects of stress are supported in human clinical trials with PTSD. In healthy male subjects, inhibition of the α_2 -adrenergic receptor with yohimbine results in an elevated plasma levels of NPY [207]. In a follow-up study of combat veterans with PTSD, baseline plasma levels of NPY were significantly lower than those in healthy control subjects [208]. Moreover, yohimbine treatment in this cohort of patients with PTSD resulted in a blunted increase in plasma NPY levels. These diminutive levels of NPY are observed in the cerebral spinal fluid (CSF) of combat-related PTSD [209]. Thus, NPY may be involved in resilience and promote adaptive coping mechanisms. However, the contributions of either peripheral or central NPY to the regulation of PTSD symptoms remain unclear. Clinical trials continue to investigate the utility of intranasal NPY, with unreported results. As such, these approaches and continued understanding of the NPY system are promising areas for future research to identify novel therapeutic targets for stress-related psychiatric disorders.

Since its discovery in the 1930s, significant research has been aimed at understanding the role of the neurokinin system in mood and anxiety. Early clinical experiments with an NK1R antagonist, MK-869 (aprepitant), suggests a novel and efficacious reduction from baseline values on the Hamilton Depression Scale and Hamilton Anxiety Scale [210]. MK-869 has good brain penetrance, oral bioavailability, and pharmacokinetic data, suggesting a >90 % blockade of the NK1 receptor, but the antidepressant effect of MK-869 was similar to that of paroxetine [210]. Similar results seen in MK-869 trial were obtained in trials with three other NK1 receptor antagonists: L-759274 [211], CP-122721[212], and casopitant[213]. However, further clinical trials of MK-869 found the drug inactive, and the results of a Phase IIa trial of casopitant were inconclusive [214]. Development of the NK1 receptor antagonist orvepitant by GlaxoSmithKline was also halted due to the occurrence of isolated seizures in Phase IIb trials. The subsequent development and clinical investigation of the NK2 receptor antagonist saredutant and the NK3 receptor antagonists osanetant and talnetant also yielded inconclusive results in the treatment of neuropsychiatric disorders [214].

Although discouraging, there are several potential solutions to improve our understanding and potential development of neuropeptide agents available to target psychiatric disorders. Neuropeptides define neuronal ensembles, and a continued characterization of these circuits is critical to understand the brain connectome in homeostatic and pathogenic states. Numerous reports indicate neuropeptides play highly specialized role(s) in the expression of stress responses [175, 206, 215]. Improved technologies in targeting and temporally controlling these circuits has already begun to clarify specific contributions to peptidergic system in fear responses and learning. Moreover, highlighting select dysfunction within neuropeptide ensembles as they contribute to symptomology and the discrete phenotypes observed in neuropsychiatric disorders, will highlight novel druggable targets. Neuropeptide system

may also improve the accuracy in diagnosis of neuropsychiatric disorders. As stated above, the concentration of numerous neuropeptides is affected by chronic stress and may have prognostic potential in clinical settings. Currently, the use of animal models has allowed researchers to generate representative states of disease, but continued improvement in animal models of neuropsychiatric disorders is required. The contribution of neuropeptide systems to these disorders and within these models can then be manipulated for development of more effective therapeutic interventions.

Dissertation Research Objective

The focus of our lab is to better understand the role of neuropeptides as neuromodulatory molecules within the amygdala. The amygdala is an anatomically and functionally distinct region, possessing glutamatergic or GABAergic neurons. Our attention is primarily focused on how neuromodulatory peptides affect these neurons as their activity ultimately affects amygdala function. Moreover, the amygdala receives and sends projections to numerous effector regions that ultimately modulate amygdala function. The objective of this dissertation is to further our understanding of the neuromodulatory mechanisms within the nuclei of the amygdala. The dissertation is divided into three studies that will address the following questions:

1. How does neuromedin B modulate neuronal function in the CeA?
2. Does neuromedin B modulate neuronal function in the BLA?
3. How does neurokinin B modulate BLA neurons?

CHAPTER 2

METHODS

Preparation of Amygdala Slices

All procedures and experiments involving animals presented herein were approved by the Institutional Animal Use and Care Committee (IACUC) of the University of North Dakota and performed in accordance with the Guide for the Care and Use of Laboratory Animals published by the National Institutes of Health, USA. For all studies, 300 μm coronal brain slices were prepared from virgin male and female Sprague-Dawley (SD) rats. In Study 1 and 2, slices were prepared from 22- to 38-day-old SD rats, whereas in Study 3 SD rats were 30- to 45-day old rats (purchased from Envigo RMS, INC., Indianapolis, IN). We did not notice any age-specific differences in the excitabilities of the neurons in these studies. For Study 2 and Study 3, the following three strains of KO mice (1–2 months old) and their corresponding age-matched WT mice purchased from Jackson Laboratory were used: TRPV1 KO mice (B6.129 \times 1-*Trpv1*^{tm1Jul}/J, strain 003770) vs. WT mice (C57BL/6J, strain 000664); TRPC4 KO mice (129S1/SvImJ-*Trpc4*^{tm1.1clph}/J, strain 030802) vs. WT mice (129S1/SvImJ, strain 002448); TRPC5 KO mice (129S1/SvImJ-*Trpc5*^{tm1.1clph}/J, strain 030804) vs. WT mice (129S1/SvImJ, strain 002448). The animals were housed in the Center for Biomedical Research at the University of North Dakota with food and water available *ad libitum*. The animal rooms were maintained on a 14/10 h light–dark cycle (lights on at 7:00 a.m.), with a room temperature of 22°C. After being deeply anaesthetized with isoflurane, animals

were transcardially perfused with an extracellular solution that contained (in mM) 130 NaCl, 24 NaHCO₃, 3.5 KCl, 1.25 NaH₂PO₄, 2.5 CaCl₂, 1.5 MgCl, and 10 glucose saturated with 95% O₂ and 5% CO₂, decapitated, and their brains were dissected out. The cerebellum was trimmed and the caudal pole of the brain was glued to the plate of a vibratome (Leica VT1200S) and then bathed in an ice-cold cutting solution. In Study 1, the cutting solution contained (in mM) 130 N-methyl-D-glucamine (NMDG)-Cl, 24 NaCO₃, 3.5 KCl, 1.25 NaH₂PO₄, 0.5 CaCl₂, 8.0 MgCl₂, and 10 glucose, saturated with 95% O₂ and 5% CO₂ (pH 7.4, adjusted with HCl). The cutting solution was modified slightly for Study 2 and 3 to contain (in mM) 250 sucrose, 104 NaCl, 19.2 NaHCO₃, 2.8 KCl, 1 NaH₂PO₄, 2 CaCl₂, 2.4 MgCl₂ and 8 glucose (saturated with 95% O₂ and 5% CO₂). Various protective cutting solutions are commonly use that are NMDG- or sucrose-based, but work in the amygdala has indicated no differences in intrinsic excitability [216]. Cuts began at the rostral pole and slices were collected from both hemispheres when the structure of the amygdala was apparent. Slices were incubated at 35°C for 1 h in the extracellular solution particular to the cutting solution of each study and kept at room temperature (22° C) until use. When an NMDG cutting solution was used, slices were incubated in the cutting solution except the NMDG-Cl was replaced with the same concentration of NaCl. For slices prepared in the sucrose cutting solution, slices were incubated at 35°C for 30 min in the extracellular solution containing (mM) 60 sucrose, 124 NaCl, 23 NaHCO₃, 3.3 KCl, 1.2 NaH₂PO₄, 2.4 CaCl₂, 1.7 MgCl₂ and 9.5 glucose (saturated with 95% O₂ and 5% CO₂) and then kept at room temperature until use.

Electrophysiology

Whole-cell patch-clamp recordings were made using a Multiclamp 700B amplifier (Molecular Devices, Sunnyvale, CA) and signals were digitized using an Axon 1550 Digidata System (Axon Instruments). Recordings in current- or voltage-clamp mode

were conducted from CeL (Study 1) and BLA (Study 2 & 3) neurons visually identified with infrared video microscopy (Olympus BX51WI) and differential interference contrast optics. Slices were continuously superfused with an extracellular solution that contained (in mM) 130 NaCl, 24 NaHCO₃, 3.5 KCl, 1.25 NaH₂PO₄, 2.5 CaCl₂, 1.5 MgCl₂ and 10 glucose, saturated with 95% O₂ and 5% CO₂ (pH 7.4) via a gravity-driven perfusion system (~1 mL/min). In experiments where extracellular Ca²⁺ was reduced, equimolar MgCl₂ was used to substitute the extracellular CaCl₂. In Study 2 and 3, the bath was maintained between 33°C and 34°C by an in-line heater and an automatic temperature controller (TC-324C, Warner Instruments). Patch recording electrodes with a tip resistance of 4-10 MΩ were pulled with a PP-830 gravity puller (Narishge, Tokyo, Japan). Upon the establishment of the whole-cell configuration, a period of at least 10 minutes elapsed prior to recording to ensure stable recording. For all studies, data were filtered at 2 kHz, digitized at 10kHz, acquired and analyzed subsequently using pClamp 10.4 or 10.7 software (Molecular Devices, Sunnyvale, CA).

Recordings of Resting Membrane Potentials, Action Potentials, Holding Currents, and Current-Voltage Relationships from Amygdala Neurons

For Study 1, recordings were made directly from local CeL GABAergic neurons, whereas in Study 2 and 3, recordings were made from BLA principal neurons. The recording electrodes were filled with (in mM) 120 K⁺-gluconate, 10 KCl, 5 NaCl, 2 MgCl₂, 10 HEPES, 0.5 EGTA, 2 ATPNa₂, 0.4 GTPNa, and 5 phosphocreatine (pH 7.3) in all studies. When the Cs⁺-containing intracellular solution was used for recordings, the intracellular K⁺-gluconate was replaced by the same concentration of Cs⁺-gluconate. For action potential (AP) recordings, kynurenic acid (1 mM) and picrotoxin (100 μM) were supplemented in the extracellular solution to block potential indirect actions from synaptic transmission. AP frequency was obtained by using the "Event Detection" and "Threshold Search" features of Clampfit 10.7 software. AP data were then exported to

Microsoft Excel and binned per minute using Excel function commands. As BLA neurons did not show spontaneous firing (Study 2 and 3), we injected a series of positive currents from 50 pA to 700 pA at an increment of 50 pA every 6 s. This protocol was applied to the same cells before and during peptide application for 3–5 min when the maximal effect was typically observed. In a subset of experiments in Study 2, a constant positive current was injected to depolarize membrane potentials near AP threshold to induce sparse AP firing. Rheobase current was defined as the current required to elicit the first AP during the positive current injection protocol. The AP half-width was defined as the time between the half-amplitude of the upslope of the AP waveform and the equivalent point on the downslope and was calculated from the rheobase sweep of 100 to 200 pA (50 pA steps) series of current injections. The time to the first AP was the time from the initiation of the current injection until the first AP fired and was calculated from the rheobase sweeps of 100 to 200 pA (50 pA steps) series of the positive current injection protocol.

Resting membrane potentials (RMPs) and holding currents (HCs) were recorded from amygdala neurons held at -60 mV in the extracellular solutions supplemented with tetrodotoxin (TTX, 0.5 μ M), kynurenic acid (1 mM), and picrotoxin (100 μ M). The intracellular solution was the K⁺-gluconate containing solution unless otherwise stated. Current-voltage (I-V) relationships were obtained by recording from amygdala neurons held at -60 mV. Cells were stepped from -140 to -40 mV for 400 ms at a voltage increment of 10 mV every 10 s. If the reversal potential was not found within this voltage range, the step range was extended to + 20 mV. In Study 1, we replaced the CaCl₂ in the extracellular solution with the same concentration of MgCl₂ to reduce the contamination of voltage-gated Ca²⁺ channels. Steady-state current values were measured within 5 ms prior to the end of the step voltage protocol.

The selective peptide agonists in each study were dissolved in extracellular solutions and bath applied to cells for at least 5 minutes, as the maximum effect was typically observed within this period. Slices were limited to a single peptide application to prevent agonist-induced receptor desensitization. Pharmacological inhibitors were applied to the cells either extracellularly or intracellularly via the recording pipettes. For extracellular application, slices were pretreated for at least 2 h to ensure permeation of reagents into the cells in the slices and the extracellular solution continuously contained the same concentration of the reagents, unless stated otherwise. For intracellular application, a period of at least 15 min followed the establishment of the whole-cell configuration to allow for diffusion of the inhibitor into the cells.

Recordings of sEPSCs, mEPSCs, and eEPSCs

Glutamatergic excitatory post-synaptic currents (EPSCs) were recorded in Study 3. Spontaneous EPSCs, (sEPSCs), miniature EPSCs (mEPSCs), and evoked EPSCs (eEPSCs) were obtained using whole-cell patch-clamp recordings from principal cells of the BLA held at -60 mV. Recording electrodes were filled with the K-gluconate recording solution that contained QX-314 (1 mM) to remove contamination from voltage-gated Na⁺-channels. To isolate glutamatergic events, the extracellular solution was supplemented with bicuculine (10 μM) to block GABA_A receptors. For recordings of mEPSCs, TTX was included in the bicuculine-supplemented external solution. The recorded sEPSC and mEPSCs were analyzed using Easy Electrophysiology (RRID:SCR_021190) or Clampfit 10.7. Results obtained from either analysis methods produced similar results. The data were then exported for analysis using a custom formula in Microsoft Excel to bin events per minute. All recorded events were visually inspected to exclude obvious artifacts. The detection threshold was established as 3 X the standard deviation of the baseline noise measured in an event-free segment. Due to

the variation of basal sEPSC and mEPSC events, any changes in the frequency of events following the application of NMB or senktide was normalized to the 5 minutes of recorded baseline. eEPSCs were obtained from BLA neurons by placing a tungsten in the afferents of the BLA (~200-350 μm from patched neuron). An A365 stimulus isolator delivered stimulations at a frequency of 10 Hz. The series resistance was carefully monitored by delivering a -5 mV voltage step following each evoked current. The synaptic current recordings were stopped if the series resistance changed by > 20%. The coefficient of variation was calculated by comparing the ratio of the standard deviation and mean of 15 consecutive events before and after NMB bath application. Paired pulse ratio (PPR) was recorded by applying two stimuli at an interval of 50 ms before and after NMB application from the same cell and calculated by equation ($\text{PPR} = \text{P2/P1}$, where P1 and P2 were the first and second EPSC amplitude, respectively). All synaptic events were digitized at 10 kHz and filtered at 2 kHz.

Stereotaxic Surgery, Microinjection, and Histology

For all studies, surgical procedures and cannula placement were performed under aseptic conditions, according to our previous publications [217-220]. Guide cannulas (23 GA, 8.5 mm length; P1 Technologies Inc., Roanoke, VA) were bilaterally implanted such that the end of the cannula was positioned 0.5-1 mm above the target brain region. For Study 1, guide cannula targeted the CeA with coordinates obtained from the rat brain atlas (from bregma: anteroposterior: -2.1-2.3 mm, mediolateral: \pm 4.1-4.2 mm; dorsoventral: -7.6 mm [221]). For Study 2 and 3, guide cannula were positioned targeting the BLA (from bregma, anteroposterior: -2 ~ -2.6 mm, mediolateral: \pm 4.9 ~ 5.0 mm, dorsoventral: -7.2-7.6 mm) [222]. Coordinate placement was adjusted to account for variation in animal weight and personal experiences with the procedure. Study 1 and 3 included male (Study 1: 368 ± 10.4 g, $n = 17$; Study 3: 195.7 ± 8.4 g, $n = 21$) and female

(Study 1: 225 ± 5.8 g, $n = 20$; Study 2: 168 ± 3.9 g, $n = 26$) SD rats, whereas Study 2 included only female (193 ± 8 g, $n = 63$) SD rats. A deep state of anesthesia was induced by 5% isoflurane and anesthesia was maintained at 3% while rats were placed in the stereotaxic frame (Stoelting Co., IL). An incision was made at the occipital bone extending forward toward the frontal bone. The connective tissue encasing the skull was cleared with cotton swabs to expose the suture lines. Cannulas were secured in place with dental acrylic bonded to 3 stainless steel screws (4.8 mm, P1 Technologies Inc., Roanoke, VA) inserted into burr holes drilled into the skull. To prevent occlusion of the guide cannulas, stainless steel stylets were screwed into the guide cannula and left in place until microinjection. Following surgery, rats were allotted a 7-10 d recovery period in which rats were monitored daily for adverse post-surgical complication. Within the recovery period, rats received daily handling for habituation of microinjection procedures. Bilateral microinjections of various compounds into the amygdala were delivered in 1 μ L volumes through an internal cannula (30 GA, 8.5 mm; P1 Technologies Inc., Roanoke, VA). Two 5 μ L Hamilton syringes fixed to an automated pump (Harvard Apparatus, MA) were used to administer drug injections at a rate of 0.2 μ L min⁻¹. Upon the completion of the microinjection, the internal cannula was left in place for an additional ~2 min to ensure adequate diffusion of reagents into the amygdala.

For Study 1, saline, NMB, tertiapin-Q, BIM23042 (all in 1 μ L volume per side) were bilaterally injected into the CeA. In Study 2, rats were bilaterally injected with saline, NMB, BIM23042, AMG9810, or tertiapin-Q. Rats in Study 3 received bilaterally injections of saline, senktide, SB218795, M084, or tertiapin-Q into the BLA via the internal cannula. Following experiments, all rats were anesthetized and bilaterally injected with 3% Chicago Sky Blue dye (Sigma). Coronal sections (80 μ m) containing the amygdala were collected on a vibrating microtome (VT1200, Leica Biosystems Inc., IL) and proper

cannula placement was confirmed. Animals with incorrect cannula placement were excluded from analysis.

Acoustic Startle and Fear-Potentiated Startle Responses

Acoustic startle response (ASR) and fear-potentiated startle (FPS) experiments were conducted in Study 1 and 2. ASR and FPS were conducted using clear cylindrical animal holders inside two identical SR-LAB startle chambers connected to a laptop with the SR-Lab software (San Diego Instruments, CA) as described [223, 224]. Experimental protocols were designed and implemented via the SR-lab software. A high-frequency loudspeaker and a single lightbulb mounted 24 cm above the animal holder in each cabinet was used to elicit the white noise bursts (90 dB, 95 dB, and 105 dB WNBs) and the visually conditioned stimulus, respectively. Foot shocks (0.5 mA) were used as a conditioned stimulus and were delivered from a removable stainless-steel floor grid within each animal holder.

The experimental paradigms used in Study 1 and 3 are shown below (Figures 8 and 24). Days 1, 3, and 4 were conducted in the same way in Study 1 and 3, whereas day 2 was specific to a particular study. On day 1, rats were moved to the behavioral testing room in their home cage for a 1 h handling session and a 30 min habituation within each animal holder in each startle chamber. On day 2 in Study 1, animals underwent a 5-min habituation prior to being presented with 21 WNBs (90 dB x 7; 95 dB x 7; 105 dB x 7; 50 ms duration) at a 30 s intertrial interval (ITI) for startle responses in the presence of a background white noise (70 dB). A subset of male and female rats was microinjected with saline or NMB (0.3 nmol) 15 min prior to ASR testing. Study 3 animals were presented with 30 WNBs (95 dB, 50 ms) at a 30 s ITI. All experiments on day 2 occurred in the presence of a 70 dB background white noise. On day 3, test compounds were microinjected 5-10 minutes prior to the fear conditioning session. Similar to days 1

and 2, animals were allotted a 5-min habituation. Fear condition consisted of a series of ten 3.7 s light cues (neutral stimuli) that co-terminated with a 0.5 s foot shock (0.5 mA, pseudorandom ITI 30-180 s) in the absence of background white noise. On day 4, acquisition of a fear response was tested using a FPS protocol. After a 5-minute habituation period within the startle chamber, rats were subjected to 30 WNBs in presence of a continuous 70 dB background white noise. The startle amplitude was defined as the maximum peak voltage recorded during the first 200 ms of the response to the WNB. A basal startle amplitude in the presence of background noise was obtained in response to the first 10 WNBs (90 dB x5; 95 dB x 5) alone without a light cue. The following 20 WNBs occurred in groups of 10 WNBs: 10 WNBs (105 dB) paired with the conditioned light cue (cued) and 10 WNBs (105 dB) occur in the absence of the conditioned light cue (non-cued) in a pseudorandom order. FPS responses in Study 1 were reported as raw startle responses as described previously [225, 226]. In Study 2, cued fear responses were reported as $[(\text{amplitude with the light cue} - \text{non-cued amplitude}) / \text{non-cued amplitude}] \times 100\%$. The non-cued fear responses showed as $[(\text{amplitude without the light cue} - \text{basal amplitude}) / \text{basal amplitude}] \times 100\%$, as previously reported [226, 227].

Recordings of Mean Arterial Pressure and Heart Rate

For Study 1, a VPR noninvasive blood pressure monitoring system (CODA-6, Kent Scientific, Torrington, CT) connected to a Powerlab system (ADInstruments Pty Ltd., Bella Vista, New South Wales, Australia) was used to measure mean arterial pressure (MAP) and heart rate (HR) in age-matched male and female SD rats. The VPR noninvasive blood pressure monitoring system provides accurate measures in comparison with more invasive approaches [228]. When possible, data were collected from an equal number of male and female rats. MAP and HR were assessed during the

light cycle and SD rats underwent a minimum of 7-days habituation via light handling in a clean towel [229]. Prior to recording, animals were placed on a warming pad to improve the recording signal and care was taken to not overheat nor over restrict the movement of the animal during the recording session. Baseline cardiovascular parameters (systolic, diastolic, mean arterial pressure, and heart rate) were recorded for at least a 10-minute habituation period during each session. A series of measurements were recorded during and immediately following drug injection and data were reported as the net change in mean arterial pressure (MAP) and heart rate (HR) from baseline as a result of saline or drug injection, as previously reported [229-231].

Vogel Conflict Test

Rats in Study 2 were assessed for anxiety-like behaviors in the Vogel Conflict Test (VCT). The VCT was performed in polycarbonate cages (42 x 25 x 20 cm) with a metal floor grid, as previously described [232, 233]. The stainless-steel drinking spout of the water bottle and floor grid were connected to an Anxiometer (Columbus Instruments, OH). When an animal contacts the spout and floor grid, the electric circuit is closed and a lick is counted by the Anxiometer. The animal received a mild electric shock (0.3 mA, 0.5 s) every 20 licks. For 2 days preceding the VCT, animals were restricted to 1 h per day of access to tap water. After the initial 23 h water deprivation, animals are habituated to the testing cage for 30 min and allowed unpunished drinking. On day 2, test compounds were microinjected 10-20 minutes prior to the VCT session. Animals were allowed a 5-minute habituation in the test cage prior to the start of the VCT. The test session was then initiated after the animal made 20 licks and a single shock (0.3 mA, 0.5 ms) was delivered. Rats received a shock every 20 licks during the 3-minute testing period. Data reported were the number of spout licks by rats during the 3-minute test session.

Data Analysis

Data in Study 1 and Study 2 are presented as the means \pm S.E.M. In Study 3, data are presented as the means \pm SD. For the *in vitro* data, “n” refers to the number of cells recorded, whereas for the *in vivo* experiments, “n” refers to the number of animals tested. Normality was assessed using the D’Agostino and Pearson tests, and data that did not pass were analyzed with the corresponding nonparametric test. Paired Student’s t-test (paired t-test), Wilcoxon matched-pair signed rank test (hereafter Wilcoxon’s test), two-sample Student’s t-test, and one-way or two-way ANOVA were used for statistical analysis, as appropriate. To minimize potential influences of variations from individual animals, each experiment was performed from slices obtained from at least four animals and one-way ANOVA was performed to ensure there was no significant difference for the data obtained from individual animals under the same treatment. One-way ANOVA followed by Dunnett’s or Tukey’s multiple comparison test was used for statistical analysis when the pooled control data were used for comparison. Two-way repeated measures ANOVA followed by Šídák’s multiple comparison test was used for statistical analysis for the AP firing frequency elicited by injections of positive currents and for the data used to construct the I-V relationship. For sEPSC cumulative probability plots, events recorded 5 min before and 5 min after reaching maximal effects were used for comparison, and bin sizes were the same between the experiments. The Kolmogorov-Smirnov test was used to assess the significance of the cumulative probability plots. ASR, FPS, and baseline cardiovascular responses were analyzed using a mixed-effects two-way ANOVA, as appropriate and significant was analyzed post hoc using the Šídák’s multiple comparisons test. Shock reactivity was analyzed using the nonparametric Mann-Whitney test. Net changes in cardiovascular values were compared using a one-way ANOVA and post-hoc differences were assessed using Dunnett’s or Tukey’s multiple comparisons test. The IC₅₀ value was calculated from raw

data measurements using non-linear regression. Statistical analysis was performed using Origin 7 (OriginLab Corporation, Northampton, MA, USA) and GraphPad Prism v9.4 (GraphPad Software Inc., San Diego, CA, USA). P-values were reported throughout the text, and significance was set at $P < 0.05$.

Chemicals

All drugs were initially prepared as a stock solution and stored at -20°C until use. The stock solution was diluted with extracellular solution to obtain the appropriate working concentration for bath application to the recording chamber. In preparations requiring dimethyl sulfoxide (DMSO), the final concentration of DMSO was below 0.1% which is physiologically inert. The complete list of drugs used in this dissertation can be found in the List of Reagents and Drugs.

CHAPTER 3

RESULTS

Study 1 - Neuromedin B-Mediated Modulation of Central Amygdala Neurons

Introduction

Neuromedin B (NMB) and gastrin-releasing peptide (GRP) are the mammalian analogues of the bombesin and the bombesin-like family of peptides originally characterized in amphibians and first isolated from porcine gastric tissue and spinal cord [234]. The biological actions of bombesin-like peptides are mediated by at least three receptors; the NMB-preferring bombesin 1 (BB1) receptors, the GRP-preferring bombesin 2 (BB2) receptors [235, 236] and the orphan bombesin 3 (BB3) receptors whose natural ligand is unknown [237, 238]. All three bombesin receptors are coupled to G proteins resulting in the activation of phospholipase C β (PLC β) which hydrolyzes phosphatidylinositol 4,5-bisphosphate (PIP₂) generating inositol 1,4,5-trisphosphate (IP₃) to stimulate intracellular Ca²⁺ release and diacylglycerol (DAG) to activate protein kinase C (PKC) [237, 239, 240], although the bombesin receptors also stimulate tyrosine phosphorylation of a number of signaling proteins [239, 241]. BB1 receptor activation regulates pituitary-thyroid function, fear and anxiety responses, satiety and tumor growth; BB2 receptors play important roles in modulating pruritus, lung development, small intestinal mucosal defense and CNS processes such as learning and memory; BB3 receptors are involved in controlling obesity and glucose intolerance, lung response to injury, tumor growth and gastrointestinal tract motility [239, 241].

However, the cellular and molecular mechanisms whereby the bombesin-like peptides modulate these physiological functions and pathological disorders have not been fully determined.

The CeA expresses not only bombesin-like peptides [242] and NMB mRNA [243], but also high densities of binding sites for bombesin-like peptides [242] and NMB [244]. Consistent with the distribution of bombesin-like peptides and their receptors in the CeA, injection of bombesin into the CeA induces an increase in mean arterial pressure [245] and reduces food intake [246, 247]. Intraperitoneal or cerebroventricular administration of bombesin induces Fos-like immunoreactivity, a marker of neuronal activation, in the CeL [248]. However, the effects of bombesin and bombesin-like peptides on neuronal excitability in the CeA and the underlying cellular and molecular mechanisms have not been determined. In this study, we studied the effects of NMB on the excitability of CeL neurons based on the results showing that high densities of NMB binding sites are distributed in the CeA [244] and administration of bombesin induces Fos expression in the CeL suggesting that activation of bombesin receptors increases neuronal activity in the CeL. Our results indicate that activation of BB1 receptors by NMB excites CeL neurons by PLC β and PKC-mediated depression of inwardly rectifying K⁺ (Kir) channels. Moreover, microinjection of NMB into the CeA reduced blood pressure and heart rate in unanesthetized male and female rats and reduced fear-potentiated startle responses. Our results may provide a cellular and molecular mechanism to explain the roles of bombesin and bombesin-like peptides in the amygdala.

NMB Increases Neuronal Excitability in the CeL

We chose NMB as an example to test the effects of bombesin-like peptides on neuronal excitability in the CeL (Figure 1, a) based on the results showing that the CeA expresses both NMB mRNA [243] and NMB binding sites [244] and administration of

bombesin induces Fos expression in the CeL [248], suggesting that activation of bombesin receptors facilitates neuronal activity. CeL neurons can be classified electrophysiologically into three types: regular firing (RS, ~54%), low-threshold bursting (LTB, ~34%), and late firing (LF, ~12%) [42]. We thus identified the types of the recorded neurons first after formation of the whole cell recording configuration by injection of a series of negative and positive currents. As neurons in the CeL did not show spontaneous firing, we injected a persistent positive current to induce discrete AP firing. We examined 33 neurons of which 23 were RS, 7 were LTB, and 3 were LF. Bath application of the selective BB1 receptor agonist, NMB at 0.3 μ M, a near-saturating concentration [74], augmented the firing frequency of APs recorded from each neuronal type (Figure 1, b-d). We therefore pooled the data recorded from each neuronal type. NMB increased the AP firing frequency to $274 \pm 38\%$ of control (Control: 0.51 ± 0.08 Hz, NMB: 1.11 ± 0.15 Hz, $n = 33$, $P < 0.0001$, Wilcoxon test, Figure 1, e), suggesting that activation of BB1 receptors excited CeL neurons. NMB-elicited augmentation of AP firing frequency was irreversible after a wash for 30 minutes (Control: 0.51 ± 0.08 Hz, wash 30 min: 1.38 ± 0.34 Hz, $n = 33$, $P = 0.0003$, Wilcoxon test, Figure 1, e). The NMB-mediated increases in AP firing frequency were sex-independent as NMB exerted similar extent of increases ($P = 0.15$, Two-sample t-test) in male ($248 \pm 53\%$ of control, $n = 17$) and female ($434 \pm 117\%$ of controls, $n = 16$) virgin rats. We thus used both sexes and kept the numbers of male and female rats as equal as possible for the remaining experiments.

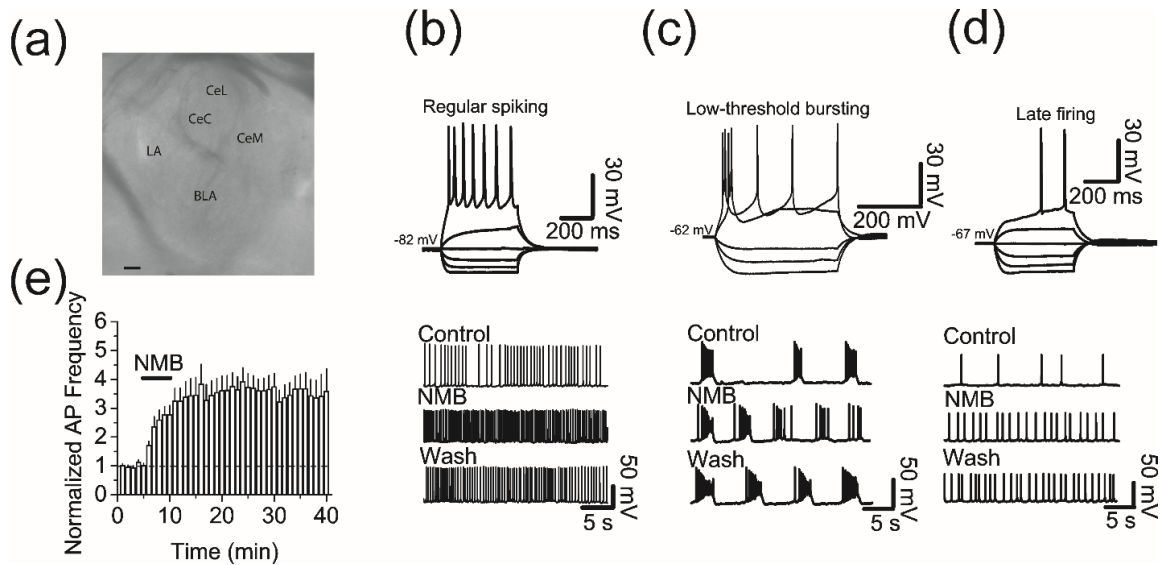


Figure 1. NMB increases AP firing frequency in CeL neurons. (a), microscopic photograph showing the location of CeL where electrophysiological recordings were conducted. LA: lateral nucleus; BLA: basolateral nucleus; CeC: capsular central amygdala; CeL: lateral central amygdala; CeM: medial central amygdala. Scale bar: 500 μ m. (b), bath application of NMB (0.3 μ M) increased AP firing frequency in regular spiking (RS) neurons in the CeL region. *Upper panel*: voltage responses elicited by injection of currents from -30 pA to 20 pA at an increment of 10 pA in a duration of 400 ms. *Lower panel*: current traces recorded from the same neuron prior to, during and after the application of NMB. The firing frequency of APs in RS neurons was increased by a 5-minute bath application of NMB. (c), bath application of NMB (0.3 μ M) increased AP firing frequency in low-threshold bursting (LTB) neurons of the CeL region. The firing frequency of APs in LTB neurons was increased by a 5-minute bath application of NMB. (d), bath application of NMB (0.3 μ M) increased AP firing frequency in late firing (LF) neurons in the CeL region. The firing frequency of APs in LF neurons was increased by a 5-minute bath application of NMB. (e), summarized time course of NMB-induced potentiation of AP firing frequency recorded from 33 CeL neurons. Adapted from [223].

NMB-Induced Excitation of CeL Neurons Requires the Functions of G Proteins and PLC β

We then sought to determine the intracellular signaling mechanisms involved in NMB-mediated excitation of CeL neurons. BB1 receptors are coupled to G α_q proteins resulting in the activation of PLC β which hydrolyzes PIP $_2$ to generate IP $_3$ to increase intracellular Ca $^{2+}$ release and DAG to activate PKC [240]. Thus, we examined the roles of this signaling pathway in NMB-mediated facilitation of neuronal excitability in the CeL. Intracellular perfusion of the selective G protein inactivator GDP- β -S (0.5 mM) prevented NMB-induced augmentation of AP firing frequency (Control : 0.73 ± 0.31 Hz, NMB: 0.65 ± 0.28 Hz, $99 \pm 19\%$ of control, $n = 10$, $P = 0.75$, Wilcoxon test; $F_{(1,41)} = 9.523$, $P = 0.0036$ vs. NMB alone, two-way ordinary ANOVA, Figure 2, a), indicating that the function of G protein is required for NMB-mediated enhancement of AP firing.

We assessed the roles of PLC β in NMB-mediated excitation of CeL neurons. Slices were pretreated with the selective PLC inhibitor, U73122 (5 μ M), for >2 h. Separate slices were treated with the inactive analogue U73343 (5 μ M) in the same fashion as the control. Under these conditions, application of NMB did not significantly augment AP firing frequency in slices pretreated with U73122 (Control: 1.36 ± 0.25 Hz, NMB 1.27 ± 0.31 Hz, $99 \pm 11\%$ of control, $n = 17$, $P = 0.8802$, Wilcoxon test, Figure 2, b), but still significantly enhanced the AP firing frequency in slices pretreated with U73343 (Control: 0.51 ± 0.10 Hz, NMB 0.98 ± 0.19 Hz, $221 \pm 35\%$ of control, $n = 18$, $P < 0.0007$, Wilcoxon test; $F_{(1,33)} = 9.25$, $P < 0.01$ vs. U73122, two-way ordinary ANOVA, Figure 2, b). These results demonstrate that PLC β is required for NMB-mediated increases in neuronal excitability in the CeL.

Intracellular Ca²⁺ Release is Unnecessary, but PKC is Required for NMB-Elicited Excitation of CeL Neurons

We investigated the involvement of Ca²⁺ release from intracellular stores in NMB-mediated facilitation of neuronal excitability. Intracellular application of the IP₃ receptor blocker heparin (2 mg/ml) through the recording pipettes failed to significantly affect NMB-mediated enhancement of AP firing frequency (Control: 0.56 ± 0.10 Hz, NMB: 1.79 ± 0.64 Hz, $299 \pm 49\%$ of control, $n = 16$, $P < 0.0006$, Wilcoxon test; $F_{(1,47)} = 0.047$, $P = 0.8282$ vs. NMB alone, two-way ordinary ANOVA, Figure 2, c), indicating that IP₃ receptors are not required for NMB-induced augmentation of neuronal excitability. Similarly, intracellular application of the sarcoplasmic-endoplasmic reticulum Ca²⁺-ATPase inhibitor thapsigargin (10 μ M) via the recording pipettes did not significantly alter NMB-mediated augmentation of AP firing frequency (Control: 0.51 ± 0.11 Hz, NMB: 0.82 ± 0.15 Hz, $174 \pm 20\%$ of control, $n = 21$, $P < 0.0001$, Wilcoxon test; $F_{(1,52)} = 0.289$, $P = 0.593$ vs. NMB alone, two-way ordinary ANOVA, Figure 2, c). We further examined the potential involvement of Ca²⁺ released from the ryanodine-sensitive store by intracellular perfusion of ryanodine (100 μ M) to inhibit ryanodine receptors. Intracellular application of ryanodine did not significantly affect NMB-mediated increases in neuronal excitability in CeL neurons (Control: 1.97 ± 0.59 Hz, NMB: 3.98 ± 1.14 Hz, $244 \pm 64\%$ of control, $n = 18$, $P = 0.0016$, Wilcoxon test; $F_{(1,50)} = 0.09$, $P = 0.77$ vs. NMB alone, two-way ordinary ANOVA, Figure 2, d). These results demonstrate that intracellular Ca²⁺ release is not involved in the NMB-elicited increases in AP firing. Interestingly, intracellular dialysis of the Ca²⁺ chelator, BAPTA (10 mM), significantly attenuated NMB-mediated increase in AP firing frequency (Control: 0.90 ± 0.19 Hz, NMB: 0.79 ± 0.14 Hz, $110 \pm 14\%$ of control, $n = 18$, $P = 0.475$, Wilcoxon test; $F_{(1,49)} = 15.69$, $P = 0.0002$ vs. NMB alone, two-way ordinary ANOVA, Figure 2, d). As PKC was involved in NMB-

elicited excitation of CeL neurons (see below) and some PKC isoforms are Ca^{2+} -dependent, one explanation for the BAPTA result is that BAPTA lowered the basal intracellular Ca^{2+} level, which may be required for the functions of Ca^{2+} -dependent signaling molecules such as PKC. Lastly, we investigated the role of extracellular Ca^{2+} in NMB-elicited augmentation of neuronal excitability by replacing the extracellular Ca^{2+} with an equal concentration of Mg^{2+} . Under these conditions, application of NMB similarly enhanced AP firing frequency (Control: 0.58 ± 0.10 Hz, NMB: 1.05 ± 0.16 Hz, $213 \pm 28\%$ of control, $n = 18$, $P = 0.003$, Wilcoxon test; $F_{(1,49)} = 0.196$, $P = 0.66$ vs. NMB alone, two-way ordinary ANOVA, Figure 2, e), indicating that NMB-mediated increase in neuronal excitability is not dependent on extracellular Ca^{2+} .

We further probed the role of PKC in NMB-mediated excitation of CeL neurons. Slices were pretreated with the selective PKC inhibitor, chelerythrine ($10 \mu\text{M}$), for >2 h, and the bath was continuously perfused with the same concentration of chelerythrine to ensure persistent inhibition of PKC. In this situation, application of NMB did not significantly increase the AP firing frequency (Control: 0.75 ± 0.18 Hz, NMB: 0.71 ± 0.17 Hz, $102 \pm 15\%$ of control, $n = 22$, $P = 0.708$, Wilcoxon test; $F_{(1,53)} = 16.57$, $P = 0.0002$ vs. NMB alone, two-way ordinary ANOVA, Figure 2, f). Moreover, pretreatment of slices with and continuous bath application of another selective PKC inhibitor, bisindolylmaleimide (Bis II, $1 \mu\text{M}$), blocked NMB-mediated increases in AP firing frequency (Control: 1.04 ± 0.32 Hz, NMB: 0.91 ± 0.26 Hz, $101 \pm 15\%$ of control, $n = 10$, $P = 0.77$, Wilcoxon test; $F_{(1,41)} = 9.519$, $P = 0.0036$ vs. NMB alone, two-way ordinary ANOVA, Figure 2, g). The involvement of PKC was further supported by bath application of the PKC activator, phorbol 12-myristate 13-acetate (PMA, $1 \mu\text{M}$), resulting in a significant increase of AP firing frequency in CeL neurons (Control: 0.68 ± 0.21 Hz, PMA: 1.74 ± 0.43 Hz, $281 \pm 70\%$ of control, $n = 14$, $P = 0.0031$, Wilcoxon test,

Figure 2, h). In slices pretreated and continuously superfused with Bis II (1 μ M), application of PMA failed to significantly increase AP firing frequency (Control: 0.42 ± 0.11 Hz, PMA: 0.33 ± 0.10 Hz, $75 \pm 9\%$ of control, $n = 15$, $P = 0.058$, Wilcoxon test; $F_{(1,27)} = 19.11$, $P = 0.0002$ vs PMA alone, Figure 2h). Moreover, application of chelerythrine (10 μ M) in the same fashion blocked PMA-induced increase in AP firing frequency (Control: 0.59 ± 0.31 Hz, PMA: 0.64 ± 0.34 Hz, $101 \pm 15\%$ of control, $n = 10$, $P = 0.63$, Wilcoxon test; $F_{(1,22)} = 9.81$, $P = 0.0048$ vs. PMA alone, two-way ordinary ANOVA, Figure 2, h). These data together indicate that PKC is required for NMB-mediated excitation of CeL neurons.

NMB Depolarizes CeL Neurons and Increases the Input Resistance and Membrane Time Constants of CeL Neurons

We then included TTX (0.5 μ M) in the extracellular solution to block Na^+ -dependent AP firing to determine the effects of NMB on passive membrane properties of CeL neurons. Bath application of NMB induced significant depolarization of CeL neurons (Control: -63.1 ± 1.8 mV, NMB: -59.6 ± 1.9 mV, net depolarization: 3.5 ± 0.8 mV, $n = 16$, $P = 0.0004$, paired t-test, Figure 3, a1-a2). To confirm that NMB-elicited excitation of CeL neurons was indeed mediated by activation of BB1 receptors, we pretreated slices with and continuously bath-applied the selective BB1 antagonist, BIM23042 (0.3 μ M) [249, 250]. In the presence of BIM23042, NMB failed to depolarize CeL neurons significantly (BIM 23042: -63.5 ± 1.2 mV, BIM 23042 + NMB: -63.3 ± 1.3 mV, net depolarization: 0.20 ± 0.16 mV, $n = 10$, $P = 0.24$, paired t-test, Figure 3, a3). Furthermore, application of PD168368 (10 μ M), another selective BB1 receptor antagonist [251], in the same fashion blocked NMB-induced depolarization (PD168368: -64.3 ± 1.9 mV, PD168368 + NMB: -64.1 ± 2.0 mV, net depolarization: 0.25 ± 0.14 mV, $n = 10$, $P = 0.12$, Wilcoxon test, Figure 3, a3). In voltage-clamp mode, NMB elicited an inward current

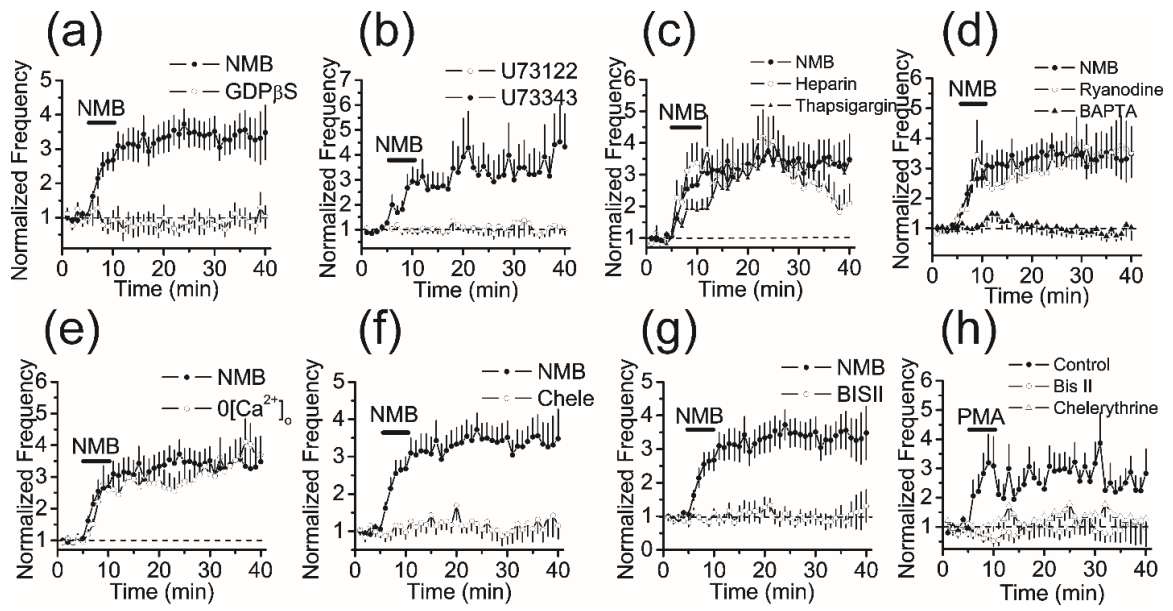


Figure 2.

G proteins, PLC β and PKC are required for NMB-mediated potentiation of AP firing frequency.

(a), intracellular dialysis of the G protein inactivator, GDP- β -S (0.5 mM), blocked NMB-induced facilitation of AP firing frequency (n = 10). (b), pretreatment of slices with the PLC inhibitor, U73122 (5 μ M), blocked NMB-induced potentiation of AP firing frequency (n = 17), whereas application of NMB still significantly enhanced AP firing frequency in slices pretreated with the inactive analog, U73343 (5 μ M, n = 18). (c), intracellular dialysis of the IP₃ receptor blocker, heparin (2 mg/ml, n = 16), or the inhibitor of the smooth-endoplasmic reticular Ca²⁺-ATPase, thapsigargin (10 μ M, n = 21) did not significantly affect NMB-induced augmentation of AP firing frequency. (d), intracellular application of ryanodine (100 μ M) to inhibit ryanodine receptors did not significantly influence NMB-elicited augmentation of AP firing frequency (n = 18), whereas intracellular perfusion of the Ca²⁺ chelator BAPTA (10 mM) blocked NMB-induced enhancement of AP firing frequency (n = 18). (e), replacement of extracellular Ca²⁺ with the same concentration of Mg²⁺ did not affect NMB-induced increases in AP firing frequency (n = 18). (f), pretreatment of slices with and continuous bath application of the selective PKC inhibitor chelerythrine (Chele, 10 μ M) blocked NMB-induced augmentation of AP firing frequency (n = 22). (g), pretreatment of slices with and continuous bath application of the selective PKC inhibitor Bis II (1 μ M) blocked NMB-induced augmentation of AP firing frequency (n = 10). (h), bath application of the PKC activator PMA (1 μ M) significantly increased the AP firing frequency (n = 14), whereas pretreatment of slices with and continuous bath application of Bis II (1 μ M, n = 15) or chelerythrine (10 μ M, n = 10) blocked PMA-induced potentiation of AP firing frequency. Adapted from [223].

at -60 mV (-19.6 ± 5.2 pA, $n = 17$, $P = 0.002$, paired t-test, Figure 3, b1-b2). Taken together, these results demonstrate that activation of BB1 receptors increases neuronal excitability through membrane depolarization.

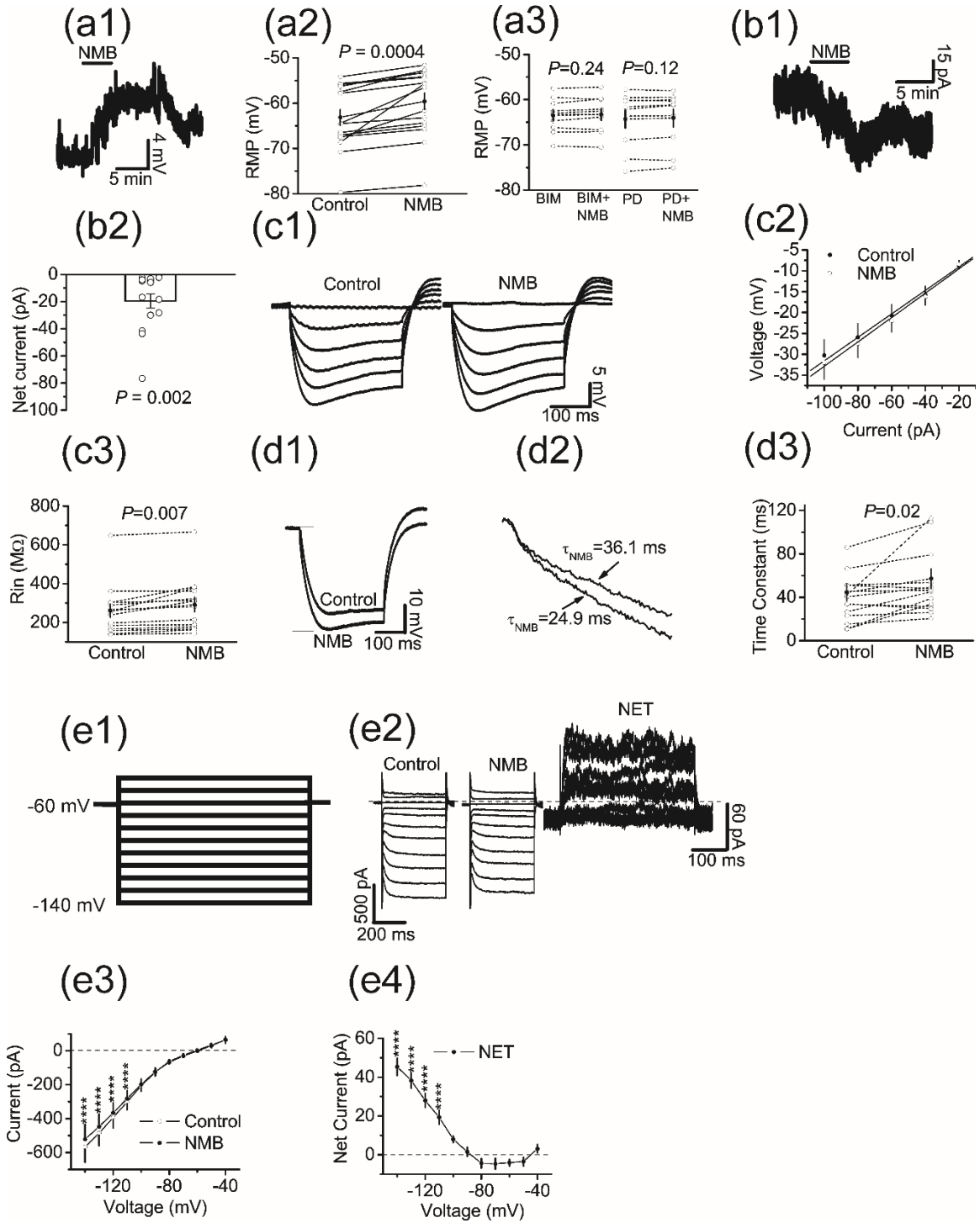
We further determined the effect of BB1 receptor activation on the input resistance of CeL neurons by injecting a series of negative currents from -20 to -100 pA with a 20 pA step every 6 s before and after the application of NMB. We then fit the current-voltage relationship to a linear function for each cell to obtain the input resistance (R_{in}) which was the slope of the linear fitting (Figure 3, c1-c3). Bath application of NMB significantly increased R_{in} (Control: 260 ± 35 M Ω , NMB: 290 ± 36 M Ω , $n = 14$, $P = 0.007$, Wilcoxon test, Figure 3, c3), indicating that NMB increased R_{in} . We acquired the membrane time constants by fitting a single exponential function to the voltage transient generated by negative current injection (-100 pA, 100 ms from the end of the baseline). Bath application of NMB significantly increased the membrane time constants (Control: 38.3 ± 5.7 ms, NMB: 51.8 ± 7.8 ms, $n = 14$, $P = 0.023$, Wilcoxon test, Figure 3, d1-d3). These results together suggest that NMB excites CeL neurons by suppressing a membrane conductance.

Activation of BB1 Receptors Inhibits an Inwardly Rectifying K⁺ Channel in CeL Neurons

We next determined the ionic mechanisms by which BB1 receptor activation depolarizes CeL neurons. As shown in Figure, 2e, the effect of NMB on CeL neurons was independent of extracellular Ca²⁺. We therefore replaced extracellular Ca²⁺ with the same concentration of Mg²⁺ to avoid contamination of voltage-gated Ca²⁺ channels. TTX (0.5 μ M) was included in the Ca²⁺-free extracellular solution to block voltage-gated Na⁺ channels. Cells were held at -60 mV and stepped from -140 mV to -40 mV for 400 ms at a voltage interval of 10 mV every 10 s (Figure 3, e1) before and after bath application of NMB when the maximal effect was observed. Steady-state currents were

Figure 3. NMB induces membrane depolarization and increases the input resistances and membrane time constants.

(a1-a3), bath application of NMB depolarized CeL neurons via activation of BB1 receptors. **(a1)**, RMP recorded from a CeL neuron before, during, and after the application of NMB. **(a2)**, summary data for NMB-induced depolarization ($n = 16$). Green circles represent the values from individual cells and the red circles represent their average. **(a3)**, pretreatment of slices with and continuous bath application of the selective BB1 receptor antagonist BIM23042 (BIM, $0.3 \mu\text{M}$, $n = 10$) or PD168368 (PD, $10 \mu\text{M}$, $n = 10$) blocked NMB-induced depolarization. **(b1-b2)**, bath application of NMB induced an inward current from CeL neurons in voltage-clamp. **(b1)**, holding current recorded at -60 mV from a CeL neuron before, during, and after the application of NMB. **(b2)**, summary of net holding currents induced by NMB ($n = 17$). Green circles represent the values from individual cells and the bar graph represent their average. **(c1-c3)**, NMB increased the input resistance (R_{in}). **(c1)**, voltage responses evoked by injection of negative currents from -100 to -20 pA at an interval of 20 pA before (*left*) and during (*right*) the application of NMB. **(c2)**, I-V relationship averaged from 14 cells. R_{in} was obtained by linear fitting of the I-V relationship. **(c3)**, summary graph for the R_{in} before and after the application of NMB ($n = 14$). **(d1-d3)**, NMB increased membrane time constants. **(d1)**, voltage response evoked by -100 pA current injection before and after the application of NMB. **(d2)**, expansion of the voltage transient shown in the box in **(d1)** to demonstrate NMB-induced enlargement of membrane time constant. **(d3)**, summary graph for membrane time constants before and after the application of NMB. **(e1-e4)**, activation of BB1 receptors excited CeL neurons through an inhibition of inwardly rectifying K^+ channels. **(e1)**, the voltage-step protocol used. Cells were held at -60 mV and stepped from -140 mV to -40 mV for 400 ms in 10 mV voltage intervals every 10 s . **(e2)**, representative currents elicited by the voltage-step protocol before and after bath application of NMB and the net currents acquired by subtraction. **(e3)**, I-V curves averaged from 13 cells before and after the application of NMB. **** $P < 0.0001$, two-way repeated-measures ANOVA followed by Šídák's multiple comparison test. **(e4)**, I-V curve of the net currents acquired by subtracting the currents in control condition from those after the application of NMB ($n = 13$). Adapted from [223].



measured within 5 ms before the end of the step voltage protocols. Under these circumstances, the currents recorded before and after the application of NMB showed inward rectification ($n = 13$, Figure 3, e2-e4), suggesting that Kir channels are expressed in CeL neurons. Subtraction of the current-voltage relationship in the control condition from that after the application of NMB displayed an inwardly rectified current-voltage curve ($n = 13$, Figure 3, e4). These results support that activation of the BB1 receptors excites CeL neurons by inhibiting Kir channels.

Micromolar concentrations (100 – 300 μM) of extracellular Ba^{2+} have been shown to block Kir channels by at least 80% [252-254]. Inclusion of 300 μM Ba^{2+} in the extracellular solution inhibited a current showing inward rectification ($n = 12$, $F_{(1,11)} = 39.65$, $P < 0.0001$, two-way repeated measures ANOVA followed by Šídák's multiple comparison test, Figure 4, a1-a3) suggesting that this concentration of Ba^{2+} inhibited Kir channels. In the presence of Ba^{2+} , application of NMB failed to elicit more currents significantly ($n = 12$, $F_{(1,11)} = 0.276$, $P = 0.61$, two-way repeated measures ANOVA followed by Šídák's multiple comparison test, Figure 4, a4-a6), demonstrating that NMB-induced excitation of CeL neurons is mediated by depression of Ba^{2+} -sensitive Kir channels.

GIRK Channels are Involved in BB1 Receptor-Mediated Excitation of CeL Neurons

We aimed at identifying the subtype of Kir channels involved in NMB-mediated facilitation of neuronal excitability. Kir channels are divided into four functional groups: 1) the constitutively active Kir2 subfamily channels including Kir2.1, Kir2.2, Kir2.3, and Kir2.4; 2) the G protein-gated GIRK (Kir3 subfamily) channels consisting of Kir3.1 (GIRK1), Kir3.2 (GIRK2), Kir.3.3 (GIRK3), Kir3.4 (GIRK4); 3) the ATP-sensitive K^+ (K_{ATP}) channels comprising Kir6.1 and Kir6.2; 4) K^+ transport channels involving Kir1.1, Kir4.1, Kir.4.2, and Kir7.1 [255]. We tested the role of the Kir2 subfamily channels in

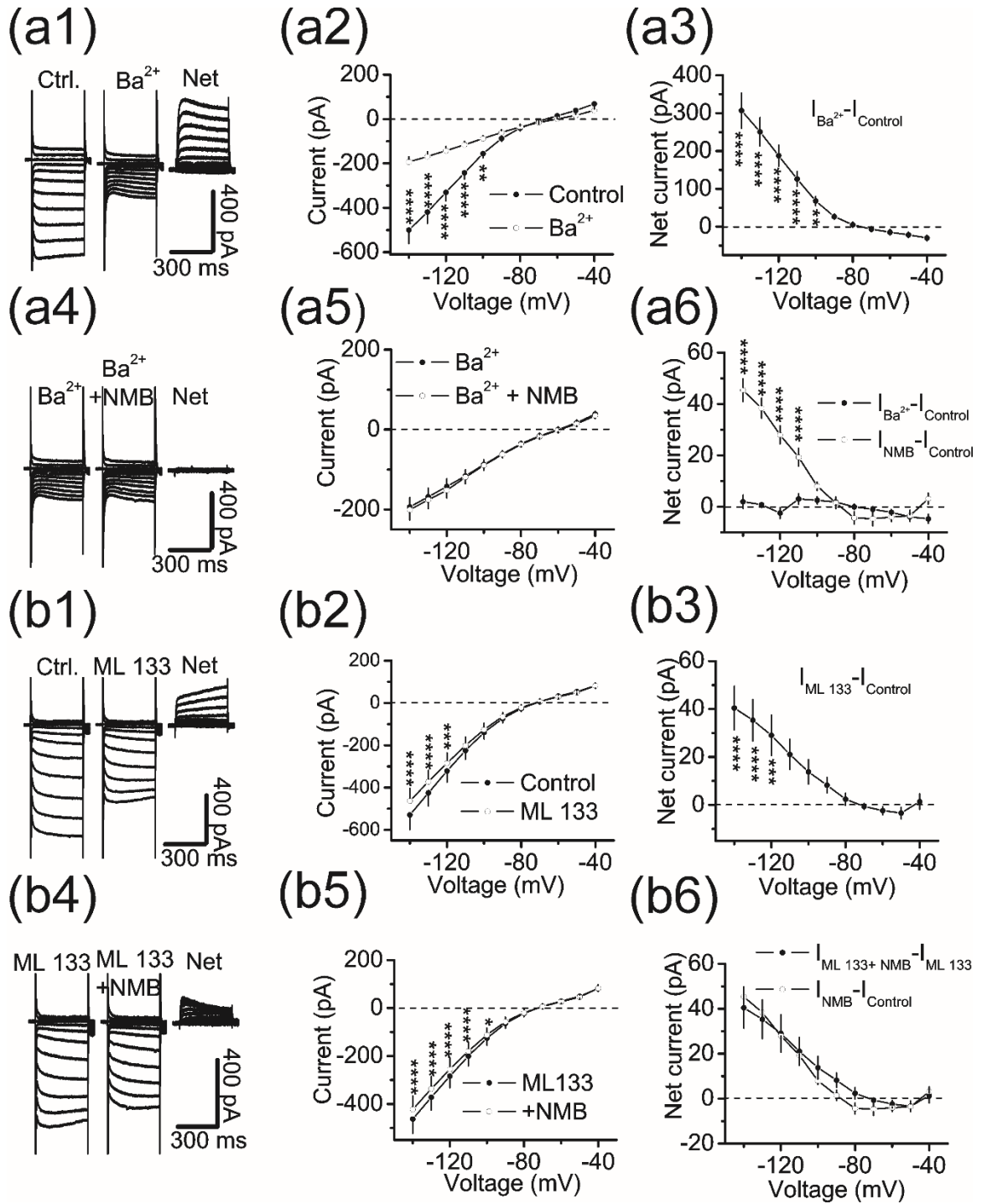
NMB-elicited depression of Kir channels by utilizing the selective Kir2 channel blocker, ML 133 (30 μ M) [256-260]. Bath application of ML 133 alone induced a significant inhibition of Kir currents from -120 to -140 mV ($n = 12$, $F_{(1,11)} = 7.288$, $P = 0.021$, two-way repeated measures ANOVA followed by Šídák's multiple comparison test, Figure 4, b1-b3). In the presence of ML 133, application of NMB still significantly depressed Kir currents at potentials -100 to -140 mV ($n = 12$, $F_{(1,11)} = 12.40$, $P = 0.005$, two-way repeated measures ANOVA followed by Šídák's multiple comparison test, Figure 5, b4-b6). Current-voltage responses elicited in the presence of ML 133 and NMB were significantly different from those obtained in CeL neurons treated with NMB alone ($F_{(1,253)} = 4.439$, $P = 0.036$, two-way ordinary ANOVA followed by Šídák's multiple comparison test, Figure 4, b6), but did not differ significantly at any recorded voltages according to post-hoc analysis. Together, these results suggest that the Kir2 subfamily channels are not involved in the NMB-mediated excitation of CeL neurons.

We further probed the role of GIRK channels in NMB-mediated inhibition of Kir channels. GIRK1 channels are strongly expressed in the BLA and cortical nuclei with low expression in the CeA [261]. Bath application of ML 297 (10 μ M), an activator of GIRK1-containing channels [262] failed to significantly affect Kir currents ($n = 9$, $F_{(1,8)} = 0.674$, $P = 0.44$, two-way repeated measures ANOVA followed by Šídák's multiple comparison test, Figure 5, a1-a3), suggesting that there were no functional GIRK1 channels in the CeL neurons and NMB-elicited excitation of CeL neurons was unlikely to be mediated by depressing GIRK1 channels.

We then used tertiapin-Q (TQ), a blocker for GIRK ($K_i = 13.3$ nM) and Kir1.1 ($K_i = 1.3$ nM) channels [263-265]. Bath application of TQ (250 nM) by itself depressed a current displaying inward rectification ($n = 10$, $F_{(1,9)} = 23.16$, $P = 0.001$, two-way

Figure 4. NMB-mediated inhibition of Kir currents is Ba²⁺-sensitive but insensitive to the Kir2 subfamily blocker ML 133.

(**a1-a6**), bath application of Ba²⁺ (300 μM) alone inhibited Kir channel currents and blocked NMB-elicited inhibition of Kir channel currents. (**a1**), currents evoked by the voltage-step protocol before (*left*) and during (*middle*) the application of Ba²⁺ (300 μM) and the net currents acquired by subtraction (*right*). (**a2**), I-V curves of the currents elicited by the voltage-step protocol before and during the application of Ba²⁺. **** $P < 0.0001$, ** $P < 0.01$. (**a3**), Net currents acquired by subtraction of the currents recorded in the control condition from those recorded from the same cell in the presence of Ba²⁺ (n = 12). Note that the Ba²⁺-sensitive currents showed inward rectification. (**a4**), currents recorded from a CeL neuron in response to the voltage-step protocol in the presence of Ba²⁺ alone (*left*) and Ba²⁺ plus NMB (*middle*). The net currents acquired by subtraction were shown in the right panel. (**a5**), I-V curves of the currents elicited by the voltage-step protocol in the presence of Ba²⁺ alone and Ba²⁺ plus NMB (n = 12). (**a6**), Net currents acquired by subtracting the currents in the presence of Ba²⁺ alone from those recorded from the same cell in the presence of Ba²⁺ plus NMB. NMB-elicited net currents in the control condition (green circles) were co-plotted as a comparison. (**b1-b6**), bath application of ML 133 (30 μM), a blocker of Kir2 subfamily channels, by itself inhibited Kir currents, but failed to block NMB-mediated inhibition of Kir currents. (**b1**), currents elicited by the voltage-step protocol before (*left*) and during (*middle*) the application of ML 133 (30 μM). The net currents inhibited by ML 133 were shown on the right. (**b2**), I-V curves of the currents elicited by the voltage-step protocol before and during the application of ML 133 (n = 12). (**b3**), net currents acquired by subtraction of the currents in the control condition from those recorded from the same cell in the presence of ML 133. Note that the ML133-sensitive currents displayed inward rectification. (**b4**), current traces recorded from a CeL neuron in response to the voltage-step protocol in the presence of ML 133 (*left*) and ML 133 plus NMB (*middle*) and the net current acquired via subtraction (*right*). (**b5**), I-V curves of the currents generated by the voltage-step protocol in the presence of ML 133 alone and ML 133 plus NMB (n = 12). (**b6**), net currents acquired by subtraction of currents recorded from CeL neurons in the presence of ML 133 from those in the presence of ML 133 plus NMB. Net currents elicited by NMB in control condition without application of ML133 were co-plotted for comparison. **** $P < 0.0001$, *** $P < 0.001$, ** $P < 0.01$, * $P < 0.05$, two-way repeated measures ANOVA followed by Šídák's multiple comparison test. Adapted from [223].



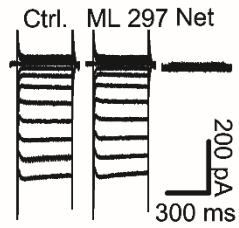
repeated measures ANOVA followed by Šídák's multiple comparison test, Figure 5, b1-b3). There were significant differences in the current-voltage curve before and during the application of TQ at a voltage range from -100 to -140 mV ($n = 10$, Figure 5, b1-b3), suggesting that CeL neurons express functional GIRK channels. Whereas application of NMB in the presence of TQ still significantly depressed Kir currents ($F_{(1,9)} = 24.95$, $P = 0.0007$, two-way repeated measures ANOVA followed by Šídák's multiple comparison test, Figure 5, b4-b6), the NMB-elicited depression of Kir currents in the presence of TQ was significantly smaller at -130 mV and -140 mV compared with the effect of NMB in the control condition [263-265] (Figure 5, b6). These results together indicate that NMB-induced excitation of CeL neurons occurred at least partially through the depression of GIRK channels.

Because TQ inhibits both GIRK and Kir1.1 channels [263-265], we probed the potential involvement of Kir1.1 channels in NMB-induced inhibition of Kir currents. Bath application of the selective Kir1.1 channel blocker, tertiapin-LQ (100 nM), which lacks effects on GIRK channels [266], failed to alter significantly the voltage-current relationship ($n = 7$, $F_{(1,6)} = 1.582$, $P = 0.255$, two-way repeated measures ANOVA, Figure 5, c1-c3), suggesting that CeL neurons do not express functional Kir1.1 channels. Application of NMB in the continuous presence of tertiapin-LQ still inhibited a comparable extent of Kir currents ($n = 7$, $F_{(1,6)} = 31.59$, $P = 0.001$, two-way repeated measures ANOVA followed by Šídák's multiple comparison test, Figure 5, c4-c6). The NMB-induced depression of Kir currents in the presence of tertiapin-LQ was not significantly different from that in the control condition at all voltages tested ($F_{(1,18)} = 2.437$, $P = 0.14$, two-way ordinary ANOVA, Figure 5, c6). These data suggest a lack of involvement of Kir1.1 channels in NMB-elicited depression of Kir currents. Together, these data suggest that activation of the BB1 receptor excites CeL neurons through the inhibition of GIRK channel.

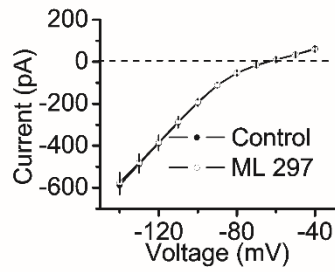
Figure 5. GIRK channels are involved in NMB-elicited depression of Kir channel currents.

(**a1-a3**), application of ML 297, the GIRK1-containing channel activator, failed to alter Kir currents. (**a1**), currents recorded from a CeL neuron in response to the voltage-step protocol before (*left*) and during (*middle*) the application of ML 297 (10 μ M) and the net current acquired by subtraction (*right*). (**a2**), I-V curves of the currents elicited by the voltage-step protocol before and during the application of ML 297 (n = 9). (**a3**), net currents acquired by subtracting the currents in the control condition from those recorded from the same cells in the presence of ML 297. Application of ML 297 did not significantly affect Kir currents at each voltage. (**b1-b6**), bath application of tertiapin-Q (TQ) by itself inhibited Kir currents and significantly depressed NMB-mediated inhibition of Kir currents. (**b1**), currents recorded from a CeL neuron in response to the voltage-step protocol before (*left*) and during (*middle*) the bath application of TQ (250 nM) and the net current generated by subtraction (*right*). (**b2**), I-V curves of the currents elicited by the voltage-step protocol before and during the application of TQ (n = 10). (**b3**), net currents generated by subtracting the currents in the control condition from those recorded from the same neurons in the presence of TQ. TQ-sensitive currents displayed inward rectification. (**b4**), currents recorded from a CeL neuron in response to the voltage-step protocol in the presence of TQ alone (*left*) and TQ plus NMB (*middle*) and the net current acquired by subtraction (*right*). (**b5**), I-V curves of the currents elicited by the voltage-step protocol in the presence of TQ or TQ + NMB (n = 10). (**b6**), net currents acquired by subtracting the currents in the presence of TQ alone from those recorded from the same cells in the presence of TQ plus NMB. NMB-elicited net currents in the control condition (green circles) were co-plotted as a comparison. Note that TQ significantly reduced NMB-elicited depression of Kir currents at -130 mV and -140 mV. ** $P < 0.01$, ordinary two-way ANOVA. (**c1-c6**), bath application of tertiapin-LQ (T-LQ) alone did not alter Kir currents and failed to significantly change NMB-mediated inhibition of Kir currents. (**c1**), currents recorded from a CeL neuron in response to the voltage-step protocol before (*left*) and during (*middle*) the application of T-LQ (100 nM) and the net current acquired by subtraction (*right*). (**c2**), I-V curves of the currents elicited by the voltage-step protocol before and during the application of T-LQ (n = 7). (**c3**), net currents acquired by subtracting the currents in the control condition from those recorded from the same cells in the presence of T-LQ. T-LQ failed to alter Kir currents at each voltage. (**c4**), currents recorded from a CeL neuron in response to the voltage-step protocol in the presence of T-LQ alone (*left*) and T-LQ plus NMB (*middle*) and the net current acquired by subtraction (*right*). (**c5**), I-V curves of the currents elicited by the voltage-step protocol in the presence of T-LQ and T-LQ + NMB (n = 7). (**c6**), net currents acquired by subtracting the currents in the presence of T-LQ alone from those recorded from the same cells in the presence of T-LQ plus NMB. NMB-sensitive net currents in control conditions were co-plotted for comparison. Application of T-LQ failed to significantly alter the NMB-induced depression of Kir currents. **** $P < 0.0001$, *** $P < 0.001$, ** $P < 0.01$, * $P < 0.05$, two-way repeated measures ANOVA followed by Šídák's multiple comparison test. Adapted from [223].

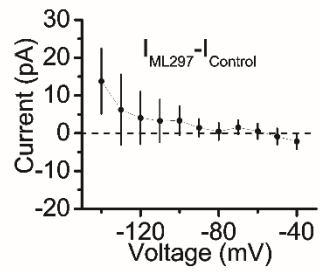
(a1)



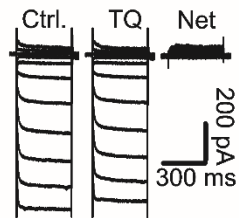
(a2)



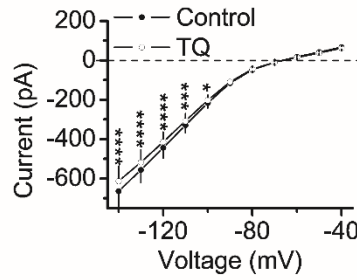
(a3)



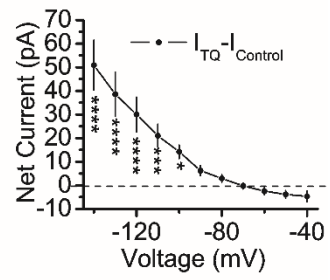
(b1)



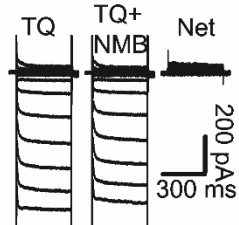
(b2)



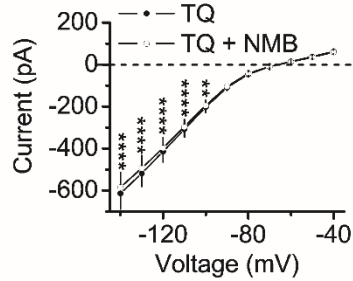
(b3)



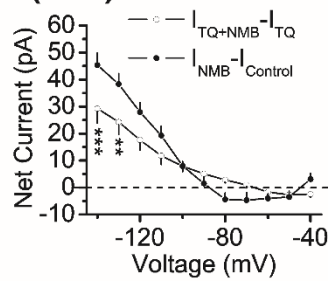
(b4)



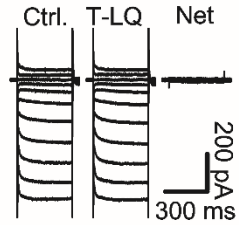
(b5)



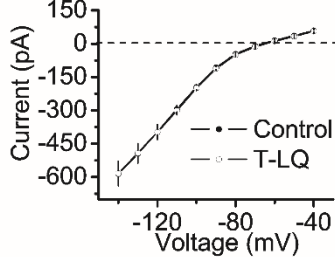
(b6)



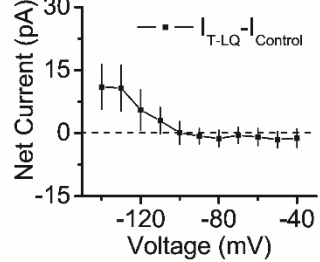
(c1)



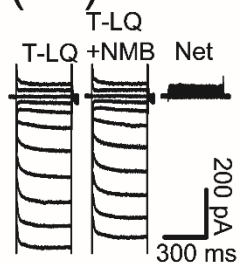
(c2)



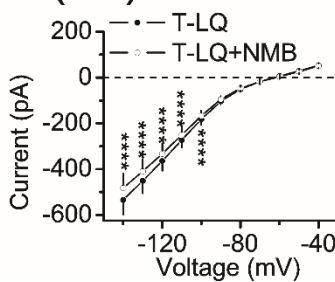
(c3)



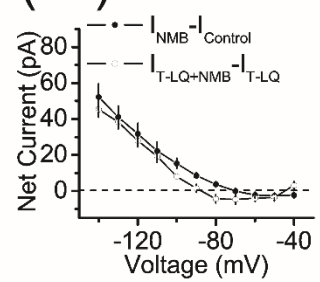
(c4)



(c5)



(c6)



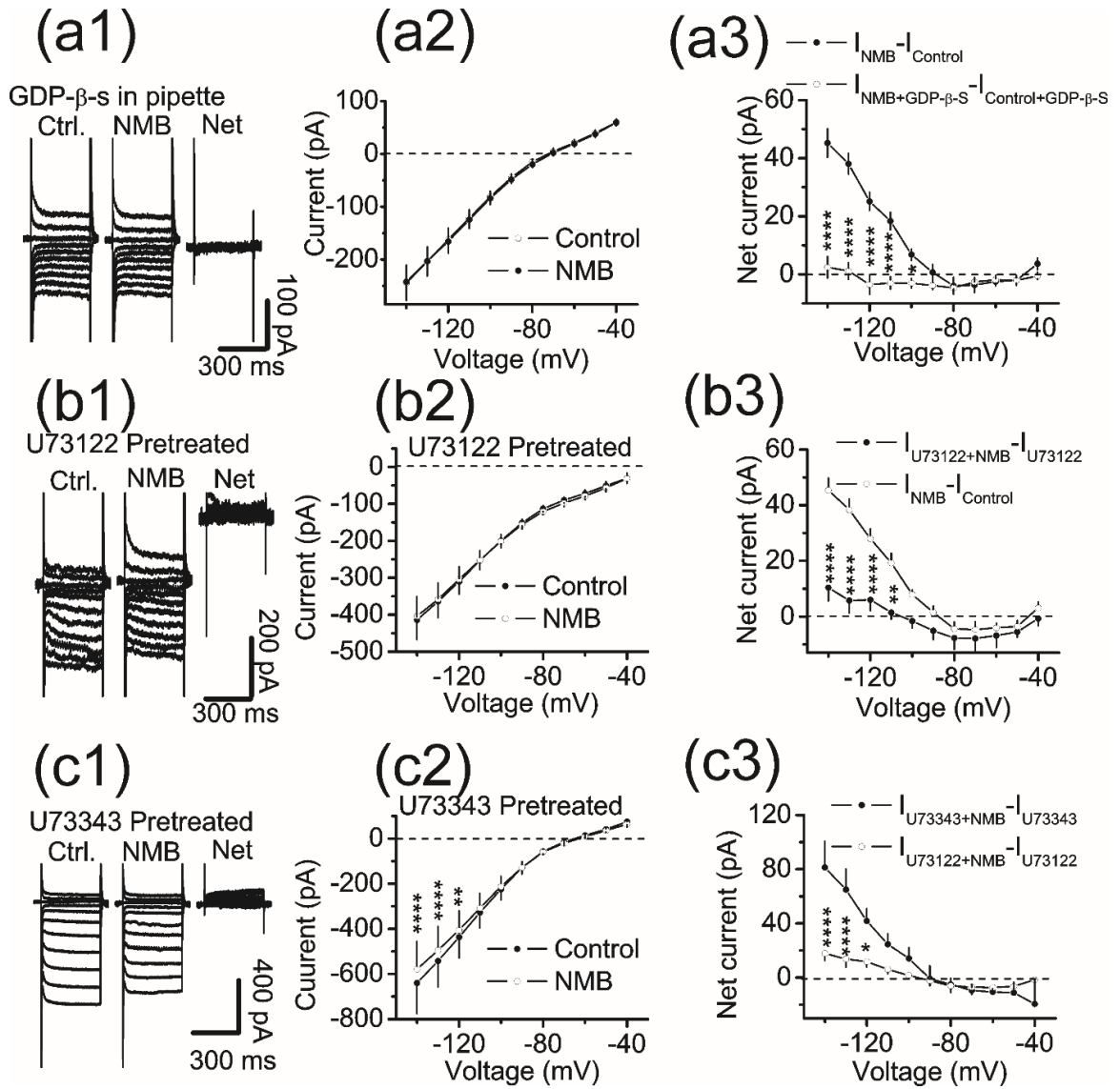
G proteins, PLC β and PKC are Required for BB1 Receptor-Mediated Depression of Kir Channels

As our results indicated that activation of BB1 receptors excited CeL neurons by depressing the GIRK type of the Kir channels, we further tested the roles of G proteins, PLC β and PKC in NMB-mediated inhibition of Kir channel currents. Inclusion of GDP- β -S (0.5 mM) in the intracellular recording solution blocked NMB-induced depression of Kir currents ($n = 14$, $F_{(1,13)} = 1.539$, $P = 0.24$, two-way repeated measures ANOVA followed by Šídák's multiple comparison test, Figure 6, a1-a3). Additionally, pretreatment of slices with the PLC β inhibitor U73122 (5 μ M) significantly reduced NMB-induced depression of Kir currents ($n = 15$, $F_{(1,14)} = 0.144$, $P = 0.71$, two-way repeated measures ANOVA, Figure 6, b1-b3), compared with the effect of NMB in slices pretreated with the inactive analog, U73343 (5 μ M, $n = 5$, $F_{(1,4)} = 22.22$, $P = 0.009$, two-way repeated measures ANOVA followed by Šídák's multiple comparison test, Figure 6, c1-c3). These results demonstrate that the activity of PLC β is required for NMB-mediated depression of Kir channels in the CeL.

We then explored the role of PKC in NMB-induced depression of Kir currents. Slices were pretreated with Bis II (1 μ M), a selective PKC inhibitor, and the same concentration of Bis II was continuously bath-applied in the extracellular solution. Bath application of NMB in this condition failed to significantly alter Kir channel currents at all voltages recorded ($n = 12$, $F_{(1,11)} = 0.032$, $P = 0.86$ two-way repeated measures ANOVA, Figure 7, a1-a3). Compared with NMB-mediated depression in the control condition, slices treated with Bis II elicited significantly smaller currents ($F_{(1,253)} = 94.63$, $P < 0.0001$ vs. NMB-alone, ordinary two-way ANOVA, Figure 7, a3), supporting a functional requirement of PKC in NMB-mediated depression of Kir channels.

Figure 6. G proteins and PLC β are involved in BB1 receptor-mediated depression of Kir channels.

(**a1-a3**), intracellular dialysis of GDP- β -S (0.5 mM) via the recording pipettes blocked NMB-elicited inhibition of Kir currents. (**a1**), currents recorded from a CeL neuron in response to the voltage-step protocol before (*left*) and during (*middle*) the application of NMB in the presence of GDP- β -S and the net current generated by subtraction (*right*). (**a2**), I-V curves of the currents elicited by the voltage-step protocol before and during the application of NMB (n = 14). (**a3**), net currents generated by subtracting the currents in control conditions from those recorded from the same neurons during the bath application of NMB with GDP- β -S in the recording pipettes. Note that inclusion of GDP- β -S in the recording pipettes blocked NMB-elicited depression of Kir currents. (**b1-b3**), pretreatment of slices with the selective PLC inhibitor, U73122 (5 μ M), significantly depressed NMB-elicited Kir currents. (**b1**), currents recorded from a CeL neuron in response to the voltage-step protocol before (*left*) and during (*middle*) the application of NMB in a slice pretreated with U73122 and the net currents acquired by subtraction (*right*). (**b2**), I-V curves of the currents generated by the voltage-step protocol before and during the bath application of NMB (n = 15). (**b3**), net currents acquired by subtracting the currents in control conditions from those during the bath application of NMB from the same neurons in slices pretreated with U73122. Note that pretreatment of slices with U73122 significantly attenuated NMB-mediated depression of Kir currents. (**c1-c3**), bath application of NMB in slices pretreated with the inactive analog U73343 (5 μ M), still significantly depressed Kir currents. (**c1**), currents recorded from a CeL neuron in response to the voltage-step protocol before (*left*) and during (*middle*) the application of NMB in a slice pretreated with U73343 and the net current acquired by subtraction (*right*). (**c2**), I-V curves of the currents recorded from the same neurons before and during the application of NMB (n = 5) in slices pretreated with U73343. (**c3**), net currents acquired by subtracting the currents in control conditions from those during the application of NMB from the same neurons in slices pretreated with U73343. Note that bath application of NMB still significantly depressed Kir currents. **** $P < 0.0001$, *** $P < 0.001$, ** $P < 0.01$, * $P < 0.05$, two-way repeated measures ANOVA followed by Šídák's multiple comparison test. Adapted from [223].



Similarly, bath application of a PKC activator, PMA (1 μ M), significantly inhibited Kir currents ($n = 13$, $F_{(1,12)} = 12.97$, $P = 0.004$, two-way repeated measures ANOVA followed by Šídák's multiple comparison test, Figure 7, b1-b3). The PMA-mediated depression was significantly reduced in slices pretreated with Bis II (1 μ M, $n = 12$, $F_{(1,11)} = 1.797$, $P = 0.21$, two-way repeated measures ANOVA, Figure 7, c1-c3). These results further support the involvement of PKC in NMB-mediated depression of Kir channels. Lastly, we determined the effects of intracellular Ca^{2+} levels on NMB-elicited inhibition of Kir channels. Intracellular perfusion of BAPTA (10 mM) via the recording pipettes significantly attenuated NMB-elicited depression of Kir currents ($F_{(1,286)} = 25.88$, $P < 0.0001$ vs. NMB alone, ordinary two-way ANOVA, Figure 7, d1-d3), supporting the involvement of the Ca^{2+} -dependent PKC isoform in NMB-mediated inhibition of Kir channels.

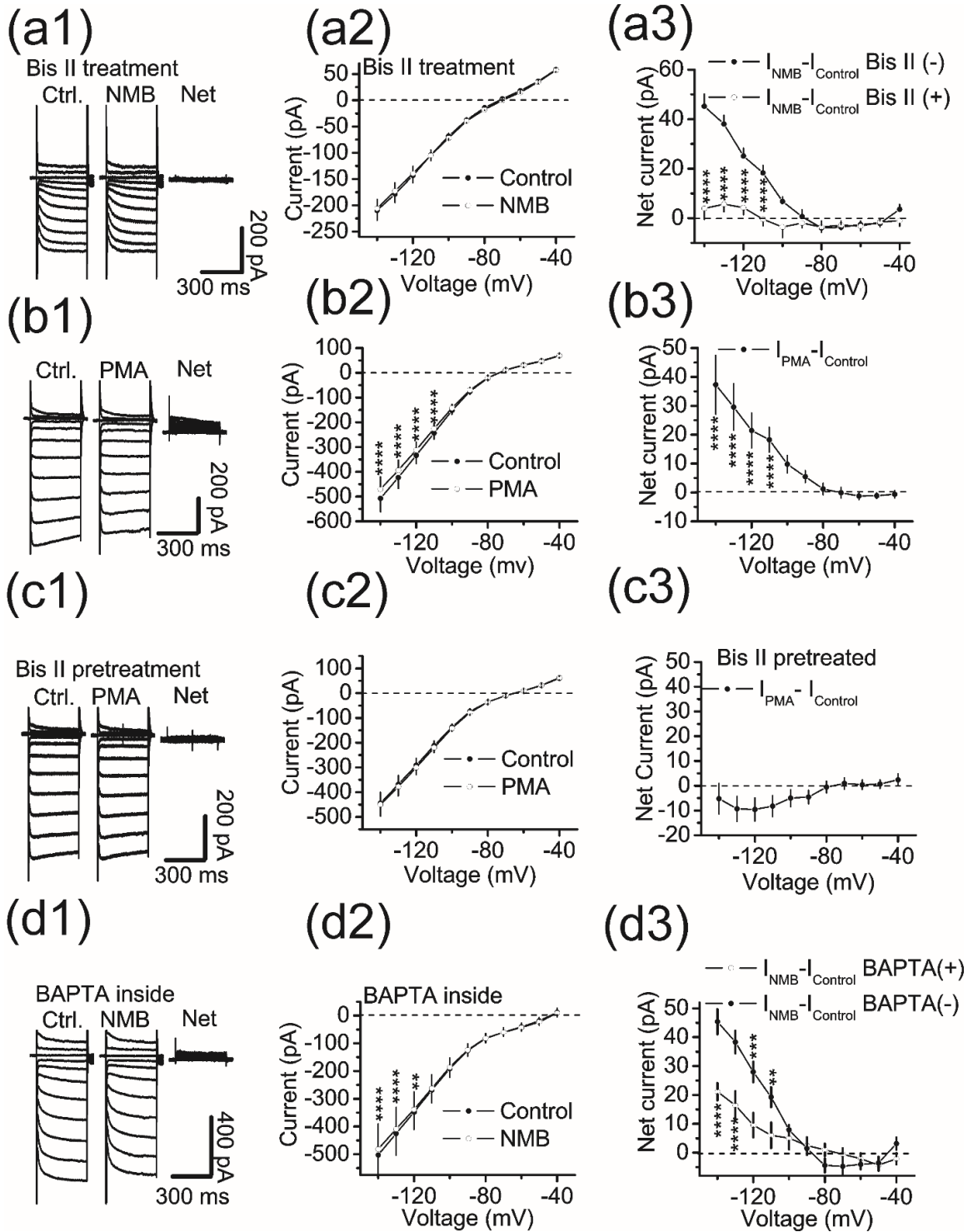
BB1 Receptor-Mediated Excitation of CeL Neurons Promotes Inhibitory Cardiovascular Responses

The distinct CeA projections to the brainstem involved in the alterations of cardiac output in response to emotionally relevant stimuli are not completely understood [71-74]. As bombesin receptors are implicated in cardiovascular responses, we tested the roles of BB1 receptor-mediated excitation of CeA neurons in modulation of cardiac function. Guide cannulae were bilaterally implanted into the CeA and NMB and/or other compounds were microinjected into the CeA to probe the effects of BB1 receptor activation on mean arterial pressures (MAP; mmHg) and heart rate (HR; bpm) (Figure 8, a & c). There were no significant differences in baseline cardiovascular responses between groups ($F_{(2.4, 24.3)} = 2.76$, $P = 0.07$, mixed-effect two-way ANOVA). A two-way ANOVA revealed saline injection did not significant effect any cardiovascular parameters

Figure 7.

PKC is involved in NMB-induced depression of Kir channels.

(**a1-a3**), pretreatment of slices with and continuous bath application of the selective PKC inhibitor, Bis II (1 μ M), blocked NMB-mediated inhibition of Kir currents at each voltage. (**a1**), currents recorded from a CeL neuron elicited by the voltage-step protocol before (*left*) and during (*middle*) the application of NMB in a slice treated with Bis II and the net currents acquired by subtraction (*right*). (**a2**), I-V curves of the currents generated by the voltage-step protocol before and during the application of NMB (n = 12) recorded from the same neurons in slices treated with Bis II. Note that application of Bis II blocked NMB-induced depression of Kir currents at each voltage. (**a3**), net currents acquired by subtracting the currents in control conditions from those during the application of NMB recorded from the same neurons in slices treated with Bis II. NMB-induced net currents in control conditions without Bis II were co-plotted for comparison (green circles). (**b1-b3**), application of the PKC activator, PMA (1 μ M), inhibited Kir currents. (**b1**), current traces recorded from a CeL neuron elicited by the voltage-step protocol before (*left*) and during (*middle*) the application of PMA and the net current acquired by subtraction (*right*). (**b2**), I-V curves generated by the voltage-step protocol before and during the application of PMA (n = 13). Note that PMA significantly attenuated Kir currents. (**b3**), net currents produced by subtracting the currents in control conditions from those recorded from the same cells during the application of PMA. (**c1-c3**), pretreatment of slices with and continuous bath application of Bis II blocked PMA-mediated depression of Kir currents. (**c1**), currents recorded from a CeL neuron in response to the voltage-step protocol before (*left*) and during (*middle*) the bath application of PMA in a CeL neuron treated with Bis II and the net current acquired by subtraction (*right*). (**c2**), I-V curves of the currents generated by the voltage-step protocol before and during the bath application of PMA (n = 12) in slices treated with Bis II. (**c3**), net currents acquired by subtracting the currents in control conditions from those during the application of PMA recorded from the same neurons in slices treated with Bis II. (**d1-d3**), intracellular application of the Ca²⁺ chelator BAPTA (10 mM) via the recording pipettes significantly reduced NMB-mediated depression of Kir currents. (**d1**), currents recorded from a CeL neuron in response to the voltage-step protocol before (*left*) and during (*middle*) the application of NMB with the intracellular solution containing BAPTA and the net current acquired by subtraction (*right*). (**d2**), I-V curves of the currents generated by the voltage-step protocol before and during the application of NMB (n = 15) with the intracellular solution containing BAPTA. (**d3**), net currents acquired by subtracting the currents in control conditions from those during the bath application of NMB from the same neurons with the intracellular solution containing BAPTA. NMB-elicited net currents in control conditions without BAPTA were co-plotted for comparison (green circles). **** $P < 0.0001$, *** $P < 0.001$, ** $P < 0.01$, * $P < 0.05$, two-way repeated measures ANOVA followed by Šidák's multiple comparison test. Adapted from [223].



(Treatment: $F_{(1,10)} = 0.007$, $P = 0.933$, two-way ANOVA). Microinjection of NMB produced a significant dose-dependent reduction in MAP ($F_{(3,39)} = 6.21$, $P = 0.0015$, one-way ANOVA; saline vs. 0.3 nmol NMB: $P = 0.035$; saline vs. 1 nmol NMB: $P = 0.0005$ via Dunnett's multiple comparisons test, Figure 9, a1, Table 1) and HR ($F_{(3,39)} = 7.55$, $P = 0.0004$, one-way ANOVA; saline vs. 0.1 nmol: $P = 0.006$; saline vs. 0.3 nmol NMB: $P = 0.0001$ Dunnett's multiple comparisons test, Figure 9, a2, Table 1). The effects of NMB were not sex-dependent, as comparison of MAP ($F_{(1,35)} = 0.198$, $P = 0.66$) or HR ($F_{(1,35)} = 0.961$, $P = 0.33$) from male and female rats showed no significant differences (Two-way ordinary ANOVA). The IC_{50} value was calculated to be 0.362 nmol, we therefore used 0.3 nmol NMB for the remaining *in vivo* experiments.

We then tested the involvement of BB1 receptors in NMB-mediated depression of MAP and HR by microinjection of the selective BB1 receptor antagonist BIM23042 (0.3 nmol) [250]. Application BIM23042 by itself had no significant effect on MAP ($P > 0.99$) or HR ($P = 0.85$). However, prior microinjection of BIM23042 prevented NMB-induced depression of MAP ($P = 0.99$, one-way ANOVA followed by Tukey's multiple comparisons test, Figure 9, a3) and HR ($P = 0.99$, one-way ANOVA followed by Tukey's multiple comparisons test, Figure 9, a4), corroborating the involvement of BB1 receptors.

Our *in vitro* results indicate that activation of BB1 receptors excites CeL neurons by depressing GIRK channels. We further probed the roles of GIRK channels in NMB-mediated suppression of MAP and HR. TQ is a selective GIRK channel inhibitor that effectively inhibits GIRK channels in picomolar range [267, 268]. Bilateral microinjection of TQ (250 pmol) by itself had no significant effects on MAP ($P = 0.97$) and HR ($P = 0.77$), but blocked NMB-elicited depression of MAP ($P = 0.96$, one-way ANOVA followed by Tukey's multiple comparisons test, Figure 9, a3) and HR ($P = 0.80$, one-way ANOVA followed by Tukey's multiple comparisons test, Figure 9, a4), indicating that GIRK channels are required for NMB-mediated depression of MAP and HR.

BB1 Receptor Activation Augments ASR but Attenuates FPS

The microcircuits of the CeA are involved in fear processing [74, 141, 269] and send projections to brainstem nuclei involved in fear expression and cardiovascular responses [74]. Whereas NMB and its receptor have been implicated in stress responses [239, 270-272], the effect of NMB on fear expression remain less understood [273-276]. FPS is a translatable paradigm used to measure the acquisition and expression of conditioned fear responses in both rodents and humans [277-279]. Taking advantage of a simple reflex (ASR), FPS measures conditioned fear by an increase in the amplitude of ASR in the presence of a previously paired cue with a foot shock. We probed the effects of BB1 receptor activation on both ASR and FPS by microinjecting NMB or saline into the CeA (Figure 8, b, c). Microinjection of NMB (0.3 nmol) into the CeA significantly augmented ASR to the 105 dB WNB compared to the rats injected with saline (0.9 % NaCl) (NMB: 1013.77 ± 214.88 ; Saline: 599.19 ± 92.10 arbitrary units, $n = 11$, $P = 0.0204$, Šídák's multiple comparisons test, Figure 9, b1). These results were independent of the sex of the rat ($F_{(1,54)} = 3.39$, $P = 0.07$). Furthermore, microinjection of NMB into the CeA (0.3 nmol) significantly reduced FPS responses to cue stimuli ($P = 0.004$, Šídák's multiple comparisons test, Figure 9, b2), with no significant effects on baseline ($P = 0.976$, Šídák's multiple comparisons test, Figure 9, b2) or non-cued responses ($P = 0.906$, Šídák's multiple comparisons test, Figure 9, b2). Microinjection of NMB into the CeA prior to fear conditioning had no significant effect on shock reactivity ($P = 0.57$, Mann-Whitney test, Figure 9, b3). Moreover, the shock reactivity amplitudes measured between male and female rats injected with saline ($P = 0.22$) or NMB ($P = 0.98$) were not significantly different, suggesting that the alterations in FPS were independent of aversive stimuli or sex of the animal. A working model of the findings of Study 1 is shown in Figure 26.

Figure 8. Schematic diagram showing the cardiovascular recording, ASR and FPS procedures and cannula placement.

(a), For recording cardiovascular parameters, animals received daily handling to habituate them to the experimental procedure for at least 7 days. Baseline measurements were recorded for 2 days. Cardiovascular parameters were recorded during and for at least 15 min after the injection (*top*). (b), In the acoustic startle response (ASR) experiments, rats were given intra-CeA saline (1 μ L in each side) or NMB (0.3 nmol in 1 μ L) 10 mins prior to the test session (*middle*). In fear-potentiated startle (FPS) experiments (*bottom*), rats were given intra-CeA saline or NMB 10 mins prior to the fear conditioning session. FPS measured as cued or non-cued fear responses were tested 24 h later. (c), cannula tip placement in a subset of experiments displayed onto an atlas figure adapted from Paxinos and Watson [221]; White arrow denotes the cannula tip placement. Adapted from [223].

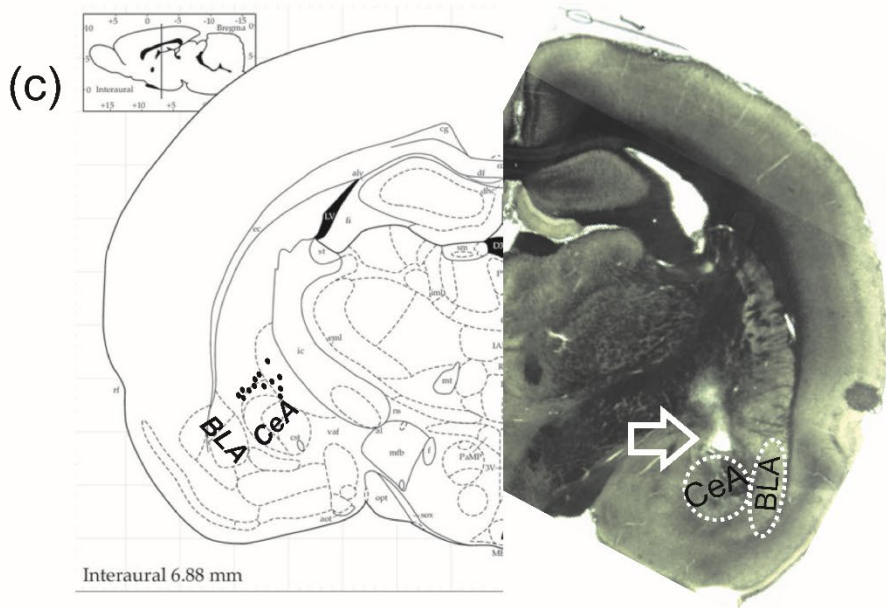
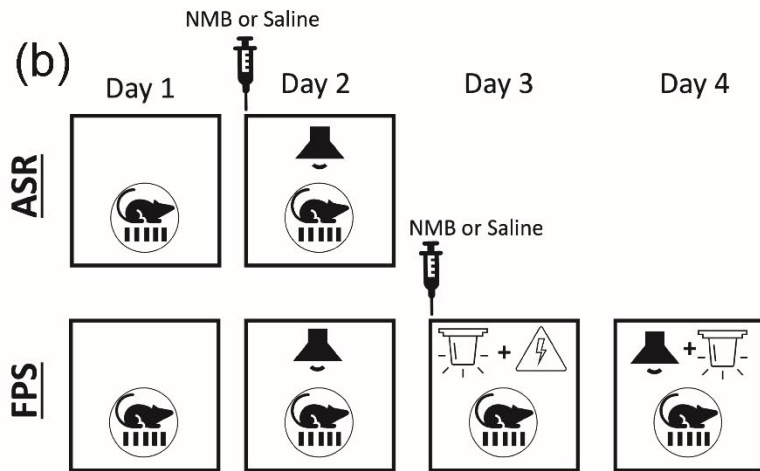
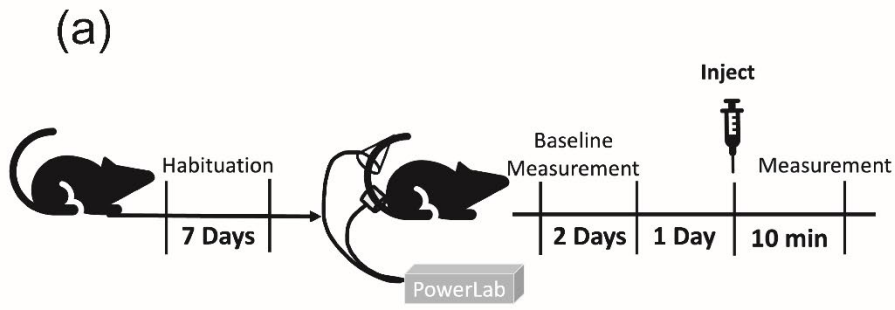
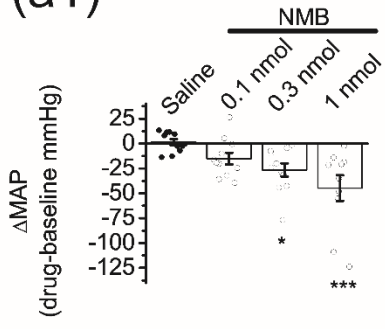


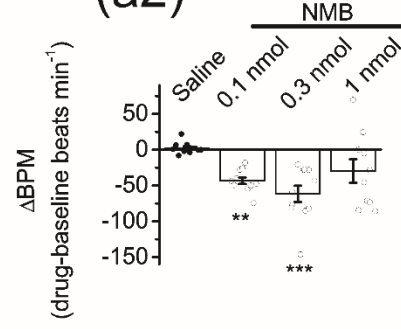
Figure 9. BB1 receptor activation in the CeA reduces cardiovascular output and affects ASR and FPS.

(a1-a4) Microinjection of NMB into the CeA lowered MAP and reduced HR through inhibition of GIRK channels. **(a1)**, NMB dose-dependently reduced MAP, and **(a2)** HR. * $P < 0.05$, ** $P < 0.01$, *** $P < 0.001$ vs saline (one-way ANOVA followed by Dunnett's test). The circles and triangles represent data obtained from male and female rats, respectively. **(a3)**, microinjection of NMB (0.3 nmol) into the CeA reduced MAP, whereas prior administration of the BB1 receptor antagonist, BIM 23042 (0.3 nmol) or GIRK channel blocker, TQ (250 pmol) blocked NMB-mediated depression of MAP. **(a4)**, microinjection of NMB (0.3 nmol) into the CeA produced bradycardia, whereas prior microinjection of the BB1 receptor antagonist, BIM 23042 (0.3 nmol) or GIRK channel blocker, TQ (250 pmol) blocked NMB-induced bradycardia. *** $P < 0.01$, **** $P < 0.0001$ (one-way ANOVA followed by Dunnett's test), **n. s.**, no significance (Tukey's test). **(b1-b3)**, microinjection of NMB increased ASR while reducing FPS. **(b1)**, microinjection of NMB (0.3 nmol) into the CeA enhanced ASR to the 105 dB WNB without altering ASR to the 90 dB or 95 dB WNBs. ** $P < 0.01$ (Two-way ANOVA followed by Šídák's multiple comparisons test). **(b2)**, application of NMB into the CeA prior to fear conditioning significantly reduced cued responses without effects on non-cued responses during the FPS testing session. ** $P < 0.01$ (Two-way ANOVA followed by Šídák's multiple comparisons test). **(b3)**, behavioral responses to foot shock on Day 3 did not differ significantly in response to NMB microinjection. The circles and triangles represent data obtained from male and female rats, respectively. Adapted from [223].

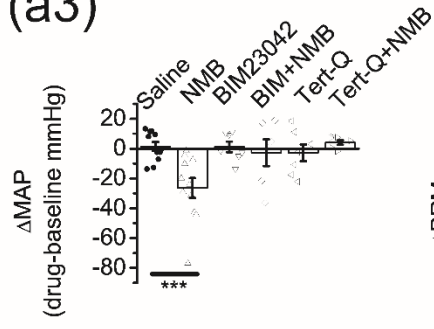
(a1)



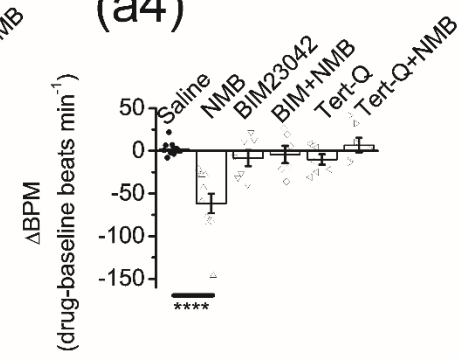
(a2)



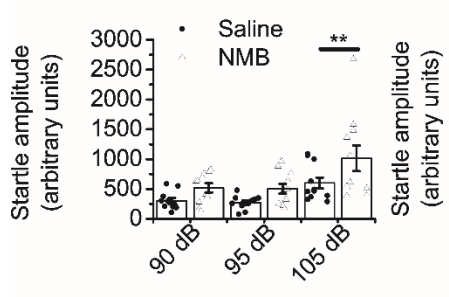
(a3)



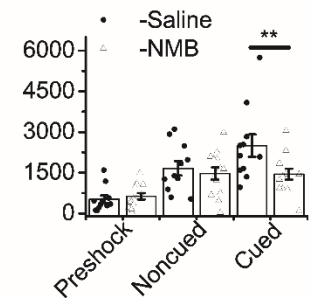
(a4)



(b1)



(b2)



(b3)

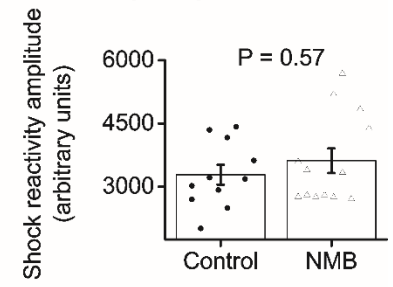


Table 1. Cardiovascular parameters Adapted from [223].

	Baseline mean (\pm SEM)	Neuromedin B (NMB) mean (\pm SEM)	<i>p</i> -value
Systolic (mmHg)	160.2 (4.8)	141.9 (3.7)	0.03
Diastolic (mmHg)	123.6 (5.0)	101.1 (4.4)	0.007
Mean arterial pressure (MAP) (mmHg)	136.5 (5.2)	110.1 (4.2)	0.001
Heart rate (HR) (bpm)	433.3 (13.8)	371.7 (8.4)	<0.001

Study 2- Activation of Bombesin-1 Receptors Excites the Principal Neurons in the Basolateral Amygdala by Multiple Signaling and Ionic Mechanisms

Introduction

Another target of bombesin-like peptides is the BLA which expresses NMB peptide and its mRNA [280], as well as high densities of bombesin-like peptide binding sites [242, 281, 282]. In line with the expression of bombesin-like peptide binding sites within the BLA, direct application of bombesin into the BLA reduces food intake and affects aversive memory [283, 284]. Bombesin-like peptide receptor activation in the BLA affects fear and anxiety-like behaviors [285, 286]. Elevations of NMB and GRP immunoreactivity are observed in the human brains of suicide patients supporting the involvement of bombesin-like peptides in neuropsychiatric disorders [275]. However, the effects of bombesin and bombesin-like peptides on neuronal excitability in the BLA and the underlying ionic and signaling mechanisms have not yet been determined. In Study 2, we investigated the effects of NMB on the excitability of BLA neurons based on the literature results showing that high densities of BB1 receptors are distributed in the BLA [287]. Using *in vitro* electrophysiological approaches in Sprague-Dawley (SD) rats and mutant mice, we showed that BB1 receptor activation excited BLA neurons through a PLC-mediated inhibition of GIRK channels and activation of TRPV1 channels; NMB increased glutamatergic transmission that is dependent on functional transient receptor potential vanilloid 1 (TRPV1) channels. Finally, microinjection of NMB into the BLA produced anxiogenic phenotypes in the Vogel Conflict Test in SD rats. Together, these results provide mechanistic insights into BB1 receptor activity in the BLA and further support the involvement of bombesin-like peptides in stress responses and anxiety disorders.

Activation of BB1 Receptors Excites BLA Principal Neurons

Because the BLA expresses high densities of bombesin-binding sites [288, 289] and BB1 receptor mRNA [290], we aimed to determine the functional outcome of NMB, a selective BB1 receptor agonist, on BLA neuronal excitability (Figure 10, A). The extracellular solution contained kynurenic acid (1 mM) to block glutamatergic transmission and picrotoxin (100 μ M) to block GABAergic transmission. The intracellular solution was the K⁺- gluconate-containing intracellular solution (see *Methods and Materials*). We bath applied a near-saturating concentration of the BB1 receptor agonist, NMB (0.3 μ M, see below), that resulted in subthreshold depolarizations (n = 18; Control: -64.6 ± 0.96 mV; NMB -61.2 ± 1.3 mV, P = 0.001, paired t-test; net depolarization: 2.82 mV, Figure 10. *Ba, Bb*). As the BLA neurons do not show spontaneous AP firing, we probed the effect of NMB on neuronal excitability by injecting a series of positive currents from 50 to 750 pA at an interval of 50 pA every 6 s prior to and after application of NMB when the maximal depolarization was obtained. Application of 0.3 μ M NMB significantly increased the number of APs elicited by the positive current injection protocol (n = 18, F_(1,17) = 26.06, P = 0.0001, two-way repeated-measures ANOVA followed by Šídák's multiple comparisons test; Figure 10. *Ca, Cb*). NMB increased AP firing in BLA neurons in slices cut from both male and female rats (Females: F_(1,6) = 7.275, P = 0.035, two-way repeated-measures ANOVA followed by Šídák's multiple comparisons test; males: F_(1,10) = 18.09, P = 0.0017, two-way repeated-measures ANOVA followed by Šídák's multiple comparisons test). NMB significantly reduced the rheobase current required to induce AP firing in BLA neurons (control: 200 ± 14 pA, NMB: 166.6 ± 14 pA, n = 18, P = 0.002, paired t-test, Figure 10. *Cc-Ce*) and reduced the delay time to the first AP waveform (Control: 161.6 ± 19.6 ms, NMB: 108.7 ± 7.3 ms, n = 18, P = 0.0003, Wilcoxon test, Figure 10. *Cf, Cg*). Enhanced BLA neuronal excitability

was not due to an alteration in AP waveform halfwidth (Control: 1.76 ± 0.25 ms, NMB: 1.29 ± 0.09 ms, $n = 18$, $P = 0.09$, Wilcoxon test, Figure 10. *Ch*). To assess the effect of NMB on passive membrane properties, current-clamped neurons were exposed to negative current injection sweeps from -50 to -200 pA with 50 pA steps for a duration of 600 ms before and after the application of NMB when the maximal effect was reached. The slope of the linearly fitted current-voltage (I-V) response was used to determine the input resistance, R_{in} . Bath application of NMB significantly increased the R_{in} (Control: 106.9 ± 16.9 M Ω , NMB: 208.0 ± 25.5 M Ω , $n = 18$, $P = 0.0006$, Wilcoxon test, Figure 10. *Da*). BLA neuron membrane time constants were obtained by fitting a single exponential function to a voltage transient elicited by the -200 pA current injection (100 ms from the end of baseline). Bath application of NMB significantly increased membrane time constants (Control: 17.4 ± 0.96 ms, NMB: 20.9 ± 1.9 ms, $n = 18$, $P = 0.004$, Wilcoxon test, Figure 10. *Db-Dd*). Together, these results suggest that NMB increases the excitability of principal BLA neurons.

Because NMB selectively activates BB1 receptors [291], and BB2 receptors are also expressed in the BLA [290], we confirmed the involvement of BB1 receptor activation in neuronal excitability. The slices were pretreated with the selective BB1 antagonist, BIM23042 (0.3 μ M) [292], and the same concentration of BIM23042 was included in the bath solution. Under these circumstances, bath application of NMB failed to significantly increase AP firing numbers ($n = 10$, $F_{(1,9)} = 2.671$, $P = 0.14$, two-way repeated measures ANOVA followed by Šídák's multiple comparison test, Figure 10. *Ea-Eb*), indicating that increased AP firing occurs via activation of BB1 receptors. Because bombesin activates both BB1 and BB2 receptors [293, 294], we pretreated slices with the selective BB2 receptor antagonist RC3095 (2 μ M) and the same concentration of RC3095 was present in the bath solution. Under these circumstances, bombesin-mediated excitation of BLA

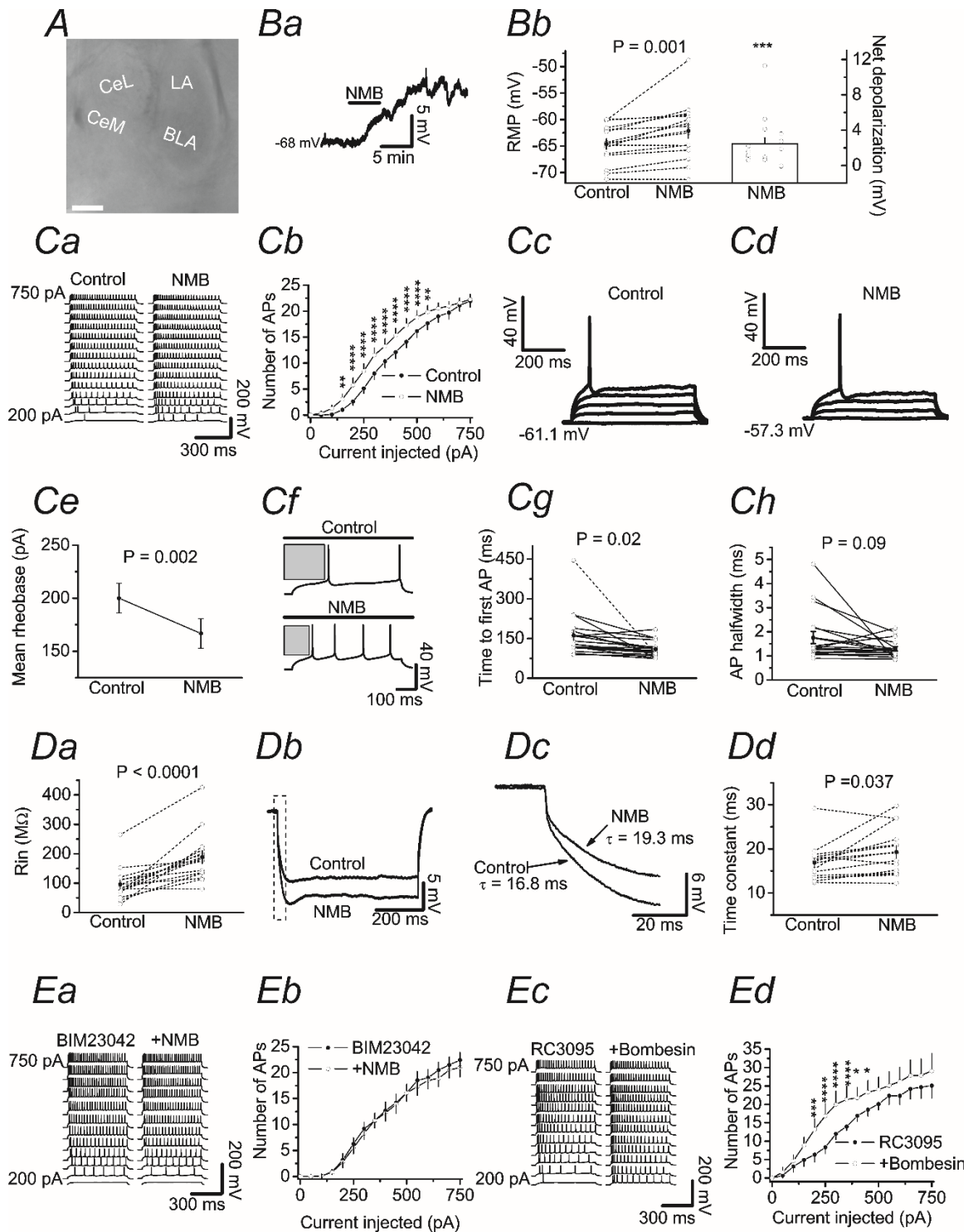
neurons should be due to the activation of BB1 receptors. Indeed, bath application of bombesin (0.3 μ M) increased the number of APs fired in response to the positive current injection protocol ($n = 9$, $F_{(1,8)} = 7.064$, $P = 0.028$, two-way ANOVA repeated measures ANOVA followed by Šídák's multiple comparisons test, Figure 10. *Ec-Ed*). Taken together, these results suggest that NMB excites principal BLA neurons through the activation of BB1 receptors.

BB1 Receptors Stimulate a Cation Current and Inhibit an Inwardly Rectifying K⁺ Current

Next, we characterized the ionic mechanisms whereby the activation of BB1 receptors facilitates the excitability of BLA neurons. Two common ionic currents mediate neuronal excitability: activation of cationic currents, and inhibition of K⁺ currents. Using a K⁺-gluconate internal solution, bath application of NMB (0.3 μ M) elicited an inward current from BLA neurons at -60 mV (-21.60 ± 2.61 pA, $n = 22$, $P < 0.0001$, Wilcoxon test, Figure 11. *Aa, Ab*). The NMB-mediated inward currents were concentration-dependent (Figure 11. *Ab*). Substituting the K⁺-gluconate internal solution for Cs⁺-gluconate to annul the contribution of K⁺ channels blocked NMB-mediated inward holding currents (-2.47 ± 4.57 pA, $n = 23$, $P = 0.59$ vs baseline, two-sample paired t-test; $P = 0.0008$ vs the NMB-induced inward currents recorded in K⁺-containing internal solution, two-sample independent t-test, Figure 11. *Ac, Ad*), supporting that depression of K⁺ currents by BB1 receptor activation is one means of enhancing BLA neuronal excitability. We further probed the ionic mechanism whereby BB1 receptor activation excites BLA neurons by measuring I-V relationships from 49 voltage-clamped BLA neurons. Twenty-four cells showed an I-V curve resembling inwardly rectifying K⁺ (Kir) channels with a reversal potential of -56.2 ± 6.3 mV (Figure 11. *Ba-Bc*), which is

Figure 10. Activation of BB1 receptors excites BLA neurons.

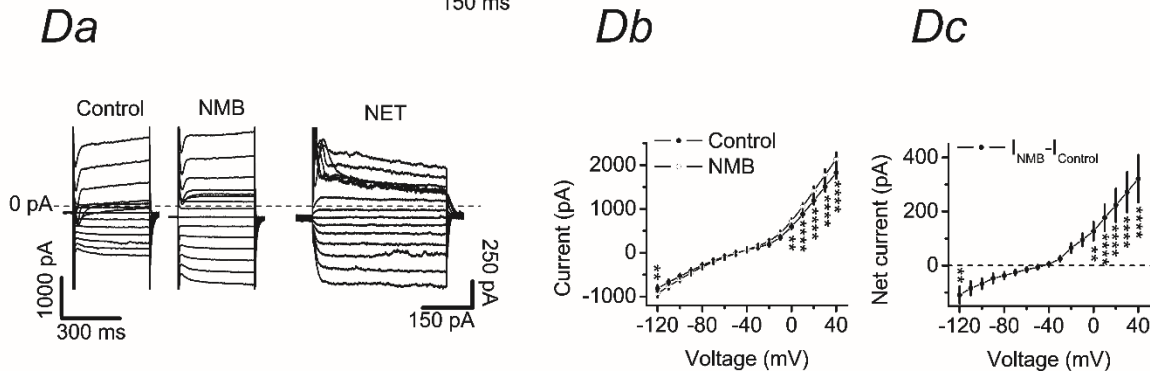
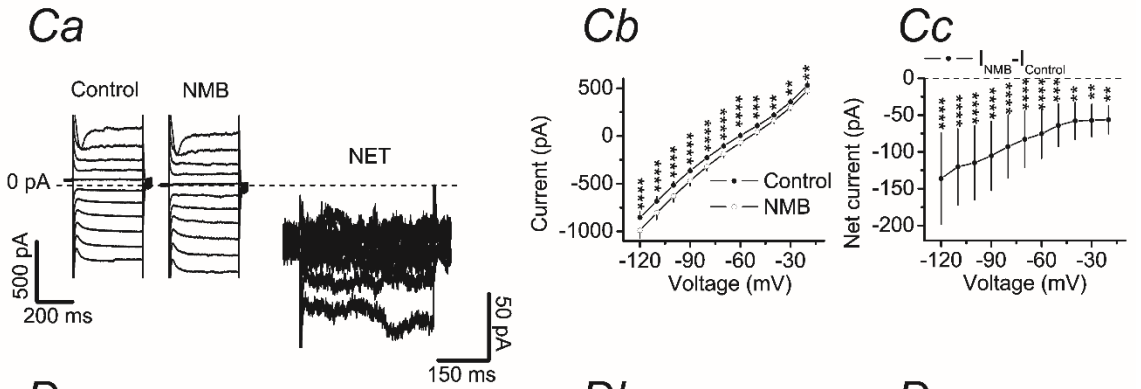
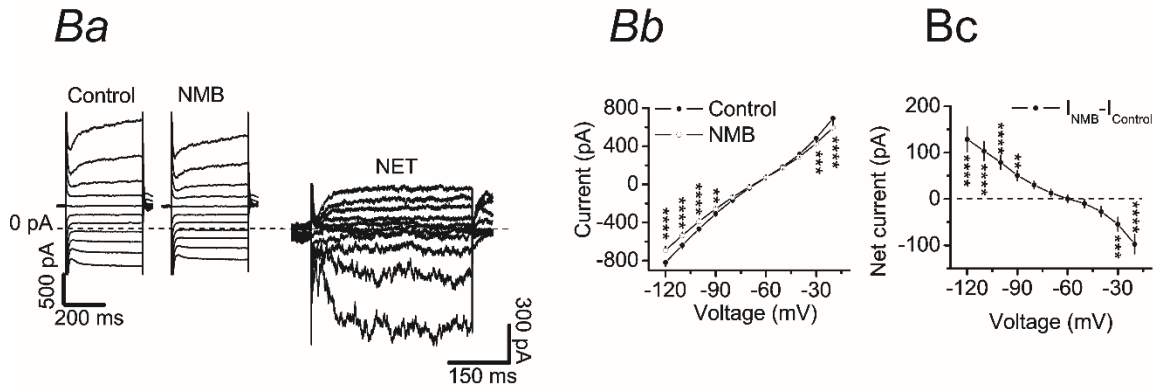
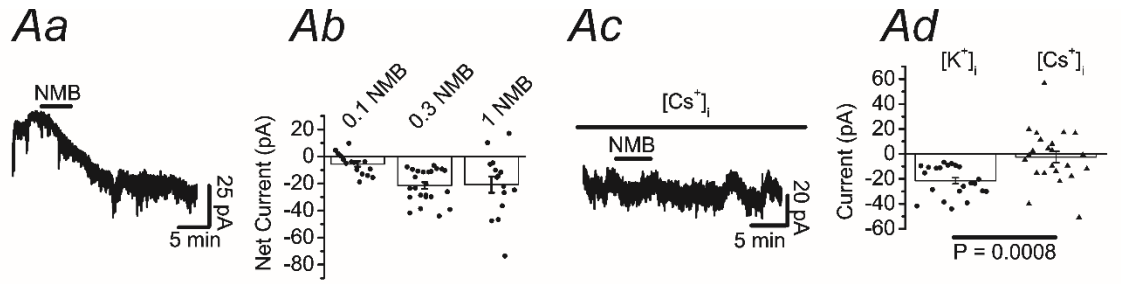
A, microscopic photograph displaying the location of the BLA where electrophysiological recordings were obtained. LA: lateral amygdala; BLA: basolateral amygdala; CeL: lateral nucleus of the central amygdala; CeM: medial nucleus of the central amygdala. *Ba & Bb*, Bath application of the selective BB1 receptor agonist, NMB, induces subthreshold depolarizations. *Ba*, a representative trace of the RMP prior to, during and after the bath application of NMB. *Bb*, summary data showing RMPs in control condition and after application of NMB from the same cells (left) and the net depolarization obtained by subtraction (right). *Ca-Cg*, bath application of NMB enhanced AP firing by lowering the rheobase current and the time to the first action potential. *Ca*, APs generated by a series of positive current injections from 50 pA to 750 pA at 50 pA increments and a duration of 600 ms every 6 s before and after bath application of NMB. *Cb*, summary of AP firing before and after NMB application. *Cc*, a representative trace of the rheobase current in a BLA principal neuron in control condition. *Cd*, a representative trace of the rheobase current in the same BLA principal neuron after NMB application. *Ce*, summary data of the mean rheobase current before and after application of NMB. *Cf*, a representative trace of the first action potential fired during the rheobase sweep before and after the application of NMB. Note the reduction in the time to the first AP denoted by the grey boxes. *Cg*, summary graph showing the time to the first AP fired in the rheobase sweep before and after NMB application. *Ch*, summary data of the AP halfwidth of the rheobase sweep. *Da-Dd*, NMB excites neurons by increasing the input resistance and elevating membrane time constants. *Da*, summary results of NMB on input resistance. *Db & Dc*, representative voltage response produced by the injection of -100 pA before and after treatment with NMB. Note the area highlighted by the dashed rectangle is magnified in *Dc*. *Dd*, summary graph for membrane time constants before and after NMB treatment. *Ea-Ed*, NMB-mediated excitation was mediated by selective activation of BB1Rs. *Ea*, APs recorded from a BLA neuron following the positive current injection protocol before (left) and after (right) bath application of NMB in a slice pretreated with the selective BB1 receptor antagonist BIM23042 (0.3 μ M). *Eb*, the relationship of APs elicited before and after bath application of NMB in slices pretreated with BIM23042. *Ec*, APs recorded from a BLA neuron following the positive current injection protocol before (left) and after (right) bath application of bombesin in a slice treated with the selective BB2 receptor antagonist RC3095 (2 μ M). *Ed*, the relationship of APs generated before and after the bath application of bombesin in slices treated with RC3095.



between the K^+ reversal potential and the reversal potential of cations, suggesting that both mechanisms are involved. Indeed, 25 recorded BLA neurons displayed an I-V curve resembling a nonselective cation channel (Figure 11. *Ca-Cc*). We then measured I-V responses with the inclusion of Cs-gluconate in our internal recording solution to block K^+ channels and applied TTX ($0.5 \mu\text{M}$) and CdCl_2 ($200 \mu\text{M}$) to block voltage-gated Na^+ and Ca^{2+} channels, respectively. The reversal potential of the NMB-elicited cation channel currents was measured by extending the voltage range to $+20 \text{ mV}$. From these experimental conditions, we obtained an I-V curve of the NMB-mediated currents with a reversal potential of $-39.1 \pm 6.6 \text{ mV}$ ($n = 13$, Figure 11. *Da-Dc*). These results suggest that BB1 receptor activation excites principal BLA neurons by opening a non-selective cation channel and depressing a Kir channel. To better understand the role of BB1 receptor activation in Kir channel depression, we measured NMB-induced inward holding currents in the presence of Ba^{2+} , as Kir channels are inhibited by Ba^{2+} in micromolar range [252, 254]. Bath application of Ba^{2+} ($500 \mu\text{M}$), by itself induced an inward holding current ($-56.51 \pm 14.29 \text{ pA}$, $n = 15$, $P = 0.001$, two-sample paired t-test, Figure 12. *A, E*) and significantly reduced NMB-elicited inward currents (Net current: $-10.48 \pm 1.40 \text{ pA}$, $n = 15$, $P = 0.010$, one-way ANOVA followed by Dunnett's test, Figure 12. *A, F*). Functionally distinct Kir channel subfamilies include Kir2, Kir3 (G protein-gated inwardly rectifying potassium (GIRK) channels), Kir6 (ATP-sensitive channels), and K^+ transport channels [255]. To test the potential involvement of the Kir2 subfamily, we used ML 133, a specific antagonist of the Kir2 subfamily [295], in NMB-elicited excitation of BLA principal neurons. Bath application of ML 133 ($30 \mu\text{M}$) by itself had no effect on holding currents (Net current: $-2.52 \pm 1.57 \text{ pA}$, $n = 19$, $P = 0.13$, one-sample t-test, Figure 12. *B, E*). When NMB was bath applied in the presence of ML 133, NMB elicited an inward current that was not significantly different from slices treated with

Figure 11. NMB-elicited excitation of BLA neurons is mediated by inhibiting a Kir channel and opening a cation channel.

Aa-Ad, bath application of NMB concentration-dependently excited BLA neurons producing an inward holding current in part by blocking a K⁺ current. *Aa*, a representative trace of the inward currents generated by the bath application of NMB (0.3 μM) in a BLA neuron. *Ab*, the relationship of the net inward current generated by application of increasing concentrations of NMB. Filled circles represent individual current values and the bars represent their means. *Ac*, a representative trace of the inward current elicited by bath application of NMB recorded from a BLA neuron using a Cs-gluconate internal recording solution. *Ad*, relationship of the net inward currents generated by bath application of NMB in BLA neurons recorded with a K-gluconate or Cs-gluconate internal recording solution. Filled symbols are individual current values, and the bars represent their mean current values. *Ba-Bc*, NMB inhibited an inwardly rectified K⁺ channel. The extracellular solution contained tetrodotoxin (0.5 μM), picrotoxin (100 μM) and kynurenic acid (1 mM) and the intracellular recording solution was the K⁺-gluconate containing internal recording solution. *Ba*, a representative current trace elicited by the voltage-step protocol before (left) and during (middle) bath application of NMB and the net current obtained by subtraction (right) from a BLA neuron. The dashed line represents zero current level. *Bb*, I-V curved averaged from 24 cells before and during the application of NMB (Two-way repeated measures ANOVA followed Šídák's multiple comparisons test; Drug: $F_{(1,23)} = 4.76$, $P = 0.039$; Voltage: $F_{(10,230)} = 296.1$, $P < 0.0001$; Drug x Voltage: $F_{(10,230)} = 27.57$, $P < 0.0001$). *Bc*, I-V curve of the net current obtained by subtracting the currents in the control condition from those after the application of NMB. The I-V curved of the NMB-mediated inhibition of Kir channels had a reversal potential of -56.2 ± 6.3 mV. *Ca-Cc*, NMB opens a cation channel. *Ca*, a representative current trace generated by the voltage-step protocol before (left) and during (middle) bath application of NMB and the net current obtained by subtraction (right) from a BLA neuron. *Cb*, I-V curve averaged from 25 cells before and during the application of NMB (Two-way repeated ANOVA; Drug: $F_{(1,24)} = 6.18$, $P = 0.02$; Voltage: $F_{(1,24)} = 225.5$, $P < 0.0001$; Drug x Voltage: $F_{(10,240)} = 1.85$, $P = 0.05$). *Cc*, I-V curve of the net current obtained by subtracting the currents in the control condition from those after the application of NMB. *Da-Dc*, NMB opened a cation channel with outward rectification recorded in extracellular solution containing tetrodotoxin (0.5 μM), picrotoxin (100 μM), kynurenic acid (1 mM), and CdCl₂ (200 μM) and the intracellular solution was the Cs⁺-gluconate containing internal recording solution. *Da*, a representative current trace elicited by the voltage-step protocol before (left) and during (middle) bath application of NMB and the net current obtained by subtraction (right) from a BLA neuron. The dashed line is the zero current level. *Db*, I-V curve averaged from 25 cells before and during the application of NMB (Two-way repeated measures ANOVA followed by Šídák's multiple comparisons test; Drug: $F_{(1,23)} = 4.89$, $P = 0.037$; Voltage: $F_{(10,230)} = 296.1$, $P < 0.0001$; Drug x Voltage: $F_{(10,230)} = 27.57$, $P < 0.0001$). *Dc*, I-V curve of the net current obtained by subtracting the currents in control conditions from those during the application of NMB. The I-V curve of the NMB-induced outwardly rectifying currents had a reversal potential of -39.1 ± 6.6 mV. **** $P < 0.0001$, *** $P < 0.001$, ** $P < 0.01$, * $P < 0.05$.



NMB in control conditions (Net current: -22.09 ± 2.87 pA, $n = 19$, $P = 0.996$ one-way ANOVA followed by Dunnett's test, Figure 12. *B, F*), suggesting that the Kir2 subfamily is not the type of Kir channels involved in NMB-mediated excitation of BLA neurons. Because BB1 receptor activation is coupled to G proteins, we tested the involvement of the GIRK channel subfamily. ML297 is a selective activator of GIRK1 containing channels, and GIRK1 channels are expressed in the BLA [296]. Bath application of a saturating concentration of ML297 ($10 \mu\text{M}$) produced significant outward currents in BLA neurons (Net current: 48.72 ± 14.29 pA, $P = 0.01$, Student's t-test, Figure 12. *C, E*), suggesting that GIRK1-containing channels are expressed in BLA neurons. The derivative of the honeybee toxin tertiapin, tertiapin-Q (250 nM, TQ), is an antagonist of GIRK channels [263, 264]. Bath application of TQ by itself produced a significant inward current in BLA neurons (Net current: -15.37 ± 2.95 pA, $p = 0.0002$, student's t-test, Figure 12. *D, E*) and co-application of NMB resulted in a significantly smaller current than in BLA neurons treated with NMB alone (Net current: -10.18 ± 2.25 pA, $P = 0.002$, one-way ANOVA followed by Dunnett's test, Figure 12. *D, F*). Together, these data suggest tertiapin-Q sensitive GIRK channels contribute to NMB-mediated excitation of BLA neurons.

TRPV1 Channels are Involved in NMB-Mediated Inward Currents

In approximately 50% of the neurons examined, the I-V curve of the NMB-elicited currents (Figure. 11) resembled that of transient receptor potential channel family, namely TRPV1, TRPC4, and TRPC5 channels [297]. Because TRPV1, TRPC4, and TRPC5 are expressed in the BLA [298-301], we tested the involvement of these channels in NMB-elicited inward currents. To probe the roles of TRPC4/5 we pretreated rat BLA neurons with the selective TRPC4/5 channel blocker M084 ($100 \mu\text{M}$)

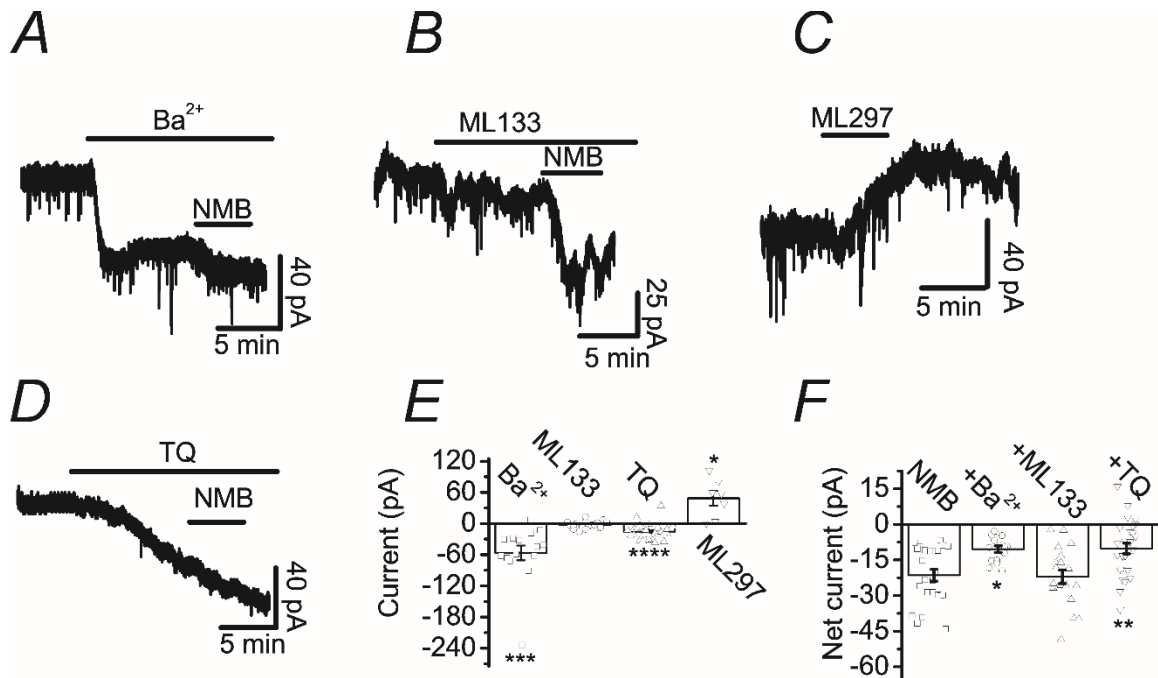


Figure 12. GIRK channels are required for BB1 receptor-elicited inward currents in BLA neurons.

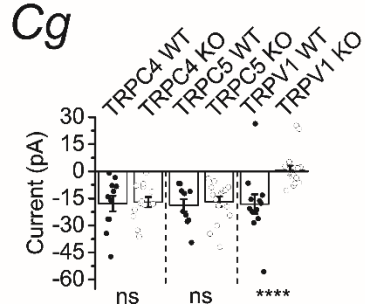
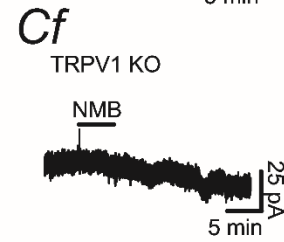
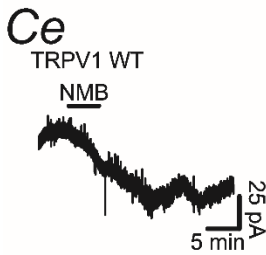
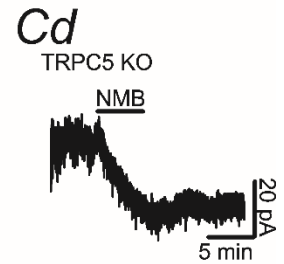
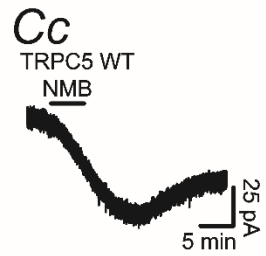
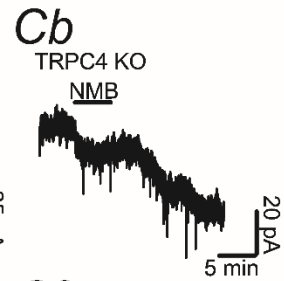
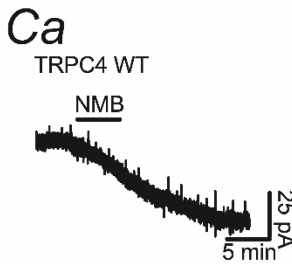
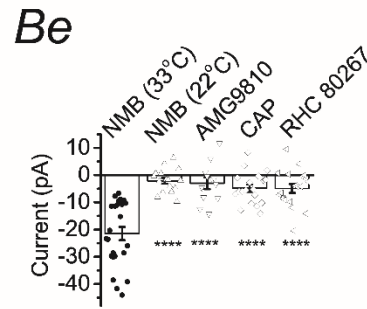
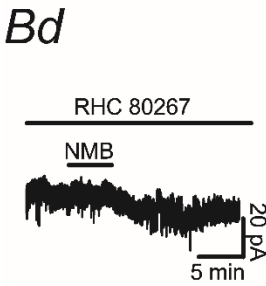
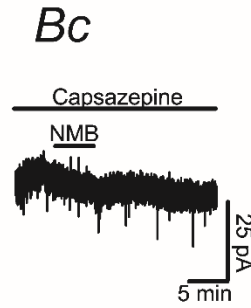
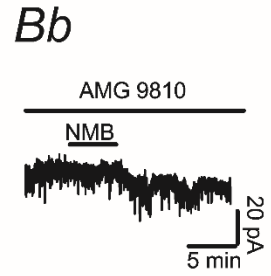
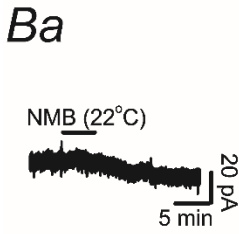
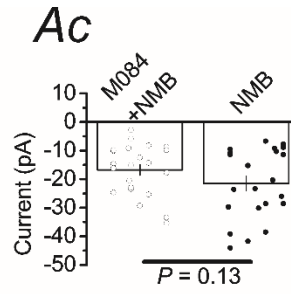
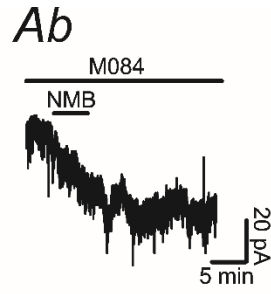
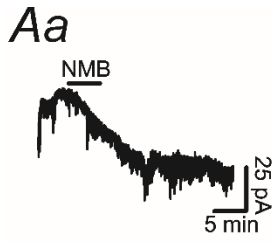
A, a current trace recorded from a BLA neurons in response to Ba²⁺ (500 μM) alone and Ba²⁺ plus NMB. B, a current trace recorded from a BLA neuron in response to ML133 (30 μM) alone and ML133 plus NMB. C, current trace recorded from a BLA neuron in response to bath application of ML297 (10 μM). D, a current trace recorded from a BLA neurons in response to tertiapin-Q (250 nM, TQ) alone and TQ plus NMB. E, summary data for the effects of Kir channel modulators on BLA neurons. **** P < 0.0001, *** P < 0.001, * P < 0.05 vs. baseline, two-sample paired t-test. F, summary graph showing the effects of Kir channel blockers on NMB-mediated inward currents. ** P < 0.01, * P < 0.05 vs. NMB alone, one-way ANOVA followed by Dunnett's test.

and the same concentration was present in the bath. Under these conditions, NMB-mediated inward currents were not altered significantly when compared to BLA neurons treated with NMB alone (Net current: M084+NMB: -16.8 ± 2.4 pA; NMB: -21.6 ± 2.6 pA; $P = 0.13$, two-way student's t-test, Figure 13. *Aa-Ac*), suggesting that TRPC4/5 channels are not involved in NMB-evoked inward currents.

The temperature sensitive TRPV1 channels are non-selective cation channels expressed in the BLA [298, 301], displaying outward rectification similar to that observed in our I-V recordings. The steady-state temperature of our recording solutions was held at 33-34°C and revealed that NMB generates a significant inward current (see Figure 11. *Aa*, Figure 13. *Aa*). As TRPV1 channels are temperature-sensitive cation ion channels [297], we recorded holding currents from rat brain slices with the recording solution held at room temperature (22-23°C). When the bath temperature was held at room temperature, bath application of NMB elicited a significantly smaller inward current than control slices held at 33-34°C (NMB 22-23 °C net current: -2.1 ± 1.1 pA; NMB 33-34 °C net current: -21.6 ± 2.6 pA, $P < 0.0001$ unpaired t-test, $P < 0.0001$ vs. NMB alone one-way ANOVA followed by Tukey's test, Figure 13. *Ba, Be*). We further evaluated the involvement of TRPV1 channels using targeted TRPV1 channel blockers. Pretreatment and bath application of the selective TRPV1 channel blocker, AMG 9810 (10 μ M) [302], significantly reduced NMB-mediated inward currents ($P = 0.19$, $n = 12$, paired t-test; $P < 0.0001$ vs. NMB alone, one-way ANOVA followed by Dunnett's test, Figure 13. *Bb, Be*). In slices treated with another TRPV1 antagonist, capsazepine (10 μ M)[303-306], NMB generated a significant inward current ($P = 0.002$, $n = 19$, unpaired t-test, Figure 13. *Bc*), but the inward current was significantly reduced when compared to currents in control slices treated with NMB alone ($P < 0.0001$, one-way ANOVA followed by

Figure 13. TRPV1 channels are involved in BB1 receptor-induced inward currents in BLA neurons.

Aa-Ac, pretreatment of slices with and continuous bath application of M084 did not significantly affect NMB-mediated inward currents. *Aa*, a representative trace of the NMB-mediated inward currents in control condition. *Ab*, a representative trace of the NMB-elicited inward currents in a slice pretreated with the TRPC4/5 channel blocker M084 (100 μ M). *Ac*, summary graph showing the relationship of currents produced by NMB in slices pretreated with M084. Circles represent the currents generated by individual cells and the bars represent the respective means. *Ba-Be*, NMB activates TRPV1 channels in rat BLA neurons. *Ba*, a representative current trace recorded at room temperature from a BLA neuron after bath application of NMB. *Bb*, a representative trace of NMB-mediated inward currents in the presence of selective TRPV1 blocker, AMG9810 (10 μ M). *Bc*, holding current trace induced by bath application of NMB in the presence of another TRPV1 channel blocker capsazepine (10 μ M). *Bd*, a representative current trace generated by bath application of NMB in the presence of the DAG lipase inhibitor, RHC 80267 (25 μ M). *Be*, summary graph showing the effects of TRPV1 channel modulators on the NMB-mediated inward currents in BLA neurons. **** $P < 0.0001$ vs NMB alone, one-way ANOVA followed by Dunnett's test. *Ca-Cg*, bath application of NMB produced significantly smaller inward currents in TRPV1 knockout mice, but not in TRPC4 or TRPC5 knockout mice. *Ca*, a representative current trace recorded from TRPC4 WT mouse before and after the bath application of NMB. *Cb*, a representative current trace recorded from TRPC4 KO mouse before and after the bath application of NMB. *Cc*, a representative current trace recorded from TRPC5 WT mouse before and after the bath application of NMB. *Cd*, a representative current trace recorded from a TRPC5 KO mouse before and after the bath application of NMB. *Ce*, a representative current trace recorded from a TRPV1 WT mouse before and after the bath application of NMB. *Cf*, a current trace elicited from a TRPV1 KO mouse before and after the bath application of NMB. *Cg*, summary graph showing the effects of NMB-generated inward currents in WT and respective KO mice. **** $P < 0.0001$ vs corresponding WT, Mann-Whitney test. n.s, nonsignificant.



Tukey's test, Figure 13. *Bc, Be*), suggesting that NMB excites BLA through the activation of TRPV1 channels. TRPV1 channels can also be activated by natural endocannabinoids, which resemble vanilloid agonists [297, 307]. The endocannabinoid 2-arachidonoylglycerol (2-AG), produced by DAG lipase following G_q-couple receptor activation, may activate TRPV1 channels [308]. We tested this possibility by pretreating and bath applying RHC 80267 (25 μM) to inhibit both α- and β-DAG lipase. Pretreatment of slices with and continuous bath application of RHC 80267 failed to block NMB-mediated inward currents significantly (Net current: -4.9 ± 1.7 pA, $P = 0.009$, $n = 18$, paired t-test; Figure 13. *Bd*), but this inward current was significantly smaller than that mediated by NMB alone ($P < 0.0001$, one-way ANOVA followed by Tukey's test, Figure 13. *Bd, Be*).

We further tested the role of TRP channels using TRPC4, TRPC5, and TRPV1 knockout mice. Bath application of NMB produced similar inward currents in TRPC4, TRPC5, and TRPV1 wild-type mice ($P = 0.86$, one-way ANOVA; Figure 13. *Ca, Cc, Ce*). The inward current produced in TRPC4 KO and TRPC5 KO was similar to the inward currents produced in corresponding wild-type mice (TRPC4 WT: -17.9 ± 4.3 pA; TRPC4 KO: -17.1 ± 2.8 pA; $P = 0.87$, unpaired t-test; TRPC5 WT: -18.9 ± 3.5 pA; TRPC5 KO: -16.8 ± 2.7 pA; $P = 0.64$, unpaired t-test; Figure 13. *Ca-Cd, Cg*). However, in male and female mice lacking the TRPV1 channel, NMB failed to produce a significant inward current (TRPV1 WT: -18.2 ± 5.3 pA; TRPV1 KO: 0.7 ± 2.3 pA; $P < 0.0001$, Mann-Whitney test; Figure 13. *Ce, Cf, Cg*). Together, these data indicate that NMB excites BLA neurons via activation of TRPV1 channels.

BB1 Receptor-Mediated Excitation of BLA Neurons is Dependent on PLC β and PLC β -Mediated Hydrolysis of PIP $_2$ and PI3/4K Signaling

We then investigated the intracellular signaling mechanisms involved in NMB-mediated excitation of BLA neurons. BB1 receptors are coupled to G $\alpha_{q/11}$ proteins [236, 239, 240] that signal through the PLC β pathway. Therefore, we examined the role of this signaling pathway in NMB-induced AP firing. Intracellular dialysis of the selective G protein inactivator GDP- β -S (0.5 mM) significantly attenuated the number of APs fired in response to the positive current injection protocol ($F_{(1,12)} = 1.513$, $P = 0.24$, two-way repeated-measures ANOVA; Figure 14. A), indicating that the function of G proteins is necessary for NMB-mediated enhancement of AP firing.

We sought to determine the functional involvement of PLC β in BB1-mediated excitability of BLA neurons. The slices were pretreated with U73122 (5 μ M), a selective PLC β inhibitor, for > 2 h. Under these conditions, application of NMB failed to augment AP firing in response to the positive current injection protocol ($F_{(1,10)} = 0.04$, $P = 0.83$, two-way-repeated-measures ANOVA, Figure 22. B). These results demonstrate that PLC β is required for NMB-mediated increases in neuronal excitability in the BLA.

Activated PLC β hydrolyzes the membrane lipid PIP $_2$ to generate the bioactive metabolites DAG and IP $_3$, and in turn removes PIP $_2$ allosteric modulation of a variety of ion channels [193, 309]. To test the role of PIP $_2$ turnover in NMB-mediated excitation, the short-chain, water-soluble analog diCi8-PIP $_2$ (20 μ M) was included in our recording solution to compensate for PIP $_2$ hydrolysis by PLC β . Restoration of PIP $_2$ blocked the NMB-evoked augmentation of AP firing ($F_{(1,15)} = 2.165$, $P = 0.16$, two-way repeated-measures ANOVA, Figure 14. C). As the levels of membrane PIP $_2$ are rapidly resynthesized following PLC-mediated signaling by the phosphorylation of phosphoinositol and phosphatidylinositol 4-phosphate (PI (4)P) at position 5 by their cognate kinases [310-312], we targeted PI3K and PI4K with wortmannin (20 μ M) to

inhibit PIP₂ resynthesis. Inhibition of PI3K and PI4K produced a significant reduction in the number of APs fired in response to the positive current injection protocol ($F_{(1,21)} = 9.05$, $P = 0.0067$, two-way ANOVA followed by Šídák's multiple comparisons test, Figure 14. *D*). Taken together, these data indicate that NMB-mediated excitation of principal BLA neurons requires membrane lipid remodeling.

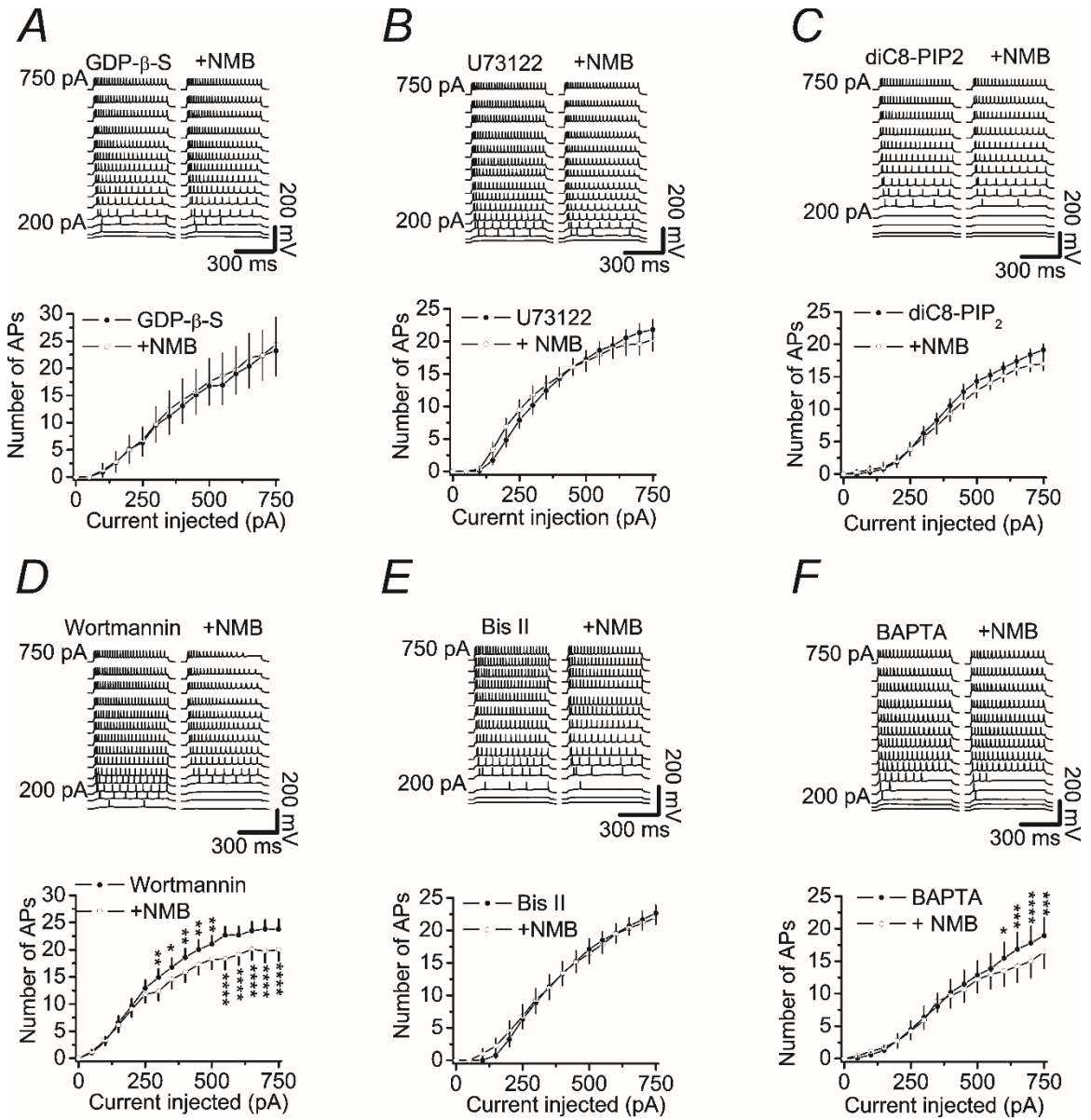
We then examined the role of PKC in NMB-mediated excitation of BLA neurons. Slices were pretreated with the selective PKC inhibitor, bisindolylmaleimide II (Bis II, 1 μ M), and this concentration was present in the extracellular recording solution. Application of NMB failed to significantly increase AP firing in slices pretreated with Bis II ($F_{(1,16)} = 0.009$, $P = 0.92$, two-way repeated measures ANOVA followed by Šídák's multiple comparisons test, Figure 14. *E*). Next, we tested the involvement of intracellular Ca²⁺ in NMB-mediated excitation of BLA neurons by inclusion of the Ca²⁺ chelator BAPTA (10 mM) in our recording electrode. Under these conditions, application of NMB failed to increase AP firing in response to the positive current injection protocol ($F_{(1,18)} = 3.96$, $P = 0.06$, two-way repeated measures ANOVA followed by Šídák's multiple comparisons test, Figure 14. *F*). Similarly, Ca²⁺ release from intracellular stores is required for NMB-mediated augmentation of BLA excitability (Supplementary Figure 1). Taken together, these data support the functional requirement for G-protein activation, membrane lipid remodeling, PKC, and intracellular Ca²⁺ for NMB-mediated increases in AP firing.

BB1 Receptor Activation Modulates Glutamatergic Transmission in the BLA

The BLA is an important site of sensory integration as it receives afferent projections from cortical and thalamic structures [313-315] and has a well-characterized involvement in fear responses [15, 316, 317] and anxiety [93, 106]. Although the neuromodulatory

Figure 14. BB1 receptor elicited excitation of BLA neurons requires PLC β -mediated intracellular signaling.

A, representative traces (upper) and summary graphs (lower) of NMB-augmented APs in response to the positive current injection protocol in the presence of intracellular GDP- β -S (0.5 mM). *B*, representative traces (upper) and summary graphs (lower) of NMB-mediated APs in the presence of the selective PLC β inhibitor U73122 (5 μ M). *C*, traces (upper) and summary graphs (lower) of NMB-augmented APs in the presence of intracellular dialyzed diC8-PIP₂ (20 μ M). *D*, representative traces (upper) and summary graphs (lower) of NMB-elicited APs in response to the positive current injection protocol from slices pretreated with the PI3K and PI4K inhibitor wortmannin (20 μ M). *E*, AP traces (upper) and summary graphs (lower) of NMB-augmented APs in the slice pretreated with the selective PKC inhibitor BISII (1 μ M). *F*, representative traces (upper) and summary graph (lower) of NMB-elicited APs in response to the positive current injection protocol in the presence of the intracellular Ca²⁺-chelator BAPTA (10 mM). **** P < 0.0001, *** P < 0.001, ** P < 0.01, * P < 0.05, two-way repeated measures ANOVA.



bombesin-like peptides have been reported to stimulate glutamatergic transmission in the spinal cord [318], olfactory bulb [319], and hypothalamus [320], little is known regarding how NMB modulates glutamate release in the BLA. To investigate the role of BB1 receptor activation in glutamatergic transmission in the BLA, we recorded sEPSCs before and after NMB application. NMB (0.3 μ M) significantly increased the frequency (baseline: 6.6 ± 1.3 Hz, NMB: 11.8 ± 1.7 Hz, $261 \pm 94\%$ of baseline, $n = 11$, $P = 0.002$ Wilcoxon test, Figure 15. *Aa-Ad*) and amplitude (baseline: 18.2 ± 0.8 pA, NMB: 21.9 ± 2.2 pA, $118 \pm 11\%$ of baseline, $n = 11$, $P = 0.009$ Figure 15. *Ae, Af*) of sEPSCs. The effect of NMB on sEPSC was irreversible for the duration of our experiments as the sEPSC frequency following 20 minutes of washing was $257.3 \pm 39\%$ of baseline ($n = 11$, $P = 0.002$, Figure 15. *Ab*). These data indicate that NMB augments spontaneous glutamatergic transmission in the BLA.

NMB-mediated increases in sEPSCs could be explained by several hypotheses, including a) NMB produces an increase in AP firing in BLA neurons to increase their excitability and glutamate release; b) NMB-mediated activation of TRPV1 channels results in elevated Ca^{2+} influx and subsequent neurotransmitter release; and c) NMB acts at postsynaptic sites to increase glutamatergic signaling. To test these hypotheses, we recorded miniature EPSCs (mEPSCs), sEPSCs, and mEPSCs targeting TRPV1 channels, and evoked EPSCs (eEPSCs). We recorded mEPSCs in the presence of TTX (0.5 μ M) to exclude action potentials and voltage-gated Ca^{2+} influx. In this condition, application of NMB enhanced the frequency (baseline: 1.3 ± 0.4 Hz, NMB: 4.1 ± 1.4 Hz, $293 \pm 55\%$ of baseline, $n = 9$, $P = 0.03$, Figure 15. *Ba-Bd*) but not the amplitude (baseline: 15.8 ± 0.4 pA, NMB: 15.9 ± 0.5 pA, $100 \pm 1\%$ of baseline, $n = 9$, $P = 0.58$, Figure 15. *Be-Bf*) of mEPSCs, indicating APs are not required for NMB-mediated spontaneous glutamatergic transmission in the BLA but the involvement of calcium

cannot be excluded. Moreover, the increase in frequency, but not amplitude may suggest a presynaptic mechanism whereby NMB enhances spontaneously released glutamate.

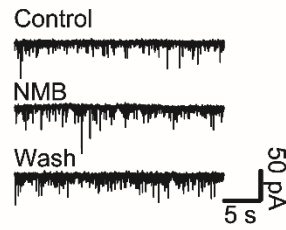
We then probed the involvement of Ca²⁺-permeant TRPV1 channels in NMB-mediated glutamatergic transmission in the BLA by treating slices with AMG9810 (10 μ M). Application of NMB failed to significantly increase the frequency (baseline: 8.9 ± 1.4 Hz, NMB: 9.3 ± 0.9 Hz, 121 ± 15 % of baseline, $n = 12$, $P = 0.69$ paired t-test, Figure 16. *Aa-Ac*) or amplitude (baseline: 19.6 ± 1.5 pA, NMB: 20.7 ± 1.6 pA, 106 ± 4 % of baseline, $n = 12$, $P = 0.15$ Wilcoxon test, Figure 16. *Ad*) of sEPSCs in BLA neurons treated with AMG9810. We then recorded sEPSCs from TRPV1 KO mice and their corresponding wildtype littermates. Application of NMB in male and female TRPV1 WT mice significantly increased the frequency of sEPSCs (TRPV1 WT: control: 5.1 ± 1.4 Hz; NMB: 12.9 ± 3.1 Hz, 308 ± 65 % of control, $n = 12$, $P = 0.007$, Figure 16. *Ba, Bc-Bd*) and the amplitude of sEPSC events (TRPV1 WT: control: 17.8 ± 0.9 pA; NMB: 24.7 ± 1.7 pA, 140 ± 12 % of control, $n = 12$, $P = 0.002$, Figure 16. *Ba, Be*). The application of NMB in TRPV1 KO mice failed to significantly increase the frequency of sEPSC events (TRPV1 KO: control: 18.6 ± 4.1 Hz; NMB: 15.9 ± 3.9 , 94 ± 11 % of baseline, $n = 11$, $P = 0.33$, Figure 16. *Bb-Bc, Bf*) and had no effect on sEPSC amplitude (TRPV1 KO: 16.5 ± 0.6 pA; NMB: 16.7 ± 0.8 pA, 100 ± 2 % of baseline, $n = 11$, $P = 0.81$, Figure 16. *Bb, Bg*). These results indicate that NMB-mediated sEPSC events require functional TRPV1 channels.

We then probed the involvement of TRPV1 channels in NMB-mediated AP-independent glutamatergic transmission. Rat brain slices were pretreated with AMG9810 to annul TRPV1 channel currents, as described above, and TTX was included in all solutions to inhibit voltage-gated Na⁺ channels. Under these conditions,

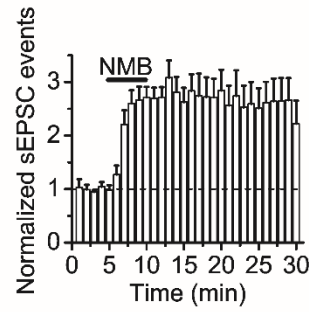
Figure 15. Activation of BB1 receptors enhances spontaneous glutamate release in BLA neurons.

Aa-Af, NMB increases the frequency and the amplitude of sEPSCs recorded from BLA neurons. *Aa*, representative trace of spontaneous EPSCs recorded from BLA neurons before, during, and after the bath application of NMB (0.3 μ M). *Ab*, time course of the sEPSC frequency averaged from 11 BLA principal neurons. *Ac*, cumulative frequency distribution averaged from 11 BLA neurons before and during the application of NMB. *Ad*, frequency of sEPSCs pooled from 11 cells before and during the application of NMB. Open circles are values from individual cells and filled circles are their mean. *Ae*, cumulative amplitude distribution average from 11 cells before and during the application of NMB. *Af*, amplitude of sEPSCs pooled from 11 cells before and during the application of NMB. *Ba-Bf*, NMB-mediated increases in glutamatergic transmission were AP-independent. *Ba*, mEPSC traces recorded from a BLA neuron before, during, and after the application of NMB. *Bb*, time course of the mEPSCs events averaged from 9 BLA neurons recorded in the presence of tetrodotoxin. *Bc*, cumulative frequency distribution averaged from 9 cells before and during the application of NMB in the presence of tetrodotoxin. *Bd*, frequency of mEPSCs pooled from 9 cells before and during the application of NMB. *Be*, cumulative amplitude distribution averaged from 9 BLA neurons before and during the application of NMB. *Bf*, amplitude of mEPSCs pooled from 9 cells before and during the application of NMB.

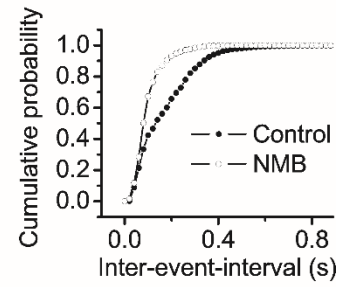
Aa



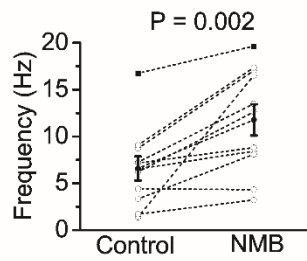
Ab



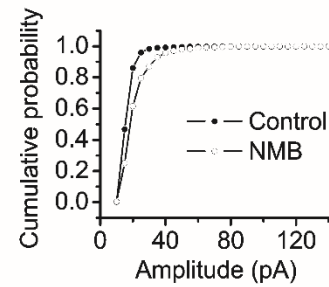
Ac



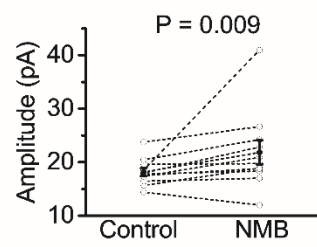
Ad



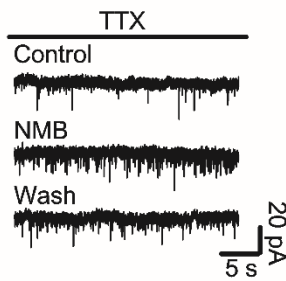
Ae



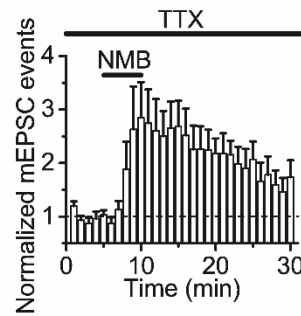
Af



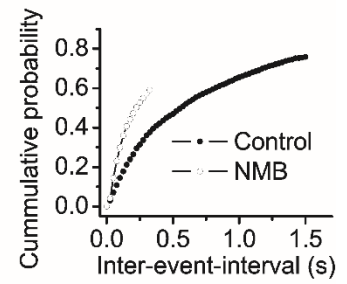
Ba



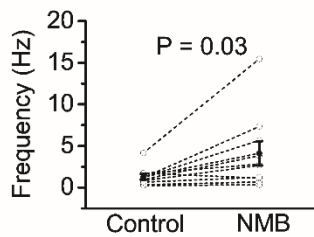
Bb



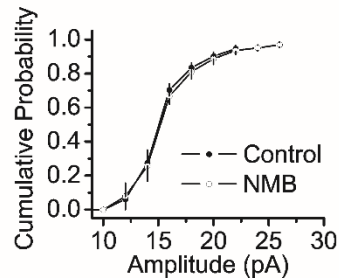
Bc



Bd



Be



Bf

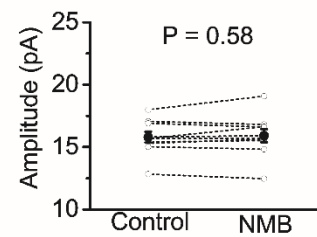
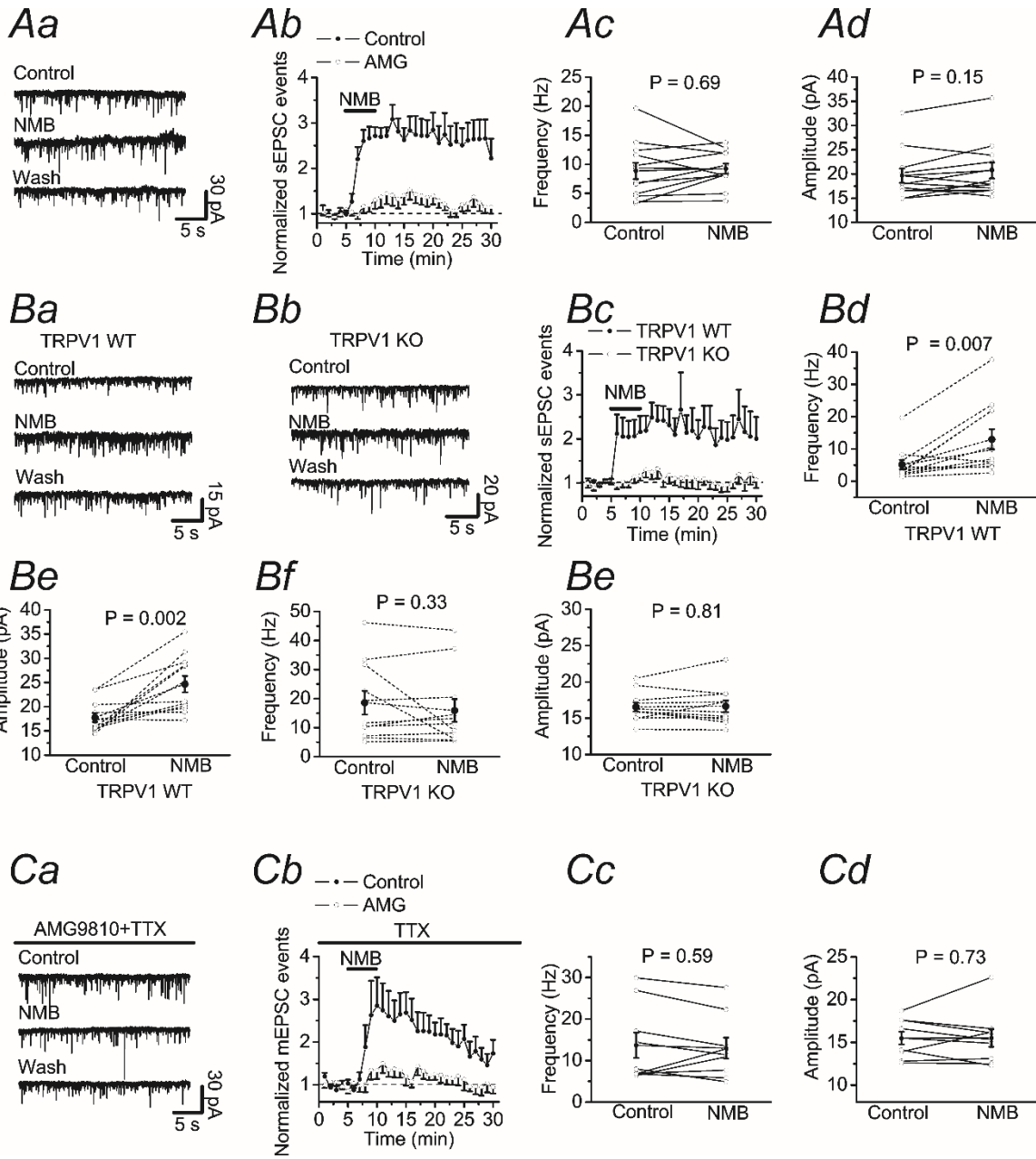


Figure 16. BB1 receptor-mediated spontaneous glutamate release requires TRPV1 channels in BLA neurons.

Aa-Ad, TRPV1 channels are required for BB1 receptor-elicited increases in spontaneous glutamate release in BLA neurons. *Aa*, representative traces of sEPSCs before, during and after the application of NMB in the presence of AMG9810 (10 μ M). *Ab*, time course of sEPSC events averaged from 12 BLA neurons. sEPSCs elicited in control conditions are co-plotted for comparison. *Ac*, frequency of sEPSCs pooled from 12 cells before and after the application of NMB in the presence of AMG9810. *Ad*, amplitude of sEPSCs pooled from 12 cells before and after the application of NMB in the presence of AMG9810. *Ba*, representative sEPSCs recorded from a BLA neuron from a TRPV1 WT mouse before, during, and after the bath application of NMB. *Bb*, representative sEPSCs recorded from a BLA neurons from a TRPV1 KO mouse before, during, and after the bath application of NMB. *Bc*, time course of sEPSC events from TRPV1 WT and TRPV1 KO mice. *Bd*, frequency of sEPSCs pooled from 12 TRPV1 WT BLA neurons before and after application of NMB. *Be*, amplitude of sEPSCs pooled from 12 TRPV1 WT BLA neurons before and after application of NMB. *Bf*, frequency of sEPSCs pooled from 11 TRPV1 KO BLA neurons before and after the application of NMB. *Bg*, amplitude of sEPSCs pooled from 11 TRPV1 KO BLA neurons before and after the application of NMB. *Ca*, representative mEPSC traces recorded before, during, and after the application of NMB in the continuous presence of AMG9810 and tetrodotoxin. *Cb*, time course of mEPSC events averaged from 9 rat BLA neurons in the presence of AMG9810 and tetrodotoxin. sEPSCs elicited in control conditions are co-plotted for comparison. *Cc*, frequency of mEPSCs pooled from 9 rat BLA neurons before and after the application of NMB in the presence of AMG9810. *Cd*, amplitude of mEPSCs pooled from 9 rat BLA neurons before and after the application of NMB in the presence of AMG9810.



application of NMB did not significantly affect the frequency (baseline: 13.7 ± 3.1 Hz, NMB: 12.9 ± 2.5 Hz, 105 ± 15 % of baseline, $n = 9$, $P = 0.59$, Figure 16. *Ca-Cc*) or amplitude (baseline: 15.4 ± 0.75 pA, NMB: 15.5 ± 1.0 pA, 100 ± 4 % of baseline, $n = 9$, $P = 0.73$, Wilcoxon test, Figure 16. *Ca, Cd*) of the mEPSC events. Taken together, these data suggest NMB can enhance presynaptic glutamate release in BLA neurons requiring TRPV1 channels.

However, if NMB potentiates glutamate release via TRPV1 channels, it stands to reason that NMB should further augment evoked EPSC because voltage-gated calcium influx will also be functional during eEPSCs. We recorded eEPSCs from BLA neurons by placing a stimulating electrode in the LA. Unexpectedly, application of NMB produced a significant, albeit transient, diminution in eEPSC amplitudes (89.3 ± 5.5 % of control, $n = 24$, $P = 0.03$ vs baseline, Figure 17. *Aa*) that returned to baseline levels during the wash of NMB in our whole-cell configuration (95.3 ± 6.2 % of control, $P = 0.46$ vs baseline, Figure 17. *Aa*). The effects of NMB on eEPSC could be due to its action on BB1 receptors at pre- or postsynaptic sites. We then differentiated the pre- and postsynaptic effects by calculating the coefficient of variation (CV) and paired-pulse ratio (PPR) of BLA EPSCs before and after the application of NMB, as alterations in these parameters are associated with altered presynaptic glutamate release. NMB significantly increased the value of CV ($n = 24$, $P = 0.008$, paired t-test, Figure 17. *Ab*), as well as the PPR ($n = 11$, $P = 0.02$ paired t-test, Figure 17. *Ac*) supporting a presynaptic mechanism. We next tested whether NMB suppressed glutamate release through a TRPV1-mediated mechanism. In slices treated with AMG9810 to block TRPV1 channels, application of NMB failed to significantly alter the amplitude of BLA eEPSCs (101 ± 3 % of baseline, $n = 9$, $P = 0.83$; Figure 17. *Ba*). These results suggest that NMB decreased eEPSCs by

a short-term depression of presynaptic glutamate release, independent of TRPV1 channels.

It is possible that the action of NMB generates a retrograde messenger to depress evoked glutamate release. The cannabinoid 1 (CB1) receptor is activated by 2-AG, an endogenous endocannabinoid generated by DAG lipase via retrograde signaling to suppress synaptic transmission [321]. To examine this possibility, slices were treated with AM251 (10 μ M), a CB1 receptor inhibitor, to block CB1 receptor activation. AM251 alone does not affect eEPSCs [307]; therefore, AM251 was included in all solutions prior to NMB application. Activation of the BB1 receptor in slices treated with AM251 produced an initial increase in BLA eEPSCs to 143 ± 16 % of baseline ($n = 16$, $P = 0.02$, Figure 17. *Bb*) that returned to baseline ($106 \pm 11\%$ of baseline, $P = 0.52$, Figure 17. *Bb*) before significantly increasing to $227 \pm 45\%$ of the baseline value throughout the wash ($P = 0.01$, Figure 17. *Bb*). Together, these results indicate that NMB potentiates spontaneous glutamate release requiring TRPV1 channels and suppresses evoked glutamate release, at least in part, through presynaptic CB1 receptor activation.

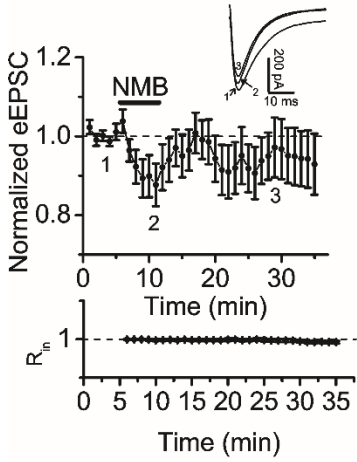
BB1 Receptor Activation in the BLA Produces Anxiogenic Phenotypes

The BLA is involved in motivational regulation and sensory processing [15] and sends projections to other brain regions involved in stress coping behavior including the BNST [322]. In our present study, we demonstrate that NMB enhanced spontaneous glutamate transmission in the BLA. Because augmented glutamate release results in anxiety [323] and NMB and its receptor have been implicated in fear and anxiety-like responses [223, 239, 272], we investigated the role of BB1 receptor activation on anxiety-like behaviors in the BLA. VCT is a well validated anxiety-model utilizing avoidance-approach behaviors in which water deprived animals are presented with a conflict between receiving a mild foot shock as they drink from a water bottle [233].

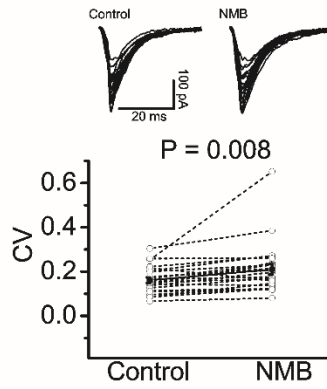
Figure 17. BB1 receptors suppress evoked glutamate release through a presynaptic mechanism.

Aa-Ac, Activated BB1 receptors suppress evoked glutamate release in BLA neurons through a presynaptic mechanism. *Aa*, time course of eEPSCs averaged from 24 BLA neurons. Current traces averaged from 10 EPSC events before (1), during (2), and after (3) application of NMB are shown in the upper right. *Ab*, SD and mean were obtained by averaging 15 consecutive EPSCs. Top shows eEPSC recorded before (left) and during (right) the application of NMB. Bottom shows the calculated CVs from 24 cells (open circles) and their average (filled circles). *Ac*, Top left, EPSCs averaged from at least 25 current traces before (black, bold) and during (grey, thin) the application of NMB. Top right, EPSCs recorded before (black, bold) and during (thin, grey) application of NMB were scaled to the first EPSC. Note that the second EPSC during the application of NMB is larger than control. Bottom, paired pulse ratio ($PPR = P2/P1$, P1 and P2 are the EPSCs evoked by two stimuli at an interval of 50 ms) recorded from 9 cells (open circles) and their average (filled circle). *Ba*, time course of eEPSC events averaged from 9 BLA neurons in the continuous presence of AMG9810. Current traces averaged from 10 EPSC events before (1), during (2), and after (3) application of NMB are displayed in the upper left. *Bb*, time course of eEPSC events averaged from 16 BLA neurons in the continuous presence of AM251. Current traces averaged from 10 EPSC events before (1), during (2), and after (3) application of NMB are shown in the upper left.

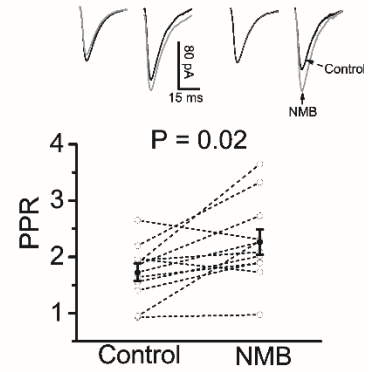
Aa



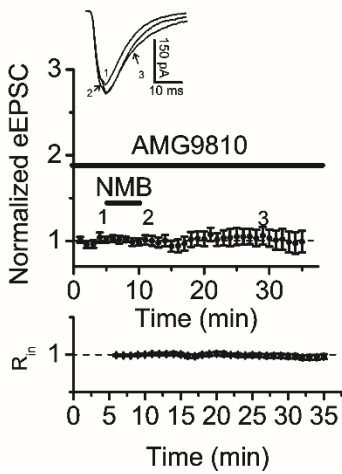
Ab



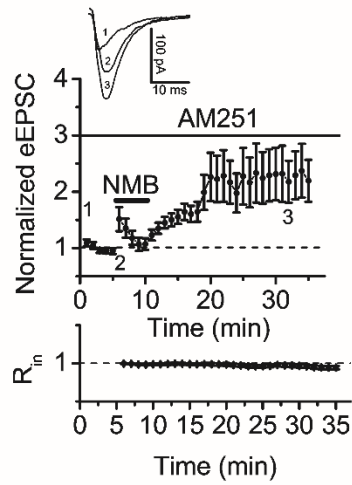
Ac



Ba



Bb



To probe the effects and underlying mechanisms of BB1 receptor activation on VCT, we microinjected NMB and/or other compounds into the BLA prior to VCT (Figure 18. A).

Microinjection of NMB into the BLA dose-dependently reduced the number of licks compared to rats injected with saline (0.9% NaCl) (Figure 18, *Ba*). Whereas microinjection of NMB at 0.1 nmol did not significantly alter the number of licks in the VCT ($P = 0.45$), the number of licks was significantly reduced in rats injected with 0.3 nmol NMB ($P = 0.038$) and 1 nmol NMB ($P = 0.0007$, one-way ANOVA followed by Dunnett's multiple comparisons test, Figure 18. *Ba*). These data suggest that application of NMB into the BLA exerts anxiogenic effects. Rats were microinjected with 1 nmol NMB in the remaining experiments to understand the role of NMB in anxiety-like behaviors. We tested the involvement of BB1 receptors in NMB-mediated anxiety-like behaviors by microinjecting the selective BB1 receptor antagonist, BIM23042 (0.3 nmol) [223, 250]. Rats injected with BIM23042 displayed a significantly larger number of licks than those injected with saline ($P = 0.032$, one-way ANOVA followed by Tukey's multiple comparisons test, Figure 18. *Bb*). Whereas microinjection of NMB following BIM23042 significantly lessened NMB-mediated anxiogenic effects (1 nmol NMB vs. BIM+NMB, $P = 0.011$, one-way ANOVA followed by Tukey's test, Figure 18. *Bb*), application of NMB counteracted the enlarged number of licks seen in rats injected with BIM23042 alone (BIM23042 vs. BIM+NMB, $P = 0.014$, one-way ANOVA followed by Tukey's test, Figure 18. *Bb*). One possibility to explain the anxiolytic effect of BIM23042 is that endogenous NMB produces anxiogenic phenotypes within the BLA. Together, these results indicate that BB1 receptors are required for NMB-mediated anxiogenic effects in the BLA.

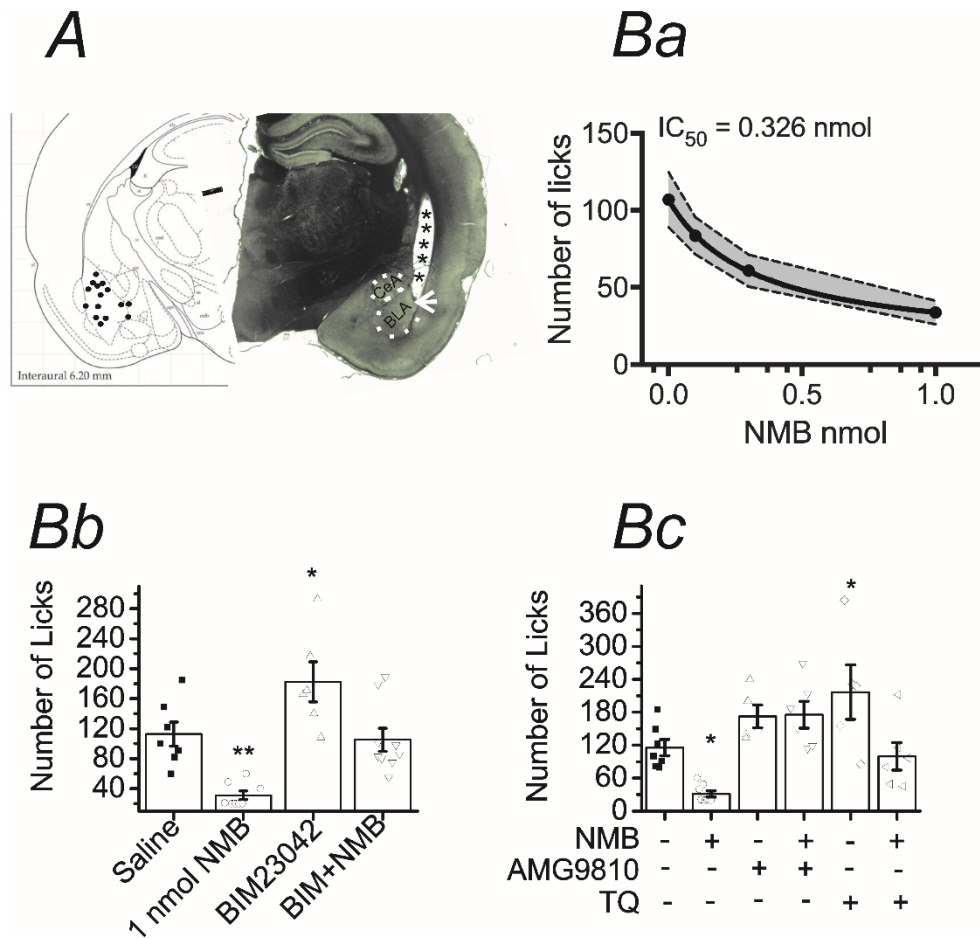


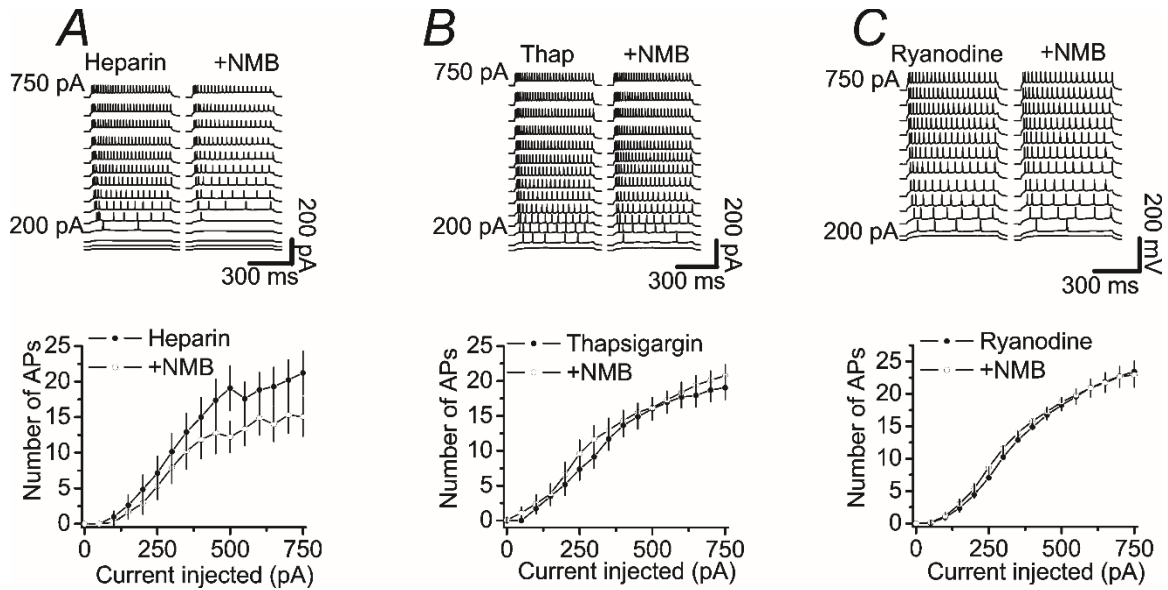
Figure 18. Application of NMB into the BLA dose-dependently increase anxiety-like behaviors.

A, Representative coronal section displaying (right) proper cannula placement and (left) cannula locations displayed onto atlas figure adapted from Paxinos and Watson [221]. Note: all cannula placements were verified, dots represent a subset of rats used in these experiments. *Ba*, microinjection of NMB dose-dependently reduced lick numbers. Shaded grey area represents SEM. *Bb*, microinjection of NMB (1 nmol) into the BLA reduced lick number, whereas prior injection of the BB1 receptor antagonist, BIM23042 (0.3 nmol), alleviated NMB-mediate anxiety-like behaviors. *Bc*, TRPV1 channel and GIRK channels are involved in NMB-mediated anxiety-like behaviors in the BLA. * $P < 0.05$, ** $P < 0.01$ vs saline (one-way ANOVA followed by Dunnett's test).

TRPV1 and GIRK Channels are Involved in BB1 Receptor-Mediated Anxiety-Like Behaviors in the BLA

Our *in vitro* results indicate that activation of BB1 receptors promotes excitability in BLA neurons by opening TRPV1 channels and depression of GIRK channels. We further explored the roles of these ion channels in NMB-mediated anxiety. Microinjection of AMG9810 at 1 nmol, an effective dose demonstrated previously [324, 325], had no effect on the number of licks (saline vs. AMG9810, $P = 0.35$, one-way ANOVA followed by Dunnett's test, Figure 18. *Bc*), but blocked NMB-induced anxiogenic effects (saline vs. AMG9810+NMB, $P = 0.26$, one-way ANOVA followed by Dunnett's test, Figure 18. *Bc*). These results demonstrate the TRPV1 channels are involved in BB1-receptor-mediated anxiogenic effects.

We then tested the involvement of GIRK channels in BB1 receptor-mediated anxiogenic effects. In rats microinjected with tertiapin-Q at 250 pmol [223, 224] the number of licks was significantly larger than in saline treated mice (saline vs. tertiapin-Q, $P = 0.03$, one-way ANOVA followed by Dunnett's test, Figure 18. *Bc*), whereas microinjection of NMB after tertiapin-Q failed to produce anxiety-like behaviors (saline vs. TQ+NMB, $P = 0.63$, one-way ANOVA followed by Dunnett's test, Figure 18. *Bc*). These results suggest that GIRK channels are involved in BB1-receptor enhancement of anxiety-like behaviors. A summary of the findings from Study 2 is shown in Figure 27.



Supplementary Figure 1. BB1 receptor-mediated excitation requires release of intracellular Ca^{2+} .

A, representative traces (upper) and summary graph (lower) of NMB-augmentation of APs in response to the positive current injection protocol in slices recorded with intracellular application of the IP_3 receptor inhibitor heparin (0.5 mg/ml). B, example of AP traces (upper) and summary graphs (lower) of NMB-mediated APs in response to the positive current injection protocol with the intracellularly dialyzed SERCA inhibitor, thapsigargin (10 μ M). C, representative AP traces (upper) and summary graphs (lower) of NMB-elicited APs in response to the positive current injection protocol with intracellular application of the RyR receptor inhibitor ryanodine (100 μ M).

Study 3- Neurokinin-3 Receptor-Mediated Modulation of Basolateral Amygdala Neurons

Introduction

The tachykinins refer to the peptides encoded in rodents by the Tachykinin 1 (Tac1) and Tac2 (TAC3 in humans) genes, which are involved in neurotransmission and neuromodulation in the central nervous system [326]. Tac1 encodes a precursor protein that produces two peptides, substance P (SP) and neurokinin A (NKA), whereas Tac2/TAC3 encodes neurokinin B (NKB). SP, NKA and NKB interact respectively with the G-protein-coupled neurokinin receptors, NK1Rs, NK2Rs, and NK3Rs [327, 328]. These receptors are coupled to the pertussis toxin-insensitive G proteins $G_{q/11}$ to activate phospholipase C β (PLC β) to hydrolyze phosphatidylinositol 4,5-bisphosphate (PIP $_2$), resulting in the production of inositol 1,4,5-triphosphate (IP $_3$) to facilitate intracellular Ca $^{2+}$ release and diacylglycerol (DAG) to activate protein kinase C (PKC) [329, 330], although activation of adenylate cyclase, resulting in accumulation of cAMP and stimulation of protein kinase A and activation of phospholipase A2 and generation of arachidonic acid have been reported as well [330]. In mammals, tachykinins serve as neuromodulators or neurotransmitters in central brain circuits, as well as in pain, stress, anxiety, depressive disorder, aggression, memory formation, inflammation and hormone regulation [330-333]. However, the cellular and molecular mechanisms underlying tachykinins-mediated modulation of these physiological functions and pathological disorders have not been fully determined.

The amygdala is one of the important targets of tachykinins, as demonstrated that the amygdala contains SP [334-336], NKA [337] and NKB [338-340]. Furthermore, the amygdala expresses NK1Rs [341, 342], NK2Rs [343, 344] and NK3Rs [345-350]. With regard to NK3Rs, high densities of NK3R protein [345-347, 351] and NK3R mRNA [349] are distributed in the BLA in animals and in humans [350]. While NKB and NK3Rs in the

CeA have been reported to be involved in the consolidation of fear memories [339, 352], the functions of NK3Rs in the BLA have not been determined. In Study 3, we showed that activation of NK3Rs in the BLA facilitated the excitability of BLA principal neurons by activating TRPC4/5 channels and depressing inwardly rectifying K⁺ (Kir) channels via PLCβ-mediated hydrolysis of PIP₂. We further showed that microinjection of senktide into the BLA increased fear-potentiated startle (FPS) response via activation of TRPC4/5 channels and depression of Kir channels. Our results provide a cellular and molecular mechanism to explain the roles of tachykinins in fear and anxiety responses.

Activation of NK3Rs Excites BLA Principal Neurons

Because high densities of NK3Rs are expressed in the BLA neurons of a variety of species including rats [345-347] and humans [347, 350] and activation of NK3Rs increases the expression of c-fos, a marker of neuronal activity, in the amygdala [348, 353], we probed the effects of NK3R activation on the excitability of principal neurons in rat BLA (Figure. 19A). The extracellular solution contained kynurenic acid (1 mM) to block glutamatergic transmission and picrotoxin (100 μM) to block GABAergic transmission. The intracellular solution was the K⁺-gluconate intracellular solution. Under these circumstances, the effects of NK3R agonists should be from the recorded neurons. Bath application of the selective NK3R agonist, senktide at 0.3 μM which is a near-saturating concentration (see below), induced subthreshold depolarization (Control: -63.8 ± 3.1 mV, Senktide: -61.1 ± 3.2 mV, $n = 20$, $P < 0.0001$, Wilcoxon test, Figure 19Ba-b). We then injected a depolarizing current to elevate the membrane potential to just above the firing threshold (-50.1 ± 4.3 mV, $n = 16$) to elicit sparse AP firing and further tested the effect of senktide on the excitability of BLA neurons. Bath application of the same concentration of senktide for 5 min significantly augmented the AP firing frequency (Control: 0.33 ± 0.23 Hz, Senktide: 3.71 ± 2.34 Hz, $n = 16$,

$P < 0.0001$, Wilcoxon test, Figure. 19Ca-c) and the persistent increases of AP firing were still observed after wash in senktide-free extracellular solution for ~ 1 h (1.80 ± 1.39 Hz, $n = 16$, $P < 0.0001$ vs. Control, Wilcoxon test, Figure. 19Ca-c). Furthermore, application of senktide significantly increased AP firing numbers elicited by injecting a series of positive currents from 50 pA to 700 pA at an increment of 50 pA ($n = 14$, $F_{(1,13)} = 21.26$, $P = 0.0005$, Two-way repeated measures ANOVA followed by Šídák's multiple comparison tests, Figure. 19Da-b). These results together indicate that bath application of senktide significantly enhanced the excitability of BLA neurons.

To test the involvement of NK3Rs, we pretreated the slices with the selective NK3R antagonist, SB 218795 (3 μ M) [354] and the bath was continuously perfused with the same concentration of SB 218795. Under these circumstances, bath application of senktide failed to increase AP firing numbers significantly ($n = 18$, $F_{(1,17)} = 1.609$, $P = 0.222$, Two-way repeated measures ANOVA followed by Šídák's multiple comparison tests, Figure. 19Ea-b), suggesting the involvement of NK3Rs. Because neurokinin B (NKB) is an endogenous agonist for NK3Rs, we also tested the effects of NKB on membrane potentials and AP firing numbers. Bath application of NKB (0.3 μ M) also elicited subthreshold depolarization (Control: -65.3 ± 4.7 mV, NKB: -61.9 ± 4.6 mV, $n = 7$, $P = 0.016$, Wilcoxon test, Figure. 19F). We then injected a persistent positive current to elevate the membrane potentials to just above the firing threshold (-49.9 ± 2.9 mV, $n = 8$) and tested the effect of NKB on AP firing. Bath application of NKB (0.3 μ M) significantly enhanced the AP firing frequency (Control: 0.35 ± 0.25 Hz, NKB: 2.99 ± 1.65 Hz, $n = 8$, $P = 0.008$, Wilcoxon test, Figure. 19Ga-c). Likewise, bath application of NKB at the same concentration significantly augmented the firing number of APs evoked by injecting the positive currents from 50 pA to 700 pA at an increment of 50 pA ($n = 13$, $F_{(1,12)} = 30.91$, $P = 0.0001$, Two-way repeated measures ANOVA

followed by Šídák's multiple comparison tests, Figure. 19Ha-b). These results together indicate that activation of NK3Rs excites the BLA principal neurons.

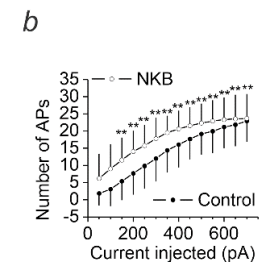
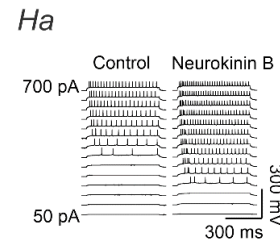
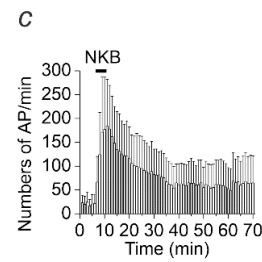
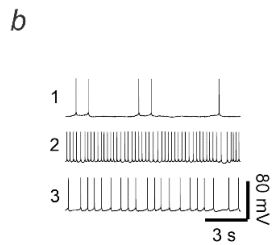
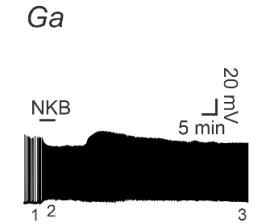
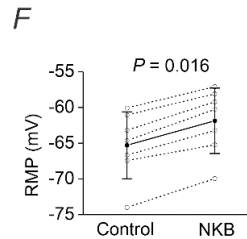
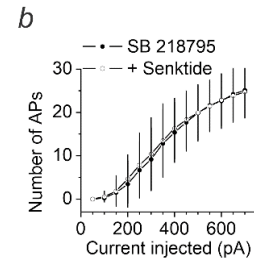
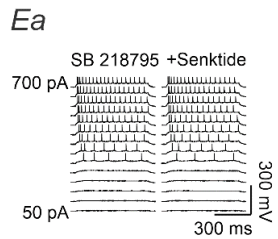
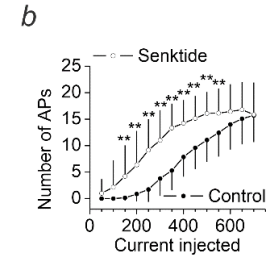
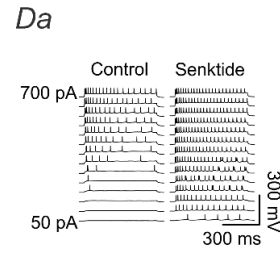
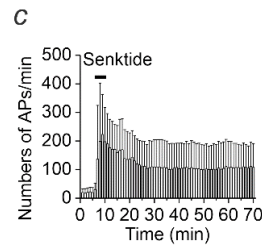
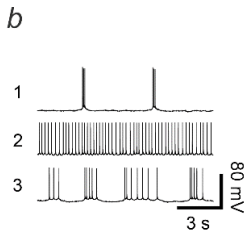
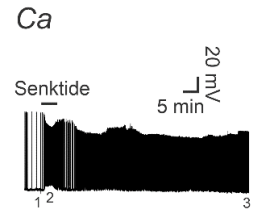
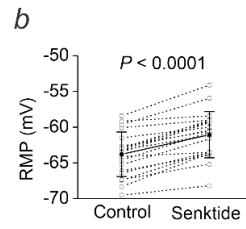
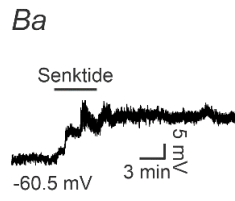
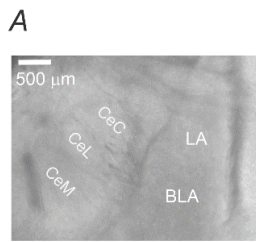
Stimulation of NK3Rs Activates a Cation Channel and Inhibits an Inwardly Rectifying K⁺ Channel

We further identified the ionic mechanisms whereby activation of NK3Rs facilitates the excitability of BLA neurons. Opening of cation channels and depression of K⁺ channels are the two common ionic mechanisms underlying neuronal excitability. Bath application of senktide (0.3 μM) elicited an inward current recorded at -60 mV with the K⁺-gluconate internal solution (-42.7 ± 20.0 pA, $n = 17$, $P < 0.0001$ vs. baseline, Wilcoxon test, Figure. 20Aa and Ad). The EC₅₀ value of senktide was calculated to be 0.064 μM (Figure. 20Ab). We therefore used 0.3 μM senktide for the remaining experiments because this is a near-saturating concentration. Replacement of the K⁺-gluconate-containing intracellular solution with the Cs⁺-gluconate-containing solution to limit the contribution of K⁺ channels significantly ($P < 0.0001$, Mann-Whitney test) reduced the senktide-induced inward holding currents (-16.7 ± 18.1 pA, $n = 25$, $P < 0.0001$ vs. baseline, Wilcoxon test; $P < 0.0001$ vs. the senktide-induced inward currents recorded in K⁺-containing internal solution, Mann-Whitney test, Figure. 20Ac-d), suggesting that depression of K⁺ channels is one mechanism responsible for NK3R-mediated excitation of BLA neurons.

We further measured the I-V relationship of senktide-induced currents to probe the ionic mechanisms whereby activation of NK3Rs excites BLA neurons. Among the 22 BLA pyramidal neurons recorded, 11 cells showed an I-V curve suggestive of non-selective cation channels, i.e., senktide elicited persistent inward currents at the voltages tested (Figure. 20Ba-Bc) and 11 cells displayed an I-V curve resembling that of the inwardly rectifying K⁺ (Kir) channels with a reversal potential at -88.7 ± 17.5 mV

Figure 19. Activation of NK3Rs excites BLA principal neurons.

A, microscopic photograph of amygdala to show the location of BLA where electrophysiological recordings were conducted. LA, lateral nucleus; BLA, basolateral nucleus; CeC, capsular central amygdala; CeL, lateral central amygdala; CeM, medial central amygdala. **Ba-Bb**, Bath application of the selective NK3R agonist, senktide (0.3 μ M), induced subthreshold depolarization of BLA neurons. **Ba**, RMP recorded from a BLA principal neuron prior to, during and after application of senktide. **Bb**, Summary data for senktide-elicited subthreshold depolarization. Empty symbols were data from individual cells and solid symbols were their averages (n = 20). **Ca-Cc**, Application of senktide increased AP firing frequency when a positive current was injected persistently to induce initial sparse AP firing. **Ca**, APs recorded from a BLA neuron prior to, during and after application of senktide when a positive current was injected persistently to induce basal sparse AP firing. **Cb**, APs recorded at the time points indicated in **Ca** in an expanded scale. **Cc**, Summary data showing senktide-induced excitation of BLA neurons (n = 16). **Da-Db**, Bath application of senktide augmented AP firing elicited by injection of a series of positive currents from 50 pA to 700 pA at an increment of 50 pA and duration of 600 ms every 6 seconds. **Da**, APs recorded from a BLA neuron evoked by the positive current injection protocol before (*left*) and during (*right*) the application of senktide. **Db**, Relationship between the injected currents and the elicited AP numbers from 14 BLA neurons. **Ea-Eb**, Senktide-elicited excitation of BLA neurons was mediated by activation of NK3Rs. **Ea**, APs recorded from a BLA neuron evoked by the positive current injection protocol before (*left*) and during (*right*) the application of senktide in a slice pretreated with the selective NK3 receptor antagonist, SB 218795 (3 μ M). The extracellular solution continuously contained the same concentration of SB 218795. **Eb**, Relationship between the injected currents and the elicited AP numbers from 18 BLA neurons prior to and during the application of senktide in the continuous presence of SB 218795. **F**, Bath application of neurokinin B (NKB, 0.3 μ M), the endogenous NK3 receptor agonist, depolarized BLA neurons. Empty symbols were data from individual cells and solid symbols were their averages (n = 7). **Ga-Gc**, Application of NKB (0.3 μ M) increased AP firing frequency when a positive current was injected persistently to induce initial sparse AP firing. **Ga**, APs recorded from a BLA neuron prior to, during and after application of NKB when a positive current was injected persistently to induce basal sparse AP firing. **Gb**, APs recorded at the time points indicated in **Ga** in an expanded scale. **Gc**, Summary data showing NKB-induced excitation of BLA neurons (n = 8). **Ha-Hb**, Application of NKB (0.3 μ M) augmented AP firing numbers evoked by injection of a series of positive currents from 50 pA to 700 pA at an increment of 50 pA recorded from the BLA neurons. **Ha**, APs recorded by the current injection protocol before (*left*) and during (*right*) the application of NKB. **Hb**, Relationship between the injected currents and the elicited AP numbers from 13 BLA neurons before and during the application of NKB. Adapted from [224].



($n = 11$) (Figure. 20Ca-Cc), close to the calculated K^+ reversal potential (-95.8 mV). One plausible explanation for the difference of the measured reversal potential and the calculated K^+ reversal potential is that the latent effect of senktide on the cation channels right-shifted the measured K^+ reversal potential. We further used Cs^+ -gluconate-containing intracellular solution to block K^+ channels and included TTX ($0.5 \mu M$) to block Na^+ channels and $CdCl_2$ ($200 \mu M$) and $NiCl_2$ ($400 \mu M$) to block Ca^{2+} channels. We measured the reversal potential of senktide-elicited cation channel currents by extending the voltage ranges to $+20$ mV. Under these circumstances, the I-V curve of the senktide-induced currents showed outward rectification with a reversal potential of -26.8 ± 18.0 mV ($n = 18$, Figure. 20Da-Dc). These results together suggest that activation of NK3Rs excites BLA principal neurons by opening a non-selective cation channel and depressing a Kir channel.

We further tested the roles of Kir channels in senktide-induced inward holding currents. Kir channels are sensitive to micromolar concentration of Ba^{2+} [355-357]. Bath application of Ba^{2+} ($500 \mu M$), by itself induced an inward holding current (-42.7 ± 20.4 pA, $n = 20$, $P < 0.0001$, Wilcoxon test, Figure. 21A, 3F) and significantly reduced senktide-elicited inward currents (-18.8 ± 13.0 pA, $n = 20$, $P = 0.0008$ vs. senktide alone, one-way ANOVA followed by Dunnett's test, Figure. 21A, 3G). Kir channels include Kir2, Kir3 (GIRK) and Kir6 (ATP-sensitive, K_{ATP}) subfamilies and the K^+ transport channels [358]. We utilized ML 133, a specific antagonist for Kir2 subfamily [256-260] to test the roles of the Kir2 subfamily in senktide-elicited excitation of BLA principal neurons. Bath application of ML 133 ($30 \mu M$) by itself did not change the holding currents significantly (-0.02 ± 7.63 pA, $n = 15$, $P = 0.847$, Wilcoxon test, Figure. 21B, 21F). In the presence of ML 133, application of senktide still elicited a comparable inward current (-40.9 ± 23.9 pA, $n = 15$, $P = 0.996$ vs. senktide alone,

Figure 20.

Senktide-elicited excitation of BLA neurons is mediated by opening a cation channel and inhibiting a Kir channel.

Aa-Ad, Activation of NK3Rs concentration-dependently excited BLA neurons.

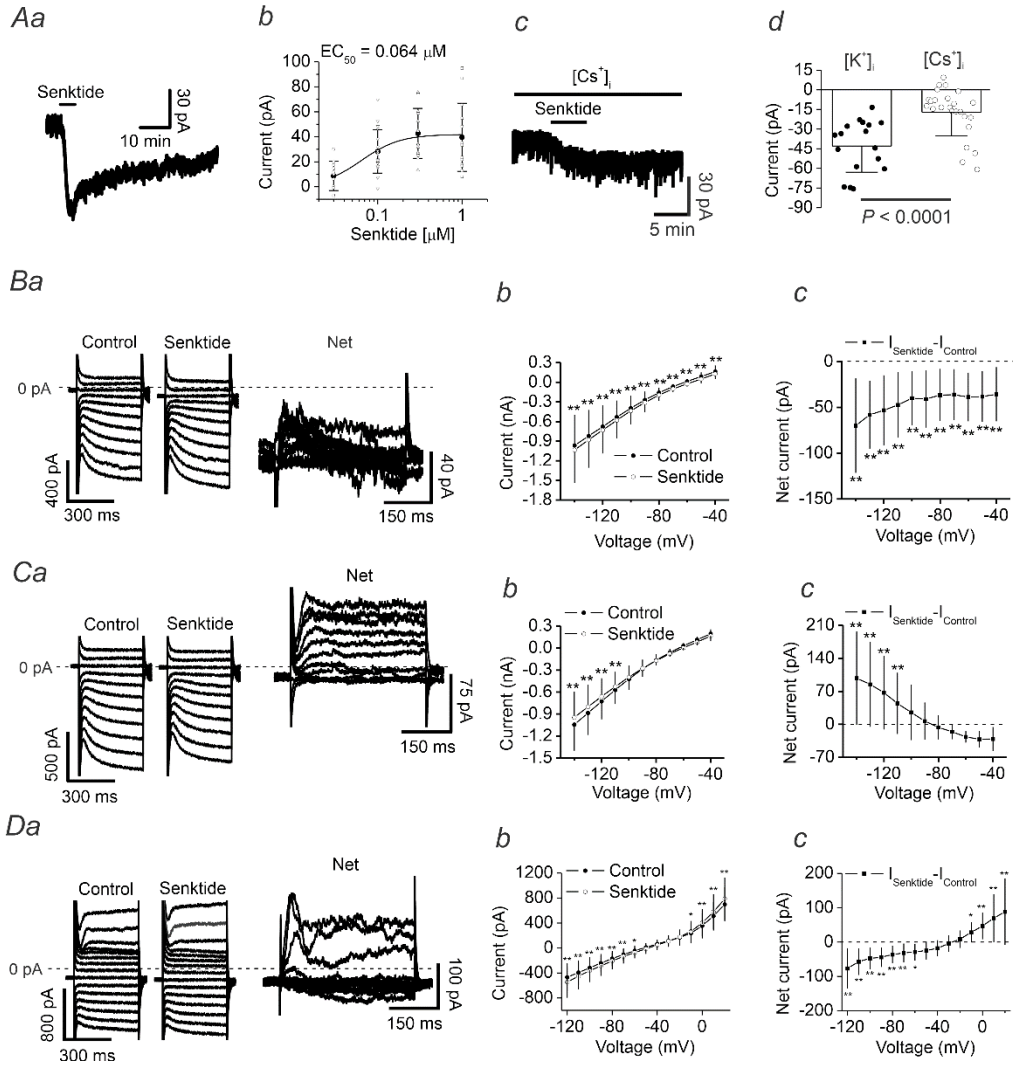
Aa, Trace of inward current induced by bath application of senktide recorded from a BLA neuron with K⁺-gluconate-containing intracellular solution.

Ab, Concentration-response curve of senktide-induced inward currents recorded with K⁺-gluconate-containing intracellular solution. The empty symbols were the inward currents from individual cells and the solid symbols were their averages. **Ac**, Trace of inward current induced by bath application of senktide recorded from a BLA neuron with Cs⁺-gluconate-containing intracellular solution. **Ad**, Summary data showing senktide-induced inward currents with K⁺-containing intracellular solution (solid circles) and Cs⁺-containing intracellular solution (empty circles). The bars were their averages.

Ba-Bc, Senktide opened a cation channel. The extracellular solution contained TTX (0.5 μM), kynurenic acid (1 mM) and picrotoxin (100 μM) and the intracellular solution was the K⁺-gluconate-containing internal solution. **Ba**, Currents elicited by a voltage-step protocol before (*left*) and during (*middle*) bath application of senktide and the net current obtained by subtraction (*right*) from a BLA neuron. The dash line was the zero current level. **Bb**, I-V curve averaged from 11 cells before and during application of senktide (Two-way repeated measures ANOVA followed by Šídák's multiple comparison test; Drug: $F_{(1, 10)} = 30.03$, $P = 0.0003$; Voltage: $F_{(10, 100)} = 42.98$, $P < 0.0001$; Drug x Voltage: $F_{(10, 100)} = 3.056$, $P = 0.002$; ** $P < 0.0001$).

Bc, I-V curve of the net current obtained by subtracting the currents in control condition from those after application of senktide. **Ca-Cc**, Senktide depressed a Kir channel. The extracellular solution contained TTX (0.5 μM), kynurenic acid (1 mM) and picrotoxin (100 μM) and the intracellular solution was the K⁺-gluconate-containing internal solution. **Ca**, Currents elicited by the voltage-step protocol before (*left*) and during (*middle*) bath application of senktide and the net current obtained by subtraction (*right*) from a BLA neuron. The dash line was the zero current level. **Cb**, I-V curve averaged from 11 cells before and during application of senktide (Two-way repeated measures ANOVA followed by Šídák's multiple comparison test; Drug: $F_{(1, 10)} = 2.553$, $P = 0.141$; Voltage: $F_{(10, 100)} = 80.87$, $P < 0.0001$; Drug x Voltage: $F_{(10, 100)} = 14.51$, $P < 0.0001$; ** $P < 0.001$).

Cc, I-V curve of the net current obtained by subtracting the currents in control condition from those during application of senktide. **Da-Dc**, Senktide opened a cation channel of outward rectification recorded in the extracellular solution containing 0.5 μM TTX, 1 mM kynurenic acid, 100 μM picrotoxin, 200 μM CdCl₂ and 400 μM NiCl₂ and intracellular solution was Cs⁺-gluconate-containing intracellular solution. **Da**, Currents elicited by the voltage-step protocol before (*left*) and during (*middle*) bath application of senktide and the net current obtained by subtraction (*right*) from a BLA neuron. The dash line was the zero current level. **Db**, I-V curve averaged from 18 cells before and during the application of senktide (Two-way repeated measures ANOVA followed by Šídák's multiple comparison test; Drug: $F_{(1, 17)} = 2.701$, $P = 0.119$; Voltage: $F_{(14, 238)} = 146.7$, $P < 0.0001$; Drug x Voltage: $F_{(14, 238)} = 27.83$, $P < 0.0001$; * $P = 0.05$, ** $P < 0.01$). **Dc**, I-V curve of the net current obtained by subtracting the currents in control condition from those during application of senktide. Adapted from [224].



one-way ANOVA followed by Dunnett's test, Figure. 21B, 21G), suggesting that Kir2 subfamily is not the type of Kir channels involved in senktide-elicited excitation. We then tested the roles of K_{ATP} channels in senktide-induced inward currents. Bath application of the selective K_{ATP} channel blocker, glibenclamide (100 μ M) did not significantly alter the holding currents in BLA neurons (-4.5 ± 13.7 pA, $n = 19$, $P = 0.490$, Wilcoxon test, Figure. 21C, 21F) and exerted no effect on senktide-elicited inward currents (-32.1 ± 22.3 pA, $n = 19$, $P = 0.261$ vs. senktide alone, one-way ANOVA followed by Dunnett's test, Figure. 21C, 21G), suggesting that K_{ATP} channels are not involved. We then tested the roles of GIRK (Kir3) subfamily in senktide-elicited excitation. Application of the selective GIRK channel blocker, tertiapin-Q (500 nM) induced an inward current by itself (-30.6 ± 18.6 pA, $n = 16$, $P < 0.0001$, Wilcoxon test, Figure. 21D, 21F), suggesting the expression of GIRK channels in the BLA principal neurons. In the continuous presence of tertiapin-Q, application of senktide induced a significantly smaller inward current (-16.0 ± 11.4 pA, $n = 15$, $P = 0.0004$ vs. senktide alone, one-way ANOVA followed by Dunnett's test, Figure. 21D, 21G), suggesting that GIRK channels are involved in senktide-mediated excitation of BLA pyramidal neurons. Consistent with the involvement of GIRK channels, application of ML 297 (10 μ M), an activator of GIRK1-containing channels [262], induced an outward current (76.3 ± 50.0 pA, $n = 7$, $P = 0.016$ vs. baseline, Wilcoxon test, Figure. 21E-F), suggesting that GIRK1 channels are functionally expressed in the BLA principal neurons, and they may be involved in senktide-elicited excitation of BLA principal neurons.

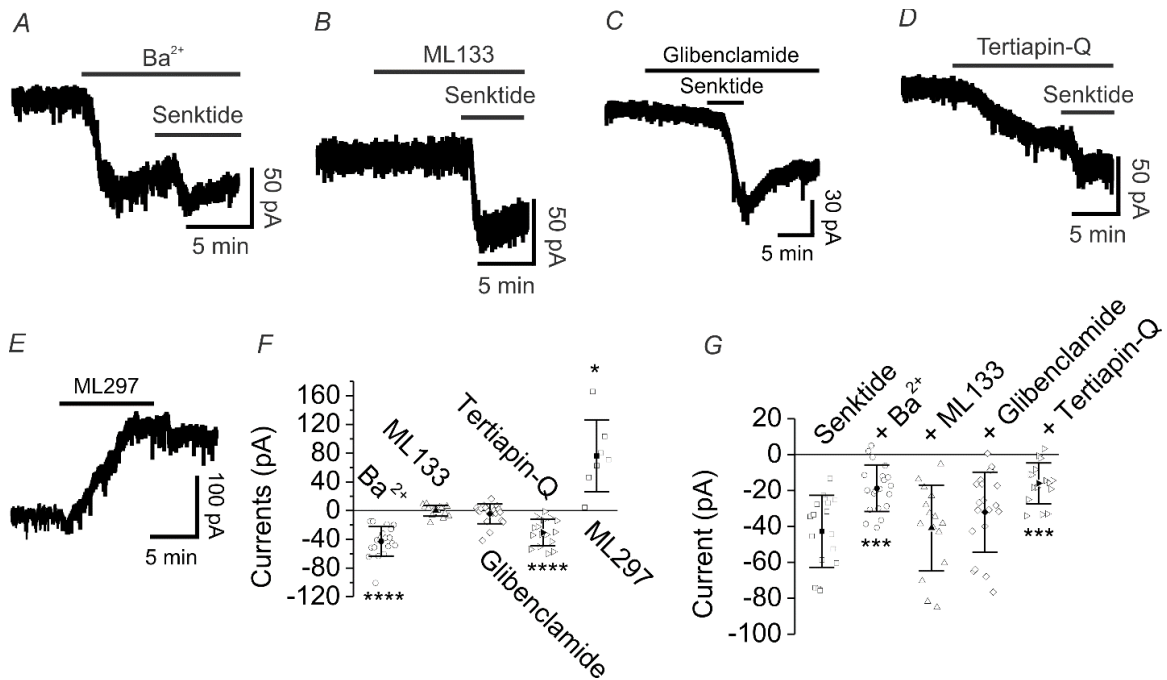


Figure 21. GIRK channels are required for NK3R-elicited inward currents in BLA neurons.

A, current trace recorded from a BLA neuron in response to Ba^{2+} (500 μM) alone and Ba^{2+} plus senktide. **B**, current trace recorded from a BLA neuron in response to ML133 (30 μM) alone and ML133 plus senktide. **C**, current trace recorded from a BLA neuron in response to bath application of glibenclamide (100 μM) alone and together with senktide. **D**, current trace recorded from a BLA neuron in response to tertiapin-Q (500 nM) alone and tertiapin-Q plus senktide. **E**, current trace recorded from a BLA neuron in response to bath application of ML297 (10 μM). **F**, summary data for the effects of Kir channel modulators on BLA neurons. **** $P < 0.0001$ vs. baseline, Wilcoxon test. **G**, Summary graph showing the effects of Kir channel blockers on senktide-mediated inward currents. *** $P < 0.001$ vs. senktide alone, one-way ANOVA followed by Dunnett's test. Adapted from [224].

TRPC4 and TRPC5 Channels are Involved in NK3R-Elicited Excitation of BLA Principal Neurons

We further identified the cation channels involved in NK3R-elicited excitation of BLA principal neurons. The I-V curve of the senktide-sensitive currents resembles that of TRPC4, TRPC5 and TRPV1 [297] channels. The BLA principal neurons express TRPV1 [298, 301], TRPC4 [359] and TRPC5 [360] channels. We next tested the roles of these channels in NK3R-mediated excitation of BLA principal neurons. Bath application of the selective TRPC4/5 channel blocker, M084 (100 μ M) alone, did not alter the holding currents significantly (3.0 ± 9.5 pA, $n = 10$, $P = 0.375$, Wilcoxon test, data not shown). Slices were pretreated with M084 (100 μ M), and the extracellular solution was perfused continuously with the same concentration of M084. Application of M084 significantly reduced senktide-induced increases in inward currents (M084 + senktide: -25.0 ± 18.8 pA, $n = 19$ vs. senktide alone: -42.7 ± 20.0 pA, $n = 17$, $P = 0.019$, Mann-Whitney test, Figure. 22Aa-c), suggesting the involvement of TRPC4/5 channels. We further tested the roles of TRPC4/5 channels by using the knockout mice for TRPC4 or TRPC5 channels. Application of senktide induced a significantly smaller inward current in slices prepared from the TRPC4 KO mice (-12.7 ± 7.8 pA, $n = 22$), compared with the corresponding WT mice (-35.5 ± 15.1 pA, $n = 17$, $P < 0.0001$ vs. TRPC4 KO mice, Mann-Whitney test, Figure. 22Ba-c), suggesting the participation of TRPC4 channels in NK3R-elicited excitation of BLA neurons. Likewise, application of senktide evoked a significantly smaller inward current in slices cut from TRPC5 KO mice (-8.7 ± 7.8 pA, $n = 22$), compared with the corresponding WT mice (-34.6 ± 18.4 pA, $n = 17$, $P < 0.0001$, Mann-Whitney test, Figure. 22Ca-c), suggesting the involvement of TRPC5 channels. We also used the TRPV1 KO mice. Application of senktide induced an inward current (-17.1 ± 13.2 pA, $n = 36$) in slices cut from TRPV1 KO mice, which was not significantly different from that obtained from the corresponding WT mice (-23.7 ± 17.2 pA, $n = 22$,

$P = 0.213$ vs. TRPV1 KO mice, Mann-Whitney test, Figure. 22Da-c), suggesting that TRPV1 channels are not required for NK3-mediated excitation of BLA neurons.

NK3R-Mediated Excitation of BLA Neurons is Dependent on PLC β and PLC β -Mediated Hydrolysis of PIP $_2$

Because activation of NK3Rs activates PLC β pathway [329, 330], we tested the roles of PLC β in NK3R-induced inward currents. Bath application of the selective PLC inhibitor, U73122 (5 μ M) had no acute effects on the holding currents recorded from the BLA neurons (-4.82 ± 6.6 pA, $n = 5$, $P = 0.188$, Wilcoxon test, data not shown). Pretreatment of slices with and continuous bath application of U73122 (5 μ M), significantly reduced senktide-evoked inward currents (-14.4 ± 8.0 pA, $n = 16$, $P < 0.0001$ vs. senktide alone, one-way ANOVA followed by Dunnett's test, Figure. 23B, 23E), suggesting the involvement of PLC β . Activation of PLC β hydrolyzes PIP $_2$ to generate IP $_3$ to increase intracellular Ca $^{2+}$ release and DAG to activate PKC. We further tested the roles of these two second messengers in NK3R-mediated inward currents. Inclusion of the IP $_3$ receptor blocker, heparin (0.5 mg/ml) in the recording pipettes failed to alter senktide-elicited inward currents significantly (-33.0 ± 19.0 pA, $n = 16$, $P = 0.221$ vs. senktide alone, one-way ANOVA followed by Dunnett's test, Figure. 23C, 23E), suggesting that IP $_3$ receptors are not involved in NK3R-induced excitation of BLA neurons. Moreover, intracellular application of the sarcoplasmic ATPase inhibitor, thapsigargin (10 μ M), to deplete Ca $^{2+}$ stores, did not alter significantly senktide-mediated inward currents (-34.0 ± 15.7 pA, $n = 19$, $P = 0.270$ vs. senktide alone, one-way ANOVA followed by Dunnett's test, Figure. 23D, 23E), suggesting that intracellular Ca $^{2+}$ release is not required for NK3R-mediated excitation of BLA principal neurons. We then probed the roles of PKC in NK3R-elicited excitation of BLA principal neurons. Pretreatment of slices with and continuous bath application of the selective PKC inhibitor, bisindolylmaleimide II (Bis II, 2 μ M), did not significantly alter senktide-induced

Figure 22. TRPC4 and TRPC5 channels are involved in NK3R-induced inward currents in BLA neurons.

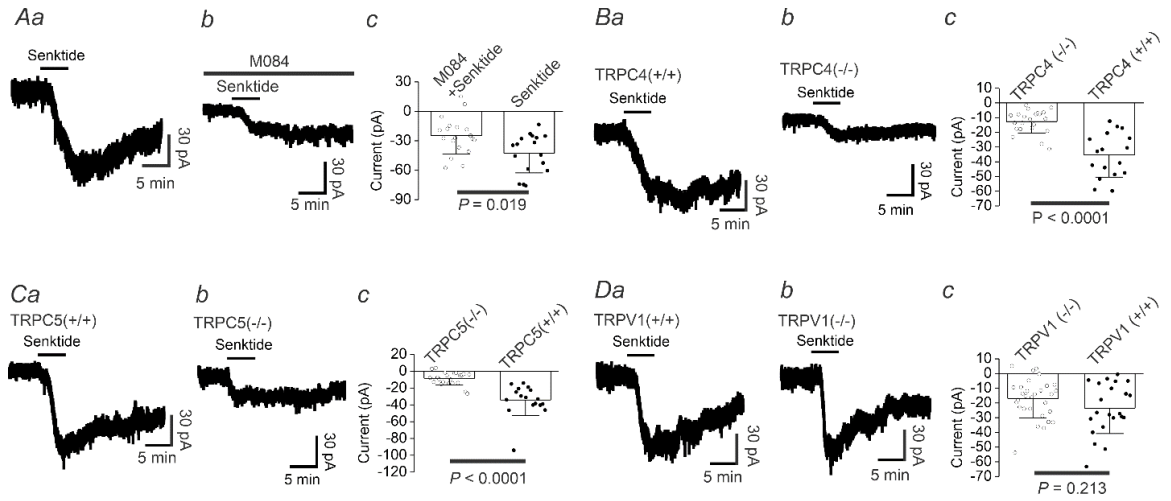
Aa-Ac: pretreatment of slices with and continuous bath application of M084 (100 μ M) significantly reduced senktide-induced inward currents. **Aa:** senktide-elicited inward current recorded from a BLA neuron in control condition. **Ab:** senktide-induced inward current recorded from a BLA neuron in a slice treated with the TRPC4/5 channels blocker, M084 (100 μ M). **Ac:** summary graph showing the decreased inward currents induced by senktide in the presence of M084. Circles represented the inward current from individual cells and the bars were their averages.

Ba-Bc: bath application of senktide induced a significantly smaller inward current in slices cut from TRPC4 KO mice (TRPC4(-/-)), compared with the corresponding WT mice (TRPC4(+/+)). **Ba:** senktide-evoked inward current recorded from a BLA neuron in a slice cut from a WT mouse. **Bb:** senktide-induced inward current recorded from a BLA neuron in a slice cut from a TRPC4 KO mouse. **Bc:** summary graph showing that senktide induced a significantly smaller inward current in TRPC4 KO mice compared with the corresponding WT mice. Circles represented the inward current from individual cells and the bars were their averages.

Ca-Cc: bath application of senktide induced a significantly smaller inward current in slices cut from TRPC5 KO mice (TRPC5(-/-)), compared with the corresponding WT mice (TRPC5(+/+)). **Ca:** senktide-elicited inward current recorded from a BLA neuron in a slice cut from a WT mouse. **Cb:** senktide-induced inward current recorded from a BLA neuron in a slice cut from a TRPC5 KO mouse. **Cc:** summary graph showing that senktide induced a significantly smaller inward current in TRPC5 KO mice compared with the corresponding WT mice. Circles represented the inward current from individual cells and the bars were their averages.

Da-Dc: TRPV1 channels were not necessary for NK3R-mediated excitation of BLA neurons. **Da:** senktide-elicited inward current recorded from a BLA neuron in a slice cut from a WT mouse. **Db:** senktide-induced inward current recorded from a BLA neuron in a slice cut from a TRPV1 KO mouse. **Dc:** summary graph indicating that senktide did not significantly alter senktide-induced inward currents in TRPV1 KO mice compared with the corresponding WT mice. Circles represented the inward current from individual cells and the bars were their averages.

Adapted from [224].



inward currents (-39.8 ± 25.4 pA, $n = 12$, $P = 0.962$ vs. senktide alone, one-way ANOVA followed by Dunnett's test, Figure. 23F, 23I). Likewise, administration of another PKC inhibitor, chelerythrine ($10 \mu\text{M}$), in the same fashion, did not significantly change senktide-elicited inward currents (-40.2 ± 22.4 pA, $n = 12$, $P = 0.975$ vs. senktide alone, one-way ANOVA followed by Dunnett's test, Figure. 23G, 23I). These data together suggest that the function of PKC is irrelevant to NK3R-mediated excitation of BLA neurons.

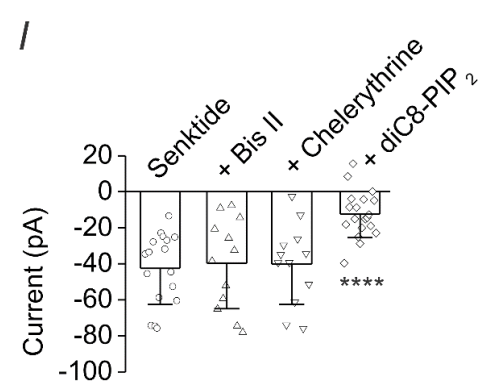
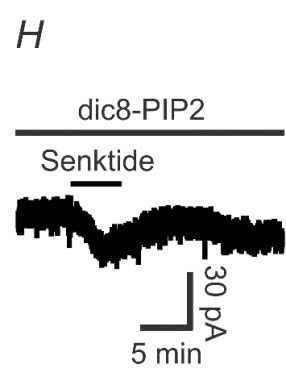
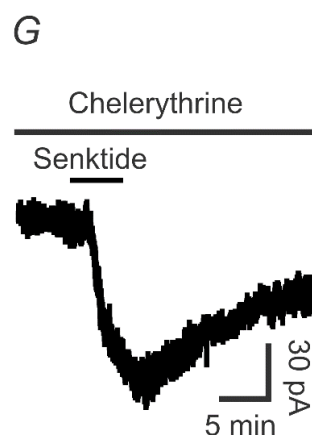
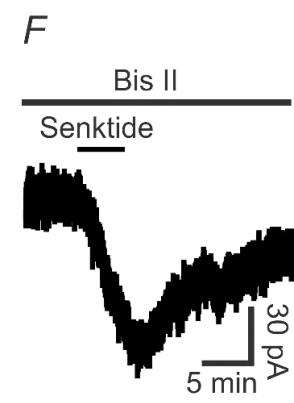
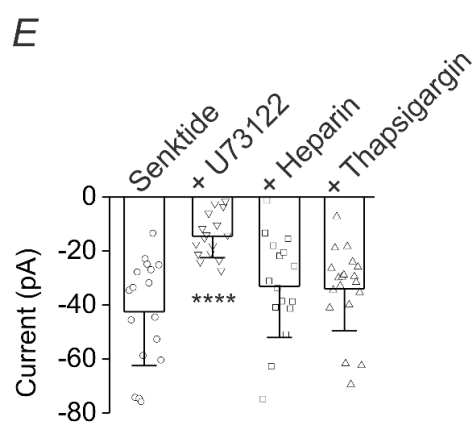
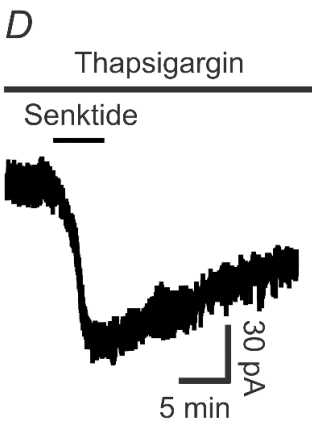
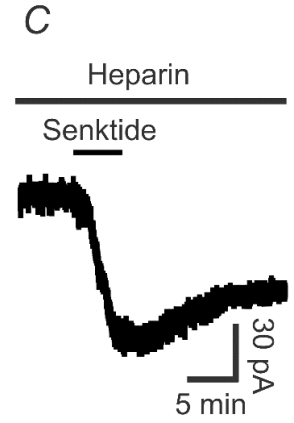
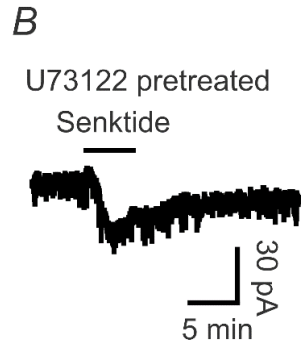
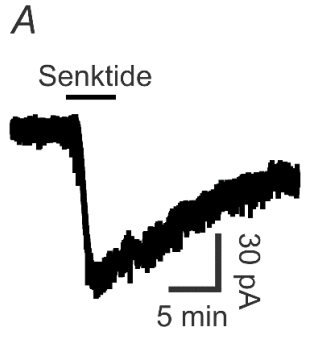
We further tested the roles of PLC β -mediated hydrolysis of PIP $_2$ in senktide-mediated inward currents. Inclusion of the diC8-PIP $_2$ ($40 \mu\text{M}$) to compensate the turnover of PIP $_2$ content elicited by PLC β significantly reduced senktide-elicited inward currents (-12.5 ± 13.0 pA, $n = 19$, $P < 0.0001$ vs. senktide alone, one-way ANOVA followed by Dunnett's test, Figure. 23H, 23I), suggesting that PLC β -mediated hydrolysis of PIP $_2$ is responsible for NK3R-mediated excitation of BLA neurons.

NK3R-Mediated Excitation of BLA Neurons Augments Cued Startle Responses

Because the BLA is closely associated with the FPS responses [277, 361-364], we tested the roles of NK3R-mediated excitation of BLA principal neurons in FPS responses. The FPS paradigm measures conditioned fear by an increase in the amplitude of a simple reflex (the acoustic startle reflex) in the presence of a cue previously paired with a shock. This test has been proven to be a valuable tool to study mechanisms involved in the acquisition and expression of conditioned fear in both rats and humans [365, 366]. We implanted cannulae into the BLA and microinjected senktide and/or other compounds into the BLA to probe the effects and the underlying mechanisms of NK3R activation on FPS by using the paradigm shown in Figure 24A. Figure 24B showed the locations of the cannula tips for a subset of experiments and the diffusion area of Chicago Sky Blue dye injected at the end of the experiments.

Figure 23. NK3R-elicited excitation of BLA neurons requires PLC β -mediated hydrolysis of PIP $_2$.

A, Inward current trace induced by bath application of senktide in control condition. **B**, Current trace evoked by senktide recorded from a BLA neuron in a slice treated with U73122 (5 μ M). **C**, Senktide-induced inward current recorded from a BLA neuron in a pipette containing heparin (0.5 mg/ml). **D**, Current trace elicited by senktide in a BLA neuron intracellularly dialyzed with thapsigargin (10 μ M). **E**, Summary graph. Empty symbols were the senktide-induced net currents from individual cells and the bars were their averages. **F**, Current trace evoked by senktide recorded from a BLA neuron in a slice pretreated and continuously bath-applied with the selective PKC inhibitor, Bis II (2 μ M). **G**, Senktide-induced current trace recorded from a BLA neuron in a slice pretreated and continuously bath-applied with the PKC inhibitor, chelerythrine (10 μ M). **H**, Current trace elicited by senktide recorded from a BLA neuron dialyzed intracellularly with diC8-PIP $_2$ (40 μ M). **I**, Summary graph. Empty symbols were the senktide-induced net currents from individual cells and the bars were their averages. Adapted from [224].



Microinjection of senktide into the BLA of rats dose-dependently increased the cued startle response compared with the rats injected with saline (0.9% NaCl) (0.3 nmol, $P = 0.047$; 1 nmol, $P = 0.008$, one-way ANOVA followed by Tukey's test, Figure. 24Ca), whereas senktide had no significant effects on the non-cued startle response ($P = 0.314$, one-way ANOVA followed by Tukey's test, Figure. 24Cb), the startle amplitude ($P = 0.063$, one-way ANOVA followed by Tukey's test, Figure. 24Cc) and the shock reactivity amplitude ($P = 0.738$, one-way ANOVA followed by Tukey's test, Figure. 24Cd), suggesting that senktide treatment had no effect on generalized stimuli in this paradigm. For the remaining experiments, we used 0.3 nmol senktide because this is an effective dose.

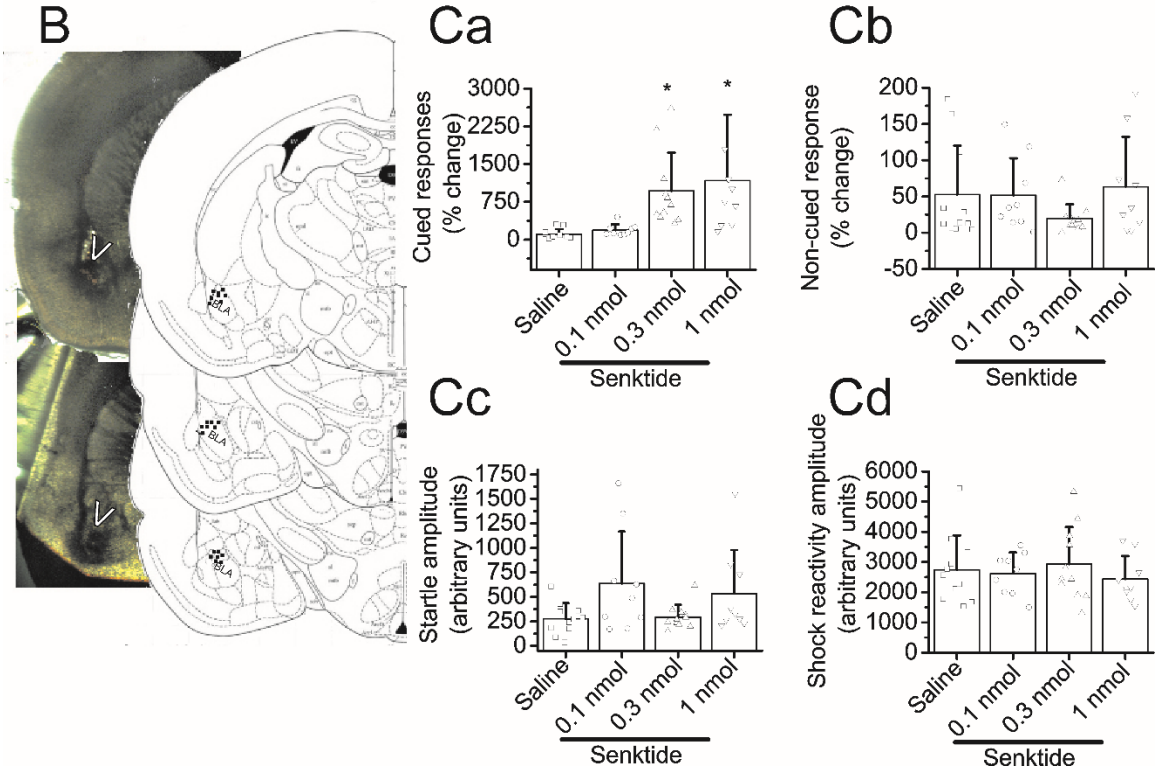
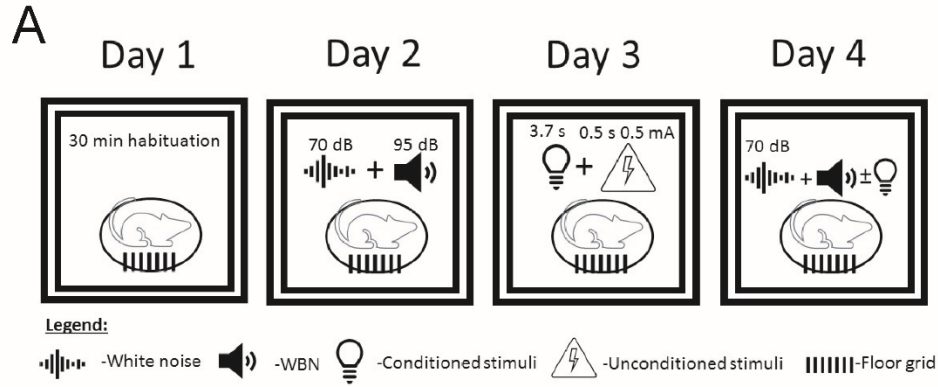
We tested the involvement of NK3Rs by microinjection of the selective NK3R antagonist, SB218795. Microinjection of SB218795 (20 nmol) by itself prior to fear conditioning had no significant effect on cued responses (saline vs SB218795, $P = 0.998$; one-way ANOVA followed by Tukey's test), but blocked the enhancement of cued responses elicited by senktide (Senktide alone vs. SB 218795 + Senktide, $P = 0.006$; SB218795 + Senktide vs. saline, $P = 0.984$; one-way ANOVA followed by Tukey's test, Figure. 25A), indicating that NK3Rs are responsible for senktide-elicited augmentation of cued-startle response in the BLA.

GIRK Channels and TRPC4/5 Channels are Involved in NK3R-Mediated Enhancement of Startle Responses

Our results indicate that activation of NK3Rs facilitated the excitabilities of BLA neurons by depression of GIRK channels and opening of TRPC4 and TRPC5 channels. We further examined the roles of these channels in senktide-mediated augmentation of startle responses. Microinjection of TQ at 250 pmol, an effective dose demonstrated previously [268, 367], failed to change significantly either the cued (saline vs. TQ,

Figure 24. Microinjection of senktide into the BLA dose-dependently enhances cued startle responses.

A, schematic representation of the experimental paradigm. Day 1, animals were habituated within the startle chambers for 30 minutes. Day 2, animals were allowed a 5-minute acclimation and presented with 30 WNBs (95 dB, 50 ms, 30 ITI) in the presence of a background white-noise (70 dB). Day 3, animals were injected with test compounds 5 minutes prior to fear conditioning. Upon placement in the startle chamber, animals were allowed a 5-minute acclimation before presentation of ten 3.7 s light cues that co-terminate with a foot shock (0.5s, 0.5 mA, pseudorandom ITI 30-180 s). Day 4, rats were allowed a 5-minute acclimation within the startle chamber prior to presentation of 30 WNBs (as on Day 2). The first ten WNBs were used for measurement of basal startle amplitude. The remaining 20 WNBs were divided such that 10 WNBs were paired with light (cued) and 10 occurred without (non-cued) in a pseudorandom order. Background noise was present during this session. **B**, (left) proper cannula placement and the diffusion area of reagents were verified with bilateral injection of 3 % Chicago Sky Blue dye into the BLA (white arrows); (right) cannula tip placements displayed onto atlas figures adapted from Paxinos and Watson [222]. Note: all animal cannula placements were verified, dots represent a subset of the rats used for the experiments. **Ca**, microinjection of senktide dose-dependently increased cued startle responses. **Cb**, BLA microinjection of senktide had no effect on non-cued startle responses. **Cc**, startle amplitude was not significantly affected by senktide microinjection. **Cd**, behavioral responses to foot shock on Day 3 did not differ significantly in response to increasing doses of senktide.



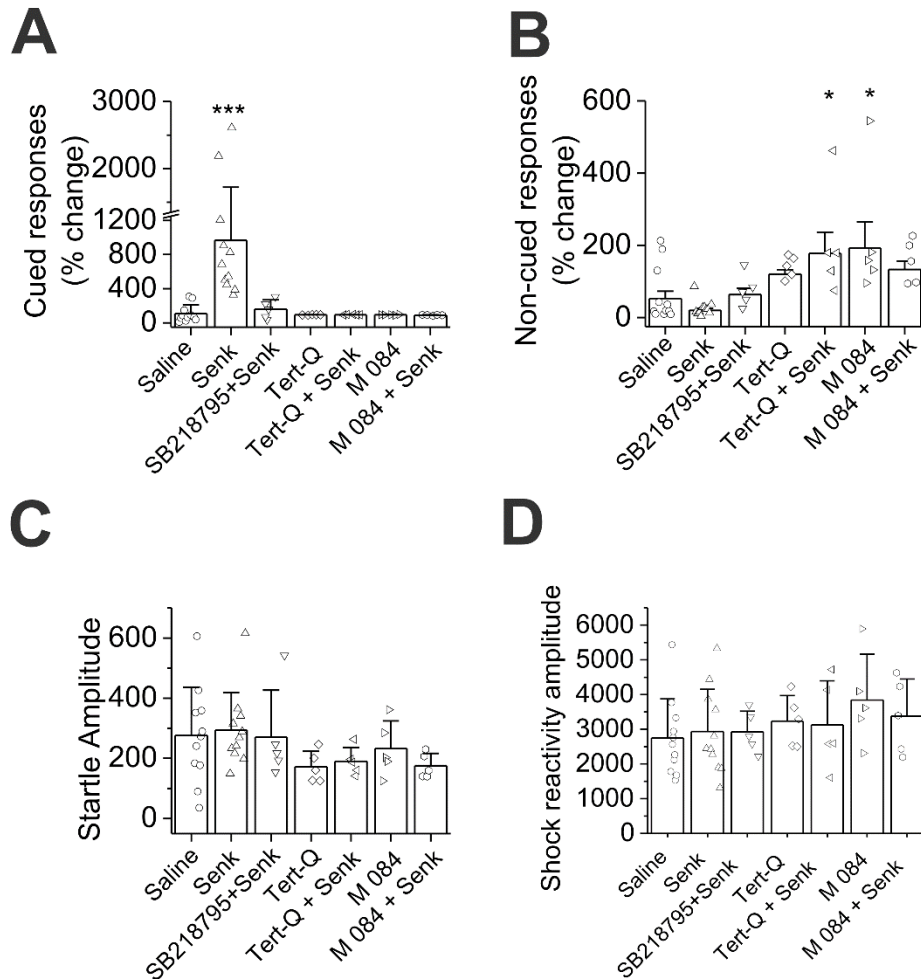


Figure 25. Roles of NK3Rs, GIRK and TRPC4/5 channels in senktide-mediated augmentation of cued startle responses.

A, Microinjection of senktide (Senk, 0.3 nmol) into the BLA enhanced cued startle responses, whereas prior administration of the NK3R antagonist, SB218795 (20 nmol), GIRK channel blocker, TQ (Tert-Q, 250 pmol) or TRPC4/5 channel blocker, M084 (100 nmol) blocked senktide-induced augmentation of cued response. **B**, non-cued startle responses of the tested compounds and significant enhancements of non-cued startle in the group of rats injected with both tertiapin-Q and senktide and the group of rats injected with M 084. * $P < 0.05$ vs. saline (one-way ANOVA followed by Tukey's test). **C**, group data for startle amplitude on Day 1. **D**, group data for shock reactivity during fear conditioning on Day 2. Adapted from [224].

$P = 0.991$; one-way ANOVA followed by Tukey's test, Figure. 25A) or the non-cued (saline vs. TQ, $P = 0.677$, one-way ANOVA followed by Tukey's test, Figure. 25B) responses. Microinjection of senktide following TQ did not alter significantly the cued startle response (TQ vs. TQ + senktide, $P = 0.992$, one-way ANOVA followed by Tukey's test, Figure. 25A), whereas significantly enhanced the non-cued response (TQ vs. TQ + senktide, $P = 0.009$, one-way ANOVA followed by Tukey's test, Figure. 25B). These results together suggest that GIRK channels are involved in NK3R-mediated enhancement of startle response.

We then tested the involvement of TRPC4/5 channels in NK3R-elicited augmentation of FPS responses. Microinjection of the TRPC4/5 channel blocker, M084 (100 nmol), into the BLA did not significantly alter the cued startle responses (Saline vs. M084, $P = 0.997$, one-way ANOVA followed by Tukey's test, Figure. 25A), but blocked senktide-induced enhancement of cued startle response (Saline vs. M084 + Senktide, $P = 0.998$, one-way ANOVA followed by Tukey's test, Figure. 25A). However, microinjection of M084 significantly enhanced the non-cued fear response, compared with the saline-injected group (saline vs. M084, $P = 0.028$, one-way ANOVA followed by Tukey's test, Figure. 25B). Administration of senktide following the injection of M084 failed to significantly increase the non-cued response further (M084 vs. M084 + senktide, $P = 0.125$, one-way ANOVA followed by Tukey's test, Figure. 25B). These results suggest that TRPC4/5 channels are involved in NK3R-elicited enhancement of startle responses.

There were no significant differences for the startle amplitudes obtained during the acoustic startle response session on Day 2 among the experimental groups ($P = 0.297$, $F_{(6,40)} = 1.26$, one-way ANOVA, Figure. 25C), suggesting that there was no endogenous between-group difference in responses to startle-inducing white-noise bursts. The shock reactivity amplitude was unaffected in any group as the result of the microinjection ($P =$

0.664, $F_{(6, 40)} = 0.68$, one-way ANOVA, Figure. 25D). Together these data suggest similar behavioral responses to startle-inducing auditory stimuli among these groups and no between-group differences in nociceptive responses to shock resulting from drug injection. Based on our experimental results, we propose a working mode to explain the cellular and molecular mechanisms underpinning NK3R-mediated excitation of BLA neurons and augmentation of FPS response (Figure. 28).

CHAPTER 4

DISCUSSION

Study 1 - Neuromedin B-Mediated Modulation of Central Amygdala Neurons

Whilst injection of bombesin into the CeA increases mean arterial pressure [245] and decreases food intake [246, 247], the cellular and molecular mechanisms whereby bombesin and bombesin-like peptides modulate these physiological functions have not been determined. As NMB peptide mRNA [243] and NMB binding sites [244] are expressed in the CeA and peripheral and central administration of bombesin increases Fos-like immunoreactivity, a marker of neuronal activation, in the CeL [248], we tested the hypothesis that activation of BB1 receptors facilitates neuronal excitability in the CeL. Our results demonstrate that BB1 receptor activation excited CeL neurons via inhibition of GIRK type Kir channels. BB1 receptor-mediated excitation of CeL neurons and depression of Kir channel currents required the functions of G proteins, PLC β and PKC, but were independent of intracellular Ca²⁺ release. We further showed that BB1 receptor activation reduced MAP and HR, depending on GIRK channel activity. In ASR and FPS testing, microinjection of NMB into the CeA increased ASR, but reduced FPS to cued stimuli. Our results may provide a cellular and molecular mechanism by which bombesin and bombesin-like peptides regulate physiological functions *in vivo* (Figure 26.)

Neuropeptides of the bombesin family increase neuronal excitability mainly by two ionic mechanisms: depression of Kir channels and activation of cation channels. For example, GRP excites spinal cord neurons [368], paraventricular thalamic neurons [369] and interneurons in the entorhinal cortex [370] by depressing Kir channels; GRP excites

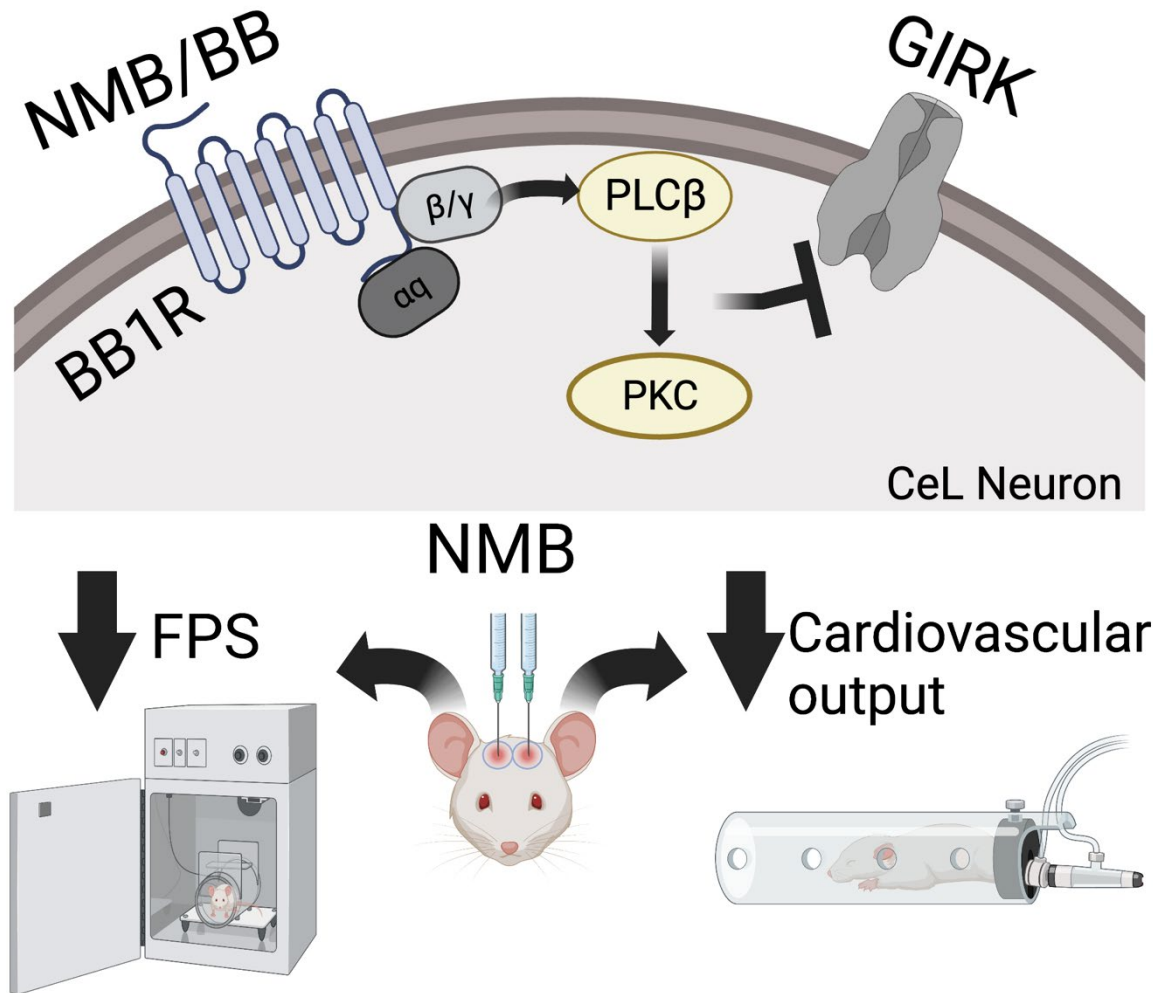


Figure 26. The proposed cellular and molecular mechanisms underpinning BB1 receptor-elicited excitation of CeA neurons and decreased FPS and cardiac output. Activation of BB1Rs by NMB results in activation of $G\alpha_q$ proteins leading to increases in PLC β activity. Activation of PLC β generates IP $_3$ to elevate intracellular Ca $^{2+}$ release from IP $_3$ -sensitive store and diacylglycerol (DAG) to activate protein kinase C (PKC). PLC β and PKC are required for depression of GIRK channels. The effects of BB1Rs on GIRK channels are responsible for BB1 receptor-mediated suppression of fear responses and cardiac output. Adapted from [223]. Created with BioRender.com

paraventricular thalamic neurons by activating TRPV1 channels [369]; both NMB and GRP excite neuropeptide Y-containing neurons in the arcuate nucleus by activation of nonselective cation channels and sodium/calcium exchangers [320] and hippocampal interneurons by activating a cation channel [371]. Consistent with this scenario, our results support a role of GIRK type Kir channels in BB1 receptor-elicited excitation of CeL neurons. Inhibition of a membrane conductance should increase input resistance and membrane time constants. Consistent with this anticipation, application of NMB augmented the input resistance and the membrane time constants of the CeL neurons. Moreover, the I-V curve of the NMB-sensitive current exhibited inward rectification with a reversal potential near the K⁺ reversal potential. Micromolar concentrations of Ba²⁺ selectively block Kir channels. Our results showed that application of 300 μM Ba²⁺ inhibited Kir channels by itself and blocked NMB-elicited depression of Kir currents, further supporting a role of Kir channels in NMB-mediated excitation of CeL neurons. Kir channels are classified into 4 functional subfamilies: Kir2 (Kir2.1, Kir2.2, Kir2.3, Kir2.4), Kir3 (GIRK channels, Kir3.1, Kir3.2, Kir3.3, Kir3.4), Kir6 (K_{ATP} channels, Kir6.1, Kir6.2), and K⁺ transport channels (Kir1.1, Kir4.1, Kir7.1) [255]. Our intracellular solution contained 2 mM ATP which would exert inhibition on K_{ATP} channels. Application of the selective Kir2 subfamily blocker ML 133 at a saturating concentration (30 μM) [372] attenuated Kir currents, suggesting that the CeL neurons express functional Kir2 subfamily channels. Consistent with our electrophysiological results, the amygdala expresses mRNAs for both Kir2.1 and Kir2.2 [373]. However, NMB-induced depression of Kir currents was not significantly altered by inclusion of ML 133 in the extracellular solution, suggesting that the Kir2 subfamily channels were not involved in NMB-elicited excitation of CeL neurons. TQ inhibits both GIRK and Kir1.1 channels [263-265], whereas tertiapin-LQ blocks Kir1.1 channels without effects on GIRK channels [266]. Application of TQ by itself elicited significant inhibition of Kir currents, whereas

application of tertiapin-LQ failed to alter Kir currents significantly. These results suggest that the CeL neurons express tonically functional GIRK channels without expression of Kir1.1 channels, consistent with the notion that GIRK channels are constitutively active [374-376]. Furthermore, NMB-induced inhibition of Kir currents was significantly reduced in the presence of TQ, but application of tertiapin-LQ failed to alter NMB-induced inhibition of Kir currents significantly. These results together suggest that activation of BB1 receptors excite CeL neurons by suppressing GIRK channels.

Our result that application of TQ alone significantly inhibited Kir channel currents satisfies the prerequisite that GIRK channels must be tonically active in the CeL neurons. Another precondition to explain our results is that the CeL neurons should physically express GIRK channels. The GIRK channels include GIRK1, GIRK2, GIRK3 and GIRK4, and these subunits are widely expressed in the brain, existing predominantly as heterotetramers of GIRK1, GIRK2 and/or GIRK3, or as homotetramers of the GIRK2 subunit [255, 377]. GIRK4 is not expressed in the amygdala [373, 378] but restricted to some neuronal populations such as Purkinje cells and neurons of the globus pallidus and the ventral pallidum, suggesting that GIRK4 channels are unlikely to be the molecular target of BB1 receptor activation in the CeL. Furthermore, our results did not support the involvement of GIRK1 channels in BB1 receptor-mediated excitation of CeL neurons, because application of ML 297, an activator selective for GIRK1-containing channels, did not affect Kir currents significantly in the CeL neurons, suggesting that there is no functional GIRK1 in the CeL neurons. Consistent with our electrophysiological data, the expression of GIRK1 mRNA has been detected more prominently in the BLA and cortical nuclei with less expression in the CeA of the amygdala [261]. Thus, the most possible subunit compositions involved in BB1 receptor-mediated excitation of CeL neurons are GIRK2 and GIRK3, which could exist as GIRK2/GIRK3 heterotetramers or GIRK2 homotetramers [255, 377]. In line with this

speculation, GIRK2 [373, 378] and GIRK3 [373] are expressed in the amygdala, and activation of both BB1 and BB2 receptors results in depression of GIRK channels including GIRK1, GIRK2 and GIRK4 expressed in *xenopus* oocytes [379]. BB1 receptors are coupled to $G\alpha_{q/11}$ resulting in activation of PLC β which hydrolyzes PIP₂ generating IP₃ to release intracellular Ca²⁺ and DAG to activate PKC [237, 239, 240]. Our results suggested that intracellular Ca²⁺ release was not required, whereas the activities of PLC β and PKC were necessary, for NMB-elicited excitation of CeL neurons and inhibition of Kir channels. Consistent with our results, PLC is required for NMB and GRP-mediated excitation of hippocampal interneurons although the involved ion channels are cation channels, not Kir channels [371]. In accordance with our results, activation of PKC phosphorylates and inhibits GIRK channels [379-381] and PLC and PKC are involved in BB1 or BB2 receptor-mediated depression of GIRK channels co-expressed in *xenopus* oocytes [379].

PKC is a serine-threonine kinase family of isozymes with different activation requirements of intracellular Ca²⁺ and DAG [382]. Classical/conventional PKC (cPKC) include PKC α , PKC β , and PKC γ and are dependent on Ca²⁺ and DAG; Novel PKC (nPKC) include PKC δ , PKC ϵ , PKC η , and PKC θ that are Ca²⁺ dependent but DAG independent; and atypical PKC (aPKC) that include PKC ζ and PKC λ which are independent of both Ca²⁺ and DAG. We demonstrated that application of the DAG analogue, PMA, significantly increased AP firing frequency but depressed Kir currents, suggesting the involvement of cPKC and nPKC. Chelation of intracellular Ca²⁺ with BAPTA via the recording pipettes blocked NMB-elicited augmentation of AP firing and lessened NMB-induced suppression of Kir currents, suggesting the involvement of cPKC. Agreeably, activation of cPKC isoforms phosphorylate and inhibit GIRK channels [383]. Our results indicate that activation of BB1 receptors enhances the excitability of

CeL neurons via PLC β and PKC-mediated depression of GIRK type Kir channels.

Consistent with our results, modulations of Kir channels [384-386], PLC β [217, 387] and PKC [388-392] affect anxiety and fear responses.

Both bombesin-like peptides and the CeA are involved in modulating fear/anxiety and appetitive behaviors [393-396], although bombesin-like peptides and their activity in the amygdala in the modulation of these physiological functions have not been fully determined. Injection of bombesin into the CeA reduces food intake [246, 247] and food ingestion increases the release of bombesin-like peptides from the CeA [397].

Consistent with our results, the function of PKC is required for amphetamine-mediated anorectic action [398]. NMB and GRP activate the hypothalamic-pituitary-adrenal axis resulting in increased release of ACTH and corticosterone [399] which are closely involved in emotional regulation. BB1 receptor knockout mice displayed decreased emotionality [400] and administration of a selective BB1 receptor agonist as well as antagonist paradoxically exerts anxiolytic effects [273, 401] and attenuates the FPS response [273]. Furthermore, the bombesin-like peptides are released from the CeA in response to stressor exposure [402]. Collectively, these results support that activation of BB1 receptors elicited by NMB modulate fear and anxiety responses. In our hands, microinjection of NMB significantly reduced FPS responses while increasing ASR with increasing intensity. We demonstrate a functional requirement of PKC for NMB-induced excitation of the CeA. In line with this, cPKC and nPKC isozymes are involved in G_q protein-mediated increased acoustic startle responses [403].

There are sex differences in the presentation of affective disorders [404] as well as sex differences in amygdala activation in response to emotionally relevant stimuli [405]. Our data indicate that NMB reduces FPS while enhancing ASR in both male and female rats. Due in part to limiting numbers of male and female rats and that bombesin-like peptide immunoreactivity in the limbic system does not vary with sex or estrous cycling

[406], the data from both sexes were pooled for the investigations of NMB on FPS and ASR. Because we did not determine the phase of the estrous cycle of the female rats in our study, one caveat of this study is that we cannot rule out the influences of the estrous cycle of the female rats on the effects of NMB. Whereas the estrous cycle of females affects anxiety-like behaviors and fear conditioning [407], FPS phenomena are dependent on CeA activity, and are not subjected to sex hormone modulation in both male and female rats [278, 279, 408, 409].

Injection of bombesin into the CeA induces an increase in MAP [245], consistent with reports of an increased response of the autonomic nervous system in fear and anxiety conditions. We demonstrated microinjection of NMB into the CeA dose-dependently reduced MAP and HR via activation of BB1 receptors and depression of GIRK channels. As bombesin non-selectively activates BB1 receptors and BB2 receptors [235, 236], the resultant increase in MAP by intra-CeA application of bombesin [245] may lend support to a hypothesis of distinct processes of each receptor on cardiovascular output from the CeA. Indeed, intraventricular application of GRP in trout produced significant increases in HR and MAP [410]. Another possibility is that BB1 receptor activation disinhibits CeA GABAergic interneurons producing increases in the baroreceptor responses and decreases in MAP and HR. Activation of CeA inhibitory projections to the dorsal vagal complex result in a decrease of the baroreceptor reflex and subsequent increases in MAP and HR [85]. As the CeA is populated by GABAergic interneurons that reciprocally inhibit each other to produce coordinated defensive responses [141, 411, 412], NMB-expressing microcircuits of the CeA may inhibit excitatory cardiovascular outputs from this nucleus. In addition, bombesin-like peptides have been demonstrated to interact with neuropeptide Y [413, 414], a peptide documented to suppress central cardiac output [415, 416]. NMB activates NPY-expressing neurons in the hypothalamic arcuate nucleus involved in energy homeostatic

processing due to co-expression of BB1 receptors [417]. As hypothalamic nuclei coordinate cardiovascular responses [418] and these nuclei receive inputs from the CeA [419, 420], NMB microinjection into the CeA may alter cardiovascular output via NMB-expressing projections to the hypothalamus. Further characterization of NMB-specific projections of the CeA is warranted.

Study 2 - Bombesin-1 Receptors Excites Neurons of the Basolateral Amygdala by Multiple Signaling and Ionic Mechanisms

Although NMB and BB1 receptor mRNA are expressed in the BLA [242, 280], the signaling and ionic mechanisms whereby activation of BB1 receptors modulates BLA principal neurons remains undetermined. Using whole-cell patch clamp electrophysiological recordings, we showed that NMB excited BLA neurons through the inhibition of GIRK channel currents and the activation of the Ca²⁺-permeable non-selective cation channel, TRPV1. The NMB-mediated increases in AP firing were dependent on the functional activity of PLC, PIP₂ turnover, PKC, and intracellular Ca²⁺ release. Furthermore, we demonstrated that activation of BLA BB1 receptors enhances sEPSCs through TRPV1 channels, but inhibits evoked glutamatergic synaptic transmission independent of TRPV1. Lastly, we demonstrated that microinjection of NMB into the BLA produces anxiety-like behaviors in the Vogel Conflict test.

NMB and GRP are excitatory neuropeptides that utilize distinct intracellular signaling and ionic mechanisms. For example, in primary sensory neurons, BB1 receptor activation stimulates PKA to enhance T-type voltage-gated Ca²⁺ channel currents independent of PLC [421]. Bombesin-like peptide excitation of hippocampal neurons requires PLC and intracellular Ca²⁺ release to activate nonselective cation channels [371]. Bombesin excites dorsal raphe neurons and entorhinal interneurons by suppressing a K⁺ conductance and GIRK channels, respectively [370, 422].

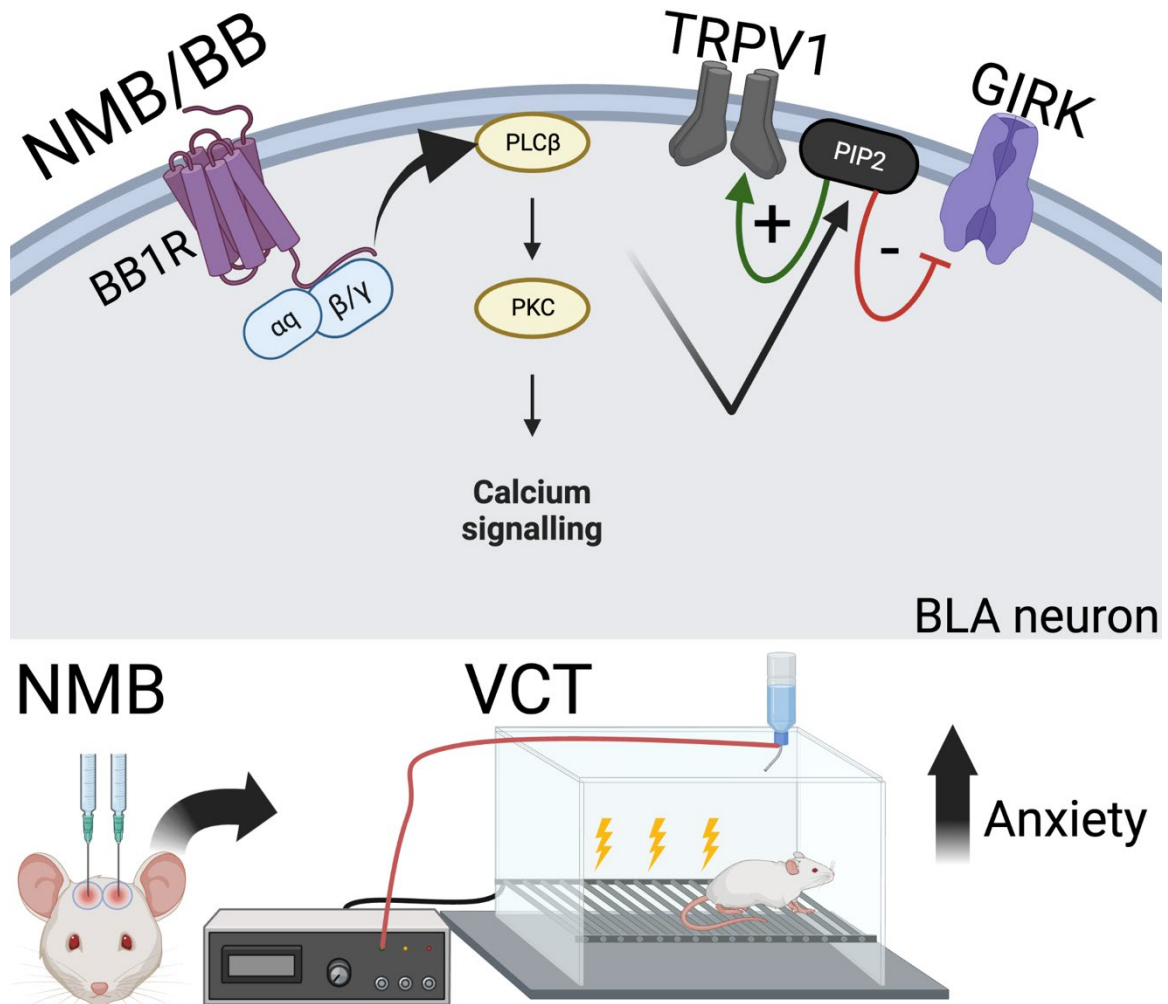


Figure 27. Working model illustrating the cellular and molecular mechanisms underpinning BB1 receptor-elicited excitation of BLA principal neurons and increased anxiety-like behaviors in the VCT. Activation of BB1Rs by NMB results in activation of G α_q proteins leading to increases in PLC β activity. Activation of PLC β catalyzes the hydrolysis of PIP $_2$ to generate IP $_3$ to elevate intracellular Ca $^{2+}$ release from IP $_3$ -sensitive store and diacylglycerol (DAG) to activate protein kinase C (PKC). PLC β -induced hydrolysis of PIP $_2$ results in depression of GIRK channels and opening of TRPV1 channels to excite BLA principal neurons. The effects of BB1Rs on GIRK channels and TRPV1 channels are responsible for BB1 receptor-induced anxiety-like behaviors in the VCT. Created with BioRender.com

In paraventricular thalamic neurons, bombesin-like peptides activate TRPV1 channels and inhibit Ba²⁺-sensitive Kir2 channels [369], whereas in preoptic GABAergic neurons bombesin activates an inward Ca²⁺-dependent cationic current [423]. NMB and GRP depolarize neurons in the arcuate nucleus by activating nonselective cation channels and Na⁺/Ca²⁺ exchangers, whereas NMB depolarizes CeL neurons by depressing GIRK channels through Ca²⁺-independent mechanisms [223, 320]. BB1 receptors are coupled to Gα_{q/11} proteins, resulting in PLC-mediated signaling. Consistent with these reports, our results indicate a functional requirement for PLCβ, PKC, and intracellular Ca²⁺ in NMB-mediated excitation of principal BLA neurons through inhibition of GIRK channels and activation of TRPV1 channels. Inhibition of PLC or PKC as well as chelation of intracellular Ca²⁺ blocked NMB-mediated augmentation of AP firing. PIP₂ tonically interacts with GIRK and TRPV1 channels, modulating their open probability [193, 424]. It is reasonable to speculate that BB1 receptor-mediated hydrolysis of PIP₂ results in the disinhibition of TRPV1 and the inhibition of GIRK channels. In agreement with this situation, our data suggest that supplementation of membrane PIP₂ by inclusion of diC8-PIP₂ in our recording electrodes attenuated NMB-mediated excitation of BLA neurons. Likewise, downstream of PIP₂, PKC activity can regulate both GIRK [425] and TRPV1 channel activity [426] through direct phosphorylation [380, 427] and/or PKC-mediated hydrolysis of membrane PIP₂ [428]. Moreover, BB1Rs and BB2Rs inhibit GIRK through PLC- and PKC-dependent mechanisms [379].

We found that NMB excited approximately 50% of the recorded neurons through activation of TRPV1 channels. Bombesin-like peptide activation of TRPV1 channels has been observed in other brain regions, including the paraventricular thalamus [369], trigeminal ganglia [429], and brainstem [319]. TRPV1 channels are temperature sensitive cation channels that display multimodal activation mechanisms and are robustly expressed in the BLA [297, 298]. Lowering the temperature of our recording

bath to 22 °C attenuated the NMB-mediated inward currents, lending support to TRPV1 involvement in the BB1 receptor-generated excitation of BLA neurons. TRPV1 activation may involve 2-AG or other endocannabinoids, as inhibition of DAG lipase significantly reduced NMB-elicited inward currents. The production of 2-AG is calcium-dependent and reduced by Ca^{2+} chelation [430, 431]. Likewise, chelation of intracellular Ca^{2+} blocked NMB-mediated excitation. Direct targeting of TRPV1 channels by pretreatment and bath application of the selective TRPV1 antagonist AMG 9810 [302] or capsazepine [303] in the recording solution significantly attenuated BB1 receptor-elicited inward currents. Finally, bath application of NMB in TRPV1 KO mice significantly reduced the elicited inward current, which was not observed in mice lacking the TRPC4 and TRPC5 channels. TRPV1 channels are involved in fear processing in the amygdala. For example, activation of TRPV1 channels in the LA modulate long-term potentiation, whereas TRPV1 KO mice show reductions in conditioned and contextual fear responses [298, 432]. As NMB has been implicated in fear and anxiety-like behaviors, these results may identify a novel pathway through which NMB and TRPV1 contribute to anxiogenic behaviors within the BLA.

We demonstrated that the activation of BB1 receptors produced a significant inward current in a subset of BLA neurons by suppressing GIRK channels. The substitution of Cs^+ in our recording solution attenuated the inward current, suggesting a BB1 receptor-mediated inhibition of a K^+ conductance. In this subset of recordings, the NMB-sensitive I-V curve displayed inward rectification, reversed near the calculated K^+ reversal potential, which was sensitive to the application of micromolar concentrations of Ba^{2+} , a Kir channel inhibitor, indicating action on an inwardly rectifying potassium channel or Kir. The four functional Kir subfamilies include Kir2 constitutively active channels (Kir2.1-2.4), GIRK or Kir3 channels (GIRK1-GIRK4), ATP-sensitive Kir6 channels (Kir6.1, Kir6.2), and the K^+ -transport channels (Kir1.1, Kir4.1, Kir4.2, and Kir7.1) [255].

Application of the saturating concentration of ML133, a specific antagonist of Kir2 channels [256, 372, 433], failed to significantly alter the inward current recorded from BLA neurons, whereas NMB-mediated inward currents were unaffected, indicating that Kir2 channels are unlikely to be involved in NMB-mediated excitation of BLA neurons. The application of the GIRK channel antagonist [263] TQ produced a significant inward current; however, in the presence of TQ, the NMB-mediated inward current was significantly reduced. GIRK channels are a family of constitutively active channels comprised of 4 subunits including GIRK1, GIRK2, GIRK3, and GIRK4 [255], which are involved in regulating intrinsic membrane excitability [374, 434, 435]. GIRK channels are expressed in a variety of neuronal populations throughout the brain as homotetramers of GIRK2 subunits or as heterotetramers of GIRK1, GIRK2, and/or GIRK3 subunits [255, 435]. The GIRK4 subunits are not expressed in the amygdala [436], whereas the GIRK1, GIRK2, and GIRK3 subunits are expressed in the BLA [437-439]. Consistent with these reports, application of the GIRK1 activator ML297 produced a significant outward current supporting the functional expression of GIRK1 subunits in the BLA. Owing to the lack of commercially available GIRK2 and GIRK3 selective antagonists and the heterotetrametric nature of these subunits, further experiments are required to determine the subunit composition of the GIRK channel inhibited by BB1 receptor activation.

We have shown that bath application of NMB significantly increased the frequency and amplitude of sEPSCs, but slightly decreased the amplitude of eEPSCs in the BLA. NMB enhanced the frequency but not the amplitude of mEPSC events recorded in the presence of TTX. The lack of NMB effects on mEPSC amplitude indicates that BB1 receptors do not modulate postsynaptic glutamate receptors but instead act to modulate glutamate release at presynaptic sites. The NMB-mediated increase in sEPSC frequency and amplitude may be the result of local increases in intracellular calcium,

which promoted the synchronized release of glutamate. In agreement with these data, TRPV1 channels may promote tonic glutamate release independent of afferent stimulation [440]. The transient inhibition of NMB-mediated eEPSCs may have resulted from the depletion of the readily releasable pool, similar to the inhibitory mechanisms proposed for bombesin in the hippocampus [370] and substance P in bronchopulmonary neurons in the solitary tract nucleus [441]. The transient suppression of eEPSC amplitude may also be the result of inhibitory signaling molecules produced following BB1 receptor activation. The two major endocannabinoids found in the brain are 2-arachidonoylglycerol (2-AG) and anandamide (AEA) [442-444]. Whereas AEA is biosynthesized via the enzymatic activities of N-acyltransferase and PLD, 2-AG is the hydrolytic product of PLC and the subsequent activity of DAG lipase [445-447]. 2-AG and AEA are released from neurons following depolarization [448-450] or activation of $G_{q/11}$ receptors [451, 452], and bind to CB1 receptors on presynaptic neurons to suppress synaptic activity [321, 451]. Oxytocinergic and vasopressinergic neurons have been demonstrated to suppress presynaptic neurotransmitter release via endocannabinoid signaling mechanisms. In magnocellular neurons, oxytocin receptor activation results in endocannabinoid release that diffuses in a retrograde direction to inhibit presynaptic glutamate release [453]. Similarly, depolarization of vasopressinergic neurons releases cannabinoids to suppress GABA release at presynaptic sites [454]. Consistent with these data, we demonstrate that NMB-mediated excitation may involve endocannabinoid release. Inhibition of DAG lipase attenuated NMB-mediated TRPV1 activation, which was required for NMB-mediated increases in AP-dependent and AP-independent glutamate release, suggesting that these channels are presynaptically located. TRPV1 channels were not involved in NMB-mediated suppression of eEPSC amplitude, whereas blockade of CB1 receptors significantly augmented eEPSC amplitude in response to NMB bath application. TRPV1 channels and CB1 receptors

differentially regulate spontaneous and evoked glutamatergic transmission in the solitary tract nucleus [307, 440]. Activation of afferent terminals produces prolonged asynchronous spontaneous release in TRPV1-positive neurons independent of CB1R activity [440], whereas evoked glutamate release in these neurons is modulated by cannabinoid 1 receptors [307]. Taken together, our results demonstrated that BB1 receptor activation in BLA neurons differentially regulates spontaneous and evoked glutamate release. Further research is needed to clarify the distinct roles of TRPV1 channels and cannabinoid signaling in NMB-mediated glutamate release.

Anxiety is a response to unpredictable or generalized threats that prepares a subject to respond to stress or danger in its environment. Anxiety paradigms are based on naturalistic behaviors that utilize generalized threats as a means to detect anxiolytic agents. For example, in elevated plus maze or open field tests of anxiety, rodents alter between their desire to explore a novel context and fear of predation in open or illuminated spaces. VCT, like other conflict-based anxiety paradigms, presents rodents with a 'conflict' between a physiological need (i.e., food or water) and punishment, where punishment is required to satiate this need. Drugs that increase punitive behaviors are considered to have anxiolytic properties, whereas drugs that reduce punitive behaviors reflect anxiogenic properties [455]. Dysregulation of glutamatergic activity within the BLA has been implicated in anxiety and anxiety-like disorders through a pathway involving the prefrontal cortex, BNST, and ventral hippocampus [15]. Activation of BLA excitatory projections to the BNST and ventral hippocampus are involved in the expression of anxiety-like behaviors [456]. Because the BLA is an important structure in the neural circuitry underlying fear and anxiety, BB1 receptor-mediated enhanced glutamate release within the BLA likely promoted information transfer out of the BLA to increase the activity of this circuit, resulting in increased anxiety-like behaviors. Moreover, intracerebroventricular application of NMDA receptor antagonists produce anxiolytic

effects in the VCT, comparable to those of diazepam [457]. BLA infusion of the selective NMDA receptor antagonists MK-801 [458] or AP5 [459] produce anxiolytic behaviors in rats and mice. Therefore, BB1 receptor-mediated depolarization could remove the voltage-dependent Mg^{2+} block of NMDA receptors, enhancing glutamatergic activity in the BLA, and promote anxiety-like behaviors. In support of our findings, intracerebroventricular application of another selective BB1 receptor antagonist, BIM23127, increased the time spent in the open arms of the elevated plus maze, a behavior associated with decreased anxiety [460]. The direct application of NMB into the dorsal raphe nucleus promotes anxiety-like behaviors, as measured by decreases in the social interaction test [461]. Taken together, our results indicate that activated BB1 receptors promote anxiety-like behaviors, and antagonists of this peptide system may be effective in the treatment of anxiety disorders.

GIRK and TRPV1 channels are attractive targets for the treatment of anxiety disorders. Our results indicate that activated BB1 receptors produce anxiety-like phenotypes in the VCT mediated by TRPV1 and GIRK channels. Inhibition of TRPV1 channels is typically associated with reductions in fear and anxiety. For example, infusion of TRPV1 antagonists into structures of the limbic system, including the BLA [462], nucleus accumbens [463], and medial PFC [464], decreases anxiety-like behaviors. TRPV1 channels are robustly expressed in the BLA, and their expression can be further increased by early life stress [465]. Activated TRPV1 channels enhance glutamatergic function and synaptic plasticity in the BLA and may contribute to hyperpathia and chronic pain [298, 466]. Consistent with these findings, treatment of rats with AMG9810 alone increased the number of punished licks, and the blockade of this channel prevented the anxiogenic action of BB1 receptor activation. The role of GIRK channels in fear and anxiety is more complex. GIRK knockout mice have shown reductions in generalized fear and deficits in conditioned fear [384, 385], whereas

wildtype mice treated with the selective GIRK channel activator, ML297 displayed decreased anxiety-like phenotypes [386]. We demonstrated that GIRK channels are involved in NMB-mediated anxiety in the BLA, and that blockade of GIRK channels prevents NMB-mediated decreases in lick numbers. GIRK channels are known targets of opioid-mediated signaling pathways and, like TRPV1 channels, are implicated in pain disorders, which are often comorbid with anxiety. Taken together, our findings may highlight a cellular and molecular mechanism to explain anxiety and pain in the BLA.

Study 3- Neurokinin-3 Receptor-Mediated Modulation of Basolateral Amygdala Neurons

While high densities of NK3Rs are expressed in the BLA [345-347, 349, 351], the actions and the underlying mechanisms of NK3R activation in the BLA have not been determined. We showed that activation of NK3Rs excited BLA neurons assessed by electrophysiologically recording AP firing, RMPs and HCs. Consistent with our electrophysiological results, intracerebroventricular injection of senktide increases the expression of c-Fos, a selective marker of neuronal activity in the BLA [348, 353]. Our results further showed that activation of NK3Rs facilitated the excitabilities of BLA neurons by depressing the GIRK type of Kir channels and opening TRPC4 and TRPC5 channels. While SP has been shown to facilitate neuronal excitability by depressing Kir channels [467-469] or by activating cation channels [470] or by both suppressing Kir conductance and activating cation channels [471-473], few studies have been conducted to determine the ionic mechanisms underlying NK3R-mediated neuronal excitation. Although SP is capable of inhibiting GIRK type of Kir channels [380, 467], the subtypes of the Kir channels involved in NK3R-mediated facilitation of neuronal excitability have not been determined. Furthermore, the cation channels underlying tachykinins-mediated neuronal excitation have not been identified. With both pharmacological approaches and KO mice, we identified that GIRK channels and TRPC4 and TRPC5 channels are the

type of Kir and cation channels involved in NK3R-induced excitation of BLA neurons. GIRK channels comprise four isoforms, namely GIRK1, GIRK2, GIRK3 and GIRK4. Consistent with our results, amygdala abundantly express GIRK1, GIRK2 and GIRK3 [373, 474]. Our result that application of the selective GIRK1 activator, ML 297, elicited an outward current in the BLA neurons, further supports the expression of functional GIRK1 channels in these neurons. GIRK channels exist as predominantly heterotetramers of GIRK1, GIRK2 and/or GIRK3, or as homotetramers of the GIRK2 subunit [358, 377]. NK3R-elicited excitation of BLA neurons might be mediated by suppression of the heterotetramers formed by GIRK1, GIRK2 and/or GIRK3, or the homotetramers of the GIRK2 subunit. Future experiments are required to identify the isoform(s) of GIRK channels involved in NK3R-elicited excitation of BLA neurons. Our results further showed that activation of NK3Rs excited about half of the BLA principal neurons by opening TRPC4 and TRPC5 channels. Consistent with our results, both TRPC4 [359] and TRPC5 [360] channels are expressed in the BLA and genetic deletion of these channels decreased fear and anxiety-related responses [359, 360].

Our results indicated that PLC β is required for NK3R-induced inward currents. This result is in line with previous results showing that PLC β 1 is involved in SP-elicited depression of Kir channels in the cholinergic neurons from the nucleus basalis [475]. Whereas previous studies failed to determine whether intracellular Ca²⁺ release is required for SP-induced depression of Kir channels, our results showed that intracellular Ca²⁺ release from the IP₃ store is unnecessary for NK3R-generated inward currents. However, there is considerable discrepancy for the roles of PKC in NK3R-produced inward currents and SP-induced inhibition of Kir channels. Whereas PKC is involved in SP-mediated inhibition of Kir channels in nucleus basalis neurons [476, 477] and SP-induced inhibition of GIRK1/GIRK4 channels expressed in *Xenopus* oocytes [380], our results failed to detect a role of PKC in NK3R-elicited inward currents in BLA neurons.

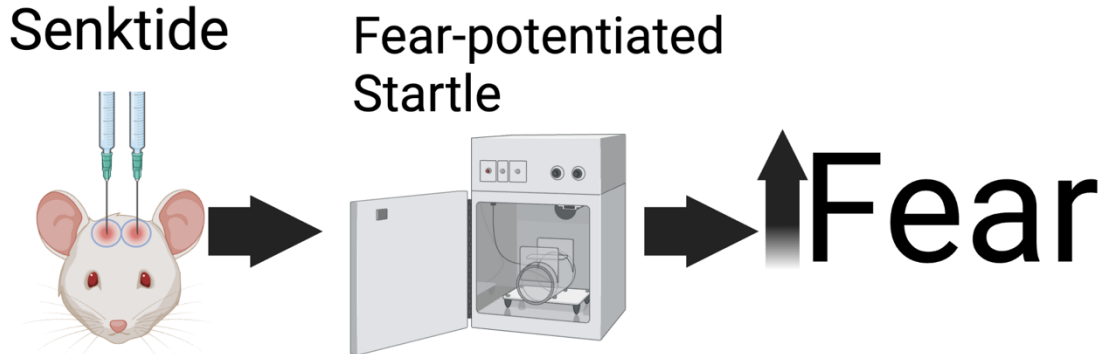
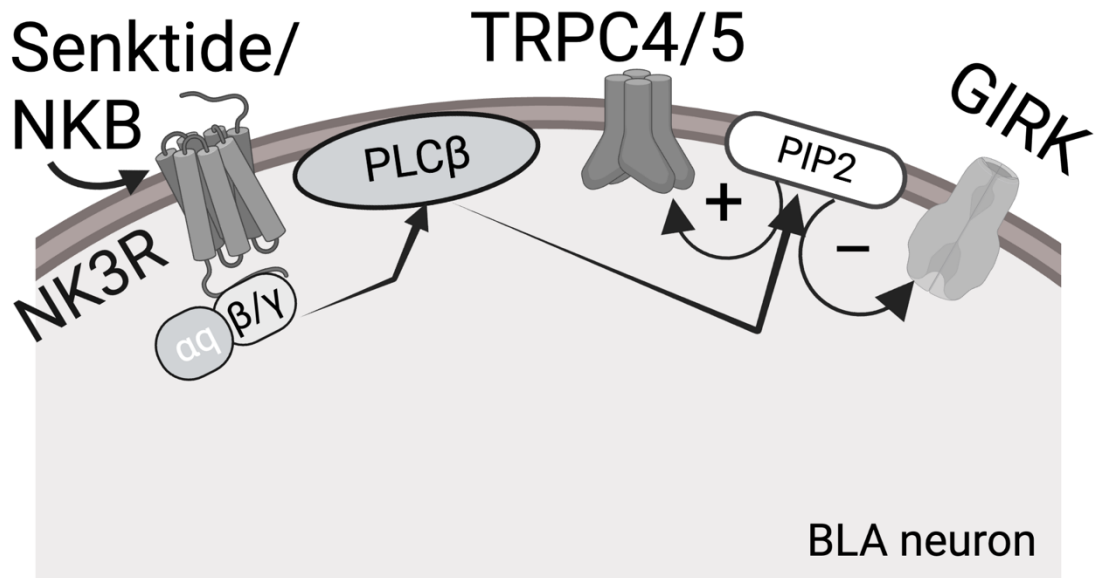


Figure 28. Working model illustrating the cellular and molecular mechanisms underpinning NK3R-elicited excitation of BLA principal neurons and augmentation of FPS response. Activation of NK3Rs by senktide results in activation of $G\alpha_q$ proteins leading to increases in PLC β activity. Activation of PLC β catalyzes the hydrolysis of PIP₂ to generate IP₃ to elevate intracellular Ca^{2+} release from IP₃-sensitive store and diacylglycerol (DAG) to activate protein kinase C (PKC). PLC β -induced hydrolysis of PIP₂ results in depression of GIRK channels and opening of TRPC4/5 channels to excite BLA principal neurons. The effects of NK3Rs on GIRK channels and TRPC4/5 channels are responsible for NK3R-induced augmentation of FPS response. Adapted from [224]. Created with BioRender.com

Several possibilities could be proposed to explain the discrepancy. First, the Kir channels depressed by SP in the nucleus basalis is distinct from the GIRK channels as the single channel conductance depressed by SP (~23 pS) is different from that of GIRK channels (32-35 pS) [467, 477]. Second, there are controversial results as to whether PKC is required for the $G_{q/11}$ -coupled receptor-mediated depression of GIRK channels. PKC has been shown to phosphorylate and depress GIRK channels [379-381, 478, 479]. There is also evidence demonstrating that the function of PKC is unnecessary for the depression of GIRK channels induced by $G_{q/11}$ -coupled receptors [480, 481].

We further tested the roles of PIP_2 , the upstream signal of PKC, in NK3R-produced inward currents, as PIP_2 has been shown to regulate functionally a variety of ion channels [192, 193]. Intracellular dialysis of diC8- PIP_2 significantly reduced senktide-induced inward currents in BLA neurons, suggesting that PLC β -elicited hydrolysis of PIP_2 is involved in NK3R-mediated excitation of BLA neurons. As our results indicate that both depression of GIRK channels and activation of TRPC4/5 channels are involved in NK3R-induced inward currents, these results also suggest that PLC β -mediated hydrolysis of PIP_2 is responsible for NK3R-elicited suppression of GIRK channels and activation of TRPC4/5 channels. Consistent with this scenario, PLC β -mediated PIP_2 hydrolysis is responsible for $G_{q/11}$ receptor-elicited depression of GIRK [480-486] and activation of TRPC4 [487] and TRPC5 [488, 489] channels. PIP_2 decreases the desensitization of TRPC5 channels and PLC β -induced hydrolysis of PIP_2 may increase the desensitization of the channels and thus facilitate the closing of the channels [489].

Fear is a response to impending threat that prepares a subject to make appropriate defensive responses including freezing, fighting, or fleeing to safety. In humans, fear is accompanied by affective feelings of dread and anticipation. The FPS paradigm has been proven to be a useful system with which to analyze neural systems involved in fear and anxiety. This test measures conditioned fear by an increase in the amplitude of a

simple reflex (the acoustic startle reflex) in the presence of a cue previously paired with a shock. The hypothesis to explain the FPS is that the conditioned stimulus activates CeA through a pathway involving the lateral geniculate nucleus, perirhinal cortex, LA and BLA. The CeA then projects directly to the acoustic startle pathway so as to modulate the startle response [277, 490, 491]. The BLA may be a neural substrate for the acquisition of conditioned fear responses [277, 361-364]. Because the BLA is an important structure in the neural circuitry underlying FPS, NK3R-mediated excitation of BLA principal neurons likely augmented the output of information from the BLA and up-regulated the activity in the circuitry, resulting in elevated FPS response. Furthermore, it has been demonstrated that the functions of NMDA receptors are required for FPS as infusion of the NMDA receptor antagonist APV into the BLA impairs FPS [492-495]. Because NMDA receptors are voltage-dependently blocked by Mg^{2+} , the subthreshold depolarization elicited by the activation of NK3Rs could relieve the Mg^{2+} -block of NMDA receptors and thus augment FPS. Consistent with our results, intracerebroventricular administration of the selective NK3R agonist, senktide, evokes gerbil foot tapping which is thought to reflect a fear-related response [496]. Likewise, NK3Rs may be responsible for the anxiogenic-like actions of SP6-11(C-terminal), a specific metabolite of SP [497]. More specifically, up-regulation of NKB and NK3Rs in the CeM facilitates the consolidation of fear memories [352]. All these results together suggest that NKB/NK3R system facilitates fear and anxiety-like responses and antagonists of NK3Rs could be potential therapeutic agents for anxiety treatment.

The results that microinjection of tertiapin-Q with senktide or M084 alone enhanced the non-cued responses (Figure 25B) are unexpected. These results may be explained by the complicated roles of Kir channels and TRPC4/5 channels in anxiety and fear responses. Conflicting results have been obtained as to the roles of GIRK channels in anxiety and fear responses. GIRK1 or GIRK2 knockout mice showed reduced anxiety-

related behavior in the elevated plus maze [385], although constitutive GIRK2 knockout mice exhibited a striking deficit in hippocampal-dependent (contextual) and hippocampal-independent (cue) fear conditioning [384]. However, application of the GIRK1 activator ML297 decreased anxiety-related behavior [386] and fear conditioning increased the activity of BLA neurons by suppression of K⁺ channels [498]. The non-cued responses may represent the background anxiety possibly due to the repeated applications of the light cues [226, 499]. TQ-mediated inhibition of GIRK channels might have already altered the anxiety level, which might have synergized with subsequent application of NK3R agonist senktide and thus an increase in non-cued responses was observed. The increasing effect of M084 on non-cued responses could be an off-target actions of M084 because M084 is an acetylcholinesterase inhibitor as well [500]. As acetylcholine efflux in the BLA has been observed during fear conditioning session [501], application of M084 could have augmented the non-cued responses by interacting with other neurotransmitters such as acetylcholine. While these results are perplexing, our results in general provide a cellular and molecular mechanism to explain the augmentation of fear response in response to NK3R activation.

Limitations and Future Experiments

Exogenous Application of NPs

The exogenous application of compounds and NPs in the *in vitro* studies may misrepresent the physiological relevance in the reported findings. Among the cell surface are numerous non-specific peptidase enzymes that degrade neuropeptides [182]. As we exogenously apply NPs, catabolism of the excess NP by the endopeptidases may prolong the half-life of endogenous peptides contributing to indirect biological activity. This indirect effect may be an important confound for these studies. In our *in vivo* work we do demonstrate endogenous action of NMB. In Study 1, we show that NMB produced reductions in FPS and cardiac output from the CeA. In Study 2, application of NMB into the BLA promoted anxiety-like behaviors. However, the indirect action of prolonged endogenous peptides is a caveat to our interpretation. In Study 3, we do not provide direct evidence of any endogenous action of NKB as we used the synthetic analogue, senktide, to activate these receptors. More on this below.

Lack of Neuronal and Circuit Specificity

In Study 1, we patched CeL neurons assuming that these neurons were GABAergic based upon morphological and electrophysiological characteristics [42, 502]. We demonstrate that NMB-mediated excitation occurred in all CeL neuronal firing pattern types (i.e., LF, RS, LTB CeL neurons). Though appropriate to generate adequate samples to study, the diversity of CeL neuronal populations based upon expression of immunohistological markers suggests we are likely oversimplifying the effects of NMB-mediated excitation in this region [141, 503]. GABAergic CeL neurons can be characterized into one of two largely non-overlapping neuronal populations based on the expression of PKC δ [504]. Whereas PKC δ -expressing CeL neurons are the LF type, SOM $^{+}$ -CeL neurons do not express PKC δ and are the RS type of CeL neuron [141].

Moreover, ~ 90% CRH-expressing CeL neurons are the LF type and overlap with PKC δ -expressing CeL neurons [503]. NMB-mediated excitation required PKC and cytosolic Ca²⁺ and our results with the DAG-analogue PMA indicate NMB-mediated depression of GIRKs requires a DAG-dependent PKC. Therefore, it is reasonable to theorize that BB1 receptors within the CeL colocalize with PKC δ -negative, SOM⁺-expressing CeL neurons. However, NMB also produced excitation in LF and LTB neurons indicating BB1 receptors may represent a unique CeL neuronal circuit. As a corollary to this hypothesis, roughly 15% of CeL neurons are both PKC δ - and SOM⁺- negative [504]. To address the question of which CeL circuits are activated by BB1 receptors, one painstaking approach would be to fix CeL slices upon the completion of the electrophysiological recording and stain for relevant immunohistological markers. A more convenient research strategy would utilize transgenic mice to characterize these CeL circuits. Future experiments could generate a NMB-GFP-Cre mouse model in which the enzyme Cre-recombinase is expressed only in NMB-positive cells. In these mice, the injection of a Cre-dependent viral vector targeting the CeL carrying a fluorescent marker controlled by a GABAergic promoter would selectively identify NMB-expressing GABAergic neurons. The combinatorial use of electrophysiology and labeling techniques can then be used to address this limitation.

Visibly identifiable NMB-expressing neurons would also allow for a series of other experiments to determine the functional outcomes of BB1 peptidergic circuit. Tracing experiments would improve our understanding of the synaptic targets of BB1-specific neurons as well as locations of synaptic inputs. Moreover, an understanding of the genetic profile of these cells could be generated in response to various stressors or treatment conditions using RNA-seq. Data obtained from these types of experiments may reveal specific genetic regulatory mechanisms that underlie specific physiological

processes downstream of BB1 receptor activation. This approach could be applied to any of the studies within this dissertation.

In Studies 2 and 3, we patched from BLA neurons presumed to be glutamatergic projection neurons based largely upon morphological features and electrophysiological characteristics [25, 37, 505]. Due to their large soma relative to BLA interneurons, this is appropriate, but a subset of PV+-interneurons may possess pyramidal-like cell bodies of similar size [45, 506, 507]. Therefore, a similar research strategy as that proposed for Study 1 could be used to identify BB1 receptor or NK3R-expressing projection neurons. In this case, injection of a Cre-dependent viral vector into the BLA carrying a fluorescent tag under the control of the CAMK promoter would be effective to selectively label these Cre-expressing neuronal populations. With this model, future experiments could use the injection of Cre-dependent tract tracers (e.g., Adenovirus, rabies virus, or cholera toxin subunit B, Fluorogold, etc.) conjugated to fluorescent probes to indicate distal targets with synaptic connections to and from NMB- or NKB-expressing BLA neurons. The improved tract tracing methods combined with transfection of inhibitory or excitatory opsin proteins would allow for specification of peptidergic system involvement in complex behavioral sequences. In conditioned-response paradigms like in Study 3, photoactivation of excitatory or inhibitory opsin proteins expressed in NKB expressing BLA will allow one to characterize the specific involvement of NK3Rs in the acquisition, consolidation, or extinction of the conditioned response [339, 352]. Alternatively, opsin transfections mediated by retrograde transport vectors in brain regions receiving inputs from Cre-expressing BLA neurons will further characterize the functional inputs to these neuron populations. These viral transfections also remove the need for exogenously applied NPs and potential confounds described above.

An additional limitation from the *in vivo* studies is the extrapolation of neuronal activity following NP or other compound injection. The *in vitro* procedures are highly

controlled to isolate aspects of NP activity, however; in our *in vivo* experiments, NPs are administered to an intact system. While we can hypothesize about the effects on regional neuronal activity and extrapolate based upon behavioral output, it remains unknown how direct NP application affects neuronal activity during these studies. In each study, NPs were administered at a set time point prior to behavioral testing, typically allowing for the maximal effect observed from the *in vitro* data. In Study 1 and 2, NMB is administered into the CeA and BLA, respectively. In Study 3, the NK3R agonist senktide was administered into the BLA. Future experiments should address this limitation with the concomitant use of local field recordings and *in vivo* Ca²⁺ imaging. Local field potentials are the synchronized rhythms of regional neuronal activity in awake and freely moving animals. Implanted electrodes near these excitable cells record the oscillatory patterns of these cells and changes in the frequency, power, or coherence of this signal reflects alterations in brain states, similar to that observed in electroencephalography [508]. A research strategy utilizing transgenic animals with an encoded Ca²⁺-indicator that upon Ca²⁺ binding fluoresces, and implanted electrodes would allow recordings of regional alterations in neuronal activity with high spatial resolution. Within this model, alterations in neuronal activity mediated by the activation of NP-expressing neurons could be observed and manipulated in real time.

NP Administration Lacks Temporal Specificity

NP release and subsequent physiological effect may be specific to the time of release as well as to the positive or negative qualities of the stimulus [509]. As mentioned, our application of NPs for behavioral testing was administered prior to testing to provide evidence of an effect in that paradigm. However, our results provide no evidence of how endogenous NMB or NKB is released in response to specific stimuli. GRAB sensors are modified G-protein coupled receptors that convert the ligand-

mediated GPCR conformation change into an optical response by the insertion of conformation-sensitive fluorescent markers at an intracellular domain [510]. These modified GPCRs allow real-time quantification of ligand-receptor interactions [509] and with simultaneous *in vivo* Ca²⁺ imaging can provide a quantitative measure of neuronal activation. Thus, improvements in *in vivo* and *in vitro* techniques will continue to describe the precise roles of NPs in neurobiological processes.

LIST OF ABBREVIATIONS

2-AG	2-arachidonoylglycerol
5-HT	Serotonin or 5-hydroxytryptophan
AEA	anandamide
AP	action potential
ASR	acoustic startle response
BA	basal nucleus of the amygdala
BB1R	bombesin-1 receptors
BB2R	bombesin-2 receptors
BLA	Basolateral nucleus of the amygdala
BM	basomedial nucleus of the amygdala
BNST	bed nucleus of the stria terminalis
CeA	central amygdala
CeL	lateral nucleus of the central amygdala
CeM	medial nucleus of the central amygdala
CRF	corticotrophin release factor
CRH	corticotrophin releasing hormone
CSF	cerebrospinal fluid
DA	dopamine
DAG	diacylglycerol
DCV	dense core vesicles
DSM-5TR	Diagnostic and Statistical Manual of Mental Disorders, Fifth Edition, Text Revision
FPS	fear-potentiated startle
GABA	γ -aminobutyric acid
GIRK	G-protein gated inwardly rectifying potassium channel
GRP	gastrin-releasing peptide
HR	heart rate
I-V	current-voltage
IP ₃	inositol 1,4,5-trisphosphate
ITCs	intercalated cells
Kir	inwardly rectifying potassium channel
LA	lateral nucleus of the amygdala
LF	late firing neurons
LTB	low-threshold bursting neurons
MAP	mean arterial pressure
NE	norepinephrine
NKA	neurokinin A
NKB	neurokinin B
NKR	neurokinin receptor
NMB	neuromedin B
NP	neuropeptide
NPY	neuropeptide Y
PFC	prefrontal cortex
PIP ₂	phosphatidylinositol 4,5-bisphosphate
PKC	protein kinase C
PLC β	phospholipase C β
PTSD	Post-Traumatic Stress Disorder

PPR	paired-pulse ratio
R_{in}	input resistance
RS	regular firing neurons
SD	Sprague Dawley rats
SNRI	selective norepinephrine reuptake inhibitor
SOM	somatostatin
SP	substance P
SSRI	selective serotonin reuptake inhibitor
Tac	tachykinin
TQ	tertiapin-Q
TRPC	transient receptor potential canonical channel
TRPV1	transient receptor potential vanilloid 1 channel
WNB	white noise bursts

LIST OF REAGENTS AND DRUGS

BAPTA	Ca ²⁺ chelator
AMG9810	TRPV1 channel antagonist
Ba ²⁺	Non-selective Kir blocker
BIM23042	BB1 receptor antagonist
Bisindolylmaleimide II	PKC inhibitor
bombesin	BB receptor agonist
CdCl	voltage gated Ca ²⁺ -channel blocker
Chelerythrine	PKC inhibitor
Glibenclamide	K _{ATP} channel blocker
Guanosine 5'-O-(2-thiodiphosphate)	non-hydrolysable GDP analog
Kynurenic acid	glutamatergic receptor antagonist
M084	TRPC4/5 inhibitor
ML133	Kir2 blocker
ML297	GIRK1 activator
Neurokinin B	endogenous NK3R agonist
Neuromedin B (NMB)	BB1 receptor agonist
PD168368	BB1 receptor antagonist
Phorbol 12-myristate 13 acetate(PMA)	PKC activator
Phosphatidylinositol diC8 (diC8-PIP ₂)	water-soluble PIP ₂ analog
Picrotoxin	GABA _A antagonist
RC3095	BB2 receptor antagonist
Ryanodine	ryanodine receptor inhibitor
SB 218795	NK3R antagonist
Senktide	NK3R agonist
Tertiapin LQ	Kir1 blocker
Tertiapin-Q(TQ)	GIRK/Kir 1 Channel blocker
Tetrodotoxin	voltage-gated Na ⁺ channel blocker
Thapsigargin	sarco-endoplasmic Ca ²⁺ /ATPase inhibitor
U73122	PLCβ inhibitor
U73343	Inactive analog of U73122
Wortmannin	PI3K/PI4K inhibitor

COPYRIGHT CLEARANCE

Study 1 and Study 3 of this dissertation are based almost entirely from publications that list Cody Boyle as the primary author. Copyright clearance was obtained from the publisher Wiley of John Wiley and sons to reproduce text, figures, and legends for this dissertation. The citations of the published manuscripts for both studies are listed below.

Boyle, C. A., & Lei, S. (2023). Neuromedin B excites central lateral amygdala neurons and reduces cardiovascular output and fear-potentiated startle. *Journal of Cellular Physiology*, 1– 24. <https://doi.org/10.1002/jcp.31020>

Boyle, C.A., Hu, B., Quaintance, K.L., Mastrud, M.R. and Lei, S. (2022), Ionic signalling mechanisms involved in neurokinin-3 receptor-mediated augmentation of fear-potentiated startle response in the basolateral amygdala. *J Physiol*, 600: 4325-4345. <https://doi.org/10.1113/JP283433>

REFERENCES

1. Papez, J.W., *A proposed mechanism of emotion*. Archives of Neurology & Psychiatry, 1937. **38**: p. 725-743.
2. Mac, L.P., *Psychosomatic disease and the visceral brain; recent developments bearing on the Papez theory of emotion*. Psychosom Med, 1949. **11**(6): p. 338-53.
3. Maclean, P.D., *Some psychiatric implications of physiological studies on frontotemporal portion of limbic system (visceral brain)*. Electroencephalogr Clin Neurophysiol, 1952. **4**(4): p. 407-18.
4. Bard, P., *THE CENTRAL REPRESENTATION OF THE SYMPATHETIC SYSTEM: AS INDICATED BY CERTAIN PHYSIOLOGIC OBSERVATIONS*. Archives of Neurology & Psychiatry, 1929. **22**(2): p. 230-246.
5. Cannon, W.B., *The James-Lange theory of emotions: a critical examination and an alternative theory*. The American Journal of Psychology, 1927. **39**: p. 106-124.
6. Brown, S. and E.A. Sharpey-Schafer, *XI. An investigation into the functions of the occipital and temporal lobes of the monkey's brain*. Philosophical Transactions of the Royal Society of London. (B.), 1888. **179**: p. 303-327.
7. Klüver, H. and P.C. Bucy, *Preliminary analysis of functions of the temporal lobes in monkeys*. Archives of Neurology & Psychiatry, 1939. **42**(6): p. 979-1000.
8. Scoville, W.B. and B. Milner, *Loss of recent memory after bilateral hippocampal lesions*. J Neurol Neurosurg Psychiatry, 1957. **20**(1): p. 11-21.
9. Liddle, P.F., et al., *Three Syndromes in Chronic Schizophrenia*. The British Journal of Psychiatry, 1989. **155**(S7): p. 119-122.
10. Balasubramaniam, V. and B. Ramamurthi, *Stereotaxic amygdalotomy in behavior disorders*. Confin Neurol, 1970. **32**(2): p. 367-73.
11. Weiskrantz, L., *Behavioral changes associated with ablation of the amygdaloid complex in monkeys*. J Comp Physiol Psychol, 1956. **49**(4): p. 381-91.
12. Nagel, J.A. and E.D. Kemble, *Effects of amygdaloid lesions on the performance of rats in four passive avoidance tasks*. Physiology & Behavior, 1976. **17**(2): p. 245-250.
13. Slotnick, B.M., *Fear behavior and passive avoidance deficits in mice with amygdala lesions*. Physiology & Behavior, 1973. **11**(5): p. 717-720.

14. Meyer, A., *Karl Friedrich Burdach and his place in the history of neuroanatomy*. J Neurol Neurosurg Psychiatry, 1970. **33**(5): p. 553-61.
15. Janak, P.H. and K.M. Tye, *From circuits to behaviour in the amygdala*. Nature, 2015. **517**(7534): p. 284-292.
16. Johnston, J.B., *Further contributions to the study of the evolution of the forebrain*. Journal of Comparative Neurology, 1923. **35**(5): p. 337-481.
17. Jones, E.G. and T.P. Powell, *An anatomical study of converging sensory pathways within the cerebral cortex of the monkey*. Brain, 1970. **93**(4): p. 793-820.
18. Herzog, A.G. and G.W. Van Hoesen, *Temporal neocortical afferent connections to the amygdala in the rhesus monkey*. Brain Res, 1976. **115**(1): p. 57-69.
19. Aggleton, J.P., M.J. Burton, and R.E. Passingham, *Cortical and subcortical afferents to the amygdala of the rhesus monkey (Macaca mulatta)*. Brain Research, 1980. **190**(2): p. 347-368.
20. Snider, R.S. and A. Maiti, *Cerebellar contributions to the Papez circuit*. J Neurosci Res, 1976. **2**(2): p. 133-46.
21. Goddard, G.V., *FUNCTIONS OF THE AMYGDALA*. Psychol Bull, 1964. **62**: p. 89-109.
22. Anand, B.K., et al., *Cerebellar projections to limbic system*. J Neurophysiol, 1959. **22**(4): p. 451-7.
23. Machne, X. and J.P. Segundo, *Unitary responses to afferent volleys in amygdaloid complex*. J Neurophysiol, 1956. **19**(3): p. 232-40.
24. McDonald, A.J., *Neurons of the lateral and basolateral amygdaloid nuclei: a Golgi study in the rat*. J Comp Neurol, 1982. **212**(3): p. 293-312.
25. McDonald, A.J., *Functional neuroanatomy of the basolateral amygdala: Neurons, neurotransmitters, and circuits*. Handbook of behavioral neuroscience, 2020. **26**: p. 1-38.
26. McDonald, A.J., *Cytoarchitecture of the central amygdaloid nucleus of the rat*. J Comp Neurol, 1982. **208**(4): p. 401-18.
27. LeDoux, J.E., C. Farb, and D.A. Ruggiero, *Topographic organization of neurons in the acoustic thalamus that project to the amygdala*. The Journal of Neuroscience, 1990. **10**(4): p. 1043.
28. Turner, B.H. and J. Zimmer, *The architecture and some of the interconnections of the rat's amygdala and lateral periallocortex*. Journal of Comparative Neurology, 1984. **227**(4): p. 540-557.

29. Millhouse, O.E., *The intercalated cells of the amygdala*. J Comp Neurol, 1986. **247**(2): p. 246-71.
30. András, T., et al., *Differential excitatory control of 2 parallel basket cell networks in amygdala microcircuits*. PLOS Biology, 2017. **15**(5): p. e2001421.
31. Faber, E.S.L., R.J. Callister, and P. Sah, *Morphological and Electrophysiological Properties of Principal Neurons in the Rat Lateral Amygdala In Vitro*. Journal of Neurophysiology, 2001. **85**(2): p. 714-723.
32. McDonald, A.J., *Neuronal organization of the lateral and basolateral amygdaloid nuclei in the rat*. J Comp Neurol, 1984. **222**(4): p. 589-606.
33. Spampanato, J., J. Polepalli, and P. Sah, *Interneurons in the basolateral amygdala*. Neuropharmacology, 2011. **60**(5): p. 765-73.
34. Hájos, N., *Interneuron Types and Their Circuits in the Basolateral Amygdala*. Frontiers in Neural Circuits, 2021. **15**.
35. Braak, H. and E. Braak, *Neuronal types in the basolateral amygdaloid nuclei of man*. Brain Res Bull, 1983. **11**(3): p. 349-65.
36. Kamal, A.M. and T. Tömböl, *Golgi studies on the amygdaloid nuclei of the cat*. J Hirnforsch, 1975. **16**(3): p. 175-201.
37. Rainnie, D.G., E.K. Asprodini, and P. Shinnick-Gallagher, *Intracellular recordings from morphologically identified neurons of the basolateral amygdala*. J Neurophysiol, 1993. **69**(4): p. 1350-62.
38. Washburn, M.S. and H.C. Moises, *Electrophysiological and morphological properties of rat basolateral amygdaloid neurons in vitro*. J Neurosci, 1992. **12**(10): p. 4066-79.
39. Faber, E.S.L. and P. Sah, *Physiological Role of Calcium-Activated Potassium Currents in the Rat Lateral Amygdala*. The Journal of Neuroscience, 2002. **22**(5): p. 1618.
40. Vereczki, V.K., et al., *Total Number and Ratio of GABAergic Neuron Types in the Mouse Lateral and Basal Amygdala*. The Journal of Neuroscience, 2021. **41**(21): p. 4575.
41. Schiess, M.C., P.M. Callahan, and H. Zheng, *Characterization of the electrophysiological and morphological properties of rat central amygdala neurons in vitro*. Journal of Neuroscience Research, 1999. **58**(5): p. 663-673.
42. Amano, T., et al., *Morphology, PKC δ expression, and synaptic responsiveness of different types of rat central lateral amygdala neurons*. J Neurophysiol, 2012. **108**(12): p. 3196-205.

43. McDonald, A.J. and F. Mascagni, *Immunohistochemical characterization of somatostatin containing interneurons in the rat basolateral amygdala*. Brain Res, 2002. **943**(2): p. 237-44.
44. McDonald, A.J. and F. Mascagni, *Colocalization of calcium-binding proteins and GABA in neurons of the rat basolateral amygdala*. Neuroscience, 2001. **105**(3): p. 681-93.
45. McDonald, A.J. and R.L. Betette, *Parvalbumin-containing neurons in the rat basolateral amygdala: morphology and co-localization of Calbindin-D(28k)*. Neuroscience, 2001. **102**(2): p. 413-25.
46. McDonald, A.J. and F. Mascagni, *Localization of the CB1 type cannabinoid receptor in the rat basolateral amygdala: high concentrations in a subpopulation of cholecystokinin-containing interneurons*. Neuroscience, 2001. **107**(4): p. 641-52.
47. McDonald, A.J., *Calbindin-D28k immunoreactivity in the rat amygdala*. J Comp Neurol, 1997. **383**(2): p. 231-44.
48. Bissière, S., Y. Humeau, and A. Lüthi, *Dopamine gates LTP induction in lateral amygdala by suppressing feedforward inhibition*. Nature Neuroscience, 2003. **6**(6): p. 587-592.
49. Li, X.F., J.L. Armony, and J.E. LeDoux, *GABAA and GABAB receptors differentially regulate synaptic transmission in the auditory thalamo-amygdala pathway: an in vivo microiontophoretic study and a model*. Synapse, 1996. **24**(2): p. 115-24.
50. Wang, Y., et al., *Multimodal mapping of cell types and projections in the central nucleus of the amygdala*. eLife, 2023. **12**: p. e84262.
51. Wolff, S.B.E., et al., *Amygdala interneuron subtypes control fear learning through disinhibition*. Nature, 2014. **509**(7501): p. 453-458.
52. Polepalli, J.S., et al., *A Specific Class of Interneuron Mediates Inhibitory Plasticity in the Lateral Amygdala*. The Journal of Neuroscience, 2010. **30**(44): p. 14619.
53. Prager, E.M., et al., *The basolateral amygdala γ -aminobutyric acidergic system in health and disease*. J Neurosci Res, 2016. **94**(6): p. 548-67.
54. Waclaw, R.R., et al., *Developmental origin of the neuronal subtypes that comprise the amygdalar fear circuit in the mouse*. J Neurosci, 2010. **30**(20): p. 6944-53.
55. Asede, D., D. Doddapaneni, and M.M. Bolton, *Amygdala Intercalated Cells: Gate Keepers and Conveyors of Internal State to the Circuits of Emotion*. J Neurosci, 2022. **42**(49): p. 9098-9109.
56. Pouille, F., et al., *Input normalization by global feedforward inhibition expands cortical dynamic range*. Nature Neuroscience, 2009. **12**(12): p. 1577-1585.

57. Royer, S., M. Martina, and D. Pare, *Bistable behavior of inhibitory neurons controlling impulse traffic through the amygdala: role of a slowly deinactivating K⁺ current*. J Neurosci, 2000. **20**(24): p. 9034-9.
58. Duvarci, S. and D. Pare, *Amygdala microcircuits controlling learned fear*. Neuron, 2014. **82**(5): p. 966-980.
59. Ehrlich, I., et al., *Amygdala Inhibitory Circuits and the Control of Fear Memory*. Neuron, 2009. **62**(6): p. 757-771.
60. Krettek, J.E. and J.L. Price, *A description of the amygdaloid complex in the rat and cat with observations on intra-amygdaloid axonal connections*. J Comp Neurol, 1978. **178**(2): p. 255-80.
61. Pitkänen, A., et al., *Intrinsic connections of the rat amygdaloid complex: projections originating in the lateral nucleus*. J Comp Neurol, 1995. **356**(2): p. 288-310.
62. Savander, V., et al., *Intrinsic connections of the rat amygdaloid complex: projections originating in the basal nucleus*. J Comp Neurol, 1995. **361**(2): p. 345-68.
63. Royer, S., M. Martina, and D. Pare, *An inhibitory interface gates impulse traffic between the input and output stations of the amygdala*. J Neurosci, 1999. **19**(23): p. 10575-83.
64. Le Gal LaSalle, G., G. Paxinos, and Y. Ben-Ari, *Neurochemical mapping of GABAergic systems in the amygdaloid complex and bed nucleus of the stria terminalis*. Brain Res, 1978. **155**(2): p. 397-403.
65. Pape, H.-C. and D. Pare, *Plastic synaptic networks of the amygdala for the acquisition, expression, and extinction of conditioned fear*. Physiological reviews, 2010. **90**(2): p. 419-463.
66. McDonald, A.J. and J.R. Augustine, *Localization of GABA-like immunoreactivity in the monkey amygdala*. Neuroscience, 1993. **52**(2): p. 281-94.
67. Paré, D. and Y. Smith, *Distribution of GABA immunoreactivity in the amygdaloid complex of the cat*. Neuroscience, 1993. **57**(4): p. 1061-76.
68. Pitkänen, A., *Connectivity of the rat amygdaloid complex*. The Amygdala, ed. Aggleton JP. 2000, New York: Oxford University Press.
69. Pape, H.C. and D. Pare, *Plastic synaptic networks of the amygdala for the acquisition, expression, and extinction of conditioned fear*. Physiol Rev, 2010. **90**(2): p. 419-63.
70. Hopkins, D.A. and G. Holstege, *Amygdaloid projections to the mesencephalon, pons and medulla oblongata in the cat*. Exp Brain Res, 1978. **32**(4): p. 529-47.

71. Galeno, T.M. and M.J. Brody, *Hemodynamic responses to amygdaloid stimulation in spontaneously hypertensive rats*. American Journal of Physiology-Regulatory, Integrative and Comparative Physiology, 1983. **245**(2): p. R281-R286.
72. Iwata, J., K. Chida, and J.E. LeDoux, *Cardiovascular responses elicited by stimulation of neurons in the central amygdaloid nucleus in awake but not anesthetized rats resemble conditioned emotional responses*. Brain Res, 1987. **418**(1): p. 183-8.
73. Mogenson, G.J. and F.R. Calaresu, *Cardiovascular responses to electrical stimulation of the amygdala in the rat*. Exp Neurol, 1973. **39**(1): p. 166-80.
74. Viviani, D., et al., *Oxytocin Selectively Gates Fear Responses Through Distinct Outputs from the Central Amygdala*. Science, 2011. **333**(6038): p. 104-107.
75. Penzo, M.A., V. Robert, and B. Li, *Fear conditioning potentiates synaptic transmission onto long-range projection neurons in the lateral subdivision of central amygdala*. J Neurosci, 2014. **34**(7): p. 2432-7.
76. Sesack, S.R., et al., *Topographical organization of the efferent projections of the medial prefrontal cortex in the rat: an anterograde tract-tracing study with Phaseolus vulgaris leucoagglutinin*. J Comp Neurol, 1989. **290**(2): p. 213-42.
77. Gabbott, P.L.A., et al., *Prefrontal cortex in the rat: Projections to subcortical autonomic, motor, and limbic centers*. Journal of Comparative Neurology, 2005. **492**(2): p. 145-177.
78. McDonald, A.J., *Cortical pathways to the mammalian amygdala*. Prog Neurobiol, 1998. **55**(3): p. 257-332.
79. Shipley, M.T. and G.D. Adamek, *The connections of the mouse olfactory bulb: a study using orthograde and retrograde transport of wheat germ agglutinin conjugated to horseradish peroxidase*. Brain Res Bull, 1984. **12**(6): p. 669-88.
80. Turner, B.H. and M. Herkenham, *Thalamoamygdaloid projections in the rat: A test of the amygdala's role in sensory processing*. Journal of Comparative Neurology, 1991. **313**(2): p. 295-325.
81. Cooper, H.M., et al., *Neuroanatomical pathways linking vision and olfaction in mammals*. Psychoneuroendocrinology, 1994. **19**(5-7): p. 623-39.
82. Doron, N.N. and J.E. Ledoux, *Organization of projections to the lateral amygdala from auditory and visual areas of the thalamus in the rat*. J Comp Neurol, 1999. **412**(3): p. 383-409.
83. Aggleton, J.P., *The amygdala: a functional analysis*. 2000: Oxford University Press.

84. Hopkins, D.A. and G. Holstege, *Amygdaloid projections to the mesencephalon, pons and medulla oblongata in the cat*. Experimental Brain Research, 1978. **32**(4): p. 529-547.
85. Saha, S., *ROLE OF THE CENTRAL NUCLEUS OF THE AMYGDALA IN THE CONTROL OF BLOOD PRESSURE: DESCENDING PATHWAYS TO MEDULLARY CARDIOVASCULAR NUCLEI*. Clinical and Experimental Pharmacology and Physiology, 2005. **32**(5-6): p. 450-456.
86. Ricardo, J.A. and E.T. Koh, *Anatomical evidence of direct projections from the nucleus of the solitary tract to the hypothalamus, amygdala, and other forebrain structures in the rat*. Brain Res, 1978. **153**(1): p. 1-26.
87. Allen, H.N., et al., *A Parabrachial-to-Amygdala Circuit That Determines Hemispheric Lateralization of Somatosensory Processing*. Biological Psychiatry, 2023. **93**(4): p. 370-381.
88. Han, W., et al., *Integrated Control of Predatory Hunting by the Central Nucleus of the Amygdala*. Cell, 2017. **168**(1): p. 311-324.e18.
89. Douglass, A.M., et al., *Central amygdala circuits modulate food consumption through a positive-valence mechanism*. Nature Neuroscience, 2017. **20**(10): p. 1384-1394.
90. Bloodgood, D.W., et al., *Kappa opioid receptor and dynorphin signaling in the central amygdala regulates alcohol intake*. Molecular Psychiatry, 2021. **26**(6): p. 2187-2199.
91. Hongjoo, J.L., et al., *Role of Amygdalo-Nigral Circuitry in Conditioning of a Visual Stimulus Paired with Food*. The Journal of Neuroscience, 2005. **25**(15): p. 3881.
92. Neugebauer, V., *Amygdala pain mechanisms*. Handb Exp Pharmacol, 2015. **227**: p. 261-84.
93. LeDoux, J.E., *Emotion circuits in the brain*. Annu Rev Neurosci, 2000. **23**: p. 155-84.
94. Kim, E.J., et al., *Dorsal periaqueductal gray-amygdala pathway conveys both innate and learned fear responses in rats*. Proc Natl Acad Sci U S A, 2013. **110**(36): p. 14795-800.
95. Omoluabi, T., et al., *Phasic and Tonic Locus Coeruleus Stimulation Associated Valence Learning Engages Distinct Adrenoceptors in the Rat Basolateral Amygdala*. Front Cell Neurosci, 2022. **16**: p. 886803.
96. Lee, S.C., et al., *Differential Recruitment of Competing Valence-Related Amygdala Networks during Anxiety*. Neuron, 2017. **96**(1): p. 81-88.e5.
97. Andersen, P., T.V.P. Bliss, and K.K. Skrede, *Lamellar organization of hippocampal excitatory pathways*. Experimental Brain Research, 1971. **13**(2): p. 222-238.

98. Bazelot, M., et al., *Hippocampal Theta Input to the Amygdala Shapes Feedforward Inhibition to Gate Heterosynaptic Plasticity*. *Neuron*, 2015. **87**(6): p. 1290-1303.
99. Orsini, C.A., et al., *Hippocampal and prefrontal projections to the basal amygdala mediate contextual regulation of fear after extinction*. *J Neurosci*, 2011. **31**(47): p. 17269-77.
100. Smith, Y., J.F. Paré, and D. Paré, *Differential innervation of parvalbumin-immunoreactive interneurons of the basolateral amygdaloid complex by cortical and intrinsic inputs*. *J Comp Neurol*, 2000. **416**(4): p. 496-508.
101. Petrovich, G.D., N.S. Canteras, and L.W. Swanson, *Combinatorial amygdalar inputs to hippocampal domains and hypothalamic behavior systems*. *Brain Research Reviews*, 2001. **38**(1): p. 247-289.
102. Felix-Ortiz, A.C., et al., *BLA to vHPC inputs modulate anxiety-related behaviors*. *Neuron*, 2013. **79**(4): p. 658-64.
103. Bocchio, M., S. Nabavi, and M. Capogna, *Synaptic Plasticity, Engrams, and Network Oscillations in Amygdala Circuits for Storage and Retrieval of Emotional Memories*. *Neuron*, 2017. **94**(4): p. 731-743.
104. Baron-Cohen, S., et al., *The amygdala theory of autism*. *Neurosci Biobehav Rev*, 2000. **24**(3): p. 355-64.
105. Schulkin, J., *Autism and the amygdala: an endocrine hypothesis*. *Brain Cogn*, 2007. **65**(1): p. 87-99.
106. Sah, P., *Fear, Anxiety, and the Amygdala*. *Neuron*, 2017. **96**(1): p. 1-2.
107. Adhikari, A., *Distributed circuits underlying anxiety*. *Frontiers in Behavioral Neuroscience*, 2014. **8**(APR).
108. Nestler, E.J., et al., *Neurobiology of depression*. *Neuron*, 2002. **34**(1): p. 13-25.
109. Belujon, P. and A.A. Grace, *Dopamine System Dysregulation in Major Depressive Disorders*. *Int J Neuropsychopharmacol*, 2017. **20**(12): p. 1036-1046.
110. Aggleton, J.P., *The contribution of the amygdala to normal and abnormal emotional states*. *Trends Neurosci*, 1993. **16**(8): p. 328-33.
111. Benes, F.M., *Amygdalocortical circuitry in schizophrenia: from circuits to molecules*. *Neuropsychopharmacology*, 2010. **35**(1): p. 239-57.
112. Craske, M.G. and M.B. Stein, *Anxiety*. *The Lancet*, 2016. **388**(10063): p. 3048-3059.
113. Hettrema, J.M., *189The Etiology of Fear and Anxiety: The Role of Environmental Exposures*, in *Anxiety Disorders*, K.J. Ressler, D.S. Pine, and B.O. Rothbaum, Editors. 2015, Oxford University Press. p. 0.

114. Steimer, T., *The biology of fear- and anxiety-related behaviors*. Dialogues Clin Neurosci, 2002. **4**(3): p. 231-49.
115. Cannon, W.B., *Bodily changes in pain, hunger, fear and rage*. ed. Appleton & Company, 1915.
116. Davis, M., et al., *Phasic vs sustained fear in rats and humans: role of the extended amygdala in fear vs anxiety*. Neuropsychopharmacology, 2010. **35**(1): p. 105-35.
117. Hasler, G., et al., *Discovering endophenotypes for major depression*. Neuropsychopharmacology, 2004. **29**(10): p. 1765-81.
118. Andrade, L., et al., *The epidemiology of major depressive episodes: results from the International Consortium of Psychiatric Epidemiology (ICPE) Surveys*. Int J Methods Psychiatr Res, 2003. **12**(1): p. 3-21.
119. Hasin, D.S., et al., *Epidemiology of Adult DSM-5 Major Depressive Disorder and Its Specifiers in the United States*. JAMA Psychiatry, 2018. **75**(4): p. 336-346.
120. Merikangas, K.R., et al., *Lifetime prevalence of mental disorders in U.S. adolescents: results from the National Comorbidity Survey Replication-- Adolescent Supplement (NCS-A)*. J Am Acad Child Adolesc Psychiatry, 2010. **49**(10): p. 980-9.
121. Kessler, R.C., et al., *Anxious and non-anxious major depressive disorder in the World Health Organization World Mental Health Surveys*. Epidemiol Psychiatr Sci, 2015. **24**(3): p. 210-26.
122. Vaidya, V.A. and R.S. Duman, *Depression--emerging insights from neurobiology*. Br Med Bull, 2001. **57**: p. 61-79.
123. Tripathi, S.J., et al., *Basolateral amygdalar inactivation blocks chronic stress-induced lamina-specific reduction in prefrontal cortex volume and associated anxiety-like behavior*. Prog Neuropsychopharmacol Biol Psychiatry, 2019. **88**: p. 194-207.
124. Price, J.L. and W.C. Drevets, *Neurocircuitry of mood disorders*. Neuropsychopharmacology, 2010. **35**(1): p. 192-216.
125. Becker, B., et al., *Fear processing and social networking in the absence of a functional amygdala*. Biol Psychiatry, 2012. **72**(1): p. 70-7.
126. Bach, D.R., R. Hurlemann, and R.J. Dolan, *Impaired threat prioritisation after selective bilateral amygdala lesions*. Cortex, 2015. **63**: p. 206-13.
127. Adolphs, R., et al., *Impaired recognition of emotion in facial expressions following bilateral damage to the human amygdala*. Nature, 1994. **372**(6507): p. 669-672.

128. Knight, D.C., H.T. Nguyen, and P.A. Bandettini, *The role of awareness in delay and trace fear conditioning in humans*. *Cogn Affect Behav Neurosci*, 2006. **6**(2): p. 157-62.
129. Qin, S., et al., *Amygdala subregional structure and intrinsic functional connectivity predicts individual differences in anxiety during early childhood*. *Biol Psychiatry*, 2014. **75**(11): p. 892-900.
130. Machado-de-Sousa, J.P., et al., *Increased amygdalar and hippocampal volumes in young adults with social anxiety*. *PLoS One*, 2014. **9**(2): p. e88523.
131. Shin, L.M., et al., *A Functional Magnetic Resonance Imaging Study of Amygdala and Medial Prefrontal Cortex Responses to Overtly Presented Fearful Faces in Posttraumatic Stress Disorder*. *Archives of General Psychiatry*, 2005. **62**(3): p. 273-281.
132. Stein, M.B., et al., *Increased Amygdala Activation to Angry and Contemptuous Faces in Generalized Social Phobia*. *Archives of General Psychiatry*, 2002. **59**(11): p. 1027-1034.
133. Rauch, S.L., L.M. Shin, and C.I. Wright, *Neuroimaging studies of amygdala function in anxiety disorders*. *Ann N Y Acad Sci*, 2003. **985**: p. 389-410.
134. LeDoux, J.E., et al., *The lateral amygdaloid nucleus: sensory interface of the amygdala in fear conditioning*. *The Journal of Neuroscience*, 1990. **10**(4): p. 1062.
135. Butler, R.K., et al., *Activation of phenotypically-distinct neuronal subpopulations of the rat amygdala following exposure to predator odor*. *Neuroscience*, 2011. **175**: p. 133-44.
136. Hitchcock, J. and M. Davis, *Lesions of the amygdala, but not of the cerebellum or red nucleus, block conditioned fear as measured with the potentiated startle paradigm*. *Behavioral Neuroscience*, 1986. **100**(1): p. 11-22.
137. Amano, T., et al., *The fear circuit revisited: contributions of the basal amygdala nuclei to conditioned fear*. *The Journal of neuroscience : the official journal of the Society for Neuroscience*, 2011. **31**(43): p. 15481-15489.
138. Whittle, N., et al., *Central amygdala micro-circuits mediate fear extinction*. *Nat Commun*, 2021. **12**(1): p. 4156.
139. Gründemann, J., et al., *Amygdala ensembles encode behavioral states*. *Science*, 2019. **364**(6437): p. eaav8736.
140. Cioocchi, S., et al., *Encoding of conditioned fear in central amygdala inhibitory circuits*. *Nature*, 2010. **468**(7321): p. 277-282.
141. Haubensak, W., et al., *Genetic dissection of an amygdala microcircuit that gates conditioned fear*. *Nature*, 2010. **468**(7321): p. 270-6.

142. Li, H., et al., *Experience-dependent modification of a central amygdala fear circuit*. *Nature neuroscience*, 2013. **16**(3): p. 332-339.
143. Tye, K.M., et al., *Amygdala circuitry mediating reversible and bidirectional control of anxiety*. *Nature*, 2011. **471**(7338): p. 358-362.
144. Senn, V., et al., *Long-Range Connectivity Defines Behavioral Specificity of Amygdala Neurons*. *Neuron*, 2014. **81**(2): p. 428-437.
145. Morel, C., et al., *Midbrain projection to the basolateral amygdala encodes anxiety-like but not depression-like behaviors*. *Nat Commun*, 2022. **13**(1): p. 1532.
146. Schildkraut, J.J., *The catecholamine hypothesis of affective disorders: a review of supporting evidence*. *Am J Psychiatry*, 1965. **122**(5): p. 509-22.
147. Cheetham, S., C. Katona, and R. Horton, *Post-mortem studies of neurotransmitter biochemistry in depression and suicide*, in *Biological aspects of affective disorders*. 1991, Elsevier. p. 191-221.
148. Leonard, B.E., *Evidence for a biochemical lesion in depression*. *J Clin Psychiatry*, 2000. **61 Suppl 6**: p. 12-7.
149. Schatzberg, A., *Recent studies on norepinephrine systems in mood disorders*. *Psychopharmacology: the fourth generation of progress*, 1995: p. 911-920.
150. Ruhé, H.G., N.S. Mason, and A.H. Schene, *Mood is indirectly related to serotonin, norepinephrine and dopamine levels in humans: a meta-analysis of monoamine depletion studies*. *Molecular Psychiatry*, 2007. **12**(4): p. 331-359.
151. Mayberg, H.S., *Limbic-cortical dysregulation: a proposed model of depression*. *J Neuropsychiatry Clin Neurosci*, 1997. **9**(3): p. 471-81.
152. Kim, J.J., et al., *Shared structural mechanisms of general anaesthetics and benzodiazepines*. *Nature*, 2020. **585**(7824): p. 303-308.
153. Sigel, E. and M. Ernst, *The Benzodiazepine Binding Sites of GABA(A) Receptors*. *Trends Pharmacol Sci*, 2018. **39**(7): p. 659-671.
154. Zanoveli, J.M., et al., *Extracellular serotonin level in the basolateral nucleus of the amygdala and dorsal periaqueductal gray under unconditioned and conditioned fear states: An in vivo microdialysis study*. *Brain Research*, 2009. **1294**: p. 106-115.
155. Parent, A., L. Descarries, and A. Beaudet, *Organization of ascending serotonin systems in the adult rat brain. A radioautographic study after intraventricular administration of [3H]5-hydroxytryptamine*. *Neuroscience*, 1981. **6**(2): p. 115-38.
156. Johnson, P.L., et al., *Pharmacological depletion of serotonin in the basolateral amygdala complex reduces anxiety and disrupts fear conditioning*. *Pharmacol Biochem Behav*, 2015. **138**: p. 174-9.

157. File, S.E., T.A. James, and N.K. MacLeod, *Depletion in amygdaloid 5-hydroxytryptamine concentration and changes in social and aggressive behaviour*. J Neural Transm, 1981. **50**(1): p. 1-12.
158. Bigos, K.L., et al., *Acute 5-HT reuptake blockade potentiates human amygdala reactivity*. Neuropsychopharmacology, 2008. **33**(13): p. 3221-5.
159. Murphy, S.E., et al., *Effect of a single dose of citalopram on amygdala response to emotional faces*. Br J Psychiatry, 2009. **194**(6): p. 535-40.
160. Godlewska, B.R., et al., *Short-term SSRI treatment normalises amygdala hyperactivity in depressed patients*. Psychol Med, 2012. **42**(12): p. 2609-17.
161. Bosker, F.J., et al., *Acute and chronic effects of citalopram on postsynaptic 5-hydroxytryptamine_{1A} receptor-mediated feedback: a microdialysis study in the amygdala*. Journal of Neurochemistry, 2001. **76**(6): p. 1645-1653.
162. Burghardt, N.S., et al., *The selective serotonin reuptake inhibitor citalopram increases fear after acute treatment but reduces fear with chronic treatment: a comparison with tianeptine*. Biological Psychiatry, 2004. **55**(12): p. 1171-1178.
163. Chen, A., C.J. Hough, and H. Li, *Serotonin type II receptor activation facilitates synaptic plasticity via n-methyl-d-aspartate-mediated mechanism in the rat basolateral amygdala*. Neuroscience, 2003. **119**(1): p. 53-63.
164. Huang, Y.Y. and E.R. Kandel, *5-Hydroxytryptamine induces a protein kinase A/mitogen-activated protein kinase-mediated and macromolecular synthesis-dependent late phase of long-term potentiation in the amygdala*. J Neurosci, 2007. **27**(12): p. 3111-9.
165. Votaw, V.R., et al., *The epidemiology of benzodiazepine misuse: A systematic review*. Drug Alcohol Depend, 2019. **200**: p. 95-114.
166. Rudolph, U. and H. Möhler, *GABAA receptor subtypes: Therapeutic potential in Down syndrome, affective disorders, schizophrenia, and autism*. Annu Rev Pharmacol Toxicol, 2014. **54**: p. 483-507.
167. Stefanits, H., et al., *GABA(A) receptor subunits in the human amygdala and hippocampus: Immunohistochemical distribution of 7 subunits*. J Comp Neurol, 2018. **526**(2): p. 324-348.
168. Pirker, S., et al., *GABA(A) receptors: immunocytochemical distribution of 13 subunits in the adult rat brain*. Neuroscience, 2000. **101**(4): p. 815-50.
169. Chandra, D., et al., *GABAA receptor gamma 2 subunit knockdown mice have enhanced anxiety-like behavior but unaltered hypnotic response to benzodiazepines*. BMC Neurosci, 2005. **6**: p. 30.
170. Fuchs, T., et al., *Disinhibition of somatostatin-positive GABAergic interneurons results in an anxiolytic and antidepressant-like brain state*. Mol Psychiatry, 2017. **22**(6): p. 920-930.

171. Smith, K.S. and U. Rudolph, *Anxiety and depression: mouse genetics and pharmacological approaches to the role of GABA(A) receptor subtypes*. *Neuropharmacology*, 2012. **62**(1): p. 54-62.
172. Marowsky, A., J.-M. Fritschy, and K.E. Vogt, *Functional mapping of GABAA receptor subtypes in the amygdala*. *European Journal of Neuroscience*, 2004. **20**(5): p. 1281-1289.
173. Botta, P., et al., *Regulating anxiety with extrasynaptic inhibition*. *Nature Neuroscience*, 2015. **18**(10): p. 1493-1500.
174. Comeras, L.B., H. Herzog, and R.O. Tasan, *Neuropeptides at the crossroad of fear and hunger: a special focus on neuropeptide Y*. *Ann N Y Acad Sci*, 2019. **1455**(1): p. 59-80.
175. Landgraf, R., *Neuropeptides and anxiety-related behavior*. *Endocr J*, 2001. **48**(5): p. 517-33.
176. van den Pol, A.N., *Neuropeptide transmission in brain circuits*. *Neuron*, 2012. **76**(1): p. 98-115.
177. Lin, E.J., *Neuropeptides as therapeutic targets in anxiety disorders*. *Curr Pharm Des*, 2012. **18**(35): p. 5709-27.
178. Jan, L.Y. and Y.N. Jan, *Peptidergic transmission in sympathetic ganglia of the frog*. *J Physiol*, 1982. **327**: p. 219-46.
179. Fuxe, K., et al., *From the Golgi-Cajal mapping to the transmitter-based characterization of the neuronal networks leading to two modes of brain communication: wiring and volume transmission*. *Brain Res Rev*, 2007. **55**(1): p. 17-54.
180. Ludwig, M. and G. Leng, *Dendritic peptide release and peptide-dependent behaviours*. *Nature Reviews Neuroscience*, 2006. **7**(2): p. 126-136.
181. Decavel, C. and A.N. Van den Pol, *GABA: a dominant neurotransmitter in the hypothalamus*. *J Comp Neurol*, 1990. **302**(4): p. 1019-37.
182. LaBella, F.S., J.D. Geiger, and G.B. Glavin, *Administered peptides inhibit the degradation of endogenous peptides. The dilemma of distinguishing direct from indirect effects*. *Peptides*, 1985. **6**(4): p. 645-60.
183. Sieburth, D., J.M. Madison, and J.M. Kaplan, *PKC-1 regulates secretion of neuropeptides*. *Nat Neurosci*, 2007. **10**(1): p. 49-57.
184. Dreifuss, J.J., et al., *Action potentials and release of neurohypophysial hormones in vitro*. *J Physiol*, 1971. **215**(3): p. 805-17.
185. Gainer, H., et al., *Action potentials and frequency-dependent secretion in the mouse neurohypophysis*. *Neuroendocrinology*, 1986. **43**(5): p. 557-63.

186. Jackson, M.B., A. Konnerth, and G.J. Augustine, *Action potential broadening and frequency-dependent facilitation of calcium signals in pituitary nerve terminals*. Proc Natl Acad Sci U S A, 1991. **88**(2): p. 380-4.
187. Ludwig, M., et al., *Intracellular calcium stores regulate activity-dependent neuropeptide release from dendrites*. Nature, 2002. **418**(6893): p. 85-89.
188. Lambert, R.C., et al., *A rise in the intracellular Ca²⁺ concentration of isolated rat supraoptic cells in response to oxytocin*. J Physiol, 1994. **478 (Pt 2)**(Pt 2): p. 275-87.
189. Zupanc, G.K., *Peptidergic transmission: from morphological correlates to functional implications*. Micron, 1996. **27**(1): p. 35-91.
190. Nordmann, J.J. and J.F. Morris, *Method for quantitating the molecular content of a subcellular organelle: hormone and neurophysin content of newly formed and aged neurosecretory granules*. Proc Natl Acad Sci U S A, 1984. **81**(1): p. 180-4.
191. Hatcher-Solis, C., et al., *G protein-coupled receptor signaling to Kir channels in Xenopus oocytes*. Current pharmaceutical biotechnology, 2014. **15**(10): p. 987-995.
192. Rodríguez-Menchaca, A.A., et al., *Dual Regulation of Voltage-Sensitive Ion Channels by PIP(2)*. Front Pharmacol, 2012. **3**: p. 170.
193. Suh, B.C. and B. Hille, *PIP₂ is a necessary cofactor for ion channel function: how and why?* Annu Rev Biophys, 2008. **37**: p. 175-95.
194. Chuang, H.H., et al., *Evidence that the nucleotide exchange and hydrolysis cycle of G proteins causes acute desensitization of G-protein gated inward rectifier K⁺ channels*. Proc Natl Acad Sci U S A, 1998. **95**(20): p. 11727-32.
195. Shekhar, A., et al., *Role of stress, corticotrophin releasing factor (CRF) and amygdala plasticity in chronic anxiety*. Stress, 2005. **8**(4): p. 209-19.
196. Funk, C.K. and G.F. Koob, *A CRF(2) agonist administered into the central nucleus of the amygdala decreases ethanol self-administration in ethanol-dependent rats*. Brain research, 2007. **1155**: p. 172-178.
197. Smith, G.W., et al., *Corticotropin Releasing Factor Receptor 1-Deficient Mice Display Decreased Anxiety, Impaired Stress Response, and Aberrant Neuroendocrine Development*. Neuron, 1998. **20**(6): p. 1093-1102.
198. Morin, S.M., et al., *Differential distribution of urocortin- and corticotropin-releasing factor-like immunoreactivities in the rat brain*. Neuroscience, 1999. **92**(1): p. 281-291.
199. Baker, D.G., et al., *Serial CSF corticotropin-releasing hormone levels and adrenocortical activity in combat veterans with posttraumatic stress disorder*. Am J Psychiatry, 1999. **156**(4): p. 585-8.

200. Sautter, F.J., et al., *Corticotropin-releasing factor in posttraumatic stress disorder (PTSD) with secondary psychotic symptoms, nonpsychotic PTSD, and healthy control subjects*. *Biol Psychiatry*, 2003. **54**(12): p. 1382-8.
201. Coric, V., et al., *Multicenter, randomized, double-blind, active comparator and placebo-controlled trial of a corticotropin-releasing factor receptor-1 antagonist in generalized anxiety disorder*. *Depression and Anxiety*, 2010. **27**(5): p. 417-425.
202. Dunlop, B.W., et al., *Evaluation of a corticotropin releasing hormone type 1 receptor antagonist in women with posttraumatic stress disorder: study protocol for a randomized controlled trial*. *Trials*, 2014. **15**: p. 240.
203. Schwandt, M.L., et al., *The CRF1 Antagonist Verucerfont in Anxious Alcohol-Dependent Women: Translation of Neuroendocrine, But not of Anti-Craving Effects*. *Neuropsychopharmacology*, 2016. **41**(12): p. 2818-2829.
204. Grillon, C., et al., *The CRH1 antagonist GSK561679 increases human fear but not anxiety as assessed by startle*. *Neuropsychopharmacology*, 2015. **40**(5): p. 1064-71.
205. Spierling, S.R. and E.P. Zorrilla, *Don't stress about CRF: assessing the translational failures of CRF(1)antagonists*. *Psychopharmacology (Berl)*, 2017. **234**(9-10): p. 1467-1481.
206. Tasan, R.O., et al., *The role of Neuropeptide Y in fear conditioning and extinction*. *Neuropeptides*, 2016. **55**: p. 111-26.
207. Rasmusson, A.M., et al., *Plasma Neuropeptide Y (NPY) Increases in Humans in Response to the α 2 Antagonist Yohimbine*. *Neuropsychopharmacology*, 1998. **19**(1): p. 95-98.
208. Rasmusson, A.M., et al., *Low baseline and yohimbine-stimulated plasma neuropeptide Y (NPY) levels in combat-related PTSD*. *Biological Psychiatry*, 2000. **47**(6): p. 526-539.
209. Sah, R., et al., *Cerebrospinal fluid neuropeptide Y in combat veterans with and without posttraumatic stress disorder*. *Psychoneuroendocrinology*, 2014. **40**: p. 277-83.
210. Kramer, M.S., et al., *Distinct Mechanism for Antidepressant Activity by Blockade of Central Substance P Receptors*. *Science*, 1998. **281**(5383): p. 1640-1645.
211. Kramer, M.S., et al., *Demonstration of the Efficacy and Safety of a Novel Substance P (NK1) Receptor Antagonist in Major Depression*. *Neuropsychopharmacology*, 2004. **29**(2): p. 385-392.
212. Ratti, E., et al., *Full central neurokinin-1 receptor blockade is required for efficacy in depression: evidence from orvepitant clinical studies*. *Journal of Psychopharmacology*, 2013. **27**(5): p. 424-434.

213. Ratti, E., et al., *Results From 2 Randomized, Double-Blind, Placebo-Controlled Studies of the Novel NK1 Receptor Antagonist Casopitant in Patients With Major Depressive Disorder*. *Journal of Clinical Psychopharmacology*, 2011. **31**(6).
214. Griebel, G. and F. Holsboer, *Neuropeptide receptor ligands as drugs for psychiatric diseases: the end of the beginning?* *Nature Reviews Drug Discovery*, 2012. **11**(6): p. 462-478.
215. van den Burg, E.H. and R. Stoop, *Neuropeptide signalling in the central nucleus of the amygdala*. *Cell and Tissue Research*, 2019. **375**(1): p. 93-101.
216. Avegno, E.M., J.W. Middleton, and N.W. Gilpin, *Synaptic GABAergic transmission in the central amygdala (CeA) of rats depends on slice preparation and recording conditions*. *Physiol Rep*, 2019. **7**(19): p. e14245.
217. Xiao, Z., et al., *Requirement of phospholipase C and protein kinase C in cholecystikinin-mediated facilitation of NMDA channel function and anxiety-like behavior*. *Hippocampus*, 2012. **22**(6): p. 1438-50.
218. Deng, P.Y., et al., *GABA(B) receptor activation inhibits neuronal excitability and spatial learning in the entorhinal cortex by activating TREK-2 K⁺ channels*. *Neuron*, 2009. **63**(2): p. 230-43.
219. Xiao, Z., et al., *Activation of neurotensin receptor 1 facilitates neuronal excitability and spatial learning and memory in the entorhinal cortex: beneficial actions in an Alzheimer's disease model*. *J Neurosci*, 2014. **34**(20): p. 7027-42.
220. Boyle, C.A., et al., *Ionic signalling mechanisms involved in neurokinin-3 receptor-mediated augmentation of fear-potentiated startle response in the basolateral amygdala*. *The Journal of Physiology*, 2022. **n/a**(n/a).
221. Paxinos, G. and C. Watson, *The Rat Brain Atlas in Stereotaxic Coordinates, 6th Edn Amsterdam*. 2007, Elsevier.[Google Scholar].
222. Paxinos, G., Watson, C., *The rat brain in stereotaxic coordinates*. 2007. **6th Edition**.
223. Boyle, C.A. and S. Lei, *Neuromedin B excites central lateral amygdala neurons and reduces cardiovascular output and fear-potentiated startle*. *Journal of Cellular Physiology*, 2023. **n/a**(n/a).
224. Boyle, C.A., et al., *Ionic signalling mechanisms involved in neurokinin-3 receptor-mediated augmentation of fear-potentiated startle response in the basolateral amygdala*. *The Journal of Physiology*, 2022. **600**(19): p. 4325-4345.
225. Ayers, L.W., et al., *Oxytocin reduces background anxiety in a fear-potentiated startle paradigm: peripheral vs central administration*. *Neuropsychopharmacology*, 2011. **36**(12): p. 2488-97.
226. Missig, G., et al., *Oxytocin reduces background anxiety in a fear-potentiated startle paradigm*. *Neuropsychopharmacology*, 2010. **35**(13): p. 2607-16.

227. Moaddab, M. and J. Dabrowska, *Oxytocin receptor neurotransmission in the dorsolateral bed nucleus of the stria terminalis facilitates the acquisition of cued fear in the fear-potentiated startle paradigm in rats*. *Neuropharmacology*, 2017. **121**: p. 130-139.
228. Feng, M., et al., *Validation of Volume–Pressure Recording Tail-Cuff Blood Pressure Measurements*. *American Journal of Hypertension*, 2008. **21**(12): p. 1288-1291.
229. Lipták, B., B. Kaprinay, and Z. Gáspárová, *A rat-friendly modification of the non-invasive tail-cuff to record blood pressure*. *Lab Anim (NY)*, 2017. **46**(6): p. 251-253.
230. Hem, N.A., et al., *A volume-pressure tail cuff method for hemodynamic parameters: Comparison of restraint and light isoflurane anesthesia in normotensive male Lewis rats*. *J Pharmacol Toxicol Methods*, 2019. **100**: p. 106601.
231. Luo, P., et al., *Stress-related arterial hypertension in Gper-deficient rats*. *Sheng Li Xue Bao*, 2017. **69**(5): p. 532-540.
232. Xiao, Z., et al., *Requirement of phospholipase C and protein kinase C in cholecystinin-mediated facilitation of NMDA channel function and anxiety-like behavior*. *Hippocampus*, 2012. **22**(6): p. 1438-1450.
233. Millan, M.J. and M. Brocco, *The Vogel conflict test: procedural aspects, gamma-aminobutyric acid, glutamate and monoamines*. *Eur J Pharmacol*, 2003. **463**(1-3): p. 67-96.
234. Minamino, N., K. Kangawa, and H. Matsuo, *Neuromedin B: a novel bombesin-like peptide identified in porcine spinal cord*. *Biochem Biophys Res Commun*, 1983. **114**(2): p. 541-8.
235. González, N., et al., *Characterization of putative GRP- and NMB-receptor antagonist's interaction with human receptors*. *Peptides*, 2009. **30**(8): p. 1473-1486.
236. Ohki-Hamazaki, H., *Neuromedin B*. *Progress in Neurobiology*, 2000. **62**(3): p. 297-312.
237. Gonzalez, N., P. Moreno, and R.T. Jensen, *Bombesin receptor subtype 3 as a potential target for obesity and diabetes*. *Expert Opin Ther Targets*, 2015. **19**(9): p. 1153-70.
238. Li, M., et al., *Bombesin Receptor Subtype-3 in Human Diseases*. *Arch Med Res*, 2019. **50**(7): p. 463-467.
239. Gonzalez, N., et al., *Bombesin-related peptides and their receptors: recent advances in their role in physiology and disease states*. *Current opinion in endocrinology, diabetes, and obesity*, 2008. **15**(1): p. 58-64.

240. Shapira, H., et al., *Neuromedin B receptor, expressed in Xenopus laevis oocytes, selectively couples to Gαq and not Gα11*. FEBS Letters, 1994. **348**(1): p. 89-92.
241. Ramos-Álvarez, I., et al., *Insights into bombesin receptors and ligands: Highlighting recent advances*. Peptides, 2015. **72**: p. 128-44.
242. Moody, T.W., et al., *Localization of receptors for bombesin-like peptides in the rat brain*. Ann N Y Acad Sci, 1988. **547**: p. 114-30.
243. Wada, E., et al., *Neuromedin B and gastrin-releasing peptide mRNAs are differentially distributed in the rat nervous system*. Journal of Neuroscience, 1990. **10**(9): p. 2917-2930.
244. Lee, M.C., et al., *Autoradiographic localization of neuromedin B binding sites in rat brain*. Molecular and Cellular Neuroscience, 1990. **1**(2): p. 161-167.
245. Brown, M.R. and T.S. Gray, *Peptide injections into the amygdala of conscious rats: effects on blood pressure, heart rate and plasma catecholamines*. Regul Pept, 1988. **21**(1-2): p. 95-106.
246. Vigh, J., et al., *Bombesin injection into the central amygdala influences feeding behavior in the rat*. Peptides, 1999. **20**(4): p. 437-44.
247. Kyrkouli, S.E., B.G. Stanley, and S.F. Leibowitz, *Bombesin-induced anorexia: sites of action in the rat brain*. Peptides, 1987. **8**(2): p. 237-41.
248. Li, B.H. and N.E. Rowland, *Peripherally and centrally administered bombesin induce Fos-like immunoreactivity in different brain regions in rats*. Regul Pept, 1996. **62**(2-3): p. 167-72.
249. Blais, K., J. Sethi, and I.V. Tabarean, *Gastrin-releasing peptide receptor mediates the excitation of preoptic GABAergic neurons by bombesin*. Neuroscience letters, 2016. **633**: p. 262-267.
250. Flynn, F.W., *Bombesin receptor antagonists block the effects of exogenous bombesin but not of nutrients on food intake*. Physiol Behav, 1997. **62**(4): p. 791-8.
251. Moody, T.W., et al., *Nonpeptide neuromedin B receptor antagonists inhibit the proliferation of C6 cells*. Eur J Pharmacol, 2000. **409**(2): p. 133-42.
252. Hu, B., N.I. Cilz, and S. Lei, *Somatostatin depresses the excitability of subicular bursting cells: Roles of inward rectifier K⁺ channels, KCNQ channels and Epac*. Hippocampus, 2017. **27**(9): p. 971-984.
253. Hu, B., C.A. Boyle, and S. Lei, *Oxytocin receptors excite lateral nucleus of central amygdala by PLCβ and PKC-dependent depression of inwardly rectifying K⁺ channels*. The Journal of Physiology, 2020. **n/a**(n/a).

254. Li, H., et al., *Roles of K⁺ and cation channels in ORL-1 receptor-mediated depression of neuronal excitability and epileptic activities in the medial entorhinal cortex*. *Neuropharmacology*, 2019. **151**: p. 144-158.
255. Hibino, H., et al., *Inwardly rectifying potassium channels: Their structure, function, and physiological roles*. *Physiological Reviews*, 2010. **90**(1): p. 291-366.
256. Wang, H.R., et al., *Selective inhibition of the K(ir)2 family of inward rectifier potassium channels by a small molecule probe: the discovery, SAR, and pharmacological characterization of ML133*. *ACS Chem Biol*, 2011. **6**(8): p. 845-56.
257. Kim, K.S., et al., *Rise and Fall of Kir2.2 Current by TLR4 Signaling in Human Monocytes: PKC-Dependent Trafficking and PI3K-Mediated PIP2 Decrease*. *J Immunol*, 2015. **195**(7): p. 3345-54.
258. Ford, N.C. and M.L. Baccei, *Inward-rectifying K(+) (Kir2) leak conductance dampens the excitability of lamina I projection neurons in the neonatal rat*. *Neuroscience*, 2016. **339**: p. 502-510.
259. Sonkusare, S.K., et al., *Inward rectifier potassium (Kir2.1) channels as end-stage boosters of endothelium-dependent vasodilators*. *J Physiol*, 2016. **594**(12): p. 3271-85.
260. Huang, X., et al., *Molecular and functional characterization of inwardly rectifying K(+) currents in murine proximal colon*. *J Physiol*, 2018. **596**(3): p. 379-391.
261. DePaoli, A.M., G.I. Bell, and M. Stoffel, *G Protein-Activated Inwardly Rectifying Potassium Channel (GIRK1/KGA) mRNA in Adult Rat Heart and Brain by in Situ Hybridization Histochemistry*. *Molecular and Cellular Neuroscience*, 1994. **5**(6): p. 515-522.
262. Kaufmann, K., et al., *ML297 (VU0456810), the first potent and selective activator of the GIRK potassium channel, displays antiepileptic properties in mice*. *ACS Chem Neurosci*, 2013. **4**(9): p. 1278-86.
263. Jin, W., et al., *Mechanisms of inward-rectifier K⁺ channel inhibition by tertiapin-Q*. *Biochemistry*, 1999. **38**(43): p. 14294-301.
264. Jin, W. and Z. Lu, *Synthesis of a stable form of tertiapin: a high-affinity inhibitor for inward-rectifier K⁺ channels*. *Biochemistry*, 1999. **38**(43): p. 14286-93.
265. Felix, J.P., et al., *Characterization of Kir1.1 channels with the use of a radiolabeled derivative of tertiapin*. *Biochemistry*, 2006. **45**(33): p. 10129-39.
266. Ramu, Y., Y. Xu, and Z. Lu, *Engineered specific and high-affinity inhibitor for a subtype of inward-rectifier K⁺ channels*. *Proceedings of the National Academy of Sciences*, 2008. **105**(31): p. 10774.
267. Mazarati, A., et al., *Regulation of Kindling Epileptogenesis by Hippocampal Galanin Type 1 and Type 2 Receptors: The Effects of Subtype-Selective*

- Agonists and the Role of G-Protein-Mediated Signaling*. Journal of Pharmacology and Experimental Therapeutics, 2006. **318**(2): p. 700.
268. Morgan, M.M., et al., *Differences in antinociceptive signalling mechanisms following morphine and fentanyl microinjections into the rat periaqueductal gray*. Eur J Pain, 2020. **24**(3): p. 617-624.
269. Ciochi, S., et al., *Encoding of conditioned fear in central amygdala inhibitory circuits*. Nature, 2010. **468**: p. 277.
270. Roesler, R., et al., *Bombesin receptor regulation of emotional memory*. 2012. p. 571.
271. Merali, Z., P. Kent, and H. Anisman, *Role of bombesin-related peptides in the mediation or integration of the stress response*. Cellular and Molecular Life Sciences CMLS, 2002. **59**(2): p. 272-287.
272. Merali, Z., et al., *Stress and eating: a dual role for bombesin-like peptides*. Frontiers in neuroscience, 2013. **7**: p. 193-193.
273. Bédard, T., et al., *Role of gastrin-releasing peptide and neuromedin B in anxiety and fear-related behavior*. Behavioural Brain Research, 2007. **179**(1): p. 133-140.
274. Merali, Z., et al., *Bombesin Receptors as a Novel Anti-Anxiety Therapeutic Target: BB₁ Receptor Actions on Anxiety through Alterations of Serotonin Activity*. The Journal of Neuroscience, 2006. **26**(41): p. 10387.
275. Merali, Z., et al., *Corticotropin-Releasing Hormone, Arginine Vasopressin, Gastrin-Releasing Peptide, and Neuromedin B Alterations in Stress-Relevant Brain Regions of Suicides and Control Subjects*. Biological Psychiatry, 2006. **59**(7): p. 594-602.
276. Ohki-Hamazaki, H., et al., *Functional Properties of Two Bombesin-Like Peptide Receptors Revealed by the Analysis of Mice Lacking Neuromedin B Receptor*. The Journal of Neuroscience, 1999. **19**(3): p. 948.
277. Davis, M., et al., *Fear-potentiated startle: a neural and pharmacological analysis*. Behav Brain Res, 1993. **58**(1-2): p. 175-98.
278. Davis, M., *Fear-Potentiated Startle in Rats*. Current Protocols in Neuroscience, 2001. **14**(1): p. 8.11A.1-8.11A.11.
279. Davis, M., *Neural systems involved in fear-potentiated startle*. Ann N Y Acad Sci, 1989. **563**: p. 165-83.
280. Wada, E., et al., *Neuromedin B and gastrin-releasing peptide mRNAs are differentially distributed in the rat nervous system*. J Neurosci, 1990. **10**(9): p. 2917-30.

281. Chaperon, F., et al., *Gastrin-Releasing Peptide Signaling Plays a Limited and Subtle Role in Amygdala Physiology and Aversive Memory*. PLOS ONE, 2012. **7**(4): p. e34963.
282. Pert, A., et al., *Bombesin: receptor distribution in brain and effects on nociception and locomotor activity*. Brain Res, 1980. **193**(1): p. 209-20.
283. Roesler, R., et al., *Bombesin/gastrin-releasing peptide receptors in the basolateral amygdala regulate memory consolidation*. European Journal of Neuroscience, 2004. **19**(4): p. 1041-1045.
284. Víg, J., L. Lénárd, and E. Fekete, *Bombesin microinjection into the basolateral amygdala influences feeding behavior in the rat*. Brain Res, 1999. **847**(2): p. 253-61.
285. Shumyatsky, G.P., et al., *Identification of a Signaling Network in Lateral Nucleus of Amygdala Important for Inhibiting Memory Specifically Related to Learned Fear*. Cell, 2002. **111**(6): p. 905-918.
286. Mountney, C., H. Anisman, and Z. Merali, *Effects of gastrin-releasing peptide agonist and antagonist administered to the basolateral nucleus of the amygdala on conditioned fear in the rat*. Psychopharmacology, 2008. **200**(1): p. 51.
287. Wada, E., et al., *cDNA cloning, characterization, and brain region-specific expression of a neuromedin-B-preferring bombesin receptor*. Neuron, 1991. **6**(3): p. 421-430.
288. Ladenheim, E.E., et al., *Distinct distribution of two bombesin receptor subtypes in the rat central nervous system*. Brain Research, 1992. **593**(2): p. 168-178.
289. Woodruff, G.N., et al., *Bombesin receptors in the brain*. Ann N Y Acad Sci, 1996. **780**: p. 223-43.
290. Wada, E., et al., *Comparison of gene expression for two distinct bombesin receptor subtypes in postnatal rat central nervous system*. Molecular and Cellular Neuroscience, 1992. **3**(5): p. 446-460.
291. Wang, L.H., et al., *Activation of neuromedin B-preferring bombesin receptors on rat glioblastoma C-6 cells increases cellular Ca²⁺ and phosphoinositides*. The Biochemical journal, 1992. **286 (Pt 2)**(Pt 2): p. 641-648.
292. Orbuch, M., et al., *Discovery of a novel class of neuromedin B receptor antagonists, substituted somatostatin analogues*. Mol Pharmacol, 1993. **44**(4): p. 841-50.
293. Mukai, H., et al., *Structure-activity relationships of mammalian bombesin-like neuropeptides in the contraction of rat uterus*. Neuropeptides, 1991. **19**(4): p. 243-250.
294. Khunawat, P. and A. Cowan, *Effects of bombesin, neuromedin B, neuromedin C and ranatensin on the rat stomach strip*. Pharmacologist, 1986. **28**: p. 171.

295. Wang, H.-R., et al., *Selective Inhibition of the Kir2 Family of Inward Rectifier Potassium Channels by a Small Molecule Probe: The Discovery, SAR, and Pharmacological Characterization of ML133*. ACS Chemical Biology, 2011. **6**(8): p. 845-856.
296. Karschin, C., et al., *Distribution and localization of a G protein-coupled inwardly rectifying K⁺ channel in the rat*. FEBS Letters, 1994. **348**(2): p. 139-144.
297. Wu, L.J., T.B. Sweet, and D.E. Clapham, *International Union of Basic and Clinical Pharmacology. LXXVI. Current progress in the mammalian TRP ion channel family*. Pharmacol Rev, 2010. **62**(3): p. 381-404.
298. Zschenderlein, C., et al., *Capsaicin-induced changes in LTP in the lateral amygdala are mediated by TRPV1*. PLoS One, 2011. **6**(1): p. e16116.
299. Riccio, A., et al., *Decreased anxiety-like behavior and Gαq/11-dependent responses in the amygdala of mice lacking TRPC4 channels*. The Journal of neuroscience : the official journal of the Society for Neuroscience, 2014. **34**(10): p. 3653-3667.
300. Riccio, A., et al., *Essential role for TRPC5 in amygdala function and fear-related behavior*. Cell, 2009. **137**(4): p. 761-772.
301. Xiao, Y., et al., *TRPV1-mediated presynaptic transmission in basolateral amygdala contributes to visceral hypersensitivity in adult rats with neonatal maternal deprivation*. Sci Rep, 2016. **6**: p. 29026.
302. Gavva, N.R., et al., *AMG 9810 [(E)-3-(4-t-butylphenyl)-N-(2,3-dihydrobenzo[b][1,4] dioxin-6-yl)acrylamide], a novel vanilloid receptor 1 (TRPV1) antagonist with antihyperalgesic properties*. J Pharmacol Exp Ther, 2005. **313**(1): p. 474-84.
303. Kwak, J.Y., et al., *A capsaicin-receptor antagonist, capsazepine, reduces inflammation-induced hyperalgesic responses in the rat: evidence for an endogenous capsaicin-like substance*. Neuroscience, 1998. **86**(2): p. 619-26.
304. Lei, S., B. Hu, and N. Rezagholizadeh, *Activation of V(1a) vasopressin receptors excite subicular pyramidal neurons by activating TRPV1 and depressing GIRK channels*. Neuropharmacology, 2021. **190**: p. 108565.
305. Yang, F. and J. Zheng, *Understand spiciness: mechanism of TRPV1 channel activation by capsaicin*. Protein Cell, 2017. **8**(3): p. 169-177.
306. Bevan, S., et al., *Capsazepine: a competitive antagonist of the sensory neurone excitant capsaicin*. Br J Pharmacol, 1992. **107**(2): p. 544-52.
307. Fawley, J.A., M.E. Hofmann, and M.C. Andresen, *Cannabinoid 1 and transient receptor potential vanilloid 1 receptors discretely modulate evoked glutamate separately from spontaneous glutamate transmission*. J Neurosci, 2014. **34**(24): p. 8324-32.

308. Zygmunt, P.M., et al., *Monoacylglycerols activate TRPV1--a link between phospholipase C and TRPV1*. PLoS One, 2013. **8**(12): p. e81618.
309. Prescott, E.D. and D. Julius, *A modular PIP2 binding site as a determinant of capsaicin receptor sensitivity*. Science, 2003. **300**(5623): p. 1284-8.
310. Willars, G.B., S.R. Nahorski, and R.A. Challiss, *Differential regulation of muscarinic acetylcholine receptor-sensitive polyphosphoinositide pools and consequences for signaling in human neuroblastoma cells*. J Biol Chem, 1998. **273**(9): p. 5037-46.
311. Cantley, L.C., *The phosphoinositide 3-kinase pathway*. Science, 2002. **296**(5573): p. 1655-7.
312. Kruse, M., et al., *Dynamics of Phosphoinositide-Dependent Signaling in Sympathetic Neurons*. J Neurosci, 2016. **36**(4): p. 1386-400.
313. Gründemann, J., *Distributed coding in auditory thalamus and basolateral amygdala upon associative fear learning*. Curr Opin Neurobiol, 2021. **67**: p. 183-189.
314. Boatman, J.A. and J.J. Kim, *A thalamo-cortico-amygdala pathway mediates auditory fear conditioning in the intact brain*. Eur J Neurosci, 2006. **24**(3): p. 894-900.
315. Berretta, S., *Cortico-amygdala circuits: role in the conditioned stress response*. Stress, 2005. **8**(4): p. 221-32.
316. Collins, D.R. and D. Paré, *Differential fear conditioning induces reciprocal changes in the sensory responses of lateral amygdala neurons to the CS(+) and CS(-)*. Learn Mem, 2000. **7**(2): p. 97-103.
317. Quirk, G.J., J.L. Armony, and J.E. LeDoux, *Fear conditioning enhances different temporal components of tone-evoked spike trains in auditory cortex and lateral amygdala*. Neuron, 1997. **19**(3): p. 613-24.
318. Wan, L., et al., *Distinct roles of NMB and GRP in itch transmission*. Sci Rep, 2017. **7**(1): p. 15466.
319. Li, F., et al., *Sneezing reflex is mediated by a peptidergic pathway from nose to brainstem*. Cell, 2021. **184**(14): p. 3762-3773.e10.
320. van den Pol, A.N., et al., *Neuromedin B and gastrin-releasing peptide excite arcuate nucleus neuropeptide Y neurons in a novel transgenic mouse expressing strong Renilla green fluorescent protein in NPY neurons*. J Neurosci, 2009. **29**(14): p. 4622-39.
321. Wilson, R.I. and R.A. Nicoll, *Endogenous cannabinoids mediate retrograde signalling at hippocampal synapses*. Nature, 2001. **410**(6828): p. 588-592.

322. Williford, K.M., et al., *BNST PKC δ neurons are activated by specific aversive conditions to promote anxiety-like behavior*. *Neuropsychopharmacology*, 2023.
323. Bergink, V., H.J. van Megen, and H.G. Westenberg, *Glutamate and anxiety*. *Eur Neuropsychopharmacol*, 2004. **14**(3): p. 175-83.
324. Fatemi, I., et al., *The role of locus coeruleus nucleus TRPV1 receptors in the development and expression of morphine dependence*. *Iran J Basic Med Sci*, 2019. **22**(10): p. 1186-1191.
325. Shirazi, M., et al., *Involvement of central TRPV1 receptors in pentylenetetrazole and amygdala-induced kindling in male rats*. *Neurological Sciences*, 2014. **35**(8): p. 1235-1241.
326. Beaujouan, J.C., et al., *A 25 year adventure in the field of tachykinins*. *Peptides*, 2004. **25**(3): p. 339-57.
327. Gerard, N.P., et al., *Molecular aspects of the tachykinin receptors*. *Regul Pept*, 1993. **43**(1-2): p. 21-35.
328. Maggi, C.A., *The mammalian tachykinin receptors*. *Gen Pharmacol*, 1995. **26**(5): p. 911-44.
329. Khawaja, A.M. and D.F. Rogers, *Tachykinins: receptor to effector*. *Int J Biochem Cell Biol*, 1996. **28**(7): p. 721-38.
330. Steinhoff, M.S., et al., *Tachykinins and their receptors: contributions to physiological control and the mechanisms of disease*. *Physiol Rev*, 2014. **94**(1): p. 265-301.
331. Onaga, T., *Tachykinin: recent developments and novel roles in health and disease*. *Biomol Concepts*, 2014. **5**(3): p. 225-43.
332. Lenard, L., et al., *Substance P and neurotensin in the limbic system: Their roles in reinforcement and memory consolidation*. *Neurosci Biobehav Rev*, 2018. **85**: p. 1-20.
333. Zieglgansberger, W., *Substance P and pain chronicity*. *Cell Tissue Res*, 2019. **375**(1): p. 227-241.
334. Cassell, M.D. and T.S. Gray, *Morphology of peptide-immunoreactive neurons in the rat central nucleus of the amygdala*. *J Comp Neurol*, 1989. **281**(2): p. 320-33.
335. Shigematsu, N., et al., *An immunohistochemical study on a unique colocalization relationship between substance P and GABA in the central nucleus of amygdala*. *Brain Res*, 2008. **1198**: p. 55-67.
336. Singewald, N., et al., *Modulation of basal and stress-induced amygdaloid substance P release by the potent and selective NK1 receptor antagonist L-822429*. *J Neurochem*, 2008. **106**(6): p. 2476-88.

337. Marcos, P., et al., *Neuropeptides in the cat amygdala*. Brain Res Bull, 1998. **45**(3): p. 261-8.
338. Lucas, L.R., et al., *Localization of the tachykinin neurokinin B precursor peptide in rat brain by immunocytochemistry and in situ hybridization*. Neuroscience, 1992. **51**(2): p. 317-45.
339. Andero, R., B.G. Dias, and K.J. Ressler, *A role for Tac2, NkB, and Nk3 receptor in normal and dysregulated fear memory consolidation*. Neuron, 2014. **83**(2): p. 444-454.
340. McCullough, K.M., et al., *Quantified Coexpression Analysis of Central Amygdala Subpopulations*. eNeuro, 2018. **5**(1).
341. Dam, T.V., B. Martinelli, and R. Quirion, *Autoradiographic distribution of brain neurokinin-1/substance P receptors using a highly selective ligand [3H]-[Sar⁹,Met(O₂)¹¹]-substance P*. Brain Res, 1990. **531**(1-2): p. 333-7.
342. Sreepathi, H.K. and F. Ferraguti, *Subpopulations of neurokinin 1 receptor-expressing neurons in the rat lateral amygdala display a differential pattern of innervation from distinct glutamatergic afferents*. Neuroscience, 2012. **203**: p. 59-77.
343. Nagano, M., T. Oishi, and H. Suzuki, *Distribution and pharmacological characterization of primate NK-2 tachykinin receptor in the central nervous system of the rhesus monkey*. Neurosci Lett, 2011. **503**(1): p. 23-6.
344. Beaujouan, J.C., et al., *Different subtypes of tachykinin NK(1) receptor binding sites are present in the rat brain*. J Neurochem, 2000. **75**(3): p. 1015-26.
345. Dam, T.V., E. Escher, and R. Quirion, *Visualization of neurokinin-3 receptor sites in rat brain using the highly selective ligand [3H]senktide*. Brain Res, 1990. **506**(1): p. 175-9.
346. Stoessl, A.J. and D.R. Hill, *Autoradiographic visualization of NK-3 tachykinin binding sites in the rat brain, utilizing [3H]senktide*. Brain Res, 1990. **534**(1-2): p. 1-7.
347. Mileusnic, D., et al., *Neurokinin-3 receptor distribution in rat and human brain: an immunohistochemical study*. Neuroscience, 1999. **89**(4): p. 1269-90.
348. Yip, J. and L.A. Chahl, *Localization of Fos-like immunoreactivity induced by the NK3 tachykinin receptor agonist, senktide, in the guinea-pig brain*. Br J Pharmacol, 1997. **122**(4): p. 715-25.
349. Nagano, M., et al., *Distribution and pharmacological characterization of primate NK-1 and NK-3 tachykinin receptors in the central nervous system of the rhesus monkey*. Br J Pharmacol, 2006. **147**(3): p. 316-23.

350. Varnas, K., et al., *Neurokinin-3 Receptor Binding in Guinea Pig, Monkey, and Human Brain: In Vitro and in Vivo Imaging Using the Novel Radioligand, [18F]Lu AF10628*. *Int J Neuropsychopharmacol*, 2016. **19**(8).
351. Yip, J. and L.A. Chahl, *Localization of NK1 and NK3 receptors in guinea-pig brain*. *Regul Pept*, 2001. **98**(1-2): p. 55-62.
352. Andero, R., et al., *Amygdala-Dependent Molecular Mechanisms of the Tac2 Pathway in Fear Learning*. *Neuropsychopharmacology*, 2016. **41**(11): p. 2714-22.
353. Smith, M.E. and F.W. Flynn, *Distribution of Fos-like immunoreactivity within the rat brain following intraventricular injection of the selective NK(3) receptor agonist senktide*. *J Comp Neurol*, 2000. **426**(3): p. 413-28.
354. Giardina, G.A., et al., *Discovery of a novel class of selective non-peptide antagonists for the human neurokinin-3 receptor. 1. Identification of the 4-quinolinecarboxamide framework*. *J Med Chem*, 1997. **40**(12): p. 1794-807.
355. Hu, B., N.I. Cilz, and S. Lei, *Somatostatin depresses the excitability of subicular bursting cells: Roles of inward rectifier K(+) channels, KCNQ channels and Epac*. *Hippocampus*, 2017. **27**(9): p. 971-984.
356. Lacey, M.G., N.B. Mercuri, and R.A. North, *On the potassium conductance increase activated by GABAB and dopamine D2 receptors in rat substantia nigra neurones*. *J Physiol*, 1988. **401**: p. 437-53.
357. Li, H., et al., *Roles of K(+) and cation channels in ORL-1 receptor-mediated depression of neuronal excitability and epileptic activities in the medial entorhinal cortex*. *Neuropharmacology*, 2019. **151**: p. 144-158.
358. Hibino, H., et al., *Inwardly rectifying potassium channels: their structure, function, and physiological roles*. *Physiol Rev*, 2010. **90**(1): p. 291-366.
359. Riccio, A., et al., *Decreased anxiety-like behavior and Galphaq/11-dependent responses in the amygdala of mice lacking TRPC4 channels*. *J Neurosci*, 2014. **34**(10): p. 3653-67.
360. Riccio, A., et al., *Essential role for TRPC5 in amygdala function and fear-related behavior*. *Cell*, 2009. **137**(4): p. 761-72.
361. Klumpers, F., et al., *Impaired acquisition of classically conditioned fear-potentiated startle reflexes in humans with focal bilateral basolateral amygdala damage*. *Soc Cogn Affect Neurosci*, 2015. **10**(9): p. 1161-8.
362. Kim, M., et al., *Infusion of the non-NMDA receptor antagonist CNQX into the amygdala blocks the expression of fear-potentiated startle*. *Behav Neural Biol*, 1993. **59**(1): p. 5-8.
363. Sananes, C.B. and M. Davis, *N-methyl-D-aspartate lesions of the lateral and basolateral nuclei of the amygdala block fear-potentiated startle and shock sensitization of startle*. *Behav Neurosci*, 1992. **106**(1): p. 72-80.

364. Campeau, S. and M. Davis, *Involvement of the central nucleus and basolateral complex of the amygdala in fear conditioning measured with fear-potentiated startle in rats trained concurrently with auditory and visual conditioned stimuli*. J Neurosci, 1995. **15**(3 Pt 2): p. 2301-11.
365. Davis, M., *Pharmacological and anatomical analysis of fear conditioning using the fear-potentiated startle paradigm*. Behav Neurosci, 1986. **100**(6): p. 814-24.
366. Grillon, C., *Models and mechanisms of anxiety: evidence from startle studies*. Psychopharmacology (Berl), 2008. **199**(3): p. 421-37.
367. Mazarati, A., et al., *Regulation of kindling epileptogenesis by hippocampal galanin type 1 and type 2 receptors: The effects of subtype-selective agonists and the role of G-protein-mediated signaling*. J Pharmacol Exp Ther, 2006. **318**(2): p. 700-8.
368. Pagani, M., et al., *How Gastrin-Releasing Peptide Opens the Spinal Gate for Itch*. Neuron, 2019. **103**(1): p. 102-117 e5.
369. Hermes, M.L., et al., *Gastrin-releasing peptide acts via postsynaptic BB2 receptors to modulate inward rectifier K⁺ and TRPV1-like conductances in rat paraventricular thalamic neurons*. J Physiol, 2013. **591**(7): p. 1823-39.
370. Zhang, H.-p., et al., *Bombesin facilitates GABAergic transmission and depresses epileptiform activity in the entorhinal cortex*. Hippocampus, 2014. **24**(1): p. 21-31.
371. Lee, K., et al., *Bombesin-like peptides depolarize rat hippocampal interneurons through interaction with subtype 2 bombesin receptors*. The Journal of Physiology, 1999. **518**(3): p. 791-802.
372. Wu, M., et al., *A potent and selective small molecule Kir2.1 inhibitor*, in *Probe Reports from the NIH Molecular Libraries Program*. 2010, National Center for Biotechnology Information (US): Bethesda (MD).
373. Karschin, C., et al., *IRK(1-3) and GIRK(1-4) inwardly rectifying K⁺ channel mRNAs are differentially expressed in the adult rat brain*. J Neurosci, 1996. **16**(11): p. 3559-70.
374. Chen, X. and D. Johnston, *Constitutively active G-protein-gated inwardly rectifying K⁺ channels in dendrites of hippocampal CA1 pyramidal neurons*. J Neurosci, 2005. **25**(15): p. 3787-92.
375. Gonzalez, J.C., et al., *Constitutive and Synaptic Activation of GIRK Channels Differentiates Mature and Newborn Dentate Granule Cells*. J Neurosci, 2018. **38**(29): p. 6513-6526.
376. Lüscher, C., et al., *G Protein-Coupled Inwardly Rectifying K⁺ Channels (GIRKs) Mediate Postsynaptic but Not Presynaptic Transmitter Actions in Hippocampal Neurons*. Neuron, 1997. **19**(3): p. 687-695.

377. Luscher, C. and P.A. Slesinger, *Emerging roles for G protein-gated inwardly rectifying potassium (GIRK) channels in health and disease*. Nat Rev Neurosci, 2010. **11**(5): p. 301-15.
378. Murer, G., et al., *An immunocytochemical study on the distribution of two G-protein-gated inward rectifier potassium channels (GIRK2 and GIRK4) in the adult rat brain*. Neuroscience, 1997. **80**(2): p. 345-357.
379. Stevens, E.B., et al., *Bombesin receptors inhibit G protein-coupled inwardly rectifying K⁺ channels expressed in Xenopus oocytes through a protein kinase C-dependent pathway*. Mol Pharmacol, 1999. **55**(6): p. 1020-7.
380. Mao, J., et al., *Molecular basis for the inhibition of G protein-coupled inward rectifier K⁺ channels by protein kinase C*. Proc Natl Acad Sci U S A, 2004. **101**(4): p. 1087-92.
381. Adney, S.K., et al., *A Critical Gating Switch at a Modulatory Site in Neuronal Kir3 Channels*. J Neurosci, 2015. **35**(42): p. 14397-405.
382. Huang, K.-P., *The mechanism of protein kinase C activation*. Trends in Neurosciences, 1989. **12**(11): p. 425-432.
383. Niemeyer, A., A. Rinne, and M.-C. Kienitz, *Receptor-specific regulation of atrial GIRK channel activity by different Ca²⁺-dependent PKC isoforms*. Cellular Signalling, 2019. **64**: p. 109418.
384. Victoria, N.C., et al., *G Protein-Gated K⁺ Channel Ablation in Forebrain Pyramidal Neurons Selectively Impairs Fear Learning*. Biol Psychiatry, 2016. **80**(10): p. 796-806.
385. Pravetoni, M. and K. Wickman, *Behavioral characterization of mice lacking GIRK/Kir3 channel subunits*. Genes Brain Behav, 2008. **7**(5): p. 523-31.
386. Wydeven, N., et al., *Mechanisms underlying the activation of G-protein-gated inwardly rectifying K⁺ (GIRK) channels by the novel anxiolytic drug, ML297*. Proc Natl Acad Sci U S A, 2014. **111**(29): p. 10755-60.
387. McOmish, C.E., et al., *PLC-beta1 knockout mice as a model of disrupted cortical development and plasticity: behavioral endophenotypes and dysregulation of RGS4 gene expression*. Hippocampus, 2008. **18**(8): p. 824-34.
388. Liu, B., J. Feng, and J.H. Wang, *Protein kinase C is essential for kainate-induced anxiety-related behavior and glutamatergic synapse upregulation in prelimbic cortex*. CNS Neurosci Ther, 2014. **20**(11): p. 982-90.
389. Lesscher, H.M., et al., *Amygdala protein kinase C epsilon regulates corticotropin-releasing factor and anxiety-like behavior*. Genes Brain Behav, 2008. **7**(3): p. 323-33.
390. Bowers, B.J., et al., *Mice lacking PKC gamma exhibit decreased anxiety*. Behav Genet, 2000. **30**(2): p. 111-21.

391. Hodge, C.W., et al., *Decreased anxiety-like behavior, reduced stress hormones, and neurosteroid supersensitivity in mice lacking protein kinase Cepsilon*. J Clin Invest, 2002. **110**(7): p. 1003-10.
392. Weeber, E.J., et al., *A role for the beta isoform of protein kinase C in fear conditioning*. J Neurosci, 2000. **20**(16): p. 5906-14.
393. Zanchi, D., et al., *The impact of gut hormones on the neural circuit of appetite and satiety: A systematic review*. Neurosci Biobehav Rev, 2017. **80**: p. 457-475.
394. Petrovich, G.D., *Learning and the motivation to eat: forebrain circuitry*. Physiol Behav, 2011. **104**(4): p. 582-9.
395. Petrovich, G.D., *Forebrain networks and the control of feeding by environmental learned cues*. Physiol Behav, 2013. **121**: p. 10-8.
396. Smith, C.M. and A.J. Lawrence, *Salt Appetite, and the Influence of Opioids*. Neurochem Res, 2018. **43**(1): p. 12-18.
397. Merali, Z., et al., *Aversive and Appetitive Events Evoke the Release of Corticotropin-Releasing Hormone and Bombesin-Like Peptides at the Central Nucleus of the Amygdala*. The Journal of Neuroscience, 1998. **18**(12): p. 4758.
398. Hsieh, Y.S., et al., *Transcriptional involvement of protein kinase C-alpha isozyme in amphetamine-mediated appetite suppression*. Eur J Neurosci, 2005. **22**(3): p. 715-23.
399. Merali, Z., et al., *Corticotropin-releasing hormone, arginine vasopressin, gastrin-releasing peptide, and neuromedin B alterations in stress-relevant brain regions of suicides and control subjects*. Biol Psychiatry, 2006. **59**(7): p. 594-602.
400. Yamada, K., et al., *Decreased marble burying behavior in female mice lacking neuromedin-B receptor (NMB-R) implies the involvement of NMB/NMB-R in 5-HT neuron function*. Brain Res, 2002. **942**(1-2): p. 71-8.
401. Merali, Z., et al., *Bombesin Receptors as a Novel Anti-Anxiety Therapeutic Target: Bombesin Receptor Actions on Anxiety through Alterations of Serotonin Activity*. The Journal of Neuroscience, 2006. **26**(41): p. 10387.
402. Merali, Z., et al., *Aversive and appetitive events evoke the release of corticotropin-releasing hormone and bombesin-like peptides at the central nucleus of the amygdala*. The Journal of neuroscience : the official journal of the Society for Neuroscience, 1998. **18**(12): p. 4758-4766.
403. Toth, M., et al., *The role of PKC signaling in CRF-induced modulation of startle*. Psychopharmacology (Berl), 2013. **229**(4): p. 579-89.
404. Rubinow, D.R. and P.J. Schmidt, *Sex differences and the neurobiology of affective disorders*. Neuropsychopharmacology, 2019. **44**(1): p. 111-128.

405. Cahill, L., et al., *Sex-Related Hemispheric Lateralization of Amygdala Function in Emotionally Influenced Memory: An fMRI Investigation*. Learning & Memory, 2004. **11**(3): p. 261-266.
406. Micevych, P.E., D.W. Matt, and V.L.W. Go, *Concentrations of cholecystokinin, substance P, and bombesin in discrete regions of male and female rat brain: Sex differences and estrogen effects*. Experimental Neurology, 1988. **100**(2): p. 416-425.
407. Johnston, A.L. and S.E. File, *Sex differences in animal tests of anxiety*. Physiol Behav, 1991. **49**(2): p. 245-50.
408. Toufexis, D., et al., *Sex Differences in Hormonal Modulation of Anxiety Measured with Light-Enhanced Startle: Possible Role for Arginine Vasopressin in the Male*. The Journal of Neuroscience, 2005. **25**(39): p. 9010.
409. Toufexis, D.J., et al., *Progesterone attenuates corticotropin-releasing factor-enhanced but not fear-potentiated startle via the activity of its neuroactive metabolite, allopregnanolone*. J Neurosci, 2004. **24**(45): p. 10280-7.
410. Le Mével, J.C., et al., *Gastrin-releasing peptide (GRP) acts centrally to stimulate the cardioventilatory system in trout*. Autonomic Neuroscience: Basic and Clinical, 2015. **192**: p. 65-66.
411. Yu, K., et al., *Central Amygdala Somatostatin Neurons Gate Passive and Active Defensive Behaviors*. J Neurosci, 2016. **36**(24): p. 6488-96.
412. Moscarello, J.M. and M.A. Penzo, *The central nucleus of the amygdala and the construction of defensive modes across the threat-imminence continuum*. Nature Neuroscience, 2022. **25**(8): p. 999-1008.
413. Bungo, T., et al., *Central bombesin inhibits food intake and the orexigenic effect of neuropeptide Y in the neonatal chick*. Physiol Behav, 2000. **70**(5): p. 573-6.
414. Mulholland, M.W. and D.M. Simeone, *Bombesin-stimulated acetylcholine release from myenteric plexus neurons*. J Surg Res, 1993. **54**(5): p. 389-92.
415. Walker, P., et al., *The role of neuropeptide Y in cardiovascular regulation*. Trends in Pharmacological Sciences, 1991. **12**: p. 111-115.
416. Yang, S.N., et al., *Cardiovascular effects of intracerebral injection of neuropeptide Y in rats*. Zhongguo Yao Li Xue Bao, 1992. **13**(2): p. 116-8.
417. van den Pol, A.N., et al., *Neuromedin B and gastrin-releasing peptide excite arcuate nucleus neuropeptide Y neurons in a novel transgenic mouse expressing strong Renilla green fluorescent protein in NPY neurons*. The Journal of neuroscience : the official journal of the Society for Neuroscience, 2009. **29**(14): p. 4622-4639.

418. Elsaafien, K., et al., *Identification of Novel Cross-Talk between the Neuroendocrine and Autonomic Stress Axes Controlling Blood Pressure*. The Journal of Neuroscience, 2021. **41**(21): p. 4641.
419. Gray, T.S., M.E. Carney, and D.J. Magnuson, *Direct projections from the central amygdaloid nucleus to the hypothalamic paraventricular nucleus: possible role in stress-induced adrenocorticotropin release*. Neuroendocrinology, 1989. **50**(4): p. 433-46.
420. Weera, M.M., et al., *Central Amygdala Projections to Lateral Hypothalamus Mediate Avoidance Behavior in Rats*. The Journal of Neuroscience, 2021. **41**(1): p. 61.
421. Zhang, Y., et al., *Neuromedin B receptor stimulation of Cav3.2 T-type Ca(2+) channels in primary sensory neurons mediates peripheral pain hypersensitivity*. Theranostics, 2021. **11**(19): p. 9342-9357.
422. Pinnock, R.D. and G.N. Woodruff, *Bombesin excites a subpopulation of 5-hydroxytryptamine-sensitive neurones in the rat dorsal raphe nucleus in vitro*. J Physiol, 1991. **440**: p. 55-65.
423. Blais, K., J. Sethi, and I.V. Tabarean, *Gastrin-releasing peptide receptor mediates the excitation of preoptic GABAergic neurons by bombesin*. Neurosci Lett, 2016. **633**: p. 262-267.
424. Ufret-Vincenty, C.A., et al., *Localization of the PIP2 sensor of TRPV1 ion channels*. J Biol Chem, 2011. **286**(11): p. 9688-98.
425. Zhang, L., et al., *Mechanosensitivity of GIRK channels is mediated by protein kinase C-dependent channel-phosphatidylinositol 4,5-bisphosphate interaction*. J Biol Chem, 2004. **279**(8): p. 7037-47.
426. Nazıroğlu, M., *Activation of TRPM2 and TRPV1 Channels in Dorsal Root Ganglion by NADPH Oxidase and Protein Kinase C Molecular Pathways: a Patch Clamp Study*. Journal of Molecular Neuroscience, 2017. **61**(3): p. 425-435.
427. Liu, B., et al., *Inhibitory modulation of distal C-terminal on protein kinase C-dependent phospho-regulation of rat TRPV1 receptors*. J Physiol, 2004. **560**(Pt 3): p. 627-38.
428. Nasuhoglu, C., et al., *Modulation of cardiac PIP2 by cardioactive hormones and other physiologically relevant interventions*. American Journal of Physiology-Cell Physiology, 2002. **283**(1): p. C223-C234.
429. Mishra, S.K., S. Holzman, and M.A. Hoon, *A Nociceptive Signaling Role for Neuromedin B*. The Journal of Neuroscience, 2012. **32**(25): p. 8686.
430. Shonesy, B.C., et al., *The initiation of synaptic 2-AG mobilization requires both an increased supply of diacylglycerol precursor and increased postsynaptic calcium*. Neuropharmacology, 2015. **91**: p. 57-62.

431. Hashimoto-dani, Y., et al., *Phospholipase C β serves as a coincidence detector through its Ca²⁺ dependency for triggering retrograde endocannabinoid signal*. *Neuron*, 2005. **45**(2): p. 257-68.
432. Marsch, R., et al., *Reduced Anxiety, Conditioned Fear, and Hippocampal Long-Term Potentiation in Transient Receptor Potential Vanilloid Type 1 Receptor-Deficient Mice*. *The Journal of Neuroscience*, 2007. **27**(4): p. 832.
433. Huang, X., et al., *Molecular and functional characterization of inwardly rectifying K⁺ currents in murine proximal colon*. *The Journal of Physiology*, 2018. **596**(3): p. 379-391.
434. Gonzalez, J.C., et al., *Constitutive and Synaptic Activation of GIRK Channels Differentiates Mature and Newborn Dentate Granule Cells*. *The Journal of Neuroscience*, 2018. **38**(29): p. 6513.
435. Lüscher, C. and P.A. Slesinger, *Emerging roles for G protein-gated inwardly rectifying potassium (GIRK) channels in health and disease*. *Nature Reviews Neuroscience*, 2010. **11**(5): p. 301-315.
436. Murer, G., et al., *An immunocytochemical study on the distribution of two G-protein-gated inward rectifier potassium channels (GIRK2 and GIRK4) in the adult rat brain*. *Neuroscience*, 1997. **80**(2): p. 345-57.
437. DePaoli, A.M., G.I. Bell, and M. Stoffel, *G protein-activated inwardly rectifying potassium channel (GIRK1/KGA) mRNA in adult rat heart and brain by in situ hybridization histochemistry*. *Mol Cell Neurosci*, 1994. **5**(6): p. 515-22.
438. Ponce, A., et al., *G-protein-gated inward rectifier K⁺ channel proteins (GIRK1) are present in the soma and dendrites as well as in nerve terminals of specific neurons in the brain*. *J Neurosci*, 1996. **16**(6): p. 1990-2001.
439. Saenz del Burgo, L., et al., *Distribution and neurochemical characterization of neurons expressing GIRK channels in the rat brain*. *J Comp Neurol*, 2008. **510**(6): p. 581-606.
440. Peters, J.H., et al., *Primary afferent activation of thermosensitive TRPV1 triggers asynchronous glutamate release at central neurons*. *Neuron*, 2010. **65**(5): p. 657-69.
441. Sekizawa, S., J.P. Joad, and A.C. Bonham, *Substance P presynaptically depresses the transmission of sensory input to bronchopulmonary neurons in the guinea pig nucleus tractus solitarius*. *J Physiol*, 2003. **552**(Pt 2): p. 547-59.
442. Devane, W.A., et al., *Isolation and structure of a brain constituent that binds to the cannabinoid receptor*. *Science*, 1992. **258**(5090): p. 1946-9.
443. Mechoulam, R., et al., *Identification of an endogenous 2-monoglyceride, present in canine gut, that binds to cannabinoid receptors*. *Biochem Pharmacol*, 1995. **50**(1): p. 83-90.

444. Sugiura, T., et al., *2-Arachidonoylglycerol: a possible endogenous cannabinoid receptor ligand in brain*. *Biochem Biophys Res Commun*, 1995. **215**(1): p. 89-97.
445. Di Marzo, V., et al., *Endocannabinoids: endogenous cannabinoid receptor ligands with neuromodulatory action*. *Trends Neurosci*, 1998. **21**(12): p. 521-8.
446. Stella, N., P. Schweitzer, and D. Piomelli, *A second endogenous cannabinoid that modulates long-term potentiation*. *Nature*, 1997. **388**(6644): p. 773-8.
447. Scotter, E.L., M.E. Abood, and M. Glass, *The endocannabinoid system as a target for the treatment of neurodegenerative disease*. *Br J Pharmacol*, 2010. **160**(3): p. 480-98.
448. Ohno-Shosaku, T., et al., *Presynaptic cannabinoid sensitivity is a major determinant of depolarization-induced retrograde suppression at hippocampal synapses*. *J Neurosci*, 2002. **22**(10): p. 3864-72.
449. Kreitzer, A.C. and W.G. Regehr, *Cerebellar depolarization-induced suppression of inhibition is mediated by endogenous cannabinoids*. *J Neurosci*, 2001. **21**(20): p. Rc174.
450. Diana, M.A., et al., *Short-term retrograde inhibition of GABAergic synaptic currents in rat Purkinje cells is mediated by endogenous cannabinoids*. *J Neurosci*, 2002. **22**(1): p. 200-8.
451. Maejima, T., et al., *Presynaptic Inhibition Caused by Retrograde Signal from Metabotropic Glutamate to Cannabinoid Receptors*. *Neuron*, 2001. **31**(3): p. 463-475.
452. Varma, N., et al., *Metabotropic glutamate receptors drive the endocannabinoid system in hippocampus*. *J Neurosci*, 2001. **21**(24): p. Rc188.
453. Hirasawa, M., S.B. Kombian, and Q.J. Pittman, *Oxytocin retrogradely inhibits evoked, but not miniature, EPSCs in the rat supraoptic nucleus: role of N- and P/Q-type calcium channels*. *J Physiol*, 2001. **532**(Pt 3): p. 595-607.
454. Wang, L. and W.E. Armstrong, *Tonic regulation of GABAergic synaptic activity on vasopressin neurones by cannabinoids*. *J Neuroendocrinol*, 2012. **24**(4): p. 664-73.
455. Vogel, J.R., B. Beer, and D.E. Clody, *A simple and reliable conflict procedure for testing anti-anxiety agents*. *Psychopharmacologia*, 1971. **21**(1): p. 1-7.
456. Cai, C.Y., et al., *Nos1(+) and Nos1(-) excitatory neurons in the BLA regulate anxiety- and depression-related behaviors oppositely*. *J Affect Disord*, 2023. **333**: p. 181-192.
457. Plaznik, A., et al., *Effects of antagonists at the NMDA receptor complex in two models of anxiety*. *Eur Neuropsychopharmacol*, 1994. **4**(4): p. 503-12.

458. Adamec, R.E., et al., *Unilateral block of NMDA receptors in the amygdala prevents predator stress-induced lasting increases in anxiety-like behavior and unconditioned startle--effective hemisphere depends on the behavior*. *Physiol Behav*, 1999. **65**(4-5): p. 739-51.
459. Masneuf, S., et al., *Glutamatergic mechanisms associated with stress-induced amygdala excitability and anxiety-related behavior*. *Neuropharmacology*, 2014. **85**: p. 190-7.
460. Bédard, T., et al., *Role of gastrin-releasing peptide and neuromedin B in anxiety and fear-related behavior*. *Behav Brain Res*, 2007. **179**(1): p. 133-40.
461. Merali, Z., et al., *Bombesin receptors as a novel anti-anxiety therapeutic target: BB1 receptor actions on anxiety through alterations of serotonin activity*. *J Neurosci*, 2006. **26**(41): p. 10387-96.
462. John, C.S. and P.J. Currie, *N-arachidonoyl-serotonin in the basolateral amygdala increases anxiolytic behavior in the elevated plus maze*. *Behav Brain Res*, 2012. **233**(2): p. 382-8.
463. Pardo-García, T.R., et al., *Blockade of the endovanilloid receptor, TRPV1, and of the endocannabinoid enzyme, FAAH, within the nucleus accumbens shell elicits anxiolytic-like effects in male rats*. *Neurosci Lett*, 2020. **732**: p. 135023.
464. Aguiar, D.C., et al., *Anxiolytic-like effects induced by blockade of transient receptor potential vanilloid type 1 (TRPV1) channels in the medial prefrontal cortex of rats*. *Psychopharmacology (Berl)*, 2009. **205**(2): p. 217-25.
465. Xiao, Y., et al., *TRPV1-mediated presynaptic transmission in basolateral amygdala contributes to visceral hypersensitivity in adult rats with neonatal maternal deprivation*. *Scientific Reports*, 2016. **6**(1): p. 29026.
466. Chahl, L.A., *TRP channels and psychiatric disorders*. *Adv Exp Med Biol*, 2011. **704**: p. 987-1009.
467. Bajic, D., et al., *Two different inward rectifier K⁺ channels are effectors for transmitter-induced slow excitation in brain neurons*. *Proc Natl Acad Sci U S A*, 2002. **99**(22): p. 14494-9.
468. Yamaguchi, K., et al., *Modulation of inwardly rectifying channels by substance P in cholinergic neurones from rat brain in culture*. *J Physiol*, 1990. **426**: p. 499-520.
469. Stanfield, P.R., Y. Nakajima, and K. Yamaguchi, *Substance P raises neuronal membrane excitability by reducing inward rectification*. *Nature*, 1985. **315**(6019): p. 498-501.
470. Aosaki, T. and Y. Kawaguchi, *Actions of substance P on rat neostriatal neurons in vitro*. *J Neurosci*, 1996. **16**(16): p. 5141-53.

471. Drew, G.M., V.A. Mitchell, and C.W. Vaughan, *Postsynaptic actions of substance P on rat periaqueductal grey neurons in vitro*. *Neuropharmacology*, 2005. **49**(5): p. 587-95.
472. Shen, K.Z. and R.A. North, *Substance P opens cation channels and closes potassium channels in rat locus coeruleus neurons*. *Neuroscience*, 1992. **50**(2): p. 345-53.
473. Koyano, K., et al., *Two signal transduction mechanisms of substance P-induced depolarization in locus coeruleus neurons*. *Eur J Neurosci*, 1993. **5**(9): p. 1189-97.
474. Sosulina, L., et al., *Neuropeptide Y activates a G-protein-coupled inwardly rectifying potassium current and dampens excitability in the lateral amygdala*. *Mol Cell Neurosci*, 2008. **39**(3): p. 491-8.
475. Takano, K., et al., *Gq/11 and PLC-beta 1 mediate the substance P-induced inhibition of an inward rectifier K⁺ channel in brain neurons*. *J Neurophysiol*, 1996. **76**(3): p. 2131-6.
476. Takano, K., et al., *Protein kinase C-mediated inhibition of an inward rectifier potassium channel by substance P in nucleus basalis neurons*. *Neuron*, 1995. **14**(5): p. 999-1008.
477. Nakajima, Y. and S. Nakajima, *Measurement of orexin (hypocretin) and substance P effects on constitutively active inward rectifier K(+) channels in brain neurons*. *Methods Enzymol*, 2010. **484**: p. 613-30.
478. Niemeyer, A., A. Rinne, and M.C. Kienitz, *Receptor-specific regulation of atrial GIRK channel activity by different Ca(2+)-dependent PKC isoforms*. *Cell Signal*, 2019. **64**: p. 109418.
479. Hu, B., C.A. Boyle, and S. Lei, *Oxytocin receptors excite lateral nucleus of central amygdala by phospholipase Cbeta- and protein kinase C-dependent depression of inwardly rectifying K(+) channels*. *J Physiol*, 2020. **598**(16): p. 3501-3520.
480. Lei, Q., et al., *Molecular mechanisms mediating inhibition of G protein-coupled inwardly-rectifying K⁺ channels*. *Mol Cells*, 2003. **15**(1): p. 1-9.
481. Mark, M.D. and S. Herlitze, *G-protein mediated gating of inward-rectifier K⁺ channels*. *Eur J Biochem*, 2000. **267**(19): p. 5830-6.
482. Cho, H., et al., *Receptor-induced depletion of phosphatidylinositol 4,5-bisphosphate inhibits inwardly rectifying K⁺ channels in a receptor-specific manner*. *Proc Natl Acad Sci U S A*, 2005. **102**(12): p. 4643-8.
483. Cho, H., et al., *Phosphatidylinositol 4,5-bisphosphate is acting as a signal molecule in alpha(1)-adrenergic pathway via the modulation of acetylcholine-activated K(+) channels in mouse atrial myocytes*. *J Biol Chem*, 2001. **276**(1): p. 159-64.

484. Keselman, I., et al., *Mechanism of PLC-mediated Kir3 current inhibition*. Channels (Austin), 2007. **1**(2): p. 113-23.
485. Meyer, T., et al., *Depletion of phosphatidylinositol 4,5-bisphosphate by activation of phospholipase C-coupled receptors causes slow inhibition but not desensitization of G protein-gated inward rectifier K⁺ current in atrial myocytes*. J Biol Chem, 2001. **276**(8): p. 5650-8.
486. Whorton, M.R. and R. MacKinnon, *Crystal structure of the mammalian GIRK2 K⁺ channel and gating regulation by G proteins, PIP₂, and sodium*. Cell, 2011. **147**(1): p. 199-208.
487. Otsuguro, K., et al., *Isoform-specific inhibition of TRPC4 channel by phosphatidylinositol 4,5-bisphosphate*. J Biol Chem, 2008. **283**(15): p. 10026-36.
488. Trebak, M., et al., *Complex functions of phosphatidylinositol 4,5-bisphosphate in regulation of TRPC5 cation channels*. Pflugers Arch, 2009. **457**(4): p. 757-69.
489. Ningoo, M., et al., *PIP₂ regulation of TRPC5 channel activation and desensitization*. J Biol Chem, 2021. **296**: p. 100726.
490. Davis, M., *Pharmacological analysis of fear-potentiated startle*. Braz J Med Biol Res, 1993. **26**(3): p. 235-60.
491. Davis, M., *Neural systems involved in fear and anxiety measured with fear-potentiated startle*. Am Psychol, 2006. **61**(8): p. 741-756.
492. Miserendino, M.J., et al., *Blocking of acquisition but not expression of conditioned fear-potentiated startle by NMDA antagonists in the amygdala*. Nature, 1990. **345**(6277): p. 716-8.
493. Campeau, S., M.J. Miserendino, and M. Davis, *Intra-amygdala infusion of the N-methyl-D-aspartate receptor antagonist AP5 blocks acquisition but not expression of fear-potentiated startle to an auditory conditioned stimulus*. Behav Neurosci, 1992. **106**(3): p. 569-574.
494. Gewirtz, J.C. and M. Davis, *Second-order fear conditioning prevented by blocking NMDA receptors in amygdala*. Nature, 1997. **388**(6641): p. 471-4.
495. Walker, D.L. and M. Davis, *Involvement of NMDA receptors within the amygdala in short- versus long-term memory for fear conditioning as assessed with fear-potentiated startle*. Behav Neurosci, 2000. **114**(6): p. 1019-33.
496. Sundqvist, M., et al., *Senktide-induced gerbil foot tapping behaviour is blocked by selective tachykinin NK1 and NK3 receptor antagonists*. Eur J Pharmacol, 2007. **577**(1-3): p. 78-86.
497. Duarte, F.S., et al., *Evidence for involvement of NK(3) receptors in the anxiogenic-like effect of SP6-11(C-terminal), a metabolite of substance P, in rats evaluated in the elevated plus-maze*. Behav Brain Res, 2016. **303**: p. 168-75.

498. Sun, P., et al., *Fear conditioning suppresses large-conductance calcium-activated potassium channels in lateral amygdala neurons*. *Physiol Behav*, 2015. **138**: p. 279-84.
499. Ayers, L., et al., *Effects of oxytocin on background anxiety in rats with high or low baseline startle*. *Psychopharmacology (Berl)*, 2016. **233**(11): p. 2165-2172.
500. Zhu, J., et al., *Synthesis, biological evaluation and molecular modeling of substituted 2-aminobenzimidazoles as novel inhibitors of acetylcholinesterase and butyrylcholinesterase*. *Bioorg Med Chem*, 2013. **21**(14): p. 4218-24.
501. Kellis, D.M., et al., *Cholinergic neurotransmission in the basolateral amygdala during cued fear extinction*. *Neurobiol Stress*, 2020. **13**: p. 100279.
502. Martina, M., S. Royer, and D. Paré, *Physiological Properties of Central Medial and Central Lateral Amygdala Neurons*. *Journal of Neurophysiology*, 1999. **82**(4): p. 1843-1854.
503. Li, J.N., K. Chen, and P.L. Sheets, *Topographic organization underlies intrinsic and morphological heterogeneity of central amygdala neurons expressing corticotropin-releasing hormone*. *J Comp Neurol*, 2022. **530**(13): p. 2286-2303.
504. Sarah, H., et al., *Intrinsic Circuits in the Lateral Central Amygdala*. *eneuro*, 2017. **4**(1): p. ENEURO.0367-16.2017.
505. Millhouse, O.E. and J. DeOlmos, *Neuronal configurations in lateral and basolateral amygdala*. *Neuroscience*, 1983. **10**(4): p. 1269-1300.
506. Yau, J.O., et al., *The Roles of Basolateral Amygdala Parvalbumin Neurons in Fear Learning*. *J Neurosci*, 2021. **41**(44): p. 9223-9234.
507. Muller, J.F., F. Mascagni, and A.J. McDonald, *Pyramidal cells of the rat basolateral amygdala: synaptology and innervation by parvalbumin-immunoreactive interneurons*. *The Journal of comparative neurology*, 2006. **494**(4): p. 635-650.
508. Seidenbecher, T., et al., *Amygdalar and Hippocampal Theta Rhythm Synchronization During Fear Memory Retrieval*. *Science*, 2003. **301**(5634): p. 846.
509. Li, H., et al., *Neurotensin orchestrates valence assignment in the amygdala*. *Nature*, 2022. **608**(7923): p. 586-592.
510. Sun, F., et al., *Next-generation GRAB sensors for monitoring dopaminergic activity in vivo*. *Nature Methods*, 2020. **17**(11): p. 1156-1166.